EFFICIENCY OF USING STEEL END CAPS IN IMPROVING THE POST-FIRE FLEXURAL BEHAVIOR OF FRP REINFORCED CONCRETE BEAMS

RAMI J. A. HAMAD

UNIVERSITI SAINS MALAYSIA

2017

EFFICIENCY OF USING STEEL END CAPS IN IMPROVING THE POST-FIRE FLEXURAL BEHAVIOR OF FRP REINFORCED CONCRETE BEAMS

by

RAMI J. A. HAMAD

This submitted in fulfilment of the
requirements for the degree of
Doctor of Philosophy

June 2017

(يَرْفَعِ اللَّهُ الَّذِينَ آمَنُوا مِنكُمْ وَالَّذِينَ أُوتُوا الْعِلْمَ دَرَجَاتٍ وَاللَّهُ بِمَا تَعْمَلُونَ خَبِيرٌ)

سورة المجادلة – 11

In The Name of Allah, the Most Beneficent, the Most Merciful

(Allah will raise those who have believed among you and those who were given knowledge, by degrees. And Allah is acquainted with what you do)

Surat Al-Mujadala -11

DEDICATION

To my mother, father, sisters, and brothers,

To my beloved wife, sons and daughter,

To all my friends in Palestine, Malaysia, Jordan and UAE,

To everyone who was there when I needed support,

To all those who wished me luck,

I dedicate this work with all my love.

ACKNOWLEDGMENT

First and foremost, I have to thank my parents for their love and support throughout my life.

All my gratitude goes to my main supervisor Prof. Dr. Megat Azmi Megat Johari and my Co-supervisor Prof. Rami Haddad for their guidance, support and patience.

Sincere thanks to all technicians in the engineering laboratories and workshops for their continuous support.

Exceptional thanks to all academic staff, administrative staff and my colleagues in the School of Civil Engineering who were of great help and support.

Last, but not least, I express my warm thanks to my wife for her moral and spiritual support, quiet patience and unwavering love.

TABLE OF CONTENTS

CHAPTER THREE: METHODOLOY

CHAPTER FOUR: RESULTS AND DISCUSSION

CHAPTER FIVE: THEORETICAL STUDY

LIST OF TABLES

LIST OF FIGURES

LIST OF ABBREVIATIONS

AFRP   Aramid Fiber Reinforced Polymer

BE   Bar Elongation

B.S.   Bond Slip Failure

BFRP   Basalt Fiber Reinforced Polymer

BPE   Bertero- Popov-Eligehausen

C.C.   Concrete Crushing Failure

C3S   Portlandite

CFRP   Carbon Fiber Reinforced Polymer

CH   Calcium Hydroxide

CIMA   Cement Industries of Malaysia Berhad

CMR   Cosenza- Manfredi - Realfonzo

CSH   Calcium Silicate Hydrate

CTE   Coefficient of Thermal Expansion

DMA   Dynamic Mechanical Analysis

DMTA   Dynamic Mechanical Thermal Analysis

DSC   Differential Scanning Calorimetry

DTG   Derivative Thermo-Gravimetric Analysis

EC   End Cap

EFM   Expected Failure Mode

EPR   Epoxy Polymer Resin

EUS   Elongation at Ultimate Strength

FA   Fly Ash

FRP   Fiber Reinforced Polymer

GFRP	Glass Fiber Reinforced Polymer
H.T.	High Temperature
HFRHSC	Hybrid-Fiber-Reinforced-High-Strength-Concrete
HPC	High-Performance Concrete
HPSCC	High-Performance, Self-Consolidating Concrete
HSC	High Strength Concrete
I.S.	Initial Stiffness
ID	Inner Diameter
LVDT	Linear Variable Differential Transducers
MK	Metakaolin Concrete
N.A.	Not Available/ Not Applicable
N.T.	Normal Temperature
NSC	Normal Strength Concrete
OD	Outer Diameter
ODF	Overall Ductility Factor
OPC	Ordinary Portland Cement
PFA	Pulverized Fly Ash
PVC	Polyvinyl Chloride polymer
RC	Reinforced Concrete
RUBS	Residual Ultimate Bond Strength
S	Shear Failure
S.R.	Reduction in Stiffness
S.Y.	Steel Yielding Followed by Concrete Crushing
SABS	Slip at Maximum Bond Strength
SAF	Stroke at Maximum Force

SEM	Scanning Electronic Microscopy
SF	Silica Fume
Sp. #	Specimen Number
SS316L	Stainless Steel Grade 316L
T.C.	Thermocouple
TGA	Thermo-Gravimetric Analysis
UBS	Ultimate Bond Strength
UD	Uni-directional
UP	Unsaturated Polyester
US	Ultimate Strength
VER	Vinyl Ester Resign
YS	Yield Strength

LIST OF SYMBOLS

°C	Celsius Degree
°F	Fahrenheit Degree
A, B, C, D	Regression Coefficients
A_f	Area of FRP Bars in Tension Region
A_v	Cross-Sectional Area of Each Stirrup
b	Concrete Section Width
c	Distance from Extreme Compression Fiber to Neutral Axis
c	Concrete Cover
c_c	Concrete Specific Heat
C	Compression Force
CE	Environmental Reduction Factor
d	Beam's effective depth
d_b	Bar's Diameter
E, F & n	Regression Coefficients
E	Elastic Modulus
E_c	Concrete Elastic Modulus
E_f	FRP's Elastic Modulus
E_L	Longitudinal Modulus of Elasticity
E_s	Steel Elastic Modulus
$E_{s,T}$	Steel Elastic Modulus at Temperature T
E_T	Bar's Elastic Modulus at Temperature T
E_T	Transverse Modulus of Elasticity
E_{el}	Absorbed Elastic Energy

E_{inel}	Absorbed Inelastic Energy
E_{tot}	Total Absorbed Energy
f'_c	Concrete Compressive Strength
$f'_{c,T}$	Concrete Compressive Strength at Temperature T
$f'_{c,0}$	Concrete Compressive Strength at Exposure Time 0.0 minutes
$f'_{c,t}$	Concrete Compressive Strength at Exposure Time t
f_c	Concrete Compressive Stress at Strain ε_c
f_{cf}	FRP Compressive Strength
$f_{c,T}$	Concrete Compressive Stress at Strain ε_c after Exposure to Temperature T
f_{cu}	Concrete Cube Compressive Strength
$f_{cu,T}$	Concrete Cube Compressive Strength at Temperature T
f_{cr}	Modulus of Rupture
f_{ct}	Concrete Tensile Strength
f_{sf}	FRP Shear Strength
f_{sp}	Concrete Tensile Splitting Strength
$f_{sp,T}$	Concrete Tensile Splitting Strength at Temperature T
f_u	Bar's Ultimate Tensile Strength
$f_{u,T}$	Bar's Ultimate Tensile Strength at Temperature T
f_f	FRP Bar's Stress
f_{ult-f}	FRP's Ultimate Strength
$f_{ult-f,T}$	FRP's Ultimate Strength at Temperature T
f_y	Steel Tensile Yield Strength
$f_{y,T}$	Steel Tensile Yield Strength at Temperature T
F	Maximum Bond Force in Reinforcement
F_a	Applied Force

F%	Fiber to Matrix volume ratio
$F_{b,u}$	Ultimate Measured Bond Force
G	Shear Modulus
h	Overall Cross-Section Height
I_{cr}	Moment of Inertia of the Cracked Transformed Section
I_e	Effective Moment of Inertia
I_g	Gross Moment of Inertia
I_m	Modified Moment of Inertia
$k_{cu,T}$	Concrete Cube Compressive Strength Reduction factor at Temperature T
k_d	Cracked Transformed Section Neutral Axis Depth
k_E	Elastic Modulus Reduction Factor
k_f	Strength Reduction Factor
$k_{sp,T}$	Concrete Tensile Splitting Strength Reduction factor at Temperature T
k_{tc}	Concrete Thermal Conductivity
L_e	Beam's Effective Length
L_d	Embedded Length
L_o	Length between Edge of the Sample and the Machine's Head Wedges
M	Bending Moment
M_a	Allowable Service Moment
M_{cr}	Cracking Moment
M_n	Beam's Nominal Moment Capacity
$M_{n\text{-}pred}$	Predicted Moment Capacities of RC Beams
$M_{n\text{-}th}$	Theoretical Moment Capacities of RC Beams
M_{ult}	Ultimate Moment Capacity
n	Elastic Modulus Ratio

n_u	Poisson's Ratio
P_c	Maximum Compression Load
P_{cr}	Cracking Load
P_{exp-cr}	Experimental Measured Cracking Load
$P_{exp-ult}$	Experimental Measured Ultimate Load Capacities of RC Beams
$P_{exp-yield}$	Experimental Measured Yield Load of Steel-RC Beams
P_{-m}	Experimental Measured Load at Concrete Strain of 0.001 (Or 0.0021)
P_{max}	Maximum Applied Force
P_n	Beam's Nominal Load Capacity
$P_{pre-ult}$	Predicted Ultimate Load Capacities of RC Beams
P_{th-cr}	Theoretical Cracking Load
P_{th-ult}	Theoretical Ultimate Load Capacities of RC Beams
P_T	Maximum Tensile Load
r	Bar's Radius
S	Slope of Line
s	Bond Slip
S_{emp}	Empirical slip at maximum bond stress
S_{exp}	Experimental slip at maximum bond stress
S	Stirrups Spacing
t	time
T	Temperature
T_m	Maximum Tensile Force in Reinforcement
T_d	Decomposition Temperature
T_g	Glass Transition Temperature
V_c	Concrete Shear Capacity

V_n	Beam's Nominal Shear Strength
V_s	Stirrups Shear Capacity
α , α_b ,	Factors
α_c	Coefficient of Thermal Expansion at Temperature T
α_L	Longitudinal Coefficient of Thermal Expansion
α_{Tr}	Transverse Coefficient of Thermal Expansion
α_T	Curve Fitting Parameter as Function of Temperature
β, $\beta 1$, β_d	Factors
β_T	Curve Fitting Parameter as Function of Temperature
Δ	Deflection
$\Delta\sigma$	Difference in Tensile Stress
$\Delta\varepsilon$	Difference in Tensile Stain
$\Delta_{exp\text{-}yield}$	Experimental Measured Deflection at Yield Load
$\Delta_{exp\text{-}cr}$	Experimental Measured Deflection at Measured Cracking Load
$\Delta_{exp\text{-}s}$	Experimental Measured Deflection at Service Load
$\Delta_{exp\text{-}ult}$	Experimental Measured Deflection at Measured Ultimate Load
$\Delta_{\text{-}m}$	Deflection at Concrete Strain of 0.001 (Or 0.0021)
$\Delta_{th\text{-}cr}$	Theoretical Deflection at Theoretical Cracking Load
$\Delta_{th\text{-}s}$	Theoretical Deflection at Service Load
$\Delta_{th\text{-}ult}$	Theoretical Deflection at Theoretical Ultimate Load
Δ_{ult}	Ultimate Deflection
δ_i	displacement at point i
θ	Rebar's Temperature
ρ	Reinforcement Ratio

ρ_b	Balance Reinforcement Ratio
$\rho_{c,T}$	Concrete Density at Temperature T
ρ_f	FRP Reinforcement Ratio
σ_i	Stress at point i
τ	Bond Stress
τ_{emp}	Empirical Bond Strength
τ_{exp}	Experimental Bond Strength
τ_{max}	Maximum Bond Stress
τ_T	Bond Strength at Temperature T
Φ	Diameter of Bar
ε_c	Concrete Strain
$\varepsilon_{c,T}$	Concrete Strain after Exposure to Temperature T
ε_{cu}	Ultimate Concrete Strain
ε_f	Strain of FRP bar at Stress f_f
ε_i	Strain at point i
ε_o	Concrete Strain at Peak Stress
ε_r	Measured Reinforcement Strain at Measured Ultimate Load
ε_R	Elongation at Rupture
ε_s	Strain of steel bar at Stress f_s
ε_{ult-f}	Strain of FRP at Ultimate Strength
ε_{ult}	Strain of Bar at Ultimate Tensile Strength
μ	Ductility Index

KEBERKESANAN PENGGUNAAN TETOPI HUJUNG KELULI DALAM PENAMBAHBAIKAN PERLAKUAN LENTURAN PASCA KEBAKARAN RASUK KONKRIT BERTETULANG FRP

ABSTRAK

Penggunaan bar Polimer Bertetulang Gentian (FRP) sebagai alternatif kepada tetulang keluli tradisional dapat membantu mengatasi masalah ketahanlasakan dalam struktur konkrit bertetulang. Kelakuan struktur FRP-RC adalah memuaskan pada suhu yang rendah sahaja, oleh itu, penggunaan bahan-bahan FRP mudah terbakar dalam perdagangan, industri dan bangunan kediaman, di mana kemungkinan berlakunya kebakaran adalah agak tinggi, boleh menjadi berbahaya. Penyelidikan lanjut diperlukan untuk menilai dan meningkatkan prestasi struktur FRP-RC di bawah keadaan kebakaran. Dalam kajian ini, kesan suhu yang tinggi ke atas sifat mekanik bar FRP / Keluli, tingkah laku ikatan antara bar-bar FRP / keluli dan konkrit, dan tindak balas lenturan rasuk konkrit dengan pelbagai jenis bar tetulang FRP telah disiasat secara mendalam. Teknik tetopi-hujung keluli baru telah dicadangkan bertujuan untuk memperbaiki tambatan bar FRP yang tertanam dalam konkrit. Untuk itu, sampel dalam bentuk bar FRP / keluli, konkrit biasa, sampel tarik keluar dan rasuk (dengan dan tanpa tetopi-hujung keluli) telah disediakan dan kemudian diawet selama 28 hari serta seterusnya diuji sebelum dan selepas didedahkan kepada suhu tinggi sehingga 500°C. Konkrit dan FRP bar mengalami pengurangan ketara dalam sifat-sifat mekanikal mereka disebabkan oleh pendedahan kepada suhu yang tinggi. Kekuatan ikatan antara bar-bar FRP dan konkrit telah berkurangan apabila terdedah kepada suhu dalam julat 125-325°C, dengan pengurangan mencapai sehingga 85%. Pengurangan ini telah dipaparkan secara negatif dalam tingkah laku rasuk konkrit bertetulang FRP yang

dipanaskan, di mana beban retak, kapasiti beban muktamad, kekakuan dan jumlah tenaga diserap telah berkurang sehingga 89%, 81%, 79%, dan 70%, masing-masing manakala pesongan pertengahan rentang dan indeks kemuluran telah meningkat dengan ketara sehingga masing-masing setinggi 50% dan 94%. Memasang tetopi hujung keluli di hujung bar FRP telah meningkatkan kekuatan ikatan mereka dengan konkrit sebelum dan selepas terdedah kepada suhu yang tinggi sehingga 325°C. Oleh itu, prestasi lenturan rasuk konkrit bertetulang FRP dengan tambatan tetopi hujung telah meningkat; beban retak, kapasiti beban muktamad, kekukuhan, pesongan pada beban muktamad, jumlah tenaga terserap dan indeks kemuluran masing-masing telah meningkat sehingga kira-kira (124%, 208%, 225%, 196%, and 453%) and (33%, 123%, 58%, 216% and 215%) sebelum dan selepas pemanasan sehingga 500 ° C, berbanding dengan rasuk kawalan tanpa tetopi-hujung keluli. Berdasarkan keputusan eksperimen, model analisis telah dicadangkan untuk meramalkan tingkah laku bahagian menaik hubungan ikatan-gelinciran antara bar FRP yang berbeza dan konkrit di bawah suhu yang tinggi. Satu kaedah teori juga tealah dicadangkan untuk meramalkan keupayaan beban muktamad teori rasuk konkrit bertetulang FRP. Ramalan kedua-dua model itu adalah bersetujuan dengan yang sangat baik dengan keputusan eksperimen.

EFFICIENCY OF USING STEEL END CAPS IN IMPROVING THE POST-FIRE FLEXURAL BEHAVIOR OF FRP REINFORCED CONCRETE BEAMS

ABSTRACT

The use of Fiber Reinforced Polymer (FRP) bars as an alternative to traditional steel reinforcement helps overcoming durability problems in reinforced concrete structures. The behavior of FRP-RC structures is satisfactory at only low temperatures, hence the application of combustible FRP materials in commercial, industrial and residential buildings, where the possibility of fire occurrence is relatively high, can be dangerous. Further research to evaluate and enhance the performance of FRP-RC structures under fire conditions is required. In this study, the effect of high temperatures on the mechanical properties of FRP/Steel bars, bond behavior between FRP/Steel bars and concrete, and the flexural response of concrete beams with different types of FRP bar reinforcement was investigated in much details. A new steel-end-caps technique was proposed aiming to improve anchorage of embedded FRP bars in concrete. For that FRP/Steel bars, plain concrete, pullout and beam specimens (with and without steel end caps) were prepared and then cured for 28 days and later tested before and after subjected to elevated temperatures of up to 500°C. Concrete and FRP bars suffered significant reductions in their mechanical properties due to exposure to high temperatures. Bond strength between FRP bars and concrete had decreased upon exposure to temperature in the range of 125 to 325°C, with the reduction reaching as high as 85%. These reductions were reflected negatively in the behavior of heated FRP-RC beams hence cracking load, ultimate load capacity, stiffness and total absorbed energy were reduced by as high as 89%, 81%, 79%, and 70%, respectively

whereas mid-span deflections and ductility indices were increased noticeably by as high as 50% and 94%, respectively. Attaching steel end caps to the ends of FRP bars had improved their bond strength with concrete before and after exposure to high temperatures of up to 325ºC. Consequently, the flexural performance of FRP-RC beams with end-cap anchorage was improved where the cracking load, ultimate load capacity, stiffness, deflection at ultimate load, and total absorbed energy were increased to reach as high as (124%, 208%, 225%, 196%, and 453%) and (33%, 123%, 58%, 216% and 215%) before and after heating up to 500°C, respectively, compared with that of control beams without end anchorage. Based on the experimental results, an analytical model was proposed to predict the behavior of the ascending part of bond-slip relation between the different FRP bars and concrete under high temperatures. Another theoretical method was also proposed to predict the theoretical ultimate load capacity of FRP-RC beams. The predictions of the two models were in an excellent agreement with the experimental results.

CHAPTER ONE
INTRODUCTION

1.1 Preface

Existing reinforced concrete (RC) structures are deteriorated when they are exposed to severe conditions such as corrosive environment. With the presence of water and oxygen, steel reinforcement, embedded in concrete, may corrode; leading to a durability problem of steel reinforced concrete structures. Maintenance and rehabilitation of the RC structure damaged by corrosion is costly (Nadjai et al., 2005; Maraveas et al., 2012) and sometimes complicated. In the U.S., the estimated costs per year for the repair of steel reinforced concrete structures damaged due to corrosion is about two hundred and seventy six Billion US dollars (Chin et al., 1997; Koch et al., 2002).

Recently, the use of non-metallic Fiber Reinforced Polymer (FRP) bars as an alternative to the traditional steel reinforcement has received a great deal of attention as an effective solution for overcoming the durability problems associated with steel corrosion in the RC structures (Galati et al., 2006).

FRP composites are materials which consist of strong reinforcing organic/inorganic fibers embedded in a rigid resin matrix. The fibers carry the applied loads and provide the stiffness and strength to the composite. There is a wide range of available FRP composites such as glass fiber reinforced polymer (GFRP), carbon fiber reinforced polymer (CFRP), and basalt fiber reinforced polymer (BFRP) with different properties. The polymeric matrix can be either thermoplastics or thermosetting polymers with the latter being the most popular type (Cao and Wu, 2008).

1

Compared to traditional reinforcing steel, FRP bars possess higher resistance to electro-chemical corrosion, tensile stresses, fatigue and electromagnetic waves. FRP possesses lighter weight, lower elastic modulus, and lower resistance to high temperature yet higher cost than conventional steel bars (Chin et al., 1997; Bisby et al., 2005a; Masmoudi et al., 2010; Maraveas et al., 2012). FRPs can be used practically either as internal reinforcing bars inside the concrete section or as externally bonded reinforcement sheets/plates using epoxy resin adhesives (Maraveas et al., 2012).

Numerous experimental and theoretical studies on the structural behavior of FRP reinforced concrete elements have been carried out in the past years. However, the contradictions in results from different research works on the significance of using FRP in reinforcing various structural elements demanded further theoretical studies and experimental programs to be carried out on the structural performance of thermally damaged elements with FRP reinforcement and their durability (Karbhari et al., 2003; Robert and Benmokrane, 2010).

Although the behavior of FRP-RC structures is satisfactory at low temperatures (Nadjai et al., 2005), the application of combustible FRP materials in commercial, industrial and residential buildings still needs more research to evaluate the structural performance in fire situations. These research works are highly needed in order to establish the design codes and practical guidelines of FRP reinforced concrete structures and guarantee their safe application (Nanni, 2001; Harries et al., 2003; Nadjai et al., 2005; Robert and Benmokrane, 2010).

The behavior of steel bars RC at high temperature is different from that of FRP bars RC. When FRP rebars are embedded in concrete and subjected to fire, the rebars will not burn due to lack of oxygen but the resin will be softened (Nadjai et al.,

2005). From previous studies, it was shown that the polymer resin used in the manufacturing of FRP composites has a service temperature called the glass transition temperature, T_g. Under elevated temperatures, such as those of fire, upon exceeding the glass transition temperature, the polymer resin exhibits visco-elastic transitions followed by irreversible thermal degradation; reducing the ability of the resin to transfer forces through fibers (Robert and Benmokrane, 2010). Thus, the mechanical properties of the resin as represented in stiffness and strength are degraded significantly and hence impairing the mechanical properties of the FRP composites (Katz et al., 1999).

The bond mechanism of FRP rebars to surrounding concrete depends on the properties of polymer matrix at the surface of the rebars. At high temperature exceeding the glass transition temperature (T_g) of the polymer matrix, the polymer surface layer is damaged therefore the matrix becomes unable to transfer stresses from the concrete to the fibers (Katz et al., 1999; Nadjai et al., 2005). The divergence in the coefficient of thermal expansion (CTE) between FRP and concrete aggravates the bonds degradation upon exposure to high temperature; additional stresses would be created in the FRP bars upon cooling. This and heat generated cracks within concrete lead to splitting cracking along the FRP bars. Ultimately, this affects the performance of bond between concrete and FRP reinforcement negatively and hence the structural response; undermining the contribution of FRP to structural applications (Galati et al., 2006).

1.2   Problem statement

a) Limited information is available on the post fire residual mechanical properties of FRP materials used in construction. Up to date, most of the studies did not precisely determine the critical exposure temperature of

different FRP composites that affects their mechanical properties and bond strength with concrete. Therefore, further research is needed to determine this critical exposure temperature and post-fire residual properties of FRPs to enable prediction of residual load capacity of corresponding reinforced concrete members.

b) There is a lack of research on the post-fire bond behavior between FRPs materials and concrete with no research works, carried out to enhance the bond between the FRP bars and concrete under fire exposure. The limited available studies reported that bond between FRP reinforcing bars and concrete deteriorates at elevated temperature leading to the slippage of bars and therefore accelerates the whole failure of the RC members. If the ends of the FRP rebars are protected enough to avoid the bars slip at elevated temperature, then the failure mechanism of FRP-RC structures will be shifted from the bars slip failure to the bars ruptures and therefore improving the fire resistance of the structures.

c) Up to date, no research works, has been carried out to enhance the pre- and post-fire behavior of FRP reinforced concrete structures.

d) Most research activities concentrated on glass FRP (GFRP) due to their lower cost. Further research is needed to investigate the elevated temperature performance of other types of FRP composites such as Carbon and Basalt FRP when used in the corresponding structural elements; especially beams.

e) Provisions for fire condition were not incorporated in various international codes to aid in design of structural elements reinforced with FRP composites. Hence, analytical equations should be proposed to provide the available codes with the necessary information to account for fire exposure.

4

1.3   Research objectives

The main objectives of this study are:

a) To investigate experimentally the residual mechanical properties of different FRP/Steel bars and the residual bond properties between these bars and concrete after exposure to elevated temperatures.

b) To investigate experimentally the flexural behavior of concrete beams, reinforced with different types of FRP bars, before and after exposure to high temperature (simulating a fire case).

c) To evaluate the efficiency of using chemically bonded steel end caps in promoting post-fire flexural behavior of FRP-RC beams and compare it with that of steel-RC beams.

d) To propose two analytical models; the first model can be used in predicting the bond-slip behavior between FRP bars and concrete after exposure to high temperature whereas the second one can be used for the evaluation and prediction of post-fire performance of the concrete beams reinforced with FRP bars with and without end cap.

1.4   Scope of work

The study includes the following:

a) Tensile tests were carried out on glass fiber reinforced polymer (GFRP), carbon fiber reinforced polymer (CFRP), basalt fiber reinforced polymer (BFRP), and steel bars to study their mechanical properties at ambient temperature ($23^{o}C$) as well as after heating to temperatures then cooling. A total of 18 specimens of each bar type were used. Three of them were tested at ambient temperature and used as controls while the remaining fifteen

specimens (in triplicates) were exposed to different elevated temperatures of 125°C, 250°C, 325°C, 375°C and 450°C.

b) Tests were performed on standard concrete cylinders and cubes to determine the splitting tensile strength, compressive strength and modulus of elasticity of the 40 MPa concrete that used in casting the beams and pullout specimens. Half of these standard specimens were tested after 28 days at ambient temperature whereas the rest were tested after exposure to a high temperature of 500°C for 90 minutes duration.

c) Traditional cubic pullout specimens were prepared using 10-mm-diameter FRP/steel bars embedded vertically in concrete cubes (150×150×150 mm) with a bond length of 100 mm and cured for 28 days then tested for bond behavior between BFRP, CFRP, GFRP and steel bars and concrete before and after exposure to high temperatures and then cooled to room temperature. A total of 60 specimens, represented triplicates of pullout specimens with the four types of used bar were tested before and after exposed to different temperature levels of 125, 250, 325 and 375°C for three hours then cooled.

d) Two FRP-RC beams were cast with eight K-Type thermocouples having a 1.0 m probe length placed at different location across the depth of two beams prior to casting, cured for 28 days then heated up in gas furnace to 500°C for four hours in order to get the temperature distribution profile throughout the beam's cross section during the heating process.

e) Twelve control specimens of 130 mm × 180 mm × 1200 mm of reinforced concrete beams were cast in triplicates using four different reinforcing bars, BFRP, CFRP, GFRP and steel bars then subjected to four-point loading test in order to study their flexural behavior, modes of failure and deflection

6

characteristics. FRP-reinforced concrete beams were designed according to ACI, 2006 (ACI 440.1R) while steel RC beams were designed according to ACI, 2005 (ACI 318R). All beams were tested as simply supported beams of 1200 mm total span, 1050 mm clear span and 350 mm pure bending moment span around the middle of the beams.

f) A loading frame with a full jack capacity of 500 kN was used in the four-point loading test. Three linear variable displacement transducers (LVDT's) were placed at three locations of each beam to measure the vertical deflection. Strain gauges were attached to the main reinforcement bars and the external concrete surface to measure the strain during testing. The response of the tested specimens was recorded using a data acquisition system before the data was analyzed to evaluate the results.

g) Similar set of twelve beams specimens were subjected to a high temperature of 500ºC for 90 minutes in gas furnace then cooled to room temperature before being tested under four-point loading test.

h) Eighteen reinforced concrete beams specimens of similar size were cast with different reinforcing bars (BFRP, CFRP, and GFRP). The FRP bars used were steel capped at their two ends using high temperature resistant epoxy adhesive. This end capping was aimed at improving bond between FRP and concrete hence the flexural behavior. Nine of these specimens were tested under four-point loading test at ambient temperature as controls whereas the remaining specimens were subjected to a high temperature of 500ºC for 90 minutes then cooled before being tested under four-point loading test.

i) Based on the bond-slip experimental results, a new analytical model was proposed to predict the bond-slip behavior between FRP bars and concrete after exposure to high temperatures.

j) Based upon the experimental data, analytical equations were presented to predict the pre- and post-fire ultimate load capacity of FRP RC beams based on the assumption of FRP rebar slippage.

1.5 Thesis structure

This thesis consists of six chapters. Chapter one presents general introduction, problem statement, objectives and scope of work. Chapter two presents the literature review of studies previously carried out on the FRP composites in construction including (different properties of FRP composites, the effect of high temperature on the FRPs properties, the pre-and post-heating bond behavior between FRP and concrete, and the performance of FRP-RC elements before and after exposure to fire). Chapter three describes the methodology including the different materials used, preparation of specimens, casting, heating, mechanical testing programs, and preface to the theoretical studies used. Experimental tests results and discussion are presented in chapter four including the pre-and post-heating mechanical properties of FRP/Steel bars and concrete, the effect of heating on bond strength between FRP/Steel bars and concrete, modes of failure and load-deflection characteristics of different tested concrete beams such as ultimate load capacity, deflection, stiffness and ductility. In chapter five, analytical studies were presented including the proposed modeling of post-heating bond-slip behavior between FRPs and concrete and then the analytical method was used for the prediction of FRP-RC beam's load capacity that based on rebars slippage assumption. Conclusions and recommendations for future work are reported in chapter six.

CHAPTER TWO
LITERATURE REVIEW

2.1   Introduction

This chapter provided brief detailing of different studies, performed on FRP composites, and concrete reinforced with FRP bars. A background about FRP materials and their practical applications; including their use for reinforcing concrete elements is presented in Sections 2.2 and 2.3. The effect of elevated temperatures on different properties of FRP composites and on the structural behavior of FRP-RC elements were presented in detailed in Section 2.4. Furthermore, Section 2.5 presented the effect of high temperatures on the properties of the concrete.

2.2   Fiber Reinforced Polymer (FRP) composites

FRP composites are manufactured from the combination of high tensile fibers and a polymer matrix to give new and useful material with better properties than their original constituents (Bisby et al., 2005b). FRPs are orthotropic material because of the use of strong fibers that are continuous and oriented in the longitudinal direction which provide the stiffness and strength of the FRP. The applied forces are transferred between the fibers through the shear stresses that developed in the polymer matrix. When one of these fibers is broken, its force is transferred to the adjacent fibers though the matrix until the total damage of fibers happen leading to the failure of the FRP (Bisby et al., 2005b; Kodur et al., 2007).

The commercial types of fibers that are used in FRP production are glass, carbon, basalt and aramid; of which have their advantages and disadvantages. Among all, carbon fibers possess the highest stiffness, the lowest low relaxation, and the best durability characteristics under high temperature and chemical attacks yet carbon

fibers are the most expensive fibers (Kodur and Baingo, 1998; Bisby et al., 2005b). Glass fibers are the most widely used in FRP production due to their low cost although they have some disadvantages such as low elastic modulus and poor durability in alkaline and moist environments. Basalt fibers have similar resistance to alkali and weathering environments as Glass fibers with a better fire endurance than carbon fibers (Hulin et al., 2013). Aramid fibers are sensitive to creep and have poor durability in moist environments (Bisby et al., 2005b), yet have good thermal stability and excellent impact resistance (Kodur and Baingo, 1998).

The applied forces are transferred and distributed between the fibers of the FRP composite through the weak matrix of polymers which have lower density than the fibers so the overall weight of these FRPs are low (Bisby et al., 2005b). There are two main types of matrix polymers; thermoplastic and thermosetting. Thermoplastic polymers include nylon, polyethylene and polyamides while thermosetting polymers include epoxies, polyesters and vinyl esters. Thermosetting polymers are cross-linked molecular structure polymers resulting from the polymerization reaction of low molecular weight polymers and cannot be welded together by heating (Cao and Wu, 2008). Thermosetting polymers are preferred to be used in FRPs production due to their higher thermal stability and chemical resistance compared with thermoplastics. The most widely used matrix in the market are epoxies and vinyl esters (Bisby et al., 2005b).

The overall FRP properties depend on the properties of the fibers and matrix, fiber volume fraction (typically in range of 60 to 70 %), fiber orientation, fiber cross sectional area and method of production (Bisby et al., 2005b). The longitudinal properties of the FRPs are governed by the properties of the fibers while the transverse properties are governed by the matrix properties (Kodur and Baingo, 1998).

Fibres are temperature-resistant material that can resist high temperature with a small reduction in stiffness and strength while the polymer resins are very sensitive to temperature and start losing their strength at low temperatures; glass, carbon and basalt fibers can resist temperature up to 450°C, 500°C and 700°C, respectively. Polymer resins can withstand relatively low exposure temperatures of 45-100°C (Cao and Wu, 2008). Kodur and Baingo, (1998) summarized the properties of FRPs and other related materials, available in the literature, in Tables 2.1 and 2.2.

Table 2.1: Mechanical properties of FRP composites and mild steel available in the literature as summarized by Kodur and Baingo, (1998)

Material	E_L GPa	E_T GPa	f_{uf} MPa	f_{cf} MPa	G GPa	f_{sf} MPa	n_u
GFRP (Glass/Epoxy)	55	18.0	1050	1050	9.0	42	0.25
GFRP (Glass/Epoxy)-UD	42	12.0	700	N.A.	5.0	72	0.30
CFRP (Carbon/Epoxy)-UD	180	10.0	1500	N.A.	7.0	68	0.28
CFRP (Graphite/Epoxy)	207	5.2	1050	700	2.6	70	0.25
Poron/ Epoxy	207	21.0	1400	2800	7.0	126	0.30
AFRP (Aramid/Epoxy)-UD	76	8.0	1400	N.A.	3.0	34	0.34
Mild Steel	200	N.A.	550	240	N.A.	380	N.A.

E_L, longitudinal modulus of elasticity, E_T, transverse modulus of elasticity, f_{uf}, ultimate tensile strength, f_{cf}, FRP compressive strength, G, shear modulus, f_{sf}, FRP shear strength, n_u, Poisson's ratio, UD, uni-directional, N.A., not available,

Table 2.2: Thermal properties of FRP composites and mild steel available in the literature as summarized by Kodur and Baingo, (1998)

Material	Coefficient of Thermal Expansion, UD, 10^{-6} m/m per °C		Thermal Conductivity, W/m °C	
	Longitudinal	Transverse	Longitudinal	Transverse
GFRP (Glass/Epoxy)	6.30	19.80	3.46	0.35
GFRP (Glass/Epoxy)-UD	7.13	N.A.	N.A.	N.A.
CFRP (Carbon/Epoxy)-UD	-0.90	27.00	48.4-60.6	0.87
CFRP (Graphite/Epoxy)	-1.44	30.60	121.1-129.8	1.04
Poron/ Epoxy	4.50	14.40	1.73	1.04
AFRP (Aramid/Epoxy)-UD	-3.60	54.00	1.73	0.73
Mild Steel	10.8-18	10.8-19	15.6-46.7	15.6-46.8

UD, uni-directional, N.A., not available,

2.3 PFRP composites in concrete construction

During the last twenty years, a great deal of attention has been given on the characteristics of FRP-RC structures. A number of research works have been carried out on the durability, fatigue, creep, bond behavior, and structural behavior as well as failure modes of these structures. A detailed literature review of the bond behavior and structural behavior of internally reinforced FRP concrete beams is presented in this section while an extensive literature review on the main topics related to the effect of elevated temperatures on FRP-RC structures are presented in the subsequent sections.

FRP materials are non-corrosive composite materials that can be applied in concrete construction effectively as alternative to steel reinforcement. These FRP materials can be applied to concrete structures in three different forms namely externally bonded FRP sheets or plates for repair or strengthening of reinforced concrete structure, main reinforcement in the form of FRP bars, and prestressed FRP tendons in prestressed concrete structures (Bisby et al., 2005a; Bisby et al., 2005b).

FRPs possess some advantages and disadvantages. Their advantages include high resistance to corrosion, high strength-to-weight ratios (10 to 15 times greater than steel), excellent fatigue characteristics (about 3 times that of steel), electromagnetic neutrality and ease as well as speed of application leading to reduced construction costs (Kodur and Baingo, 1998; Bisby et al., 2005a; Bisby et al., 2005b). On the other hands, the disadvantages include high material cost, low ductility with low strain at brittle failure, low shear strength due to poor mechanical properties of the matrix, rapid and severe loss of bond, reduced strength and stiffness at elevated temperatures, poor creep and expansion properties in the case of aramid FRP, and low resistance to alkali environments in the case of glass FRP (Kodur and Baingo, 1998; Kodur et al., 2005; Bisby et al., 2005b).

Many design codes and design guidelines were published in order to help in the design of concrete structures with internal FRP bars reinforcement such as American code ACI 440.1R-15 (2015), ISIS 2006-Design Manual No.3 and Canadian standards CAN/CSA-S806-02 (R2007). The American Code ACI 440.4R-04 (2004) is used to design prestressed concrete structures with FRP tendons.

Similarly, design guidelines were published to help in the design of concrete structures strengthened externally with epoxy bonded FRP composites such as ACI 440.2R-08, ISIS 2001-Design Manual No.4 and TR55 Design guidance for strengthening concrete structures using fibre composite materials by concrete society.

2.3.1 Bond between FRP bars and concrete

The bond behavior of FRP bars and concrete is different than that between conventional steel and concrete due to the different material properties and surface texture. In general, the bond mechanism consists of three components: chemical adhesive, friction, and the mechanical interlocking between the bar surface deformation and the surrounding concrete. At low bond stresses, the chemical adhesive between the paste and the imperfections of the bar's surface is the main resisting mechanism. When adhesion fails, the friction and mechanical interlocking start working with the start of bar slip and cracks formation. .

Chemical bonds can't be formed between the FRP bars and concrete due to the water repellent nature of the resin which is used in the FRP rebar production (Katz, 2001). Hence, FRP bars to concrete bonds mechanism depends on the bar's mechanical interlocking and the friction between the surface and the surrounding concrete. Special surface treatment should be added to plain bars in order to enhance their bonds with concrete. Different surface treatments are available such as sand coating, helical wrapping, molded deformation, irregular surface humps by adding excess of resin and

braiding of the fibers. Combinations of different surface treatment of FRP bars can improve the bond strength to values close to that of steel (Katz, 2001). Bar diameter, embedment length, FRP bar's modulus of elasticity, concrete strength, concrete cover and bars surface treatment are the main factors that were considered in the evaluation of the bond behavior. Recent findings stated that the bond between FRP bars and concrete was inversely related to bar diameter due to the increase of voids formation at larger contact surfaces (Masmoudi et al., 2010).

Each FRP composite has different properties because of the wide variety of fiber to resin interfaces which make predicting their bond behavior with concrete difficult (El Refai et al., 2014). Add to this, the bond strength is also sensitive to the setup adopted in the experiments. As a result, many reports were published with varying estimation of bond strength between FRP composites and concrete, all of which are lower than values stipulated for bond strength between steel and concrete (Tastani and Pantazopoulou, 2006). Nevertheless, most of the available design codes of FRP-RC structures assume perfect bond between the FRP reinforcement and the surrounding concrete at ambient temperature (Xiaoshan and Zhang, 2013).

The objectives and overall findings of different research studies that carried out on bond behavior between FRP bars and concrete are presented in Table 2.3.

Table 2.3: Different research studies that carried out on bond behavior between FRP composites and concrete

Reference	Objectives	Overall Finding
Ehsani and Saadatmanesh, (1996)	1- To use the experimental work results in developing an analytical equation for the evaluation of bond strength of straight and hooked GFRP bars to concrete based on experimental work	1- For straight GFRP bars, minimum embedded length of 380mm is recommended. 2- For hooked GFRP bars, minimum embedded length of 150mm is recommended.
Cosenza et al., (1999)	1- To investigate the bond behavior of GFRP bars and concrete with bar embedment length ranging from 5 to 30 times the bar diameter. 2- To predict a model to simulate the bond-slip curves.	1- The failure modes were bar's pullout failure, rebars failure accompanied by pullout failure, and rebar rupture failure for different embedment lengths of $(5d_b)$, $(10d_b)$, and (greater than $10d_b$), respectively. 2- Pullout failure was due to the damage of both ribs at outer surface of the bar and the surrounding concrete. 3- Concrete strength had negligible effect on the bond strength. 4- The bond stress distribution along the embedded length can't be considered as constant.
Brik, (2003)	To evaluate experimentally the bond strength between both plain basalt rebars and modified basalt rebars and concrete.	1- Plain rebars showed lower bond strength than that of modified rebars with 4 to 8 slots surface slots. 2- Plain rebar specimens failed due the pullout of the basalt rebars while the modified rebar specimens failed by the rupture of the rebar itself.
Belarbi and Wang, (2004)	To study the effect of incorporating short fibers in concrete and bar's type, embedment length, and surface treatement on the bond behavior between FRP rebars and concrete reinforced with randomly distributed short polypropylene fibers.	1- Lower bond strength in case of CFRP than GFRP due to smoother surface of the former. 2- The addition of short fiber to concrete changed the failure mode from concrete splitting failure to much more ductile rebar pullout failure. 3- Bond strength was increased by increasing the embedment length in case of the CFRP bars yet the opposite was noticed for the GFRP bars.

Table 2.3: continued

Reference	Objectives	Overall Finding
Tastani and Pantazopoulou, (2006)	To investigate experimentally and analytically the effect of the bar diameter and surface roughness, the concrete cover to bar diameter ratio, and the effect of externally bonded FRP sheets on the bond mechanics of GFRP bars with normal strength concrete.	1- The bond strength of large diameter smooth bars is smaller than that of small diameters. 2- The bond strength of deformed bars was insensitive to the bar size. 3- Using FRP jacketing had changed the failure mode from a sudden concrete splitting failure to a more ductile bar's pullout failure due to the confinement pressure effect of the jacketing. 4- Damage of the bar itself by peeling off was noticed at higher concrete strengths.
Liao et al., (2009)	To investigate the effect of winding methods on the bond capacity between the FRP rebars and concrete.	1- The GFRP bar's lug/ core interface of the transverse wound specimens is the weakest link where the failure can occur. 2- FRP rod with 90 degree winding without axial winding have a lower bond strength than longitudinal and oblique angle winding.
Baena et al., (2009)	To study experimentally the effect of FRP bar type (glass or carbon), bar diameter, bar surface texture, and concrete strength on the bond behavior between FRP bars and concrete	1- The bond strength increased and the failure mode changed by increasing the concrete compressive strength 2- The bar surface treatment has important effect on the bond strength especially when high strength concrete is used. 3- The bond strength increased when bar's area to space ratio and concrete lug ratio increased. 4- The bond strength decreases with the increase of the bar diameters. 5- The slip of glass FRP bars were greater than those of the carbon. 6- The new equations, proposed to simulate the ascending branch of the bond-slip curves, showed a better agreement with the experimental data than the double branch and CMR analytical models.

Table 2.3: continued

Reference	Objectives	Overall Finding
Munoz, (2010)	To study the effect of the concrete strength, FRP type (GFRP and CFRP), bar diameter and bar surface treatment on the bond behavior between FRP bars and concrete.	1- The failure mode of the rebars was at the bar to concrete interface due to the de-bonding of the rebar itself. 2- The surface treatment has a great effect on the bond strength of FRP bars and this effect increases with the increase of concrete strength. 3- Sand coated FRP bars had a higher bond strength with concrete. 4- The concrete compressive strength affects the failure modes of the pullout tests but doesn't affect the ultimate bond strength of the FRP bars. 5- Bond strength is inversely proportional to the bar diameter.
Goraya et al., (2011)	To study experimentally the effect of surface texture on the bond strength between sand coated GFRP bars and concrete specimens using the pullout test.	1- The sand coating of the FRP bars had improved the friction between the bars and the concrete and therefore had increased their bond strength. 2- Using sand coating treatment can offset the absence of ribs in plain GFRP rebars and improves the bond strength between the FRP bars and concrete. 3- The failure mode of the plain bars was pullout failure while the failure mode of the sand coated bars was represented in concrete splitting failure.
Mazaheripour et al., (2013)	To study experimentally the effect of bar diameter, embedment length, surface characteristics of the bars, and concrete cover thickness on the bond behavior of GFRP bars and steel fiber reinforced self-compacting concrete.	1- All tested specimens failed by pullout of the bars without showing concrete splitting due to the effect of steel fibers in blocking the grow of any micro-crack in concrete and maintaining the crack width at small value 2- A higher bond strength resulted when larger concrete cover thickness was used due to the increase in concrete cover shear capacity. 3- Increasing the embedment length of the bars had decreased the bond strength due to the nonlinear distribution of the bond stress along the embedment length. 4- The bond strength for ribbed bars was higher than that of sand coated bars regardless of the bar diameter and embedment length.

Table 2.3: continued

Reference	Objectives	Overall Finding
El Refai et al., (2014)	To study experimentally the effect of FRP bar type (glass and basalt), bar diameter and embedment length on the bond behavior between basalt and glass FRP bars and concrete under direct pullout test.	1- The bond strength of BFRP was about 75% of that of GFRP because of the higher modulus of elasticity of the latter. 2- The bond strength of FRP bars is inversely proportional to both bar diameter and embedment length. 3- Pullout failure mode was noticed for BFRP samples whereas different failure modes such as pullout failure, concrete splitting failure and bar rupture was noticed for GFRP bars specimens. 4- The failure mode depended on the embedment length of the bar where concrete splitting was noticed in case of $7d_b$ (short) embedded length while bar rupture before bond strength was attained was noticed in case of $15d_b$ (long) embedded length. 5- The FRP bar's surface treatment has a large effect on the bond behavior of the FRP bars. A good bond behavior up to peak followed with a sudden failure was noticed in case of sand coated GFRP whereas the bond failure was smooth in case of BFRP with spiral grooved sand coated surface.

2.3.2   Performance of concrete beams with FRP internal reinforcement bars

Ductility is an important design requirement of any element. It is defined as the ability of the element to absorb the inelastic energy without any reduction in the flexural capacity of the element. FRP bars exhibit a linear stress-strain behavior up to failure and do not show any post-yield behavior as in the case of steel reinforcement (Bisby et al., 2005b; Nadjai et al., 2005; Rafi and Nadjai, 2011b). Therefore, FRP bars have poor ductility compared with steel bars. FRPs have higher strength than steel but lower strain at failure (Bisby et al., 2005). These mechanical properties of FRPs result in non-ductile flexural behavior of concrete beams reinforced with FRP bars with higher deflection and cracking than steel-RC beam. Due to the brittle behavior of FRP bars, concrete becomes the ductile component of the FRP-RC beams and the ductility of these beams depends mainly on the properties of the concrete (Aiello and Ombres, 2002; Rafi and Nadjai, 2011b). Due to the previous statement, the design criterion for FRP reinforced concrete structures shifts to the serviceability limit states that check the structural behavior aspect instead of the strength requirement to ensure functionality and safety during the expected life of the structures. Therefore, FRP-RC beams are designed as over-reinforced in order to achieve concrete failure (crushing of concrete) before FRP rebar's failure (Aiello and Ombres, 2002; Nadjai et al., 2005; Qu et al., 2009; Issa and Elzeiny, 2011; Al-Sunna et al., 2012; Pawłowski and Szumigala., 2015). The objectives and overall findings of different research studies that carried out on FRP-RC structures are presented in Table 2.4.

The traditional ductility definition of steel-RC elements is the ratio of post yield deformation to the yield deformations (Wang and Belarbi, 2005). This definition can't be applied to FRP-RC elements due to the linear elasticity of the FRP bars. Other

methods, such as energy based method and deformation based method, were proposed by researchers to calculate the ductility index of FRP-RC elements.

Energy based approach, defined the ductility as the ratio between the elastic energy and the total energy, as shown in Figure 2.1.
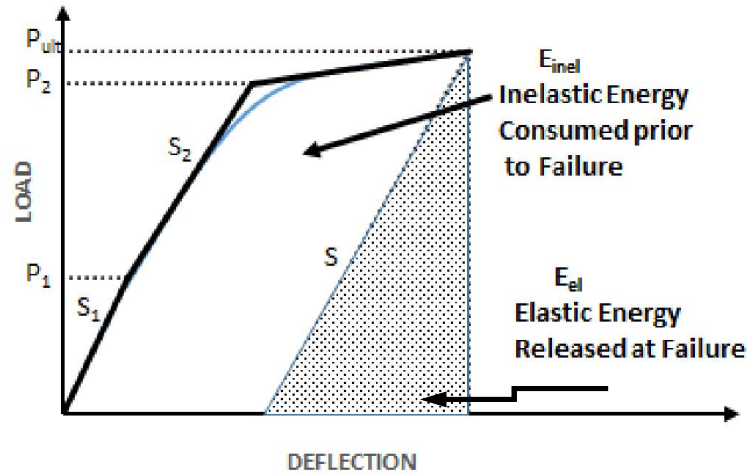
Fig. 2.1 Ductility index explanation proposed by Naaman and Jeong (1995)

Naaman and Jeong, (1995) defined the total energy as the total area under the load-deflection curve while the elastic energy is the area of right triangle formed at the failure load with hypotenuse slope equal to the weighted average slope of the two initial straight lines of the load deflection curve (Figure 2.1). Naaman and Jeong (1995) proposed Equations 2.1 and 2.2 to compute the ductility index, μ. A minimum limit of between 3 and 4 is proposed for design purposes.

$$\text{Ductility Index } \mu = \frac{1}{2}\left(\frac{E_{el} + E_{inel}}{E_{el}} + 1\right) \tag{2.1}$$

$$S = \frac{P_1 S_1 + (P_2 - P_1)S_2}{P_2} \tag{2.2}$$

where   S1, S2, and S are slopes of lines.

Deformation based approach, was introduced by Mufti et al., (1996) and the overall ductility factor was defined as the product of the strength factor and the deformability factor (Overall Ductility Factor = Deformability factor x Strength factor).

20

The deformability factor is the ratio of ultimate deflection to the deflection when the maximum concrete compressive strain equals to 0.001 and the strength factor is the ratio of the ultimate moment to the moment when the maximum concrete compressive strain is 0.001.

$$\text{Overall Ductility Factor} = \frac{\Delta_{ult}}{\Delta_{\varepsilon_c=0.001}} \times \frac{M_{ult.}}{M_{\varepsilon_c=0.001}} \qquad (2.3)$$

Table 2.4: Different research studies that carried out on FRP-RC structures.

Reference	Objectives	Overall Finding
Alsayed et al., (2000)	1- To study experimentally the flexural behavior of FRP-RC beams. 2- To examine the load versus deflection equations provided by the ACI code. 2- To suggest minimum reinforcement needed to avoid the sudden brittle failure due to the rupture of the FRP reinforcement.	1- The ultimate design theory (concrete crushing failure) can predict the flexural capacity of the FRP-RC beams accurately. 2- The mid-span deflections calculated based on ACI equations were under-estimated compared with the experimental values. 3- The proposed models accurately estimated the service load deflection and showed a good agreement with the measured experimental results. 4- A model, suggested for calculating the minimum reinforcement of FRP-RC beams, showed a good agreement with the experimental results
Aiello and Ombres, (2002)	To study experimentally and theoretically the effect of concrete cover thickness, reinforcement ratio, and the mechanical properties of concrete and reinforcement on the structural behavior of hybrid FRP-steel reinforced concrete beams.	1- FRP reinforcement provide a better flexural capacity while the steel reinforcement provide the ductility and rigidity for the beams 2- The rigidity of the hybrid RC beams were higher than the steel-RC beams after cracking. 3- The crack width and spacing of hybrid RC beams was lower and number of cracks were higher than that of the FRP-RC beams. 4- The use of steel reinforcement with FRP reinforcement reduced the deformability of the RC beams.

Table 2.4: Continued

Reference	Objectives	Overall Finding
Brik, (2003)	To evaluate experimentally the ultimate flexural capacity of basalt rebar reinforced concrete beams. Plain basalt rebars and modified basalt rebars (with slots and corrugations) were used.	1- The tested beams with modified bars have higher ultimate moments than the first crack moments due to the good bond between the rebar and concrete. 2- At ultimate failure stage, the beams were suffering from large cracking and deflections. 3- At failure, no slip was noticed in any of the tested beams; indicating a good bond between the basalt rebars and concrete. 4- In general, pure flexural failure mode was observed whereas some beams have primary flexural failure followed by secondary shear failure. 5- The measured ultimate moment capacities of the beams with modified basalt bars were higher than the calculated moment capacities according to ACI Code.
Wang and Belarbi, (2005)	To study the flexural behavior of the polypropylene-fiber-reinforced-concrete beams reinforced with FRP rebars. Variables used in this experiment were FRP type (Glass and Carbon), bar diameter and concrete type (plain versus polypropylene-fiber-reinforced-concrete).	1- The addition of short discrete fibers to the FRP-RC beams improved their flexural behavior, increased their ductility index by 40% and reduced the crack widths measured at service load. 2- All beams failed due to concrete crushing with linear strain of the reinforcement up to failure. 3- The ultimate compressive strain of the fiber-reinforced-concrete beams at failure exceeded 0.004 value. 4- The actual measured deflection at service load for all beams (with plain concrete and FRC) matched the calculated deflection according to ACI code, 2015.
El-Sayed et al., (2005)	1- To propose a new modification to the shear design equations for FRP-reinforced concrete beams given by ACI 440.1R-03	1- A good agreement was found between the proposed equations and the experimental results available in the literature.

Table 2.4: Continued

Reference	Objectives	Overall Finding
El-Sayed et al., (2005)	2- To verify the new proposed equation using the experimental results of 15 research works available in the literature. 3- To compare the proposed equations with major design equations proposed by the available design codes namely: ACI 440.1R-03, ISIS 2006- Design Manual No. 3 and CAN/CSA-S806-02	The experimental results of 15 research works available in the literature confirmed that the equations given by ACI 440 code underestimated the shear strength of FRP-RC beams whereas the new proposed equations showed a better prediction of the shear strength than those prescribed by the previously mentioned codes.
Qu et al., (2009)	1- To investigate experimentally and theoretically the flexural behavior of hybrid (GFRP-Steel) reinforced concrete beams. Type of reinforcement, reinforcement ratio and the ratio of GFRP to steel were studied as main parameters. 2- To adopt the equations of ACI440.1R-06 for the predictions of ultimate load capacity, crack width and deflection of hybrid FRP-steel RC beams.	1- The best ductility, serviceability and ultimate load capacity were found in Hybrid GFRP-steel RC beams having a normal effective reinforcement ratios. 2- The steel reinforcement improved the ductility of the hybrid FRP-Steel RC beams while the FRP reinforcement improved the flexural strength. 3- A good agreement were noticed between the experimental results and ACI code analytical models results. 4- The model proposed by Bischoff, P.H., (2007) for the prediction of the effective moment of inertia provided a good prediction of the mid-span deflection of Hybrid FRP-Steel RC beams up to service load only. 5- Equations provided by ACI440.1R-06 for the prediction of crack width showed a good agreement with the experimental results.
El-Gamal et al., (2010)	1- To study experimentally the flexural behavior of concrete beams reinforced with different bars (GFRP or steel) at different reinforcement ratios.	1- Higher reinforcement ratios increased the beams stiffness. 2- Using more reinforcement bars with smaller diameters was more efficient than using less bars with larger bar sizes because of the former higher contact area and greater contribution to crack control.

Table 2.4: Continued

Reference	Objectives	Overall Finding
El-Gamal et al., (2010)	2- To compare the measured mid-span deflections with that calculated using CAN/CSA-S806-2002, and ACI440.1R-2006	3- A good agreement between the experimental deflection values and the predicted values using the CAN/CSA-S806-2002 code whereas ACI440.1R-2006 code underestimated the deflection values.
Issa and Elzeiny, (2011)	To study experimentally and theoretically the flexural behavior of GFRP-RC cantilever beams. The main parameters were the reinforcement type (GFRP and steel), reinforcement ratio, and concrete compressive strength.	1- The theoretical ultimate flexural capacity, predicted using ACI code's formulas (ACI440.1R, 2006), were found to be 30% lower than the experimental values. 2- The strains of the FRP rebars at failure were much lower than their rupture strains while the failure strain of steel rebars were higher than their yield strain. 3- The experimental average cracking loads were about 31% of the average ultimate loads.
Al-Sunna et al., (2012)	1- To investigate the flexural behavior of GFRP and CFRP-RC beams and slab with different reinforcement ratios. 2- To examine the accuracy of the ACI440 and Eurocode 2 design equations used to calculate the short-term deflection	1- The assumption of plane section remains plane after bending is not valid for FRP-RC beams and slab at high levels of loading. 2- Considering only the flexural behavior of FRP-RC elements in prediction of the overall deflection of these elements will lead to underestimate the deflection values. 3- Shear cracking, shrinkage and loss of bond were found to have a significant contribution to the overall deflection of FRP-RC structures. 4- ACI 440.1R-06 equations used for predicting the deflection of FRP-RC elements underestimated the deflection especially for cases of moderate to high ratios of reinforcement. 5- Equations of Eurocode-2 offered a better prediction for the deflection of FRP-RC for all of the reinforcement ratios studied in this experimental program

Table 2.4: Continued

Reference	Objectives	Overall Finding
Nor et al., (2013)	To investigate the flexural behavior of concrete beams reinforced with CFRP strips and compared their behavior with the performance of steel RC beams; while considering the effect of concrete cover.	1- CFRP-RC beams with or without concrete cover had a higher ultimate strength than that of steel reinforced concrete. 2- Concrete beams reinforced with externally bonded CFRP strips showed higher load capacity than those with CFRP strips with concrete cover layer. 3- Beams with externally bonded strips showed a sudden failure due to the de-bonding and slip-off of the CFRP reinforcing strips.
Xiaoshan and Zhang, (2013)	To investigate experimentally the flexural behavior and bond-slip behavior of FRP-RC beams. Two main parameters were considered in this study including the FRP rebar type (Glass, Carbon & Basalt) and the bar's surface texture.	1- The behavior of all beams was linear up to the first crack then the load-deflection curves changed to be none linear with many slopes. 2- The rebar's surface texture plays a very important role in the bond-slip behavior between the rebar and the surrounding concrete. 3- The beams reinforced with basalt FRP rebars had higher ultimate moment capacity than that of beams reinforced with smooth surface GFRP and CFRP rebar due to the spiral indentations in the BFRP rebar's surface.
Pawłowski and Szumigala., (2015)	To study experimentally and numerically the flexural behavior of simply supported BFRP RC beams including the failure mechanism, deflection and ductility. The main parameter used in this study was the reinforcement ratio.	1- The reinforcement ratio had a significant effect on the flexural strength, stiffness and failure mode of these beams. 2- Under-reinforced Beams failed suddenly due to the rupture of the FRP bars while over-reinforced beams failed in ductile behavior due to concrete crushing. 3- Mid-span deflections increased with the decrease in the reinforcement ratio. 4- The service load of BFRP-RC beams (at deflection of L/250) was about 28~39% of the ultimate load capacity.

2.4 Performance of FRP composites exposed to high temperatures

2.4.1 Introduction

Fire resistance of FRP reinforced concrete structures is a critical subject area that should be studied intensively. Unfortunately, the little work, which has been done recently, does not provide enough data to cover the gap between the urgent need and available information (Bisby et al., 2005a).

In order to evaluate the fire resistance and post-heating residual strength of FRP-RC structures, the reduced materials properties of both concrete and FRP as a function of temperature and time should be evaluated (Kodur and Baingo, 1998; Ellis, 2009). These properties are thermal, mechanical and deformation properties (Kodur and Baingo, 1998). Mechanical properties includes the tensile and compressive strength, modulus of elasticity and ultimate strain. Thermal properties includes the thermal conductivity, specific heat and mass loss. Deformation properties includes the thermal expansion and creep.

The thermal behavior of FRP composites such as temperature distribution and heat transfer depends on their thermal properties, while the mechanical properties control their structural response (Bai et al., 2008).

Numerous different types of FRP composites are available commercially due to the variability in their formulations with respect to fiber and matrix type, fiber volume fractions, fiber orientations, and modulus of elasticity of the fibers and matrix. Consequently, varying test results of thermal and mechanical behaviors in fire are reported making the available data not applicable for all types of FRP composites used in construction (Chin et al., 1997; Bisby et al., 2005a; Chowdhury et al., 2007).

Polymer matrix exhibits four different phases when exposed to elevated temperature; glassy, leathery then rubbery and decomposed phase (Bai et al., 2007b; Cao and Wu, 2008).

When FRP composites are exposed to fire, firstly the composite material is heated up to reach a temperature which cause significant changes in the resin, whereby it transforms from glassy state to leathery state. This temperature is the glass transition temperature T_g of the polymer matrix and is typically in the range of 65–120°C (Bisby et al., 2005a). Then, further heating continues to reach a temperature which breaks the chemical bonds and modular chains of the resin. This temperature is the decomposition temperature of the resin T_d and typically in the range of 300 to 400°C. Decomposition starts forming other material phases such as liquids, smoke and gases. At higher temperatures, ignition and then combustion of the composite occur (Chowdhury et al., 2007; Bai et al., 2008).

The overall fire performance of FRP Rebars, which consist of long but not continuous fibers embedded in the polymer matrix, depends on the properties of the polymer matrix (Kodur et al., 2005). When FRP rebars are exposed to high temperature, the resin decomposes and bonds between the fibers and the decomposing resin are damaged. Consequently, FRPs suffer from significant irreversible degradation in thermal and mechanical properties, as well as bond properties (Bisby et al., 2005a; Kodur et al., 2005; Wang et al., 2007; Chowdhury et al., 2007). Glass and aramid fiber composites show a significant reduction in strength at high temperature while carbon fiber composites are insensitive to high temperature (Bisby et al., 2005a; Lublóy et al., 2005).

Ezzeldin and Shrive, (1999) noticed that exposure of FRP to 200 and 300°C for 24 hours changes the surface color to become darker, indicating the loss of some resin.

Within the first hour of exposure to 500°C, the resin evaporated leaving the FRP composite as a bundle of loose fibers.

2.4.2 Effect of fire on thermal properties of FRP

Most of the international codes did not provide any equation to predict the thermal properties of FRP composites such as the thermal conductivity, specific heat, glass transition temperature, and mass loss as a function of temperature. Also, limited research works on these thermal properties of different types of FRP composites at elevated temperatures have been carried out as summarized in Table 2.5.

Thermal conductivity of any material represents its capacity to conduct heat. FRP composites are unidirectional composite materials where the longitudinal thermal conductivity is controlled by the fibers while the transverse conductivity is controlled by the matrix. Most of FRP composites, except CFRP, have low longitudinal and transverse thermal conductivity (Kodur and Baingo, 1998; Chowdhury et al., 2007).

Different investigation and testing techniques have been used to study the thermal properties of FRP composites such as dynamic mechanical thermal analysis (DMTA), thermogravimetric analysis (TGA), and differential scanning calorimetry (DSC) (Chowdhury et al., 2007). DMTA analysis tests are used to determine the glass transition temperature of the FRP composites, TGA is used to measure the mass variation of the specimens, while the DSC is used to measure the energy changes in the material as a function of time and temperature (Pires , 2012).

Based on the data and information obtained from the DMTA, TGA, and DSC, it was found that the thermo-physical and thermo-mechanical properties of FRP composites are functions of both temperature and time (Bai and Keller, 2009). Kodur et al., (2005) proved that the FRP reinforcement has lower thermal conductivity and heat capacity than the steel reinforcement.

Table 2.5: Different research works that carried out on the thermal properties of FRP composites under high temperatures

Reference	Objectives	Overall Finding
Bai et al., (2007a)	To propose analytical relations between high temperatures and the thermal properties of GFRP composites such as specific heat and thermal conductivity.	The corresponding relations are depicted graphically in Fig. 2.2. As shown the thermal conductivity showed a severe drop at a temperature of about 250°C whereas the specific heat showed an increase up to 200°C then it became almost constant.
Bai et al., (2007b & 2008)	To propose an analytical model to predict the effect of high temperatures on the thermal properties of FRP composites such as the decomposition degree, mass transfer, specific heat capacity, and thermal conductivity.	1- Little changes were noticed in the mass of the FRP composites before decomposition starts. 2- In temperature range of 200°C to 400°C, a rapid decrease in thermal conductivity of FRP composites was noticed due to decomposition of resin and adhesion between fiber layers. 3- The specific heat capacity of FRP composites is proportional to temperature up till the peak point between 450°C - 600°C..
Chowdhury et al., (2007)	To study experimentally the thermal properties of different FRP composites at elevated temperature such as: mass loss, glass transition temperature, specific heat, and thermal conductivity using TGA, DMTA and DSC tests.	1- 95% of epoxy sample original mass was retained until 300°C followed by a rapid drop in the mass between 320°C and 510°C due to severe degradation of their material properties. 2- Glass and carbon fibers retained 90% of their original mass until 750°C. 3-The epoxy used has 93°C and 320°C of Tg and Td, respectively.
Robert and Benmokrane, (2010)	To investigate the effect of extreme temperature on the fiber, the matrix, and the fiber/matrix interface using scanning electron microscopy (SEM), thermo-gravimetric physical analysis (TGA), and differential scanning calorimetry (DSC).	1- The TGA indicated that FRP composites lost 18% of their weight at temperature between 300-450oC. 2- Analysis showed micro-cracks in the heated specimens which explained the large decrease of the mechanical properties.
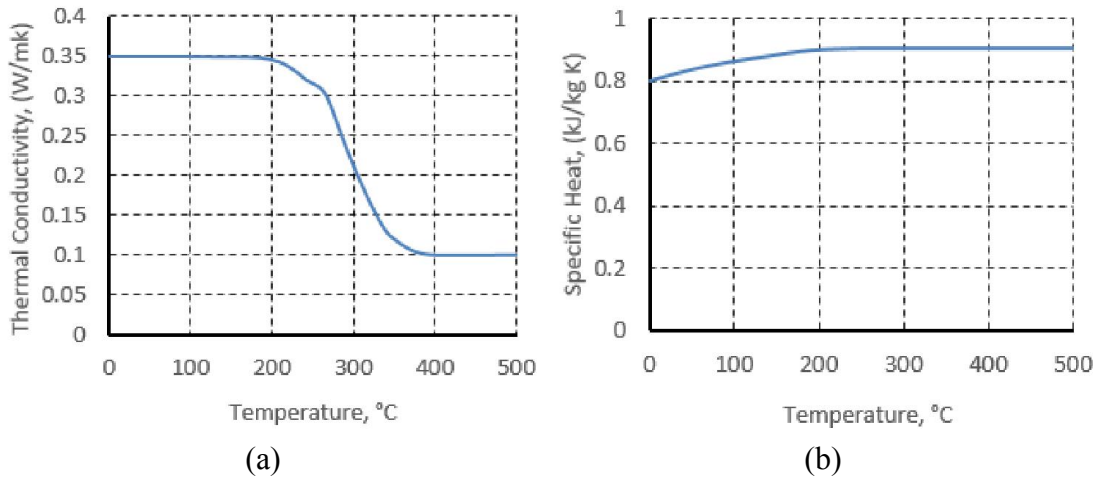
Fig. 2.2 Effect of temperature on thermal properties of GFRP proposed by Bai et al.,
(2007a)

2.4.3   Effect of fire on mechanical properties of FRP

The effect of high temperature on the mechanical properties of FRP composites
such as tensile strength, modulus of elasticity and ultimate strain have been
investigated in many studies; the objectives and overall findings of these research
studies are presented in Table 2.6.

FRP materials are anisotropic unidirectional materials where the fibers in the
longitudinal direction of the FRP rebar govern the uniaxial properties of the rebar such
as tensile strength and stiffness while the polymer governs the properties of the rebar
in the transverse direction such as the shear and bending strength (Bisby et al., 2005a).

Thermal properties of fibers are better than of the polymer because the fibers are
more resistant to thermal changes, hence the thermal mechanical properties of the FRP
composites are governed by the polymer matrix properties (Katz et al., 1999; Bisby et
al., 2005a; Robert and Benmokrane, 2010). Transverse properties of FRP bars such as
shear and bending strength are reduced significantly at elevated temperatures beyond
T_g because of the degradation in the resin shear transfer capacity (Katz et al., 1999;
Bisby et al., 2005a; Robert and Benmokrane, 2010).

Table 2.6: Different research works that carried out on the mechanical properties of FRP composites under high temperatures

Reference	Objectives	Overall Finding
Crea et al., (1997)	To evaluate experimentally the changes in the tensile mechanical parameters of FRP rods after exposure to elevated temperatures.	1- Significant effects of heat on the ultimate strength and elastic modulus of the FRP rods. 2- The ultimate strength was decreased constantly with increasing temperature whereas the elastic modulus showed varying behavior; depending upon exposure temperature
Kodur and Baingo, (1998)	To present the variation of strength of different construction materials with temperature using the limited available data reported in the literature	1- Graphical curves were presented in Fig. 2.3. 2- Up to 100°C, strength loss of FRP was very little yet experienced significant reductions at higher temperatures reaching 75% strength loss at 250°C.
Nadjai et al., (2005)	To use the available data reported in the literature in order to propose equations that can be used to calculate the reduced mechanical properties of the heated FRP materials as function of temperature.	The following equations were proposed, where kf and kE can be obtained from Table 2.7. $$k_f = \frac{\text{Reduced Tensile Strength at Temperature (T)}}{\text{Ultimate Tensile Strength at Ambient Temperature}} = \frac{f_{uf,T}}{f_{uf,20}} \quad (2.4)$$ $$k_E = \frac{\text{Reduced Modulus of Elasticity at Temperature (T)}}{\text{Modulus of Elasticity at Ambient Temperature}} = \frac{E_{f,T}}{E_{f,20}} \quad (2.5)$$
Bai et al., (2007b)	1- To investigate experimentally the changes in mechanical properties of GFRP composites after exposure to elevated temperatures using Dynamic Mechanical thermal analysis (DMTA). 2- To develop a new temperature-dependent mechanical properties model based on the chemical kinetic theory.	1- The results was shown in Fig. 2.4. 2- By increasing temperature to the glass transition temperature, a sudden decrease in the E-modulus happened. 3- The coefficient of thermal expansion for the GFRP material dropped sharply to zero after exceeding the glass transition temperature.

Table 2.6: Continued

Reference	Objectives	Overall Finding
Wang et al., (2007)	To study experimentally the mechanical properties of FRP bars such as strength and stiffness at elevated temperatures and compared them with that of steel bars.	1- The FRP bars have a linear stress–strain relation at elevated temperatures until failure at about 500°C. 2- At elevated temperatures of 350°C, the FRP bars start suffering a severe reduction in tensile strength, up to failure (zero strength) at 500°C. 3- The elastic modulus of the FRP bars remained unchanged until 300–400°C (90% residual elastic modulus) followed by a sharp drop at higher temperatures. 4- The tensile strength of CFRP bars is much greater than that of GFRP bars at ambient temperature, but reductions in GFRP strengths are smaller than those in CFRP bars at elevated temperatures because the decomposition of the binding resin rather the fiber resistance dictates the ultimate strength of the composite.
Cao and Wu, (2008)	To investigate the effect of elevated temperature (up to 200°C) on the mechanical properties of FRP sheets such as carbon, glass and basalt FRP sheets.	1- Linear stress-strain relationships up to failure for all types of FRP sheets from 120°C to 200°C. 2- Increasing the temperature resulted in reducing the tensile strength of all types of FRP sheets significantly. 3- The residual tensile strengths of CFRP, BFRP, and GFRP sheets at 200°C were 70%, 65%, and 62%, respectively 4- The elastic modulus remained unchanged at temperature below 200°C due to temperature-resistant characteristics of the fibers which control the elastic modulus of the FRPs; according to the rules of mixtures of composites.
Robert and Benmokrane, (2010)	To investigate the mechanical properties of GFRP bars such as tensile, shear and flexural properties at temperatures ranging from -100°C to 315°C	At very high temperatures exceeding the matrix glass-transition temperatures, the strength and stiffness of the bars decreased considerably. The residual tensile, shear and flexural strengths of GFRP bars were (70%, 90%, and 25%) and (45%, 20%, and 5%) after exposure to 150°C and 350°C, respectively

Table 2.6: Continued

Reference	Objectives	Overall Finding
Wang et al., (2011)	To study the mechanical properties of CFRP plates at high temperatures of up to 700°C.	1- Tensile strength of CFRP plate was reduced significantly at the temperature ranges of 20–150°C and 450–700°C, with small reduction between 150-450°C. 2- At 300 and 700°C, the residual tensile strengths were 50% & 7% respectively. 3- The stress-strain relationship is linear up to failure below 520°C and nonlinear beyond which due to loss of fiber from oxidation. 4- Equation 2.6 was proposed to predict the residual tensile strength of the CFRP plate at any temperature. This equation was calibrated using the experimental results and equation's coefficient was given in Table 2.8. $$\frac{f_{uf,T}}{f_{uf,20}} = A - \frac{(T-B)^n}{C} \qquad (2.6)$$
Chowdhury et al., (2011	To investigate experimentally the mechanical properties of CFRP coupons such as tensile strength when exposed to temperatures of up to 200°C under various types of loadings..	1- At temperature range of 86°C to 200°C, the range of residual (tensile strength) and (elastic modulus) of CFRP coupons was (40 to 60%) and (50% to 80%) of their original values. 2- The loss of tensile strength and stiffness was as due to load sharing between fibers when temperature exceed the resin's T_g. 3-Analytical models were developed based on the test results to predict the stress-strain behavior of FRP under exposure to high temperature.
Wang and Zha, (2011)	To study experimentally the effect of high temperature of up to 500°C on the mechanical properties of GFRP bars.	1- The stress-strain curves for GFRP bars were linear even at high temperatures. 2- The ultimate tensile stress of the rebars was reduced by 22% at the temperature range of 80-120°C (the glass transition temperature of epoxy resin T_g) and by 67% at about 400°C (corresponds to fibers' softening temperature). 3- The elastic modulus remained unchanged below Tg then started declining linearly when the temperature exceeds Tg.

Table 2.6: Continued

Reference	Objectives	Overall Finding
Fu et al., (2011)	1- To analyze the changes happened in GFRP rebars after exposure to high temperature	1- The GFRP rebars were suffering from vitrification, carbonization, and decomposition due to exposure to high temperature therefore, their mechanical properties such as the tensile strength and the ultimate tensile elastic modulus deteriorated.
Pires, (2012)	1- To study experimentally the mechanical properties of GFRP pultruded profiles such as the tensile, shear, stiffness and compressive strengths before and after exposure to elevated temperatures (up to 250°C). 2- To evaluate the glass transition of the GFRP pultruded materials using differential scanning calorimetry and thermos-gravimetric analysis tests.	1- Linear reduction in tensile strength of GFRP profiles from ambient temperature until 250°C where the residual tensile strength was 54% of their ambient temperature strength. 2- The stiffness, shear and compressive strengths of the GFRP profiles exposed to 250°C were 56%, 11% and 5% of their ambient temperature values, respectively. 3- A model was proposed to estimate the mechanical properties of FRP as a function of temperature. This model showed good agreement with the experimental results.

Table 2.7: Reduction factors k_f and k_E as proposed by Nadjai et al., (2005)

Rebar Type	Temperature range					
	0≤T≤100	100≤T≤300	300≤T≤400	400≤T≤475	475≤T≤500	500≤T
GFRP	k_f=1-0.0025T			k_f=0.0		
AFRP	k_f=1.0	k_f=1.333-0.00333T		k_f=0.0		
CFRP	k_f=1.0	k_f=1.267-0.00267T			k_f=0.0	
AFRP	k_E=1.0	k_E=1.25-0.0025T	k_E=2.0-0.005T	k_E=0.0		
CFRP	k_E=1.0	k_E=1.175-0.00175T	k_E=1.625-0.00325T			k_E=0.0

Table 2.8: Coefficient A, B, C, and n as proposed by Wang et al., (2011)

Temperature (°C)	Coefficients			
	A	B	C	n
22≤T<150	1.0	22	200	0.9
150≤T<420	0.59	150	490	0.7
420≤T<706	0.48	420	76,000	1.8
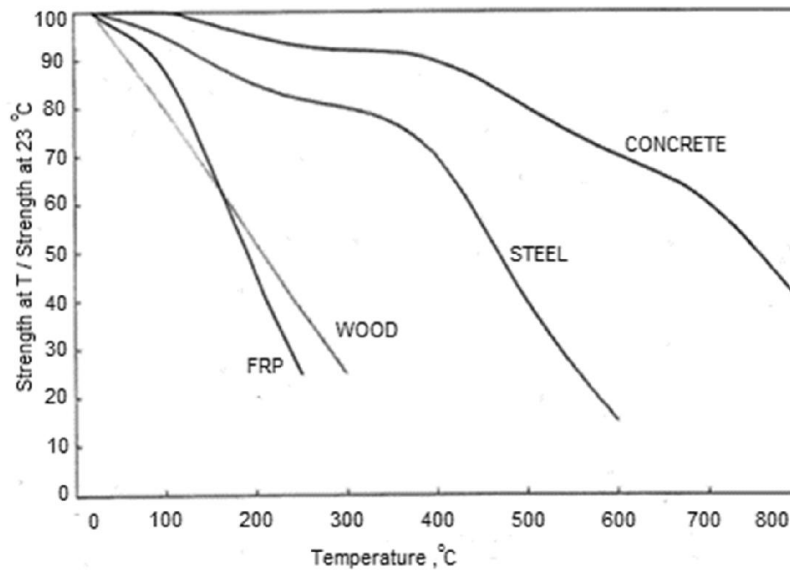
Fig. 2.3 Effect of temperature on strength of different construction materials, presented by Kodur and Baingo, (1998)

| | |
| (a) | (b) |
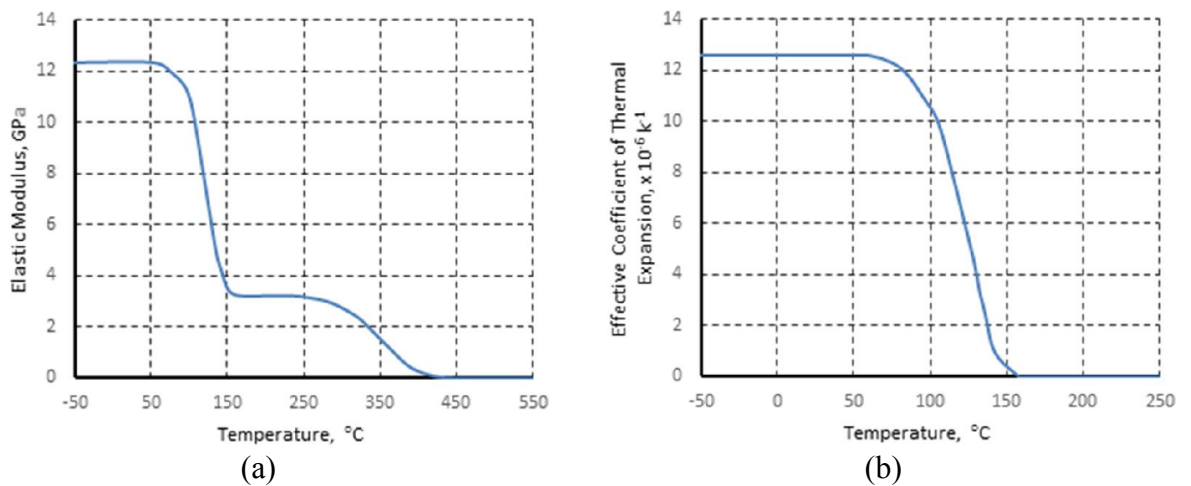
Fig. 2.4 Effect of temperature on (a) elastic modulus and (b) effective coefficient of thermal expansion of GFRP, proposed by Bai et al., (2007b)

2.4.4   Effect of fire on deformation properties of FRP

Limited studies have been carried out on the effect of fire on deformation properties of FRP composites. The creep strain of CFRP composites at constant stress of 76 MPa upon exposure to elevated temperature was studied by **Gates, (1991)**. At 150°C, creep strain started to increase and was magnified by 18 times at 200°C after 150 second of constant stress application. Fig. 2.5 shows the variation of creep strain versus creep time for different exposure temperatures.
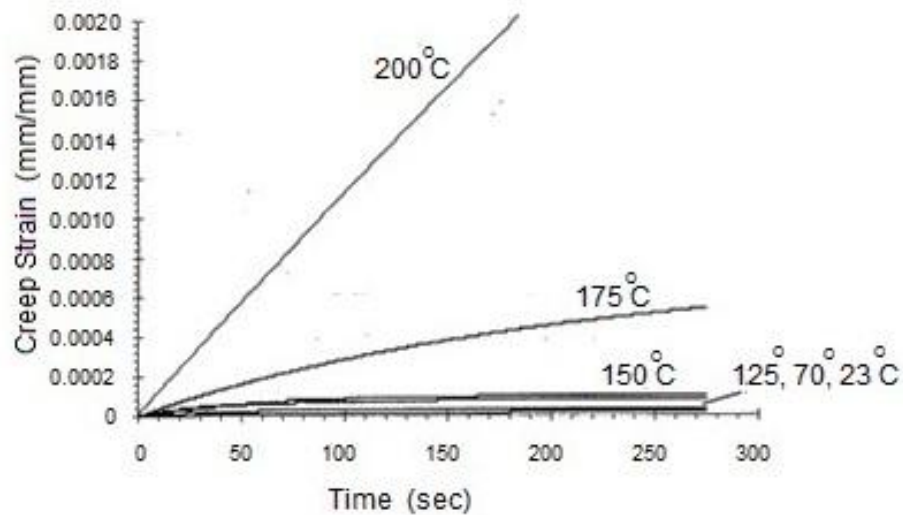
Fig. 2.5 Effect of temperature on FRP's creep strain under constant tensile loading 76 MPa, presented by Gates (1991)

2.4.5   Effect of fire on bond strength between FRP composites and concrete

Many researchers stated that bond development between FRP bars and concrete is similar to steel/concrete bonds and depends on bars type, shape, diameter and surface deformation (Rafi et al., 2007). In contrast, the bond behavior between concrete and FRP composites at elevated temperatures is different than that between concrete and conventional steel. Therefore, the bond behavior is considered as a critical factor in ascertaining the performance of FRP reinforced concrete elements during fire conditions. Hence, possible bond strength degradation with temperature should be considered in the structural design of FRP-RC structures (Katz et al., 1999). To date, limited research has been carried out to study the effect of elevated temperatures on the bond strength between FRP composites and concrete.

Bond strength between internal FRP reinforcements and concrete depends on the characteristics of resin polymer at the surface of the FRP bar (Lublóy et al., 2005; Rafi et al., 2007). The mechanical properties and microstructure of the polymer resin, especially at the surface layer of the rod, are negatively affected by high temperatures above T_g leading to a loss of bond between FRP and concrete (Bisby et al., 2005a).

36

Consequently, using thicker polymer layer at the surface of the FRP bars affects bonds strength negatively at high temperature (Katz et al., 1999).

FRP composites are anisotropic materials with different coefficients of thermal expansions (CTE)s in longitudinal and transverse directions. The coefficient of thermal expansion for FRPs in longitudinal direction is lower than that of concrete, but it's much higher than that of concrete (5-10 times) in transverse direction; therefore, due to different transverse CTE of FRP bars and concrete, high radial pressure on the surface of the reinforcement are created causing bursting thermal stresses within the concrete. When these thermal stresses reach the concrete tensile strength (f_{ct}), micro-cracks occurs leading to weakening of bonds especially when lower concrete covers are used (Lublóy et al., 2005; Galati et al., 2006; Bai et al., 2007b; Bellakehal et al., 2014). These radial cracks would not only affect the bonds between the concrete and rebar but also damage the concrete cover and cause splitting cracks and eventually degradation of the member stiffness (Rafi et al., 2007; Bellakehal et al., 2014). The bond strength between FRP bars and concrete is severely affected even at relatively low elevated temperatures (Bisby et al., 2005a). Rapid loss in bond strength, to 60% of room temperature strength, has been noticed at 100ºC. At temperatures of 200ºC, bond strengths decrease to 10~20% of its room temperature strength. It was also confirmed that bond is totally lost at a higher temperature of 300ºC and greater (Chin et al., 1997; Bisby et al., 2005a).

In steel reinforced concrete structure, the bond between steel reinforcement and concrete depends greatly on the concrete compressive strength so the reduction in steel/concrete bonds is similar to the reduction in concrete compressive strength (Rafi et al., 2007). However, in the case of heated FRP-RC, reduction in the heated concrete strength due to internal vapor pressure contributes to the reduction in bond strength

between FRP bars and concrete although it is not considered as a major factor for bond

loss (Katz et al., 1999). Table 2.9 summarized the available research works that carried

out on the effect of high temperatures on the bond between FRP bars and concrete.

Table 2.9: Different research works that carried out on the effect of high temperatures on the bond between FRP bars and concrete

Reference	Objectives	Overall Finding
Katz et al., (1999)	To study the effect of high temperatures ranging from 20ºC up to 250ºC on the bond properties between FRP/steel bars and concrete. The variables investigated were temperature and different bond treatment methods.	1- Increasing the temperature from 20ºC up to 250ºC has resulted in a decrease in the bond strength by 80% to 90% due to the change in properties of the polymer at the surface of the rebar. 2- Steel rebars lost 38% of its bond strength with concrete when temperature was increased up to 250°C. 3- The bond stiffness, which is the slope of linear portion of pullout load versus slip curve, was decreased by increasing the temperature. 4- At 300°C, the axial strength of the FRP rods was not significantly affected.
Zin et al., (2004)	To study experimentally the effect of high temperature of 350°C on bond behavior between FRP bars and concrete. Carbon FRP (phenol resin) and Aramid FRP (cross-bridged polyamonoamide resin) were used.	1- The bond strength at room temperature of the FRP rebars was smaller than that of the steel rebars. 2- Aramid FRP lost 50% and 70% of its original bond strength with concrete when temperature was raised to 170°C and 300°C, respectively. 3- Carbon FRP has lost 20% of its original bond strength when heated to only 250°C. 4- The bond strength of FRP rebar which is made phenol resin is better than that of cross-bridged polyamonoamide resin

Table 2.9: Continued

Reference	Objectives	Overall Finding
Lublóy et al., (2005)	To study the effect of elevated temperature up to 250°C on the bond behavior of CFRP wires embedded in concrete cube specimens with different concrete covers.	1- The bond strength increased with the increase of concrete cover up to 100°C while concrete cover had no effect at temperature of 200°C. 2- With 30 mm concrete cover, bond strength was reduced to approximately 50% and 20% of that at room temperature when temperature increased to 100°C and 200°C, respectively. 3-Three types of bond failure modes were distinguished; pullout failure, concrete cover splitting failure, and resin matrix deterioration failure.
Abbasi and Hogg, (2005a)	To study the effects of water and alkaline environments on bond strength of GFRP rebars with concrete at different temperatures (up to 120°C) and different treatment periods (up to 8 months).	1- The bond strength was insensitive to alkaline environments while bond strength decreased when the temperature of the test was increased. 2- At 120°C, the residual bond strength was 60% of that at ambient temperature. Two modes of failure were observed during testing; pullout of the rebar and splitting of the concrete cover.
Galati et al., (2006)	To investigate experimentally the effect of concrete cover, bonded length, and exposure to thermal cycles to a maximum temperature of 70°C on the bond performance of FRP reinforced concrete specimens.	1- Exposure to relatively high temperatures induced a significant degradation on the bond strength. 2- The bond degradation was attributed to the weakening of the matrix of the GFRP bar due to the thermal treatment. Hence, the matrix material shears off from the fibers, at relatively low loads, leading to bond failure. 3- When loaded up to the ultimate load, slip was almost zero at the free end of the untreated specimens while higher slips values were attained at the same peak load for the thermally treated ones.
Masmoudi A. et al., (2010)	To investigate the thermal effect on the bond behavior between GFRP/steel bars and concrete.	1- Temperature up to 60°C had a negligible effect on the bond behavior while heating up to 80°C reduced the bond strength by 22% and 28% for 8 mm and 16 mm diameter bars, respectively,

Table 2.9: Continued

Reference	Objectives	Overall Finding
Masmoudi A. et al., (2010)		2- An analytical model has been proposed to predict the bond strength between GFRP bars and concrete for temperatures below 80°C.
Masmoudi R. et al., (2010)	To study experimentally the bond between GFRP rebars and concrete after exposure to high temperature (up to 80°C) for 4 months period	1- The bond strength showed a minor reduction at 40°C and 60°C, yet noticeable reduction of 14% at 80°C. Based on the experimental data, an analytical model was proposed for bond-slip relationship.
Maluk et al., (2010)	To discuss experimentally the effect of fire on the bond between high performance, self-consolidating, fibre reinforced concrete (HPSCC) and CFRP or steel prestressing bars.	1- At around 170°C temperature, the bond strength of the CFRP tendons in concrete was reduced by 17 % in average since the exposure temperature had bypassed the glass transition temperature of the matrix. 2- Based on the experimental results, an analytical model was proposed to determine the cracking temperature at which first cracking appeared.
Maluk et al., (2011)	To examine the bond strength between concrete and CFRP tendon at elevated temperature as compared with that between concrete and steel prestressing wires.	1- The bond strength under elevated temperatures depends upon some interrelated factors, such as the thermal expansion coefficient of concrete and reinforcement, type of prestressing, degradation extent of the concrete, release of concrete moisture, and loading condition. 2- The elevated temperature affected the bond strength of CFRP tendons more than the tensile strength. 3- The temperature of the rebar surface was found around 165°C at failure stage. 4- The residual bond strength of heated CFRP specimens was between 73% and 96% as compared to 71% and 86% for specimens with steel reinforcement.
Petkova et al., (2012)	To study the effect of heating up to 300ºC on the bond between externally bonded FRPs and concrete specimens	20%, 50%, and 70% reduction in the bond capacity after heating up to 150°C, 200°C, and (250°-300°C), respectively.

2.4.6 Fire tests on FRP-RC structures

When structures are exposed to fire, they sustain their loads to a certain time before the structure deflects more than the allowable values or collapses completely, whichever comes first; this time is called as the fire endurance for buildings (Abbasi and Hogg, 2005b; Abbasi and Hogg, 2006; Rafi et al., 2007). According to regulations of the building control authorities, the length of this time depends on the use of structure, number of storeys and the floor area (Abbasi and Hogg, 2005b; Rafi et al., 2011). The minimum fire resistance period of majority of structures is 90 minutes as per UK building regulations (Abbasi and Hogg, 2006). Most of international building codes suggests minimum cross-sectional dimensions and minimum concrete cover of 50 mm to have good fire endurance rating (Rafi et al., 2011).

For any FRP-RC member exposed to fire, there are two different critical temperatures. The first is the temperature at which the FRP matrix surface is softened or burned at an early stage causing interface cracking and de-bonding between the FRP and concrete (Abbasi and Hogg, 2006), while the other critical temperature is that causes the rebar to lose 50% of its ambient temperature strength, designating structural failure under fire (Nigro et al., 2012).

The theoretical failure of steel-RC flexural elements under fire exposure occurs when the mid span deflection of the element exceeds the allowable deflection, computed as 1/30 of the element span length (BS 476-20:1987). Another criterial CAN/CSA-S806-02(R2007), stipulates that FRP-RC structures fail when the FRP bar loses 50% of its strength at ambient temperature (Rafi et al., 2011). Due to lacking data on the thermal mechanical properties of wide variety of FRP products which are currently available in the market, the critical temperature for FRP was not precisely defined (Nigro et al., 2011c) but from the literature (Wang et al., 2007; Robert and

Benmokrane, 2010; Wang et al., 2011; Wang and Zha, 2011; Rafi et al., 2011; Pires, 2012) it is assumed to range from 250°C to 500°C. Accordingly, a minimum concrete cover thickness should be used to limit the temperature rise in the FRP bars to below their critical temperature.

The failure of any FRP-RC elements, exposed to fire, depends on three parameters that should be taken into consideration during the design of FRP-RC members in fire situations. These parameters are strength of FRP, maximum rebar's temperature and the FRP rebar's anchorage length (length of RC element's end zone that is not directly subjected to fire) (Nigro et al., 2011a). If the anchorage length was enough to avoid the pull-out of the FRP bars, then failure mechanism of FRP-RC elements is shifted from bars slip failure to the bars rupture at their strength limit unless if the anchorage applied is not satisfactory (Nigro et al., 2012). In order to evaluate fire resistance and post-heating residual strength of FRP-RC structures, the reduced materials mechanical properties of both concrete and FRP as a function of temperature and time should be evaluated (Kodur and Baingo, 1998; Ellis, 2009).

The mechanical properties of FRP rebar such as strength and stiffness as a function of temperatures were evaluated in previous studies as shown in Table 2.6 therefore, the properties of FRP rebar and concrete strength can be estimated at any time if the temperature distribution of FRP RC element cross section is known (Abbasi and Hogg, 2005b). The degradation of compressive strength and modulus of elasticity of concrete after exposure to high temperature can be evaluated according to Eurocode ENV-EC2 Part1.2 (Nadjai et al., 2005). Once the properties of the FRP rebars and concrete during fire exposure are estimated as a function of time, modified design expressions of the FRP-RC beams can be used to predict the flexural and shear strength as a function of time (Abbasi and Hogg, 2005b; Adelzadeh et al., 2014).

As summarized in Table 2.10, few experimental data is available on the behavior of FRP-RC structures under exposure to fire therefore, more experimental studies are required in order to understand deeply the structural behavior of FRP RC members when subjected to large temperature variations and fire conditions.

Table 2.10: Different research works that carried out on fire tests on FRP-RC structures

Reference	Objectives	Overall Finding
Kodur and Baingo, (1998)	1- To carry out a parametric study in order to determine the parameters that affect the fire resistance of FRP–RC slabs 2- To provide an analytical evaluation of the minimum concrete cover to keep the bar's temperature lower than the critical bar's temperature.	1- The fire resistance of FRP-RC slabs depends on FRP rebar type, concrete cover thickness and aggregate type. 2- The effects of FRP bar type on the fire resistance of any RC element depends on the FRP bar's critical temperature. 3- By increasing the concrete cover thickness, the time needed to reach the FRP bar's critical temperature can be delayed. 4- Carbonate aggregate RC slabs show a better fire resistance than that with siliceous and quartz aggregates due to slow temperature rise in the former. 4- The slab thickness has no effect on the fire resistance of the slab since the failure is governed by the bar's critical temperature.
Zin et al., (2004)	To study the flexural behavior of carbon fiber reinforced concrete (CFRP-RC) beams and aramid fiber reinforced concrete (AFRP-RC) beams at exposure to 200°C	1- CFRP and AFRP-RC beams can be used upon exposure to high temperature up to 200°C although the performance of CFRP beams was better compared with AFRP-RC beams. 2- The load and deflection of the CFRP-RC were not affected until 200°C because the bond between the concrete and FRP rebars was maintained. 3- The ultimate load of the AFRP-RC beams was reduced at 200°C with noticeable deflection due to the deterioration of the bond at such a temperature.

43

Table 2.10: Continued

Reference	Objectives	Overall Finding
Nadjai et al., (2005)	To study experimentally and analytically the behavior of hybrid FRP/steel rebar reinforced concrete beams at normal and high temperatures.	1- The concrete cover of the FRP reinforced concrete beams greatly affect their structural response with 50 mm concrete cover considered as the minimum concrete cover for FRP reinforced beams, exposed to high temperatures. 2- The analytical model, based on slice method, showed a good agreement with the experimental data of the structural behavior of FRP RC beams at room temperature and elevated temperatures.
Nadjai et al., (2005)	To study the temperature distribution of RC beams, exposed to fire on three sides.	1- The temperature contours were parallel to the beams faces exposed to fire. 2- The temperature inside the beam depends on three factors: beam's cross-section dimensions, ambient temperature and fire exposure period.
Kodur et al., (2005)	To investigate experimentally the thermal performance of CFRP and GFRP-RC slabs in fire and compared the results with those from steel-RC slabs. Effect of FRP type, concrete cover, slab thickness and aggregate type on the fire resistance of these slabs were studied.	1- The FRP bar type and concrete cover to the reinforcement have the major effect on the fire resistance of the FRP-RC slabs while the slab thickness has a minor effect. 2- Increasing the thickness of concrete cover would minimize the temperature rise in the FRP bars therefore enhances the fire resistance of the FRP-RC slabs. 3- Using carbonate aggregate instead of siliceous aggregate would lower the bar's temperature therefore enhance the fire resistance of the slab by 10 to 15%.
Abbasi and Hogg, (2005b)	1- To predict a general equation for estimating the time-temperature distribution of RC beams. 2- To develop an analytical expressions to predict the strength and stiffness of concrete matrix with FRP rebars as reinforcement at elevated temperatures.	1- The rebar temperature (θ) when a RC beam is exposed to standard fire, with respect to time (t) and concrete cover (c) can be predicted using Eq. 2-7. 2- The beam's concrete strength after exposure to high temperatures as function of exposure time (t) can be predicted using Eq. 2-8. $\theta = [\langle 345.log(8t+1)\rangle + 20] - \left[767.exp^{-t\left(0,001.exp^{\langle\frac{7.602}{c-23.623}\rangle}\right)}\right]$ (2.7) $f'_{c,t} = (1 - 0.0031t)\, f'_{c,0}$ (2.8)

Table 2.10: Continued

Reference	Objectives	Overall Finding
Abbasi and Hogg, (2005b)		3- The reduction factor in FRP rebars' strength (k_f) and reduction factor in stiffness(k_E) , as a function of time and concrete cover when the concrete beams are exposed to fire test, can be predicted using Eqs. 2.9 and 2.10. $$k_f = \begin{cases} 1 - 0.007t & for\ 105\ mm\ concrete\ cover \\ 1 - 0.0073t & for\ 70\ mm\ concrete\ cover \\ 1 - 0.01t & for\ 30\ mm\ concrete\ cover \end{cases} \qquad (2.9)$$ $$k_E = \begin{cases} 1 - 0.0044t & for\ 105\ mm\ concrete\ cover \\ 1 - 0.0046t & for\ 70\ mm\ concrete\ cover \\ 1 - 0.0063t & for\ 30\ mm\ concrete\ cover \end{cases} \qquad (2.10)$$
Abbasi and Hogg, (2006)	To evaluate the effect of fire exposure on the flexural behaviour of concrete beams reinforced with continuous GFRP rebars in order to determine the fire resistance of these FRP reinforced concrete beams.	1- GFRP reinforced concrete beams had a fire resistance period between 94 to 128 minutes therefore met the 90-minutes minimum fire resistance requirements. 2- At failure under service load capacity, deflection was found between L/27 to L/23 which is less than the BS476 failure criteria deflection of L/20. 3- Fire penetrates the beams through the cracks which occurred during testing; leading to the failure of the beams. 4- 70 mm minimum clear concrete cover is recommended for GFRP-RC beams under fire conditions. 5- Concrete moisture content and the aggregate as well as chemical composition of cement are the factors that affect the temperature distribution across the sample cross section due to external heating.
Rafi et al., 2007 and Rafi and Nadjai, (2008)	To study experimentally the fire resistance of concrete beams reinforced internally with CFRP rebars.	1- Concrete crushing failure was noticed in the CFRP beams while crushing of concrete after yielding of steel reinforcement was noticed in steel RC beams. 2- During heating, temperature distribution across the cross-section of the beam was non-uniform.

Table 2.10: Continued

Reference	Objectives	Overall Finding
Rafi et al., 2007 and Rafi and Nadjai, (2008)		3- The loss of bonds between FRP and concrete was a major factor contributing to the failure of FRP RC beams where CFRP rod slipped at one end of the beams forcing an existing crack to propagate quickly towards the compression zone leading to failure of beam at compression surface. 4- The stiffness of CFRP reinforced beams was less than the stiffness of steel-reinforced beams at normal temperature whereas the stiffness of CFRP-RC beams was more than that of the steel-RC beams at high temperature. 5- CFRP-RC beams were less ductile than steel-RC beams at high temperature 6- The ends of the tested beams were not exposed directly to the fire therefore, at 120°C, the behavior of the beams changed to a tied arch, because FRP to concrete bonds were lost at the middle of the beams while the FRP rods were still anchored at the cold ends of the beam. The beams failed when these end anchorages were lost
Ellis, (2009)	1- To investigate the effect of high temperatures of up to 400°C on the residual tensile strength, bond between GFRP and concrete, and the residual flexural capacity of GFRP-RC beams. 2- To develop an analytical model for predicting the post-fire strength of GFRP-RC beams	1- By increasing the temperature, the residual tensile strength, modulus of elasticity properties and the residual bond strength of GFRP bars had decreased. 2- The reduction in the mechanical properties of the FRP bars after cooling was less than the reduction observed by other researchers when similar FRP bars were tested during the heating process. 3- Flexural behavior of GFRP-RC beams was negatively affected by the exposure to elevated temperatures. 4- An increase in FRP bars ductility was noticed in the post-heating tensile tests. 5- The proposed analytical model showed conservative results in comparison with the experimental results.

Table 2.10: Continued

Reference	Objectives	Overall Finding
Wang et al., (2009)	1- To use a finite element method to simulate the mechanical performance of FRP-RC columns in fire. 2- To predict the temperature distribution through the cross section of the column. The size of section and concrete cover were studied as major parameters that affect the fire resistance of the columns.	1- An empirical formula, shown below (Eq. 2-11), was developed to predict the fire resistance time of FRP-RC columns in term of section side length of a square section (b) and concrete cover thickness (c). Fire resistance time $= 0.38478c^2 - 0.00147b^2 + 3.71374b$ (2.11) 2- The fire resistance of FRP-RC columns can be improved by increasing the cross-section size and/or the concrete cover; with a greater effect of the latter. 3- The small ratio of FRP rebar in concrete had a little effect on the temperature distribution within the columns.
Carvelli et al., (2011)	To investigate the behavior of GFRP-RC beams already heated to localized elevated temperatures (230 and 510°C).	The geometry of the reinforcement in the overlapping areas affected both the beam's ultimate load capacity at room and elevated temperatures while this overlapping geometry had minor effect on the beam's initial stiffness.
Nigro et al., (2011a & 2011b)	1- To evaluate the fire resistance and deformability under fire conditions of simply supported GFRP rebars RC slabs. The slab's edge cold zones not directly exposed to fire were considered as the FRP bar anchorage length. 2- To examine the effect of concrete cover (c) on temperature distribution through the concrete cross section.	1- The slabs with short anchorage length failed due to the slip of bars in the short anchorage zone while the rebar's tensile stress at midspan zone (direct fire exposed zone) was still lower than their tensile rupture strength. 2- Longer anchorage zone slabs failed at mid-span due to FRP tensile rupture at 500°C without showing any sign of slip at cold edge zones. 3- With larger concrete cover, the attainment of high temperature in the bars was delayed further and hence, the reduction in bars strength was minimized. 4- Longer anchorage length prevented bars' slip, therefore increased the slabs fire resistance significantly by using larger concrete covers. A minimum of 500 mm cold zone length is recommended. 5- Continuous FRP bars from side to side of the concrete elements and bended at the end of the slab is recommended to increase the cold zone anchorage length.

Table 2.10: Continued

Reference	Objectives	Overall Finding
Nigro et al., (2011a, 2011b)		6- An analytical model for predicting temperatures of FRP rebars in concrete slab as a function of concrete cover was provided as shown in Fig. 2.6.
Nigro et al., (2011c)	To evaluate the fire resistance of simply supported GFRP-RC slabs similar to the slabs tested in their previous work Nigro et al., (2011a & 2011b) but with GFRP bars being bent at the 250 mm from the fire-unexposed end zone of the slabs aiming at increasing the cold zon anchorage length of the FRP rebars.	1- After 15 minutes of fire exposure, the temperature of the FRP bars at the fire exposed zones reached 100°C at which the bond between the FRP bars and concrete starts weakening. Hence, the fire-unexposed anchorage length of the FRP reinforcement controlled mainly the structural response of the member. 2- The slabs with short anchorage length (250 mm) and bent bars at the end have an equivalent structural behavior to the slabs with 500 mm anchorage length and straight bars, suggested that the required large fire-unexposed anchoring zone length can be reduced if the reinforcement bars are bent at the ends.
Rafi et al., (2011)	To investigate experimentally the thermal structural behavior of GFRP, CFRP and steel reinforced concrete beams at high temperature. Rebar temperature of 500°C was considered as the critical temperature	1- The CFRP-RC beams failed by concrete crushing with higher load capacity, and stiffness than GFRP and steel RC beams before and after fire exposure. 2- GFRP and steel RC beams had similar reduction in stiffness after exposure to elevated temperature. 3- Non-uniform temperature distribution across the beam's cross-section.
Rafi and Nadjai, (2011a, 2011b)	1- To study experimentally the stiffness, ductility, energy absorption, and failure pattern and fire resistance of hybrid (steel–CFRP) RC beams at high temperatures as compared to those of CFRP-RC beams, and steel-RC beams.	1- The double layers of CFRP reinforcement had better strength and stiffness but less ductility than hybrid (steel–CFRP) RC beams which in turn had better strength, stiffness and ductility than FRP RC or steel RC beams. 2- FRP-RC beams showed better stiffness than steel RC beams. 3- Similar modes of failure were noticed for all tested beams at normal and high temperature. Failure of CFRP rebar RC beams was brittle and sudden. 4- The fire endurance time for FRP-RC beams can be extended by anchoring FRP bars sufficiently at the ends where protection from direct fire was provided.

Table 2.10: Continued

Reference	Objectives	Overall Finding
Rafi and Nadjai, (2011a, 2011b)	2- To study the effect of varying concrete cover and reinforcement arrangement on the behavior of Hybrid (steel-CFRP) and CFRP-RC beams at high temperatures.	5- All tested beams exposed to elevated temperature failed in flexure due to the crushing of concrete that was proceeded by slip failure of CFRP bars. FRP bars at the slipped ends were found to be abraded while those of the other ends were found undamaged and completely bonded with the concrete. 6- At temperatures above the polymer resin's glass transition temperature, the FRP bars de-bonded from the surrounding concrete and therefore FRP RC beams behaved as tied arches with rods adequately anchored at the ends. 7- The behavior of FRP bars control the initial behavior of the beam, whereas the final phases of beam behavior were controlled by the steel therefore, behaviors of hybrid beams were a combination of beam action and arch action. Failure of the anchored ends led to rapid failure..
Nigro et al., (2012)	To predict analytically the bond stress and slip of FRP bars embedded in concrete at high temperature and to calculate the minimal required anchoring length.	1- For long fire exposure time and relatively small stresses in bars, minimum anchorage length of 150 mm is required for all concrete cover thickness. 2- The minimum required anchorage length never exceed 320 mm regardless of concrete cover thickness and fire exposure times.
Hulin et al., (2013)	To study experimentally the fire behavior of thin plates made from high performance concrete (HPC) and reinforced with basalt FRP (BFRP) mesh.	1- The bonds between concrete and FRP mesh were lost when exposed to elevated temperatures due to burning away of the epoxy coating at contact interface between the BFRP and concrete. Therefore, voids were developed allowing the pore pressure to be released and concrete spalling to be delayed. 2- At fire exposure, the mechanical resistance of the BFRP reinforced plates was reduced due to the loss of bonds between BFRP mesh. 3- The bending resistance of BFRP-HPC plates was much lower than HPC plates reinforced with steel.

Table 2.10: Continued

Reference	Objectives	Overall Finding
Bellakehal et al., (2014)	To study experimentally and analytically the thermo-structural behavior of FRP-reinforced concrete slabs when subjected to combined mechanical loads and thermal cycles (from -30 to +60°C). Three parameters were considered, concrete cover thickness, FRP bar type, and temperature variation	1-The exposure to mechanical and thermal loads simultaneously had no effect on the bar's transverse thermal strain at temperatures range of -30 to +40°C. After 40°C, the mechanical loads started reducing the radial pressure resulting in decreasing the concrete tensile stresses and thus the radial cracks occur. 2- The thermo-mechanical behavior of FRP bars in the FRP-RC slabs was confirmed to be linear elastic. 3- The transverse thermal strains were decreased when the FRP bar diameter was increased due to the reduction of transverse coefficient of thermal expansion of bigger FRP bars. 4- Small effect of concrete cover thickness variation on the bar's transverse thermal strain was noticed at temperature in the range of -30 to +60°C. 5- The proposed analytical model results of transverse thermal strains of FRP bars showed good correspondence with the experimental work results.
Adelzadeh et al., (2014)	To investigate numerically the fire endurance of GFRP -RC slab, exposed to elevated temperatures using temperature domain and strength domain approaches.	1- A model was proposed based on an assumption that the bond between the FRP bars and concrete would not degrade. Hence, the model can be applied only to cases where bar's anchorage are used at the ends. 2- Temperature domain approach, which depended on specifying the critical temperature of the rebars to be the failure criteria, was found to be more conservative and not entirely applicable to FRP reinforced concrete members. 3- Placing the required slabs reinforcement into two layer instead of one layer (same required amount), had increased the fire endurance of the slabs. 4- The fire endurance of the slabs can be increased drastically by increasing the slab thickness or the concrete cover thickness.
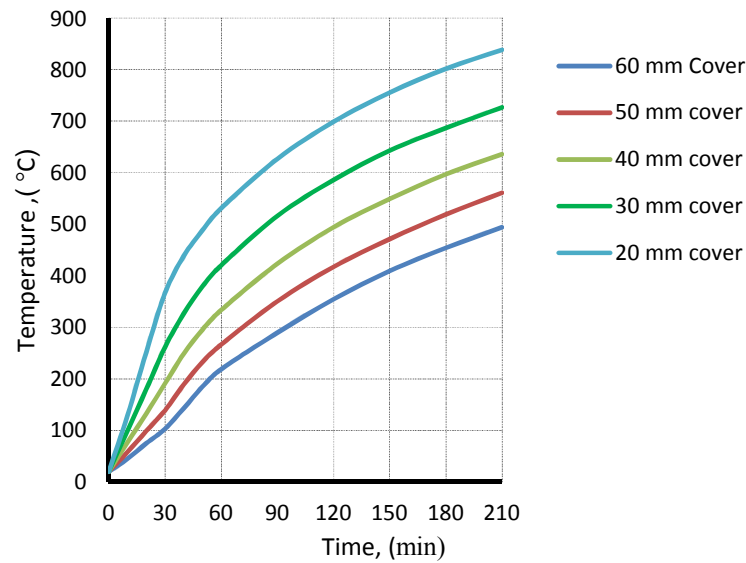
Fig. 2.6 Temperature vs time as a function of concrete cover, presented by
Nigro et al., (2011a)

2.5 Concrete under high temperature

When concrete is exposed to high temperature, the concrete starts losing its strength, where the main loss occurs mostly at 500°C due to the degradation of the hydrate structure, and the surface layer of concrete spalls. The extent and rate of this damage depends on aggregate type, moisture content, concrete permeability, fire severity and rate of temperature increase (Newman and Choo, 2003).

When structural elements are subjected to fire, several changes take place inside concrete, initially concrete loses its absorbed and free evaporable water and ultimately loses its bound water resulting in loss of concrete strength. At temperatures between 150°C and 300°C, water is lost due to the start of degradation of hydration products such as calcium silicate hydrates and calcium hydroxide resulting in more strength loss. At 350-400°C, calcium hydroxide transforms to calcium oxide and more strength loss occurs. At 500°C, concrete losses 50% to 75% of its original strength. The loss of strength continues with temperature rise up to 850-900°C but 550-600°C is considered

as the limit where concrete become useless (Newman and Choo, 2003). Additional damage is induced in concrete due to the difference between coefficient of thermal expansions of aggregate and the surrounding cement paste and the increase in the volume of some types of aggregates at high temperature. Consequently, the aggregate contributes to concrete spalling and strength loss. Limestone aggregates show a better fire resistance than siliceous aggregate because limestone has a lower coefficient of thermal expansion which is closer to that of cement paste (Newman and Choo, 2003).

European committee for standardization, Eurocode EN 1992-1-2 (2004) provides temperature-dependent relationships (Eqs. 2-12 through 2-15) of the concrete physical properties such as density, thermal conductivity and specific heat.

The mass unit ($\rho_{c,T}$) of concrete at temperature T is as follows:

$$
\rho_{c,T} = \begin{cases}
\rho_{(20°C)} & \text{for } 20°C \leq T \leq 115°C \\
\rho_{(20°C)} \times \left(1 - \dfrac{0.02 \times [T - 115]}{85}\right) & \text{for } 115°C < T \leq 200°C \\
\rho_{(20°C)} \times \left(0.98 - \dfrac{0.03 \times [T - 200]}{200}\right) & \text{for } 200°C < T \leq 400°C \\
\rho_{(20°C)} \times \left(0.95 - \dfrac{0.07 \times [T - 400]}{800}\right) & \text{for } 400°C < T \leq 1200°C
\end{cases}
\tag{2.12}
$$

The specific heat c_c of dry concrete at temperature T is as follows:

$$
c_c = \begin{cases}
900 & \text{for } 20°C \leq T \leq 100°C \\
900 + (T - 100) & \text{for } 100°C < T \leq 200°C \\
1000 + \dfrac{T - 200}{2} \quad \left(\dfrac{J}{kg\,K}\right) & \text{for } 200°C < T \leq 400°C \\
1100 & \text{for } 400°C < T \leq 1200°C
\end{cases}
\tag{2.13}
$$

The upper and lower limit thermal conductivity of normal weight concrete at temperature T up to 1200°C can be calculated from Eq. 2-14 and 2-15, respectively.

$$
k_{tc} = 2 - 0.24 \left(\frac{T}{120}\right) + 0.012 \left(\frac{T}{120}\right)^2 \quad (W/m\,k)
\tag{2.14}
$$

$$k_{tc} = 1.36 - 0.163 \left(\frac{T}{120}\right) + 0.0082 \left(\frac{T}{120}\right)^2 \ (W/m\,k) \tag{2.15}$$

According to Eurocode EN 1992-1-2, the reduced compressive and tensile strength of damaged concrete due to high temperature can be represented by the following equations:

$$f_{cu,T} = k_c \times f_{cu} \tag{2.16}$$

$$k_c = \begin{cases} 1.0 & \text{for } T \leq 100°C \\ 1.067 - 0.00067T & \text{for } 100°C < T \leq 400°C \\ 1.44 - 0.00167T & \text{for } 400°C < T \leq 900°C \\ 0.0 & \text{for } 900°C \leq T \end{cases} \tag{2.17}$$

$$k_{sp,T} = \begin{cases} 1.0 & \text{for } T \leq 100°C \\ 1.0 - \left(\dfrac{T - 100}{500}\right) & \text{for } 100°C < T \leq 600°C \end{cases} \tag{2.18}$$

Lie, (1992) provided time dependent relationships for the thermal conductivity, specific heat capacity and thermal expansion coefficient of concrete as shown below:

- k_{tc} is the thermal conductivity of concrete at Temperature T

$$k_{tc} = \begin{cases} 1.355 \ (W/m°C) & \text{for } 0°C < T \leq 293°C \\ 1.7162 - 0.001241T \ (W/m°C) & \text{for } 293°C < T \end{cases} \tag{2.19}$$

- α_c coefficient of thermal expansion at Temperature T

$$\alpha_c = (0.008T + 6) \times 10^{-6} \ (m/m°C) \tag{2.20}$$

- The specific heat c_c and the density of concrete ρ at Temperature T

$$\rho_c c_c = \begin{cases} 2.566 \times 10^6, & \text{for } 0°C < T \leq 400°C \\ (0.1765T - 68.034) \times 10^6, & \text{for } 400°C < T \leq 410°C \\ (-0.05043T + 25.00671) \times 10^6, & \text{for } 410°C < T \leq 445°C \\ 2.566 \times 10^6, & \text{for } 445°C < T \leq 500°C \\ (0.01603T - 5.44881) \times 10^6, & \text{for } 500°C < T \leq 635°C \\ (0.16635T - 100.90225) \times 10^6, & \text{for } 635°C < T \leq 715°C \\ (-0.22103T + 176.07343) \times 10^6, & \text{for } 715°C < T \leq 785°C \\ 2.566 \times 10^6, & \text{for } 785°C \leq T \end{cases} \tag{2.21}$$

Many experimental studies were conducted to investigate the behavior of concrete at high temperature as summarized in Table 2.11.

Table 2.11: Different research works that carried out on the behavior of concrete under high temperatures

Reference	Objectives	Overall Finding
Faiyadh and Al-Ausi, (1986)	To study the effect of exposure to high temperature (range of 20-800°C) on the splitting tensile strength of fiber reinforced concrete.	1- Both fiber reinforced concrete and plain concrete have similar behavior under high temperature. 2- The tensile strength of plain concrete was less than that of fiber reinforced concrete for all temperature exposures. 3- The residual tensile strength of steel fiber concrete was higher than that of glass fiber concrete. 4- The reduction in the tensile strength was more significant in water-cooled specimens than that in air-cooled specimens, which in return was more than that for hot specimens.
Mohamedbhai, (1986)	To study the effect of the duration of high temperature exposure (up to 800°C) and rates of heating and cooling on the residual strength of heated concrete.	1- The effect of heating duration, heating rate and the cooling rate on the residual strength of concrete is very significant but this effect decreases by increasing the exposure temperature. 2- By increasing the heating duration, the loss in concrete strength increases. 3- After one hour of exposure to different temperatures ranges from 200, 400, 600 and 800°C, the residual concrete strength were 80%, 70%, 60% and 30%, respectively of its original strength at ambient temperature.
Dias et al., (1990)	To study the effect of high temperature (up to 700°C) on the mechanical properties of hardened cement paste such as residual strength, static and dynamic modulus of elasticity.	1- At 120°C, a significant drop in the concrete strength then followed with strength regain up to 300°C and a rapid strength loss with temperature after 300°C. 2- The change in the dynamic modulus of elasticity under high temperature was greater than that in static modulus of elasticity. 3- Strength and static modulus of elasticity were improved in specimens which were subjected to preloading before testing.

Table 2.11: Continued

Reference	Objectives	Overall Finding
Hertz, (1992)	To investigate the behavior of silica fume steel-fibers reinforced concrete under high temperatures in the range of 300 and 600°C.	1- The presence of steel fibers in the silica fume concrete does not reduce the explosion risk of the silica fume concrete when exposed to high temperature.. 2- Toxic gasses emitted from heating of specimens due to the presence of superplasticizers in the concrete mixtures.
Sarshar and Khoury, (1993)	To examine the effect of high temperatures (20°C to 600°C) on the compressive strength of cement paste and concrete with silica fume, blast furnace slag and pulverized fuel ash as replacement of ordinary Portland cement.	1- The replacement of ordinary Portland cement by 10% silica fume did not show any improvement in concrete performance yet using pulverized fuel ash in the concrete improved the thermal properties of concrete. 2- The firebrick aggregate concrete showed a better performance than concrete with Lytag aggregate where the best results obtained for firebrick/slag concrete. 3- The application of 15% initial pre-heating load improved the residual strength for firebrick concrete but not so for Lytag concrete. 4- The residual strength of cement paste specimens decreased by increasing the heating rate from 1 °C/min to 3 °C/min. 5- The heating duration had a small effect on the residual strength of concrete subjected to lower temperature ranges but had no effect at higher ranges. 6- After cooling, specimens exposed to 100% relative humidity atmosphere for 28 days regained some of their strength.
Lin et al., (1996)	To study the effect of fire on the microstructures of concrete prepared using Portland cement type I and siliceous aggregates. Scanning electron microscopy (SEM) examinations was used.	1- At temperature between 300 and 500°C, cracking appeared around the aggregate boundaries and the cracking enlarged with the increase of temperature. 2- Between 440 and 580°C, calcium hydroxide (CH) decomposed then calcium silicate hydrate (CSH) destructed at temperature between 600 to 700°C. 3- Rehydration process occurred upon re-curing of heat-damaged samples in air or in water resulting in the formation of CH and CSH products.

Table 2.11: Continued

Reference	Objectives	Overall Finding
Chan et al., (1999)	To study the effect of high temperature (up to 1200°C) on the compressive and tensile splitting strength as well as on the pore structure of high strength (HSC) and normal strength concretes (NSC).	1- Both NSC and HSC lost their strength in similar manner and the critical temperature range was 400°C to 800°C. 2- A coarsening in the microstructure of both HSC and NSC was noticed after exposure to high temperature. 3- Deterioration of the permeability-related durability of HSC concrete due to high temperature exposure was higher than that of NSC.
Chan et al., (2000)	To study the effect of high temperature (up to 800°C) on the mechanical properties and pore structure of normal-strength concrete and high performance concrete.	1- The residual compressive strength of HPC was higher than that of normal-strength concrete although the strength degradation rate was higher in HPC than normal-strength concrete. 2- The pore structure of HPC concrete was changed after exposure to high temperature confirming the deterioration of the concrete mechanical properties.
Poon et al., (2001)	To study the effect of high temperature (up to 800°C) on the mechanical and durability properties of normal and high strength concrete containing silica fume, fly ash, and blast furnace slag.	1- Concrete containing fly ash and blast furnace slag has better performance than pure cement concretes at high temperatures below 600°C. 2- High strength concrete containing silica fume was suffering from explosive spalling at high temperatures while concrete specimens with fly ash and blast furnace slag showed intensive fine cracks network without any spalling. 3- The loss in the permeability-related durability was more than the compressive strength loss and the replacement of cement with either fly ash or blast furnace slag improved the residual strength and durability. 4- The optimum percent of replacement of cement by fly ash in HSC was 30% whereas the optimum percent of replacement of cement by blast furnace slag in normal strength concrete was 40%.

Table 2.11: Continued

Reference	Objectives	Overall Finding
Xu et al., (2001)	To investigate the effect of high temperature on the residual mechanical and durability properties of concrete containing pulverized fly ash (PFA).	1- The residual compressive strength of concrete specimens containing PFA and heated up to 250°C was higher than the unheated concrete compressive strength. 2- The increase in the compressive strength was attributed to the hardening of cement paste due to drying and additional hydration of cementitious materials. 3- At 450°C, the residual strength were 85-96% of the original strength whereas at 650°C and 800°C, the residual strength were 50% and 20%, respectively. 4- The deterioration of durability started at temperature lower than the temperature needed to start deterioration of the compressive strength. 5- The use of PFA in concrete improved its fire resistance and this improvement was clearer for maximum exposure temperatures of 450°C and 650°C.
Mahdy et al., (2002)	To study the effect of high temperature (up to 700°C) on the compressive strength of heavy weight high strength concrete including silica fume and magnetite sand.	1- The compressive strength decreased when temperature increased up to 100°C followed by strength recovery at temperature range between 100°C and 300°C. 2- Above 300°C, compressive strength decreased sharply. 3- When silica fume was used together with magnetite sand, the residual compressive strength for concrete was improved. 4- Using lower content of aggregates in concrete resulted in a higher residual compressive strength.
Poon et al., (2003)	To study experimentally the effect of elevated temperatures (up to 800°C) on the performance of normal and high strength metakaolin concrete (MK).	1- The compressive strength of MK concrete increased up to 200°C followed by a severe loss in compressive strength and durability above 200°C. 2- The loss of strength of MK concrete at high temperatures was more than that of SF, FA and OPC concretes. 3- The severity of the explosive spalling, observed in MK concretes at exposure to high temperature, increases by increasing the MK contents

Table 2.11: Continued

Reference	Objectives	Overall Finding
Li et al., (2004)	To study experimentally the effect of high temperatures (200°C to 1200°C) on compressive, splitting tensile strength, and bending strengths of high strength concrete (HSC).	1- The loss of strength starts from temperature of 400°C. 2- The residual compressive strength of concrete samples exposed to 200, 400, 600, and 1000°C were 82.3%, 63.2%, 58.1%, and 27.3% of the ambient temperature compressive strength, respectively, whereas the residual splitting tensile strength were 85.7%, 81.8%, 51.9%, and 16.4%, respectively. 3- The residual bending strength of the heat-damaged specimens were 84.5%, 43.7%, 16.3%, and 7.4% of its original bending strength, respectively. 4- By increasing the specimen size, the strength loss became less.
Chen and Liu, (2004)	To investigate the effect of high temperatures on the residual strengths of high-strength concrete (HSC) and hybrid-fiber-reinforced high-strength concrete (HFRHSC).	1- The residuals compressive and splitting tensile strengths were higher in case of fiber-reinforced HSC than of normal HSC; indicating that the use of short fibers in high-strength concrete can be beneficial to resist high temperatures. 2- Normal HSC started spalling when exposed to high temperatures above 400ºC. 3- HSC containing high melting point fibers, such as carbon or steel fiber, started spalling at 800ºC whereas HSC with polypropylene fibers showed no spalling when exposed to high temperatures. 4- Adding carbon and steel fibers in HSC can delay the time when spalling occurs, while adding PP fibers can eliminate the spalling under high temperatures therefore the best fire resistance and residual properties can be obtained by using mix of high melting point fiber and low melting point fiber in the HSC. 5- The power of the explosive spalling increased with exposure temperature.
Georgali and Tsakiridis, (2005)	To study the effect of fire on the strength and the internal structure of concrete.	1- The change in concrete color to pink coincided with the major loss in concrete strength. 2- The residual concrete strength after exposure to fire reached about 30%.

Table 2.11: Continued

Reference	Objectives	Overall Finding
Georgali and Tsakiridis, (2005)		3- The cement pastes at the external layer exposed to fire were suffering from complete spalling and dehydration process while the inner contained crystals of $Ca(OH)_2$ upon SEM testing. 4- Rapid cooling (due to fire-extinguishing) after overheating resulted in significant internal shrinkage cracking toward to the core axis.
Alarcon-Ruiz et al., (2005)	To study experimentally the chemical and physical changes in cement paste after exposure to elevated temperatures starting from 100°C to 800°C for 24 hours.	1- Portlandite $Ca(OH)_2$, formed during the cooling, has lower decomposition temperature than the original portlandite therefore it can be used in determining the temperature history of fire-damaged concrete.

2.6 Summary

This chapter provided brief review of different studies, performed on the FRP materials and their practical applications in construction, the effect of elevated temperatures on FRP composites, the pre- and post-heating bond between FRP bars and concrete and the pre- and post-heating structural behavior of FRP-RC elements. As can be noticed, most research works concentrated on GFRP bars due to their relatively low cost. Up to date, most of the available studies did not precisely determine the critical exposure temperature of FRP composites that affects their properties and bond strength with concrete. There is a lack of research on the post-fire structural behavior of FRP-RC elements with no research works, carried out to enhance the behavior of FRP reinforced concrete under fire exposure. Provisions for fire condition were not incorporated in available design codes of FRP-RC structures. Hence, new analytical equations are urgently needed to be incorporated to aid in design of structural elements reinforced with FRP composites under fire conditions.

CHAPTER THREE
METHODOLOGY

3.1   Introduction

The testing program, materials used, specimens' preparation, heat treatment, and testing are presented in this chapter. Properties of materials used are presented in Section 3.2. The testing program is presented in Section 3.3. Preparation of different types of specimens is presented in Section 3.4. The heating processes is presented in Section 3.5. Finally, the different load tests are described in Section 3.6. Flow chart of methodology showing the steps used in this work is presented in Fig. 3.1.
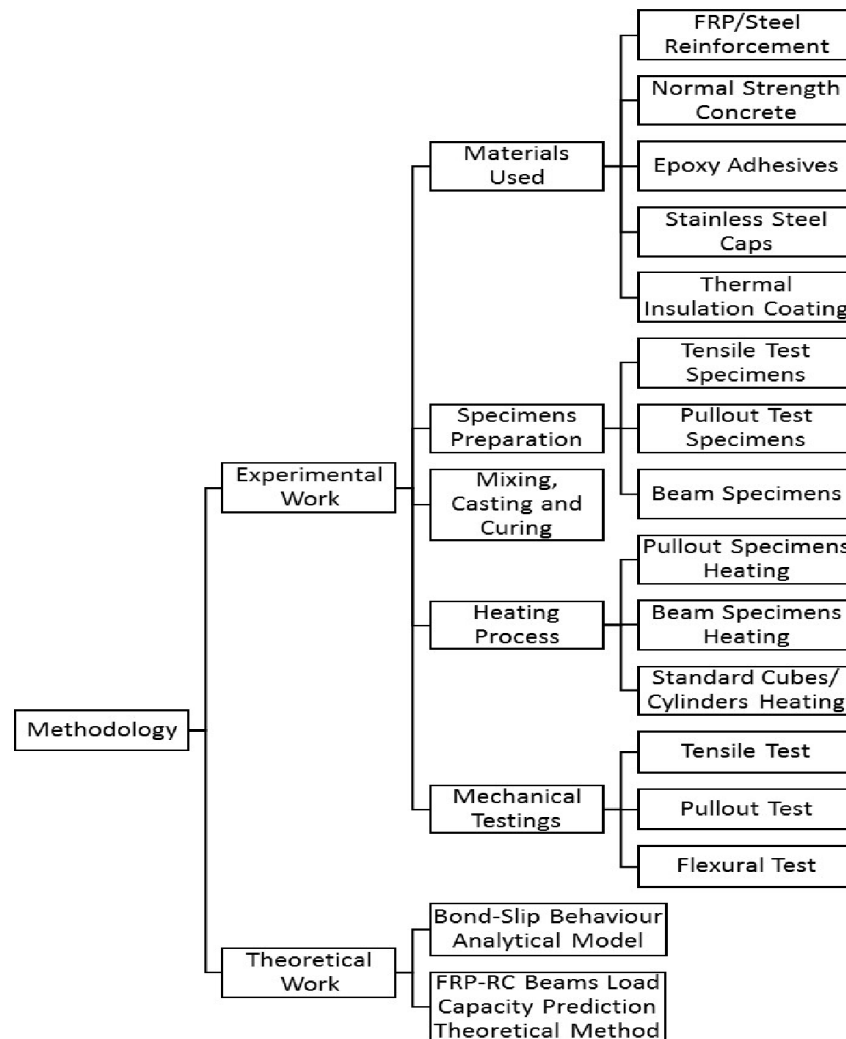
Fig. 3.1 Flow chart of methodology

3.2 Materials

3.2.1 Reinforcement bars

3.2.1(a) FRP bars

Three types of FRP bars with two nominal diameters (6 and 10mm) were used in various reinforced specimens, prepared in this work. Fig 3.2 shows bars of 10 mm diameter having different surface treatment of helically wrapped GFRP, and BFRP, and sand-coated CFRP bars, used as main tensile reinforcement. The properties of the used FRP bars as provided by the manufacturer are summarized in Table 3.1.

3.2.1(b) Reinforcing steel bars

Steel bars of 10 mm diameter were used as the main reinforcement in RC beam and pullout specimens, whereas 6 mm bars were used as reinforcement in stirrups. The mechanical properties of the 10-mm-bars with the geometric configuration shown in Fig. 3.11 were obtained at 23°C and after heating up to 450°C then cooling to room temperature; results are summarized in Table 3.2.

Table 3.1 Mechanical properties of different used FRP bars as per manufacturer data sheet.

Type	$f_{ult\text{-}f}$ MPa	ε_{uf} %	E_f GPa	α_{Tr} x10^{-6}/°C	α_L x10^{-6}/°C	F %	Type of matrix
CFRP-6mm	2068	1.7	124	89	-0.9	70%	VER
CFRP-10mm	1896	1.6	124	89	-0.9	70%	VER
GFRP-6mm	900	2.1	40	22	5.4	N.A.	UP
GFRP-10mm	800	2.1	40	22	5.4	N.A.	UP
BFRP-6mm	1100	2.1	65	23	6	N.A.	EPR
BFRP-10mm	1000	2.1	65	23	6	N.A.	EPR

$f_{ult\text{-}f}$, maximum tensile strength; ε_{uf} , maximum strain at ultimate strength; E_f, FRP's modulus of elasticity; F%, fiber to matrix volume ratio; α_L, Longitudinal coefficient of thermal expansion; α_{Tr}, Transverse coefficient of thermal expansion; VER, Vinyl Ester Resin; UP, Unsaturated Polyester; EPR, Epoxy Polymer Resin; N.A. , not applicable.

Table 3.2: The mechanical properties of reinforcing steel bars collected from our experimental work

Temperature (°C)	YS (MPa)	US (MPa)	EUS (%)
23	570	638	8.48
450	541	622	8.94

YS, Yield Strength; US, Ultimate Strength; EUS, Elongation at Ultimate Strength
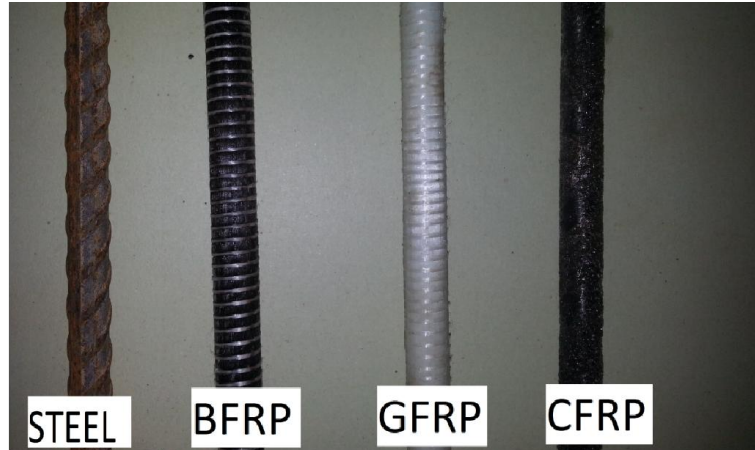
Fig. 3.2: Different reinforcement bars used in this study

3.2.2 Concrete

Normal strength concrete having 28-days-compressive strength of 40 MPa was used in preparing the various specimens. Concrete mixture proportioning is presented in Table 3.3. The average measured slump was found 90±2 mm which allowed for good compaction without excess bleeding. The modulus of elasticity for the concrete was calculated based upon experimentally obtained stress-strain curves. The coefficient of thermal expansion of concrete was estimated at 11.5×10^{-6}/°C based upon the mix proportions and the thermal properties of the used concrete components. The typical CTE ranges for granite aggregate, sand and 0.5 w/c cement paste is $(7-9) \times 10^{-6}$/°C, $(11-12) \times 10^{-6}$/°C, and $(18-20) \times 10^{-6}$/°C, as per the US Department of Transportation- Federal Highway Administration report FHWA, 2007.

Table 3.3 Concrete mix proportioning, based upon Ismail et al., (2011)

Water kg/m³	Cement kg/m³	Coarse Aggregate kg/m³	Fine Aggregate kg/m³	Target Compressive Strength, MPa	Target Slump, mm
207	416	1139	619	40	90

3.2.2(a) Water

Tap water obtained from a domestic water supply pipe at the civil engineering's concrete laboratory was used for all concrete work of this study.

3.2.2(b) Cement

Ordinary Portland cement Type-I produced by Cement Industries of Malaysia Berhad (CIMA), and known commercially as Blue Lion cement, was used in this work. The cement has sulfate content of less than or equal to 3.5%, chloride content of less than or equal to 0.1%, soundness of less than or equal to 10 mm and minimum initial setting time of 75 minutes which comply with the Malaysian Standards, MS EN 197-1, (2014).

3.2.2(c) Coarse aggregate

Crushed granite coarse aggregate of 10 mm maximum aggregate size, obtained from a location near Bukit Mertajam, was used in producing the normal strength concrete of this study. The specific gravity and water content was determined according to ASTM test method C127, and found to be 2.66, and 0.5%, respectively.

3.2.2(d) Fine aggregate

Natural river sand, obtained from river located near Nibong Tebal- Penang, was used in this study as fine aggregate. The specific gravity and water content was determined according to ASTM test method C128, and found to be 2.7, and 0.6%, respectively. Sieve analysis of fine particles was performed according to ASTM test method C136 and a fineness modulus of 3.0 was obtained. Properties of fine and coarse aggregates are summarized in Table 3.4.

Table 3.4: Properties of fine and coarse aggregates

	Fine Aggregate	Coarse Aggregate
Specific Gravity	2.7	2.66
Water Content, %	0.6	0.5
Fineness Modulus	3.0	N.A

N.A., Not Applicable

3.2.3 High tensile strength epoxy

Epoxy adhesive having the commercial designation CONCRESIVE 1441S, and manufactured by BASF-Malaysia, was used to adhere grip steel pipes to the FRP bars free ends before tension and pullout tests. These steel pipes provide a confinement pressure on the bar to prevent its slippage or local failure due to the damage of the bars ends under tension. This gray color epoxy was obtained by mixing two parts, Part-A of white color base and Part-B of black color reactor, at volumetric ratio of 2:1, respectively, as per the manufacturer recommendation. Properties of this epoxy as per manufacturer technical data sheet are given in Table 3.5.

3.2.4 High temperature resistant epoxy adhesive

An epoxy adhesive of ultimate stability and strength at high temperature of up to 650°F (343°C) was used to bond the proposed stainless steel end caps to the FRP reinforcement bars used in reinforcing certain groups of concrete beams. This aimed at improving bond between FRP and concrete hence the flexural behavior.

Duralco 4703 Adhesive used was manufactured by Cortronics Corp., and has an excellent resistance to most chemical solvents, acids and bases with high stability under exposure to high temperature. This epoxy can be obtained by mixing two parts: Part1 as resin and Part 2 as hardener at a mix ratio of 100:22 by weight. Properties of the adhesive is summarized in Table 3.6.

Table 3.5: Properties of CONCRESIVE 1441S epoxy as provided by BASF-Malaysia

Tensile Strength after 7 days of cure	10 MPa
Compressive Strength after 7 days of cure	83 MPa
Slant Shear Strength after 7 days of cure	> 35 MPa (100% concrete failure)
Elastic modulus in compression	4600 MPa
Density (Mixed)	1.25 kg/L
Surface temperature for application	26 °C
Initial Cure/ Full Cure Time	1 day/7 days

Table 3.6: Duralco 4703 epoxy properties

Tensile Strength at room Temperature	81.4 MPa
Tensile Strength at 260°C	69.2 MPa
Bond Strength at room temperature	20.7 MPa
Bond Strength at 260°C	8.3 MPa
Thermal Expansion	3.9×10^{-5} /°C
Elongation	2%
Cure Time and Temperature	2 hrs at 175°C

3.2.5 Stainless steel end cap

Stainless steel caps were fabricated by welding Grade 316L pipes of 100 mm length, external diameter of 17.2 mm and thickness of 2.3 mm, to small plates made of the same metal (50x50x6.0 mm) as shown in the sketch at Fig. 3.3. This steel caps were aimed at improving bond between FRP and concrete hence the flexural behavior of end-capped-FRP reinforced concrete beams. The mechanical and thermal properties of the stainless steel cap are shown in Table 3.7.

Table 3.7: Properties of SS316L stainless steel used as per supplier data sheet

Temperature	Tensile Strength MPa	Yield Strength MPa	Elongation in 50 mm (%) *	Coefficient of Thermal expansion x 10^{-6} /°C *
68°F / 20°C	608	302	50	15.9
600°F / 316°C	465	193	48	16.2
1000°F / 539°C	444	179	46	17.5

* As per AISI: A designer handbook series No. 9004, High-temperature characteristics of stainless steel, American Iron and Steel Institute, page 42-42.
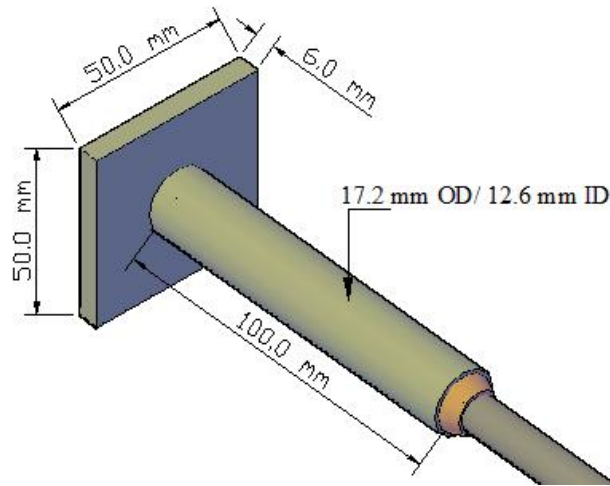
Fig.3.3: SS316L End Cap

3.2.6 High temperature thermal insulation coating

High-temperature thermal insulation coating (RLHY-12), manufactured by Beijing Ronglihengye Technology Corporation, Ltd - China, was used to insulate the bar's end caps hence maintain their temperature during heating at low values. The coating has a high temperature resistance range from -80°C to 800°C and heat conductivity of 0.03W/m.K only. This insulation coating was used specifically to insulate the stainless steel caps fixed to the ends of the FRP bars to prevent melting of the adhesive used to adhere the caps to the FRP bars. According to the manufacturer's technical data sheet, a thick layer of 4 mm of coating can reduce the temperature between the external and internal side of the coating to 40%. Table 3.8 shows the temperature at the internal side of various coating thicknesses with respect to an external temperature of 500°C. The insulation material was applied to the caps with average thickness of 4.0 mm as shown in Fig. 3.4.

Table 3.8: Temperature reduction for different insulation thicknesses by special coating as per the manufacturer's technical data sheet

Thickness of Coating, mm	12	10	8	6	4	2
From 500°C, temperature decreased to	45°C	55°C	80°C	130°C	200°C	300°C

Fig.3.4: Different FRP bars with steel end caps, with and without thermal insulation coating (RLHY12)

3.3 Testing program

To achieve the objectives of this study, the following tests were carried out.

1) Concrete strengths test

The compressive and splitting tensile strength of concrete was determined using standard cylinders and cubes specimens before and after being subjected to elevated temperatures of up to 500°C.

2) Tensile tests on reinforcing bars

The tensile mechanical properties of different bars used in the present work were determined at room temperature and after heating to 125, 250, 325, 375 and 450°C and cooling to room temperature. Detailings of the testing program are shown in Fig. 3.5

3) Bond tests using pullout specimens

The bond characteristics between FRP/Steel bars and concrete was studied using standard pullout cube specimens before and after exposure to high temperatures of 125°C, 250°C, 325°C, and 375°C. Fig. 3.6 shows the Detailings of the testing program.

4) Temperature Profile Evaluation

The temperature profile across the depth of two concrete beams was determined by embedding type-k thermocouples at eight different locations. Measurements were acquired while the specimens were heated in gas furnace up to 500°C for four hours.

5) Flexural response of concrete beams

The flexural response off 130x180x1200 mm concrete beams reinforced with different reinforcement types (BFRP, CFRP, GFRP and steel bars) was determined under four points loading. Flexural behavior and its characteristics, and modes of failure were acquired and monitored, respectively. Beams are divided into two main groups: the first group were tested at ambient temperature 23°C and used as controls whereas the other were tested after exposure to a high temperature of 500°C for 90 minutes. Designations of NT and HT were used for control and heated specimens, respectively. Each group was divided into two secondary groups corresponding to cases without or with rebar's steel end cap. Steel caps were fixed to the ends of FRP bars using high temperature resistant epoxy adhesive. Detailings of this testing program are shown in Fig. 3.7.
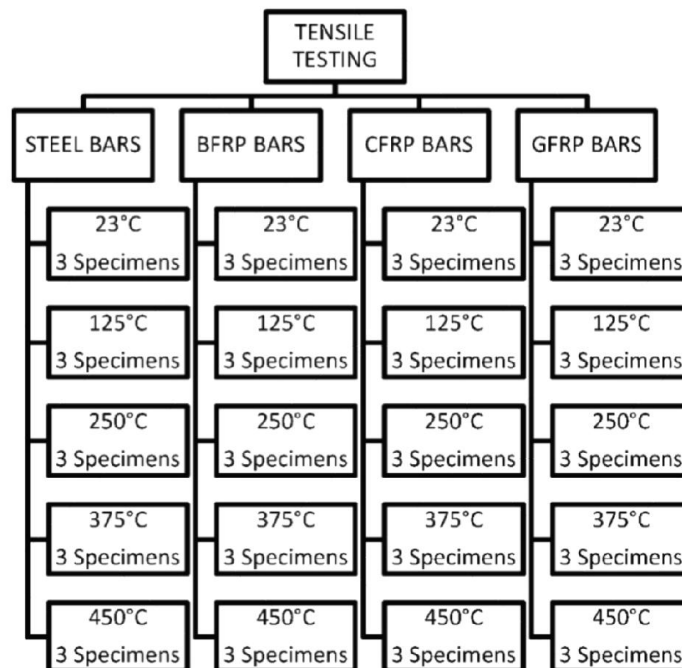
Fig. 3.5: Detailing of testing program via tensile test for FRP/steel bars
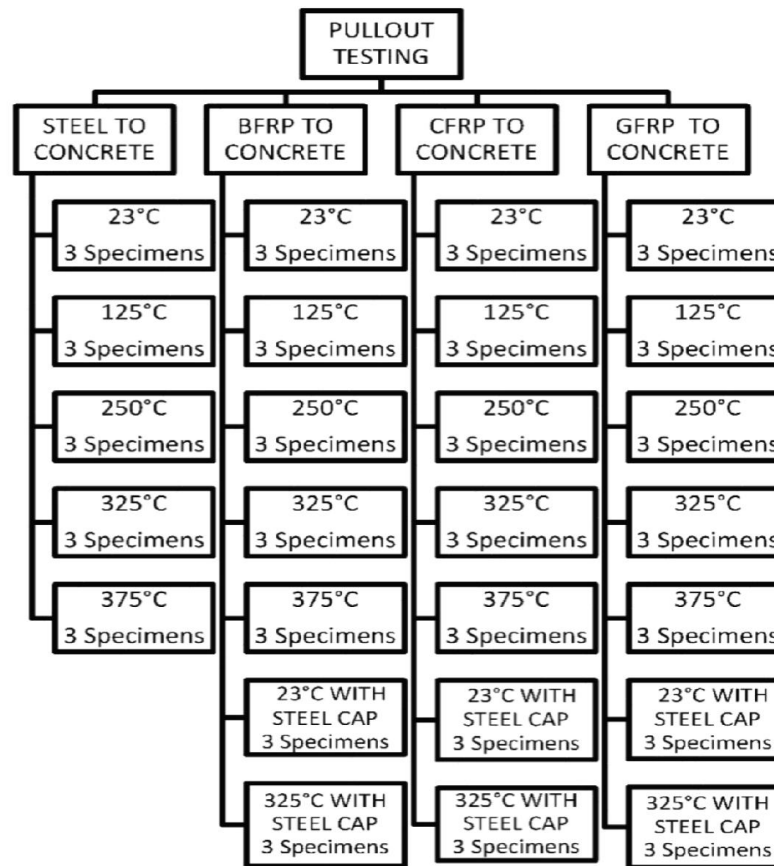
Fig. 3.6: Detailing of testing program via pullout tests
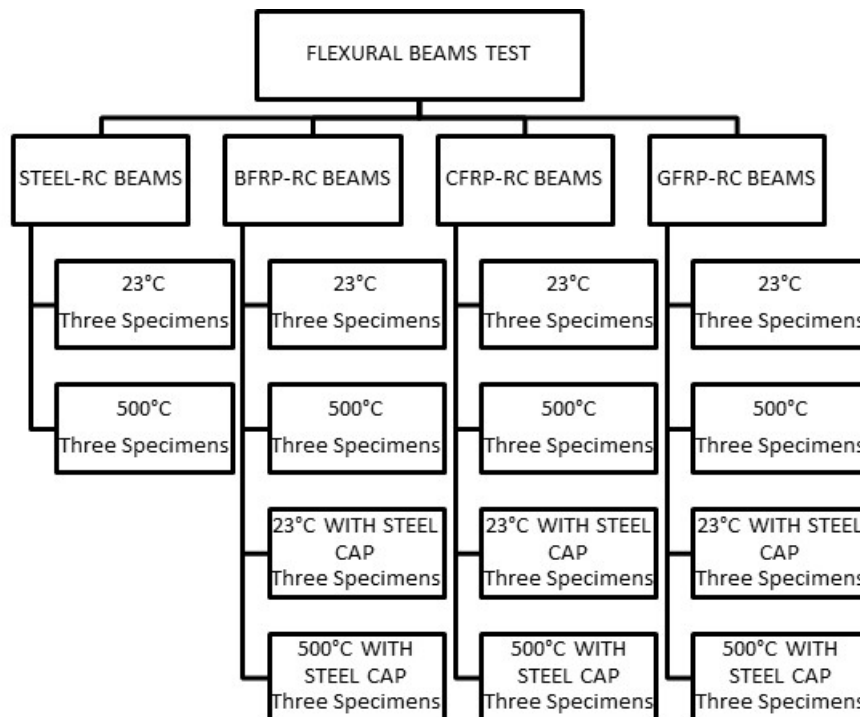
Fig. 3.7: Detailing of testing program for different beams in flexure

3.4   Specimens preparation

3.4.1   Preparation of tensile testing specimens

BFRP, CFRP, GFRP and steel bar specimens of 600 mm length and 10 mm diameter were prepared for tensile tests. A total of 18 specimens of each bar type was used. Three of them were tested at ambient temperature and used as controls while the remaining fifteen specimens (in triplicates) were exposed to different elevated temperature equal to 125°C, 250°C, 325°C, 375°C and 450°C.

Specimens were heated up with 10°C/min heating rate in an electric furnace allowing the hot air to circulate in the oven until reaching the required target temperature then kept at this target temperature for 30 minutes to ensure a uniform temperature distribution in the FRP specimens (Abbasi and Hogg, 2005a; Wang et al., 2007). After heating, the specimens were left to cool in air ready for tensile testing. It was noticed that all FRP bars heated up to 450°C were totally damaged, hence were not tested for mechanical properties as shown in Fig. 3.8. Figures. 3.9 through 3.12 show the physical status of various bars after exposure to various high temperatures.
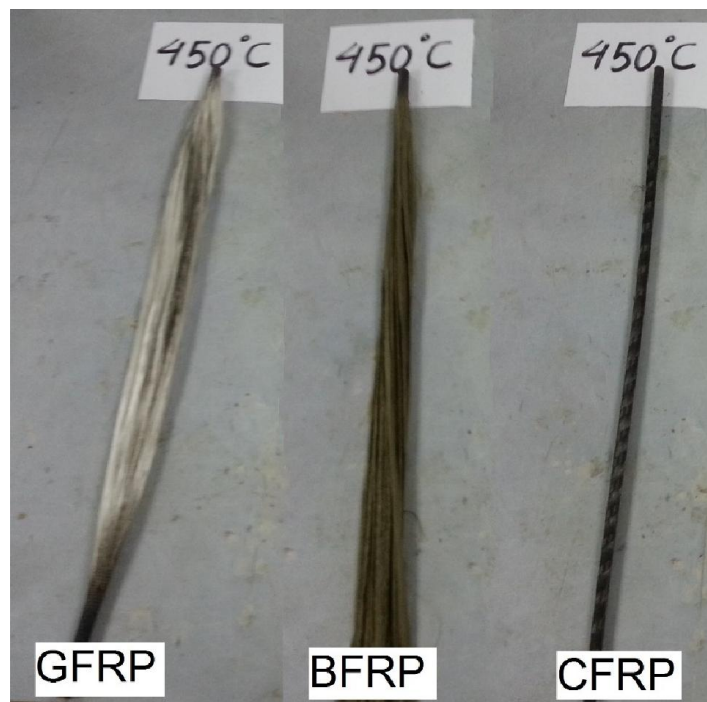
Fig 3.8: Damaged FRP bars after exposure to 450°C

Fig 3.9: GFRP bars before and after exposure to different high temperatures
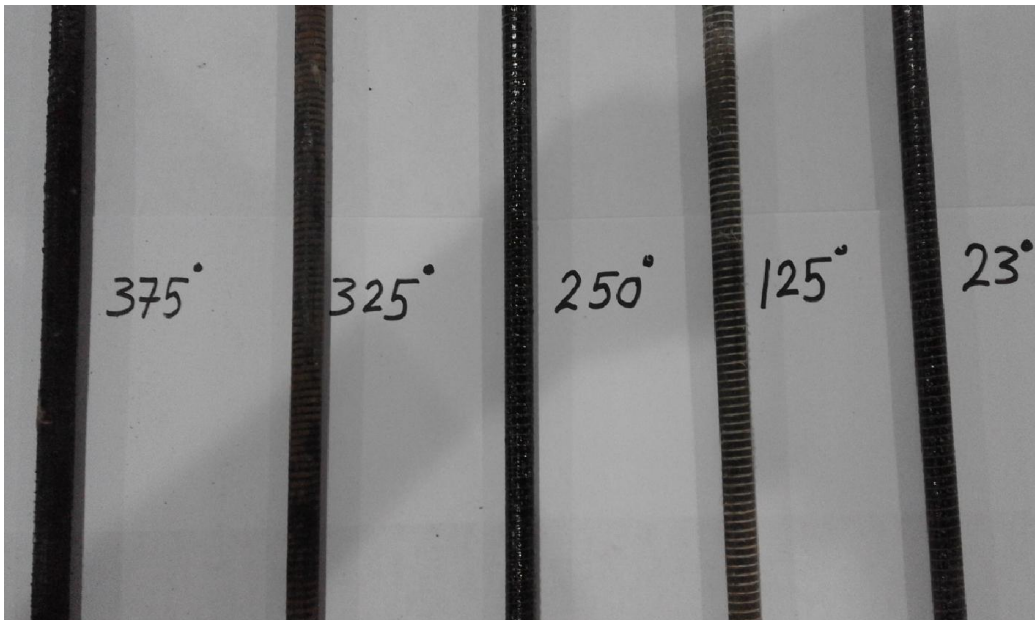
Fig 3.10: BFRP bars before and after exposure to different high temperatures
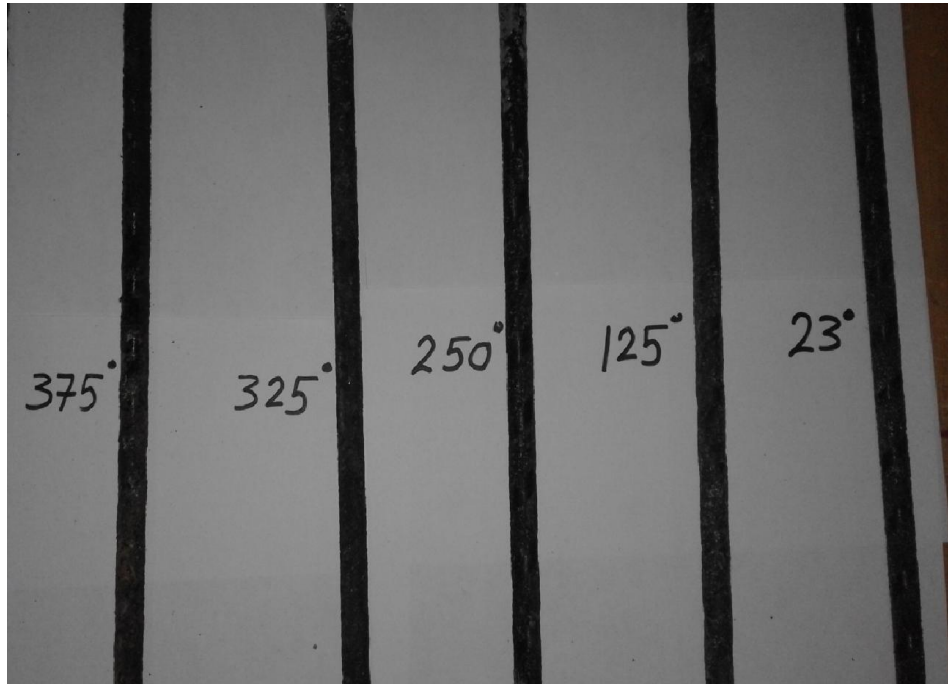
Fig 3.11: CFRP bars before and after exposure to different high temperatures
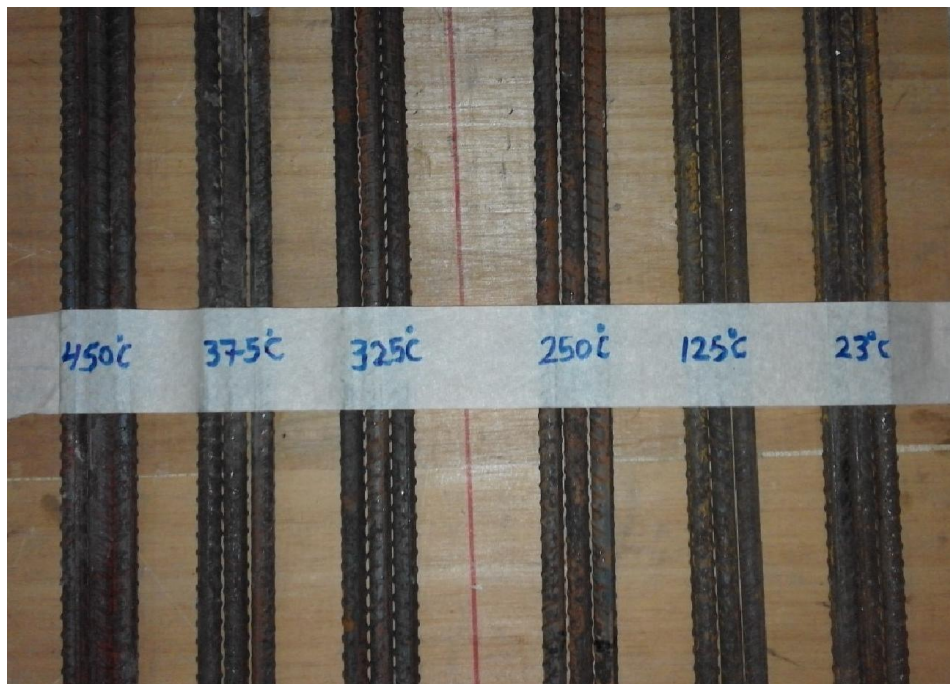
Fig. 3.12: Steel bars after exposure to different elevated temperatures ready for tensile test

Internally threaded steel pipes of a length, an outer diameter and a thickness of 200, 42 and 4 mm, respectively, were bonded to both ends of the FRP bars using a high tensile epoxy (CONCRESIVE-1441S) to enable testing of the bars without end

failure caused by the testing machine grips. Air pockets formation during adhesion was avoided to prevent any anchorage slippage during testing or undesired local failure due to the crushing of the bars ends. The threaded steel pipes were adhered to the FRP bars after their heat treatment as shown in Fig. 3.13.

Additional samples were prepared with bonded steel pipes of a length, an outer diameter and a thickness of 100, 20 and 3 mm, respectively, as shown in Fig. 3.14, and used to test the exact elastic modulus of the different specimens using an extensometer.

Fig. 3.13: Samples of FRP bars before and after exposure to different elevated
temperatures, ready for tensile strength test

Fig. 3.14: Samples of FRP bars before and after exposure to different elevated
temperatures, ready for elastic modulus determination

3.4.2 Preparation of pull-out testing specimens

Traditional pullout specimens were prepared using 10-mm-diameter FRP/steel bars embedded vertically in concrete cubes (150×150×150 mm) with a bond length of 100 mm. The latter was achieved using bond breakers consisting of PVC pipes of 25 mm length each, as shown in the schematic of Fig. 3.15(a). The de-bonded areas were created to prevent any localized artificial confinement of the bond length due to compressive load on concrete; specially at the loaded end and to ensure a uniform temperature distribution along the entire bar length. Fig. 3.15(b) shows the wooden mold in which the pullout specimens were cast as well as the locations of the PVC breakers.

A total of 78 pullout specimens were prepared, cured, and stored at room temperature of 23°C for 28 days before being tested in two groups. The first group, of 60 specimens, represented triplicates of pullout specimens with the four types of bar reinforcement embedded in concrete blocks without anchorage using steel end caps. These were tested before and after exposure to different temperature levels of 125, 250, 325 and 375°C for three hours then cooled. The second group, of 18 specimens, represented triplicates of pullout specimens with FRP bars anchored at their ends with the steel end caps. These were tested before and after exposure to 325°C.
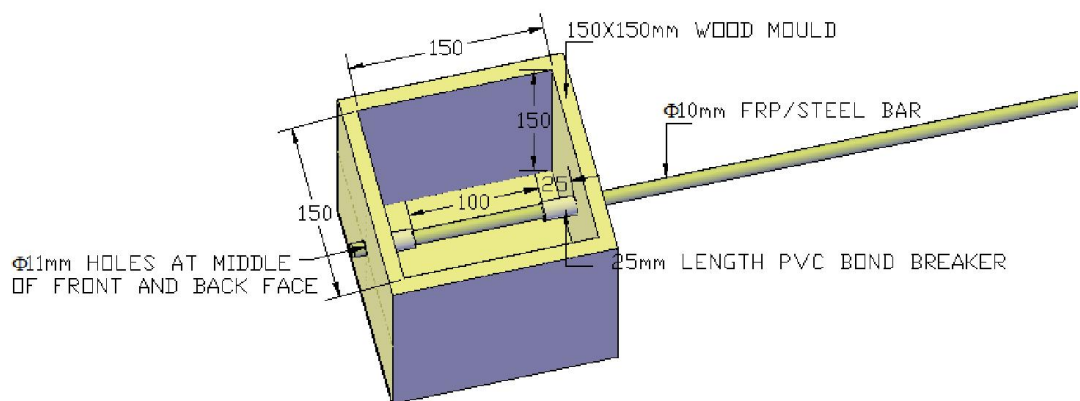
(a) A schematic of pullout test specimen mold with bars embedded to the desired length

(b) A picture of pullout test specimen mold with bars embedded to the desired length

Fig. 3.15: Detailing of the geometric dimensions of pullout test specimen molds
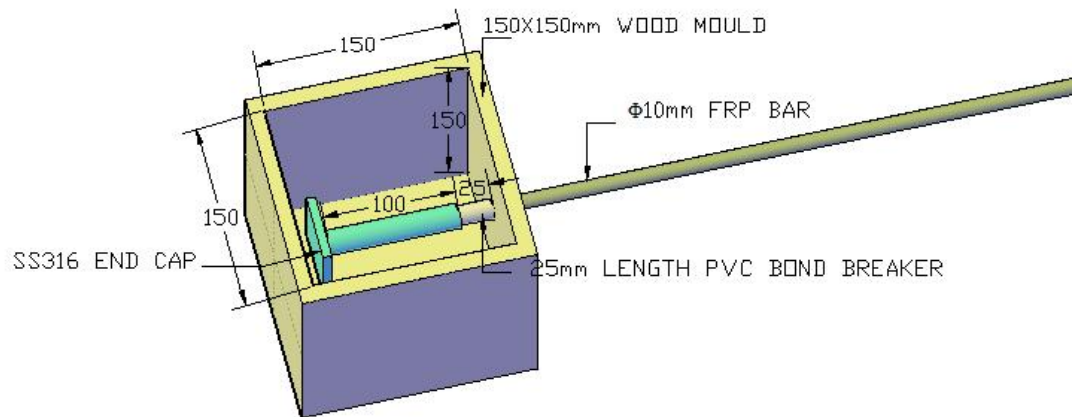
(a) A schematic of pullout test specimen with SS316L steel end cap mounted along the embedment length of the bar

(b) A picture of pullout test specimen with thermally insulated SS316L steel end cap mounted along the embedment length of the bar

Fig. 3.16: Detailing of pullout specimens with steel end cap anchorage

3.4.3   RC beams preparation

A total of 44 concrete beams (130×180×1200 mm) reinforced with different reinforcement types (BFRP, CFRP, GFRP and steel bars) were cast, then cured for 28 days and tested for flexural response and modes of failure according to experimental program of Fig. 3.7. All beams were cast in plywood molds of 10 mm thickness, as shown in Fig 3.17.

Fig. 3.17: Wooden molds for concrete beams

FRP-reinforced concrete beams were designed according to ACI, 2006 (ACI 440.1R) while steel RC beams were designed according to ACI, 2005 (ACI 318R). FRP-RC beams were designed as over-reinforced with reinforcement ratio (ρ) greater than the balanced reinforcement ratio (ρ_b) while the steel RC beams were designed as under-reinforced with (ρ) lower than (ρ_b).

For all cast beams, two bars of 10 mm diameter were used as main bottom tensile reinforcement and two top 6.0-mm-diameter bars were used. Steel stirrups of 6.0 mm diameter were used for shear reinforcement at a spacing of 70 mm; the reinforcement detailing is shown in Fig. 3.18. Special steel spacers were positioned underneath and at the sides of the reinforcement cages to achieve a cover of 25 mm.

Each type of FRP-RC beams are divided into two groups corresponding to cases without or with rebar's steel end cap as shown in Fig. 3.19. Steel caps were fixed to the ends of FRP bars using high temperature resistant epoxy adhesive. Fig. 3.20 shows the reinforcement cages in the wooden mold, ready for casting.
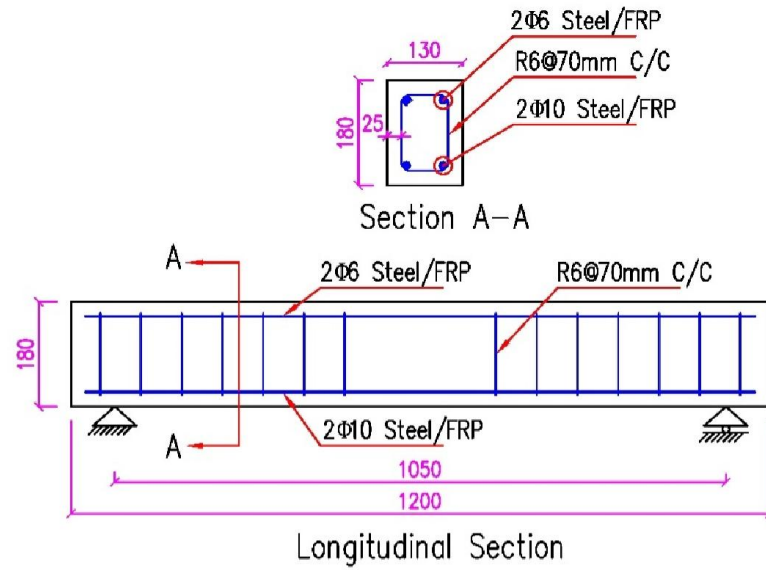
Fig. 3.18: Reinforcement Details

Fig. 3.19: Typical reinforcement cages with and without steel end caps

Fig. 3.20: Reinforcement cages inside the wooden molds

Prior to the placement of reinforcement cages in the molds, contact strain gauges were adhered to the main bottom reinforcement. A strain gauge, manufactured by Kyowa Electronic Instruments-Japan and having a length of 5.0 mm and gauge length of 3.0 mm, was adhered to the mid-length of the main reinforcement bar. The bar surface was first smoothed using sandpaper then cleaned from dusts and impurities using a volatile liquid before the strain gauge was attached. A layer of silicone sealant covered by aluminum foil tape was used to protect the fixed stain gauges during casting as shown in Fig 3.21.

Fig. 3.21: Strain gauge at reinforcement bar

For beams subjected to high temperature, special type of high temperature resisting strain gauges that can resist up to 300°C were used. Three layers of protection were used in order to reduce the temperature that will reach the gauges. After attaching the strain gauge using high temperature adhesive, it was coated with ceramic paste layer, then wrapped by ceramic wool layer followed by Teflon tape. A minimum of one inch of protection on both side of the fixed gauge is required to absorb the heat and reduce the temperature that reaches the gauge by 100-150°C.

An additional strain gauge was fixed to the second main reinforcement of the specimens which was already subjected to heating. This strain gauge was used as an alternative in case the one which was installed prior to heating didn't work.

For this purpose, a small hole of approximately 30×30×30 mm was created during casting at the main reinforcement level and then later filled with a ceramic wool to protect the neighboring FRP bar during heating, as shown in the pictures of Fig. 3.22. After burning of RC beams, ceramic wool was removed before the strain gauge was fixed to the reinforcement bar and protected by silicone sealant, as shown in Fig 3.23, and finally the hole was filled with concrete which was allowed to cure for two weeks prior to testing.

(a) Hole created	(b) Hole filled with ceramic wool
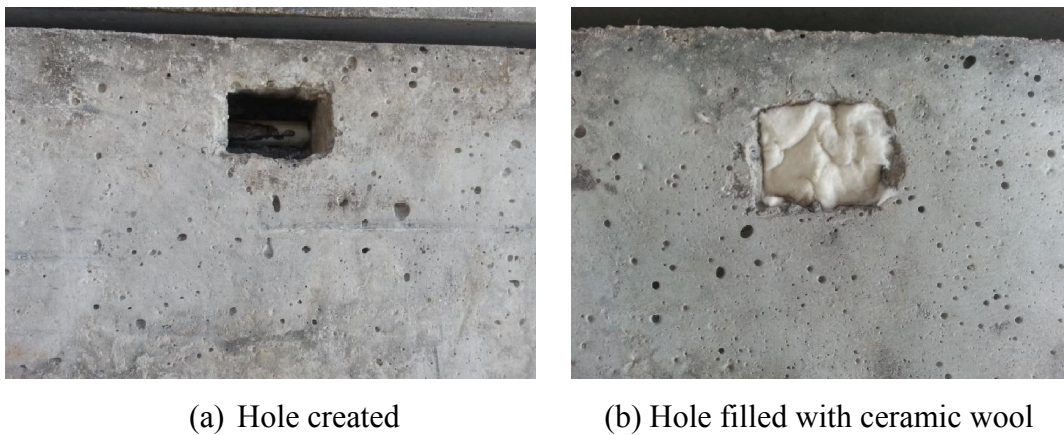
Fig. 3.22: Hole at bottom of RC beam used for later fixation of strain gauges

Fig. 3.23: Fixation of strain gauge after burning of RC beam

To monitor the temperature changes across the beam's depth during heating, four K-Type thermocouples having a 1.0 m probe length were placed at different location across the depth of two beams prior to casting, as shown in Fig. 3.24. This allowed acquiring the temperature variation across the beams, while being subjected to a high temperature of 500°C for four hours.
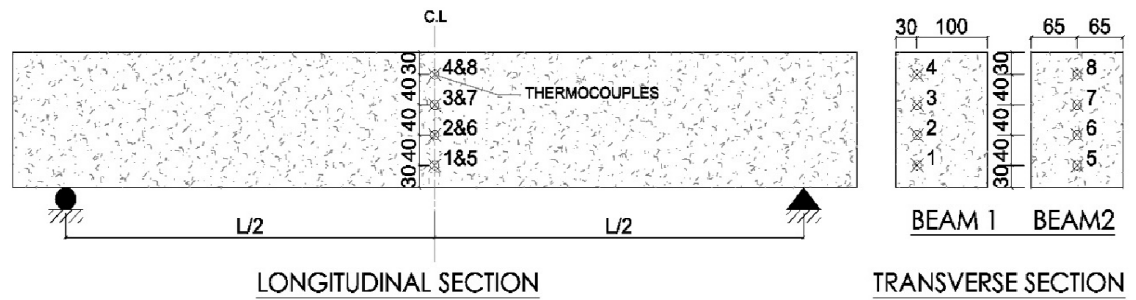
Fig. 3.24: Locations of thermocouples

A strain gauge, manufactured by Kyowa Electronic Instruments-Japan and having a gauge length of 40.0 mm, was fixed at the middle of the top surface of all concrete beam prior to flexural testing. To do so, concrete surface, where the strain gauge is to be attached, was smoothed using a grinder and sandpapers then cleaned from dusts and impurities using a volatile liquid. After fixing the strain gauge, a thin layer of silicone sealant was used to protect the strain gauges from any damage during the testing procedures as shown in Fig 3.25.

Fig. 3.25: Strain gauge at beam's mid-span top surface

3.5 Mixing, casting, and curing of different specimens

Mixing

A titling drum mixer of 0.15 m^3 capacity was used in mixing the concrete ingredient following the ASTM standard C192. Initially, a little spray water was used to wet the inner surface of the mixer, followed by placing the total amount of coarse and fine aggregates in the mixer, which was initially dry mixed, followed by adding half of water with the mixer running to wet their surface and ensure full absorption of the water. Cement and water was added carefully and gradually until total cement

amount is blended. Remaining water was added to produce a workable mix. Mixing continued for 3 minutes followed by a 3-minutes rest then a 2-minutes final mixing. The slump, measured according to ASTM standard C143 as showing in Fig. 3.26, was found to be about 90 mm.

Casting of pullout specimens

Pullout specimens were cast according to the following sequences:

1. The wooden cubic molds were oiled followed by placing the FRP/steel bar in the mold as shown in Figures 3.15 and 3.16.

2. Concrete was placed in the wooden molds in three layers. A vibration table was used to achieve a good compaction then a smooth surface of the specimens was produced using a trowel.

3. Specimens were left in their wooden molds for 24 h and covered with wet burlap before being de-molded.

Casting of RC beams

Concrete beams specimens were cast according to the following sequences:

4. The wooden molds were oiled and the reinforcement cages were placed in the mold as shown in Fig. 3.20.

5. Mixed concrete was placed in the wooden molds in three layers. Each layer was consolidated by inserting the steel rod of an electric internal poker vibrator vertically between the reinforcing bars to achieve a good compaction then the surface of the beams was finished smooth by a trowel as shown in Fig 3.27.

6. After casting, the beams were left in their wooden molds for 24 h and were covered with wet burlap before being de-molded.

Casting of standard concrete specimens:

For controlling the quality of the concrete used in making the pullout and beams specimens, standard concrete cylinders of 100 diameter × 200 mm length and 100×100×100 mm cubes were cast in layer, at the same time of casting RC beams and pullout specimens, compacted using a vibrating table then de-molded after 1 day of casting.

Fig. 3.26: Slump test

Fig. 3.27: RC beams after casting in the wooden molds

Curing

All specimens were de-molded 24 hours after casting and cured for 21 days at room temperature (23°C) by spraying water daily and cover them tightly by plastic membrane to reduce the evaporation of sprayed water from concrete surface as shown in Fig 3.28. By the end of three weeks curing, the specimens were left for a week in the laboratory air before being heated or tested.

Fig. 3.28: Water spray curing of RC beams

3.6   Heating processes

3.6.1   Heating of pull-out specimens

Pullout specimens were heated to 125°C and 250°C in an electric furnace at a rate of 10°C/min and in a gas furnace at a rate of 100°C/min when heated at higher temperatures of 325°C and 375°C. The target temperature was maintained constant for 3 hours to achieve uniform distribution of the heat across the cubic concrete blocks. Fig. 3.29 shows the heating scheme used for the pullout specimens.

In order to maintain bond between the steel end caps and FRP bars, and prevent explosive separation between FRP bars and concrete, a thermal insulating coat (RHLY-12) was applied to the steel caps prior to concrete casting. Thermal insulating coat was also applied on the exposed length of the FRP bars prior to heating in order to protect them from direct gas fire flames that may damage the FRP bars. Fig. 3.30 shows how the insulation material was applied on the exposed length of the FRP bars. The pullout specimens inside the gas furnace after heating are shown in Fig. 3.31.

After cooling of the pullout specimens in the laboratory air, threaded steel pipes with a length, an outer diameter and a thickness of 100, 20 and 3 mm, respectively, were bonded to the free end of the FRP bars using high tensile epoxy adhesive (CONCRESIVE-1441S). These allowed pullout of the FRP bars without end rupture because of the effect of stress concentration at the tensile machine's gripper's location. Fig. 3.32 shows the pullout specimens with the threaded steel pipes, ready for testing.
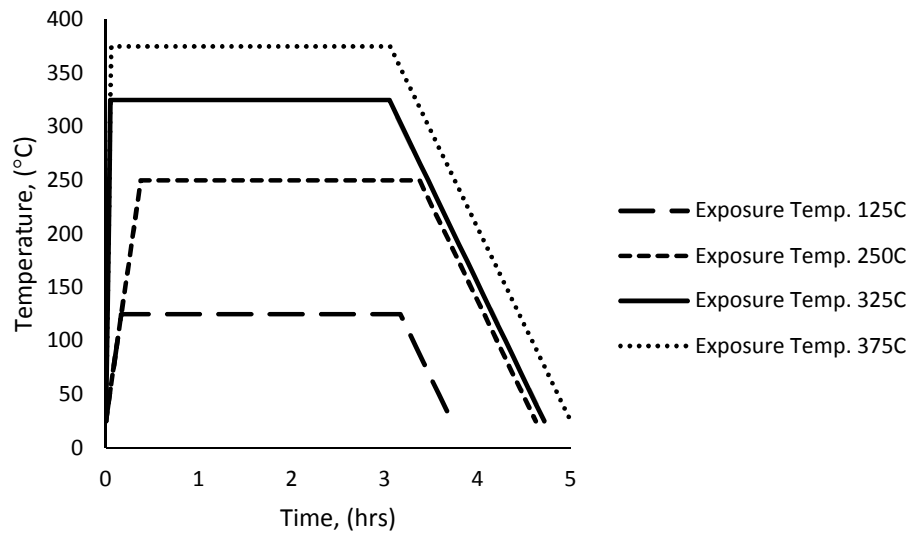
Fig. 3.29: Heat scheme for pullout specimens

Fig. 3.30: Pullout specimen with external
thermal insulation coating protection

Fig. 3.32: Pullout specimen with
top steel pipe ready for testing

Fig. 3.31: Pullout specimens in gas furnace after heating

3.6.2 Heating of beam specimens

A gas furnace having an internal dimensions of ($1.0 \times 1.0 \times 1.0$ m^3) with a movable top tight cover was used in this experimental program. The furnace is lined internally with insulating bricks. Each side wall of the furnace has one gas-fired nozzle burner and one fixed thermocouples to control the temperature inside this furnace during heating process. The average temperature, calculated from these side wall thermocouples, is used to control the furnace temperature automatically in accordance with the proposed heating curve.

The two RC beams, cast with K-Type thermocouples, were heated up to 500°C and kept constant for four hours to obtain the temperature profile across the beam's depth during the heating process. According to the thermocouples readings, it was found that the beams reach a uniform temperature of approximately 460°C at the end of the heating duration. It was also found that the temperature, at the location of the main bottom reinforcement, had reached 325°C after 92 minutes of heating.

Based on the obtained temperature profile and in order to avoid significant degradation in the mechanical properties of FRP reinforcement, it was decided to maintain a maximum temperature of 500°C, to which the beams were exposed, for a duration of 90 minutes only.

After three weeks of curing, the specimens were left for a week in the laboratory air before being heated in gas furnace at maximum temperature of 500°C for 90 minutes following the curve shown in Fig 3.33; two beams were heated at the same time, as shown in Fig 3.34.

3.6.3 Heating of concrete standard specimens

At the age of 28 days, half of the concrete cubes and cylinders were tested for compression and splitting tensile strength, respectively, while the remaining cubes and cylinders were placed in the gas furnace and heated up to 500°C for 90 minutes following the curve shown in Fig. 3.33, then left to cool in air before testing.
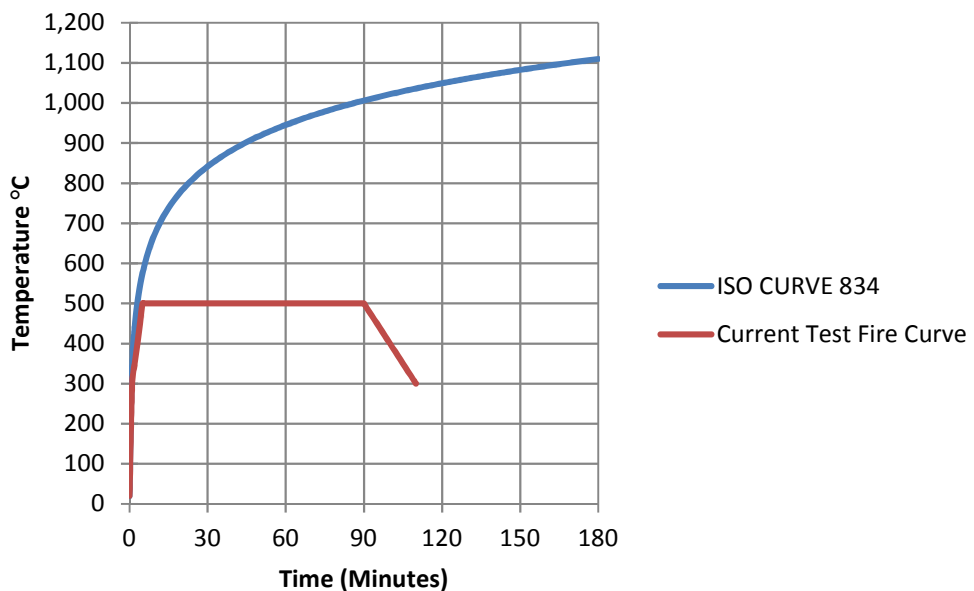
Fig. 3.33: Heating time-temperature schedule

Fig. 3.34: Two RC beam inside the furnace ready for heating

3.7 Mechanical testing

3.7.1 Tension test of FRP/steel bars

The tensile tests on FRP/steel bars were conducted at room temperature (23°C) according to ASTM D7205 using a Universal Testing Machine of 1000 kN maximum capacity. The tensile testing was performed using a standard constant head stroke rate of 3.0 mm/min until failure according to ASTM D7205/D7205M–06 recommendations. The tensile force was transmitted from the upper and lower jaws of the testing machine to the bars using epoxy bonded steel pipe at two ends of the tested bars as shown in Fig. 3.35. Loads versus displacement data were acquired automatically, before being analyzed for ultimate tensile stresses or stress-strain characteristics. An extensometer was installed on certain bars representing the different materials (steel/FRP) to enable acquiring the exact strain values as shown in Fig. 3.36. The accurate tensile chord elastic modulus was calculated according to ASTM standards, 2006 (D7205/D7205M–06) using the following equation:

$$E = \Delta\sigma/\Delta\varepsilon \tag{3.1}$$

where:

$\Delta\sigma$ is the difference in tensile stress between the start and end strain points.

$\Delta\varepsilon$ is the difference in tensile stain between the start and end strain points.

According to ASTM standards, 2006, (D7205/D7205M–06) the start and end points were defined as points of 0.001 and 0.003 strain. In case of ultimate strain ε_{ult} of less than 0.006, the start and end points were redefined as point of strain equal to $0.25\varepsilon_{ult}$ and $0.5\varepsilon_{ult}$.
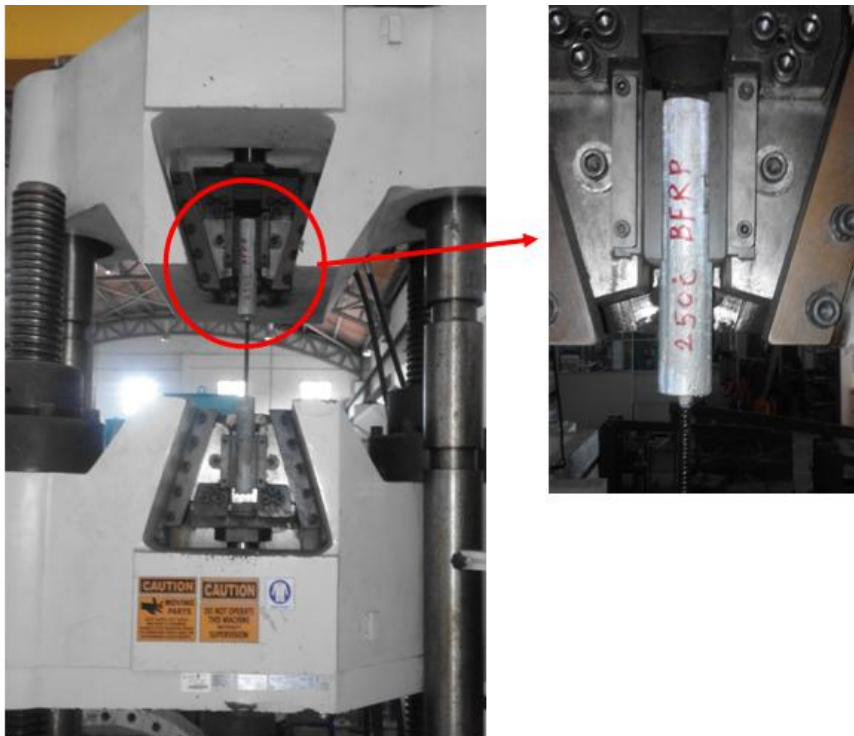
Fig. 3.35: FRP/steel bars attached to the jaws of the testing machine using epoxy bonded pipes
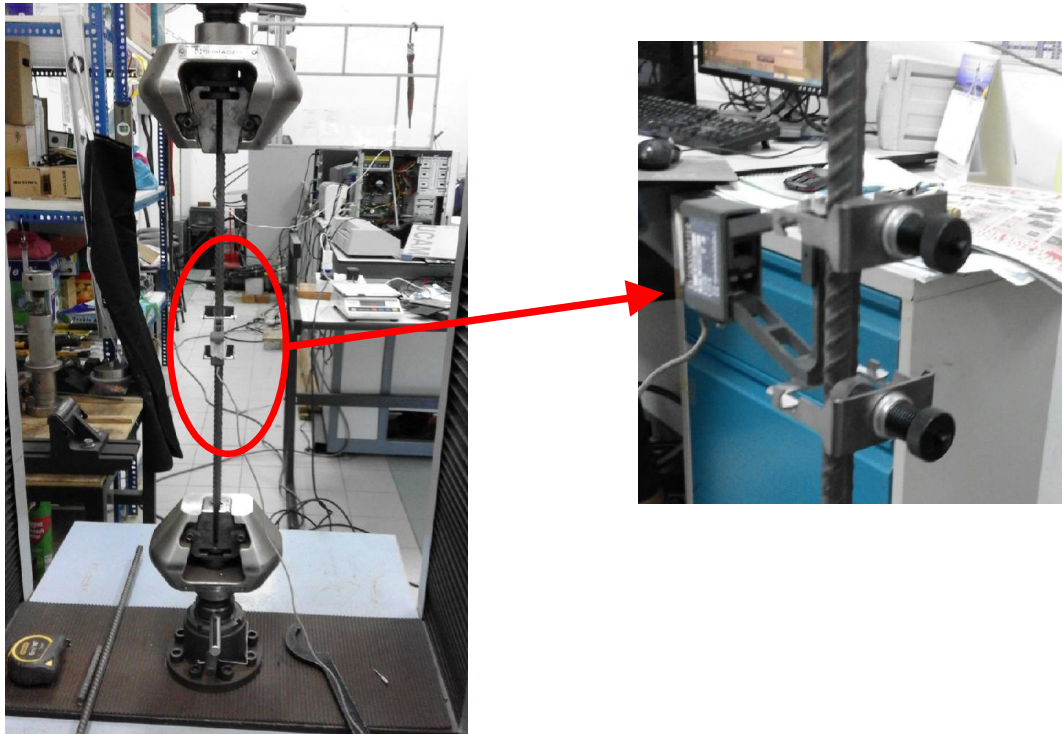
Fig. 3.36: Testing setup for obtaining the exact stress-strain diagram for steel/FRP bars using an extensometer

3.7.2 Pull-out test

Pullout tests were conducted at room temperature (23°C) according to ACI440.3R-04 recommendations using a Universal Testing Machine of 1000 kN maximum capacity. The concrete cubes were hold below the movable head of the testing machine whereas the free end of the bar was fastened to the fixed top head of the testing machine, as shown in Fig. 3.37. A built-in LVDT was used to measure the displacement between the two heads of the machine.

All pullout tests were carried out with a displacement-rate control of (1.2 mm/min) loading rate as per ACI440.3R-04 recommendations. Load and displacement readings were taken every second until bond failure.

The average bond strength was calculated from the following equation:

$$bond\ strength\ (\tau) = \frac{Max.\ Applied\ Load}{\pi * Bar\ Diameter * Embedded\ Length} = \frac{P}{\pi * d_b * L_d}$$

(3.2)

The actual bond slip (s) was calculated from the following equation

$$s = (Measured\ reading\ from\ the\ machine)$$
$$- (Elongation\ of\ the\ bar\ during\ testing\ )$$

$$(3.3)$$

$$Elongation\ of\ the\ bar = \frac{Max.\ Applied\ load\ *\ Length\ L_O}{\pi\ *\ Elastic\ Modulus\ *\ (Bar\ Radius)^2} = \frac{P\ *\ L_O}{\pi\ *\ E\ r^2}$$

$$(3.4)$$

Where Lo= is the length between edge of the concrete cube to the edge of head wedges.

Fig. 3.37: Pullout test arrangement

3.7.3 Flexural response test

Control and heated beams were tested as simply supported beams of 1200 mm total span, 1050 mm clear span and 350 mm pure bending moment span around the middle of the beams. A structural testing frame with a load cell of 500 kN maximum force capacity was used for testing. A linear variable displacement transducers (LVDT) was placed at the middle point of the bottom surface of the beam to measure the mid-span deflection, while another two LVDT's were placed at 350 mm distance from the center line of the beam as shown in the schematic and picture of Fig. 3.38.

All beams were tested under monotonically increasing load up to failure while LVDT's, strain gauges and load cell readings, were recorded using a data acquisition system. Cracks propagation were observed visually, marked and photographed.
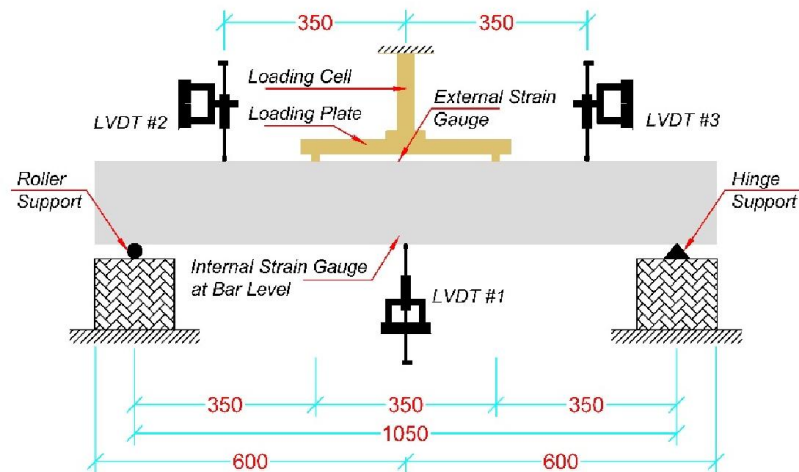
(a) Schematic presentation
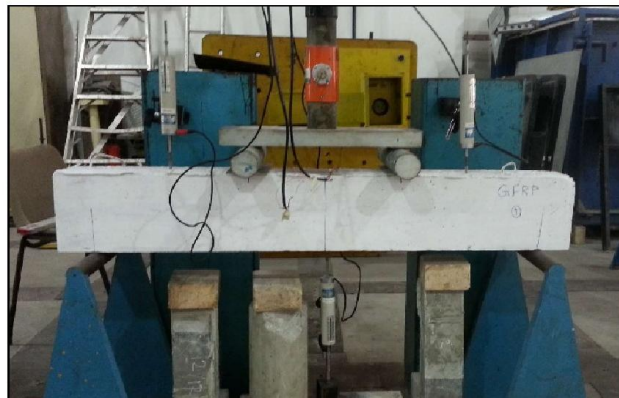
(b) Actual test Setup

Fig. 3.38: Flexural test arrangement, setup and positioning of the LVDT's

3.7.4 Compressive and splitting test of concrete

Three cube samples of (100 x 100 x 100 mm) and two concrete cylinders of (100 diameter x 200 mm height) were prepared for each batch along with four beams specimens, and cured then tested for compressive strength and modulus of elasticity. Half of these specimens were tested after 28 days at ambient temperature whereas the rest were tested after exposure to a high temperature of 500°C for 90 minutes duration.

Compression test on concrete cubes was performed using a universal compression machine of maximum capacity of 3000 kN at rate of 0.3 MPa/sec whereas that of cylinders was performed using a universal testing machine of maximum capacity of 1000 kN at rate of 0.3 MPa/sec. The compressive strength of concrete cylinders was performed according to ASTM C39; whereas that of cubic specimens was performed according to BS standards, 2009 (BS EN 12390-3:2009).

The testing setups for both types of specimens are shown in Fig. 3.39 and Fig. 3.40. Strain gauge was fixed to the concrete cylinder to measure the actual compressive strain.

Fig. 3.39: Cube compressive strength test

Fig. 3.40: Concrete cylinder compressive strength test

Similar to compressive strength, the tensile splitting strength of concrete was determined at 28 days under room temperature using a universal testing machine of maximum capacity of 1000 kN, before and after exposure to of 500°C for 90 minutes duration. The splitting tensile test at each temperature was conducted using two concrete cylinders (100 diameter × 200 mm height), prepared for each casting batch, at rate of 1.0 MPa/min according to ASTM, 2004 (ASTM C496/C496M-11). The splitting tensile test setup is shown in Fig. 3.41.

Fig. 3.41: Concrete cylinder splitting tensile strength test

3.8   Theoretical Work

Different theoretical studies were performed and presented in more details in chapter Five. The theoretical work was separated into two main parts. The first part includes the empirical prediction of post-heating bond behaviour between FRP bars and concrete, which is presented in details in section 5.2, whereas the second one includes the theoretical prediction of the load carrying capacity, mid-span deflection and cracking load for beams with FRP/steel bars without and with end anchorage, before and after exposure to 500°C, which is presented in details in section 5.3.

3.9 Summary

In this chapter, the details of the experimental and theoretical parts of this research work were presented. The experimental part, including the materials used, the specimens' preparation, the heating processes of different specimens and the mechanical tests, was presented in sections 3.2 through 3.6. Four different mechanical tests were performed. The first test was the tensile test that carried on FRP/steel bars to study their mechanical properties before and after exposure to different high temperatures. The ultimate tensile strength, the ultimate strain and the elastic modulus of each tested bar were collected and discussed in section 4.3. The un-heated and heat-damaged concrete specimens were subjected to compressive and tensile splitting tests to investigate their residual mechanical properties; results were discussed in section 4.4. The third test was the pullout test that carried out to study the pre-and post-heating bond behavior between different FRP/steel bars and concrete. Characteristics of bond-slip curves of all tested pullout specimens were discussed in section 4.5. Finally, concrete beams with FRP/steel bars, with and without end anchorage before and after exposure to 500°C, were subjected to four-point loading test to study their flexural performance. The load-deflection characteristics, strains, cracking pattern and failure modes of all tested beams were discussed in section 4.6. The detailed theoretical work are presented in chapter 5.

CHAPTER FOUR
RESULTS AND DISCUSSION

4.1 Introduction

The results of all experimental works performed are presented in this chapter. The temperature profile for the RC beams used is presented in Section 4.2. The post-heating mechanical properties of the different reinforcing bars and concrete are presented in Sections 4.3 and 4.4, respectively. The post-heating bond behavior between FRP/steel bars and concrete is presented in Section 4.5. Finally, the flexural performance of concrete beams with FRP/steel bars with and without end anchorage, before and after exposure to 500°C, is discussed in Section 4.6 including detailed discussions on different load-deflection characteristics of the tested beam specimens.

4.2 Temperature profile for RC beams

Two RC beams were heated up to 500°C and then the temperature was maintained at 500°C for four hours in order to draw the temperature distribution profile of the beam during the heating process. A proper heat distribution inside the furnace and equal heating of the beams at all directions (bottom, sides and top) was obtained by the use of gas-fired nozzle burners and fixed thermocouples at all sides of the furnace. Eight K-Type thermocouples (four thermocouples for each beam) were distributed through the cross section of the beam. The temperature readings were collected and illustrated in Fig. 4.1.

The temperature readings indicated that the beams had reached a uniform temperature of approximately 460°C at the end of the heating duration. It was found that the temperature of thermocouple (#1) located at same level of the main bottom reinforcement bar's had reached 325°C in 92 minutes. This was considered as a

critical temperature for the FRP bars with a (40-50%) loss of its ultimate tensile strength. Accordingly, the period of heating at 500°C was limited to 90 minutes.
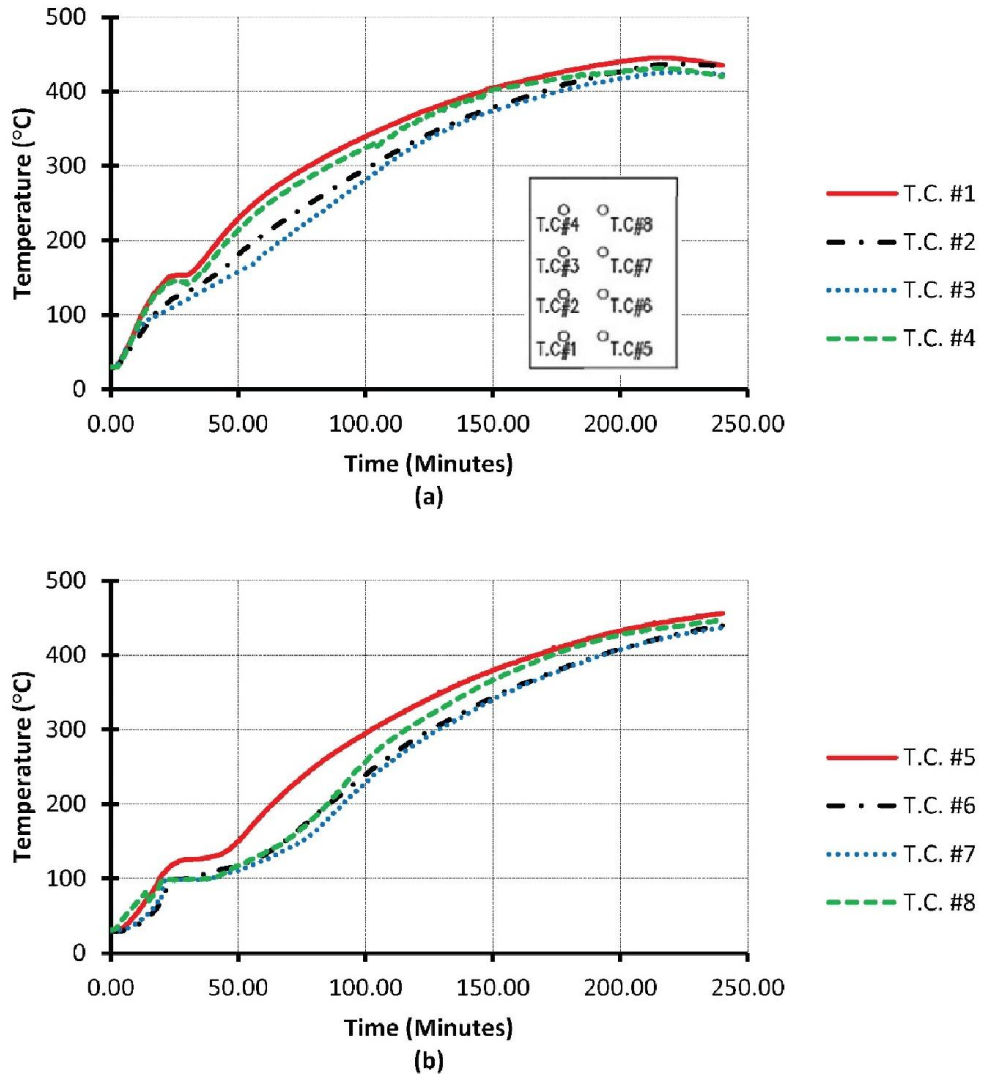
Figure 4.1: Temperature profile for RC beams heated to 500°C

Fig.4.1 shows that with 30 mm concrete cover, the temperature at the location of main reinforcement bars had reached 325°C in 92 minutes. Abbasi and Hogg, (2005b) provided Eq. 2.7 that can be used to predict the beam's main reinforcement rebar's temperature upon exposure to standard fire as a function of time and concrete cover. For example, when concrete beam with 30 mm concrete cover is subjected to standard fire test, the furnace's temperature reached 945°C after 60 minutes whereas

the main reinforcement bar's temperature reached 316°C. After 90 minutes of standard fire, the furnace temperature reached 1005°C whereas the main reinforcement bar's temperature reached 436°C. By increasing the concrete cover to 50 mm, the main reinforcement bar's temperature reached 326°C after 90 minutes of standard fire heating. Similarly, Nigro et al., (2011a) provided an analytical model to predict the temperature of FRP bars as a function of concrete cover and time. Nigro's model, presented in Fig 2.6, showed that the temperature rise in the rebars can be delayed further by using larger concrete cover. A minimum of 50 mm concrete cover is required to maintain the reinforcement bar's temperature below the critical temperature (325°C) upon exposure to standard fire.

4.3   Post-heating mechanical properties of reinforcement bars

4.3.1   Characteristics of FRP bars at different temperature exposures

The effects of elevated temperature on mechanical properties of FRP such as the tensile strength, modulus of elasticity and ultimate strain were determined experimentally then the results were compared with predictions by the relevant analytical models such as Nadjai's model (Nadjai *et al*., 2005) and Wang's model (Wang et al., 2011).

Typical stress-strain curves of the different FRP bars before and after exposure to high temperatures in the range of 23°C to 450°C are shown in Figs. 4.2 to 4.4 and their average characteristics are summarized in Table 4.1; the stress-strain diagrams and corresponding characteristics for individual specimens are reported in Figs. A-1 to A-3 and Tables A-1 to A-3 of Appendix A.

Table 4.1: Average characteristics of stress-strain diagram for different FRP bars at different temperatures (mean ± standard deviation)

FRP Type	Temp.	f_{ult-f} MPa	ε_{ult-f} x10^{-6}	E_f GPa	$f_{ult-f,T}$ / f_{ult-f}	$E_{f,T}$ / E_f
GFRP	23°C	816.49 ± 79.35	22200.00	47.14 ± 1.50	1.00	1.00
	125°C	703.29 ± 30.96	18700.00	44.87 ± 1.69	0.86	0.95
	250°C	552.25 ± 18.91	15900.00	40.91 ± 1.13	0.68	0.87
	325°C	452.97 ± 46.42	14100.00	37.40 ± 2.60	0.55	0.79
	375°C	76.74 ± 15.11	4000.00	24.50 ± 2.96	0.09	0.52
BFRP	23°C	939.99 ± 41.95	21400.00	65.58 ± 4.24	1.00	1.00
	125°C	757.62 ± 21.31	16100.00	63.02 ± 2.85	0.81	0.96
	250°C	662.37 ± 44.89	14800.00	57.74 ± 2.04	0.70	0.88
	325°C	514.28 ± 26.92	13000.00	51.89 ± 2.51	0.55	0.79
	375°C	122.28 ±33.23	7910.00	30.73 ± 4.68	0.13	0.47
CFRP	23°C	1572.07 ± 59.78	17000.00	119.08 ± 4.02	1.00	1.00
	125°C	1438.33 ± 54.48	16700.00	109.76 ± 6.16	0.91	0.92
	250°C	1152.30 ± 57.44	14000.00	100.56 ± 5.69	0.73	0.84
	325°C	700.02 ± 76.58	9500.00	81.10 ± 1.35	0.45	0.68
	375°C	454.41 ± 47.57	11500.00	56.23 ± 3.93	0.29	0.47
	450°C	164.27 ± 26.47	4800.00	43.81 ± 9.94	0.10	0.37

f_{ult-f}: ultimate tensile strength, ε_{ult-f}: strain at ultimate tensile strength, E_f :tensile chord modulus of elasticity
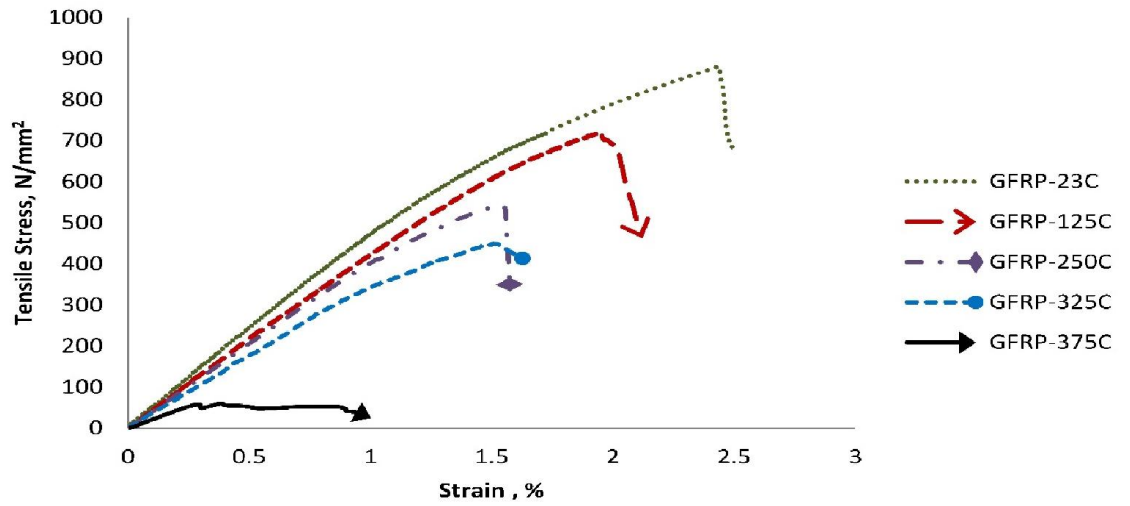
Figure 4.2: Typical stress-strain curves of GFRP bars at different temperatures
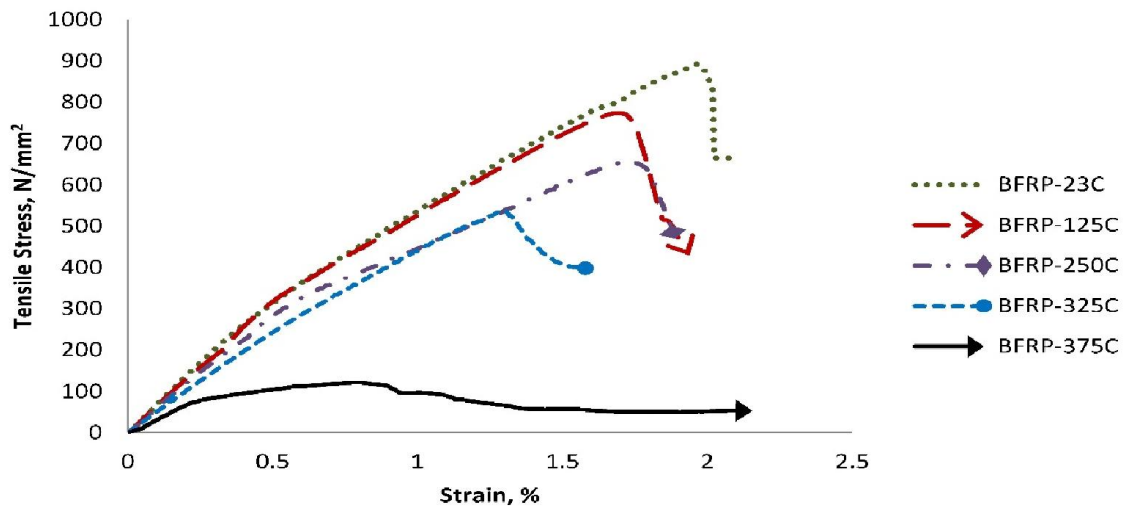
Figure 4.3: Typical stress-strain curves of BFRP bars at different temperatures
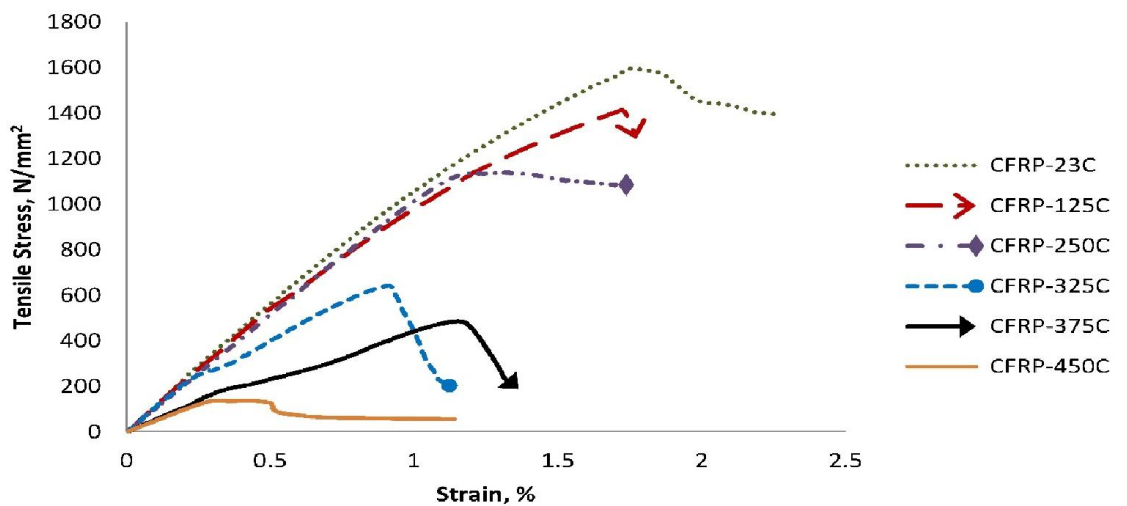
Figure 4.4: Typical stress-strain curves of CFRP bars at different temperatures

The stress-strain relationship of the different FRP bars was almost linear up to

failure for temperatures in the range from 23°C up to 325°C yet became non-linear at

higher temperatures due to the loss of bonds between fibers resulting from the damage of epoxy resin. The tensile stiffness and elastic modulus were reduced significantly especially prior to failure because the stress distribution among the fibers become non-uniform prior to failure; Fig. 4.5 shows the condition of the fibers upon heating to high temperature.

Table 4.1 indicates that the average tensile strengths of three specimens of GFRP, BFRP and CFRP bars at ambient temperatures were 816.5, 940 and 1572MPa, respectively. Their corresponding modulus of elasticity values were 47.14, 65.58, and 119.08 GPa, respectively. After exposure to high temperatures, FRP suffered reductions in their tensile strength proportional to the exposure temperature. The critical temperature which caused a significant degradation in the tensile strength of FRP bars in the range of 45 to 55% was 325°C. At this critical temperature, the different FRP bars suffered 21~32% loss in their elastic moduli. A higher rate of strength and elastic modulus loss was noticed at 450°C when the GFRP and BFRP bars melted hence lost their tensile strength capacity totally whereas the CFRP bars retained 10% and 37% of their tensile strength and elastic modulus, respectively.

Upon exposure to (125°C, 250°C, 325°C and 375°C), GFRP, BFRP and CFRP bars lost (14%, 32%, 44% and 91%), (19%, 30%, 46% and 87%) and (9%, 27%, 55% , 71%) of their ambient temperature strength, respectively. See Table 4.1.

The longitudinal elastic modulus of FRP is governed by the properties of the fibers hence reduction in elastic modulus with temperature was smaller than that of tensile strength. The residual elastic modulus of GFRP, BFRP and CFRP bars after exposure to (125°C, 250°C, 325°C and 375°C) was (95%, 87%, 79% and 52%), (96%, 88%, 79% and 53%), (92%, 84%, 68%, and 47%) of their ambient temperature elastic modulus, respectively.

It was observed that fracture failure of FRP bars exposed to lower elevated temperatures (250°C and below) happened suddenly within the specimen's middle length while those heated to 325°C and greater showed some repeated minor load drops before failure, hence tests were terminated before bars separation happened; see Fig. 4.5. Consequently, small differences between triplicate readings were noticed at temperatures below 325°C whereas significant differences were noticed at higher exposure temperature because of the decomposition of the matrix polymer which affected the bonds between the fibers hence the bar's mechanical properties.

Figure 4.5: Failure of heated FRP bar in tensile testing

The experimental results were used to assess the accuracy of the available analytical models such as the Nadjai's and Wang's models (Nadjai *et al*., 2005 and Wang et al., 2011). As shown in Figs. 4.6 and 4.7, Nadjai's model tended to overestimate the predicted reductions in tensile strength and elastic modulus of GFRP and BFRP bars yet showed a good agreement with those of CFRP bars. On the other hand, Wang's model tended to overestimate the reductions in tensile strength of FRP bars at temperatures below 325°C yet significantly underestimated those reductions especially at higher temperatures than 325°C. The reduction in tensile

strength and elastic modulus of FRP bars is almost linear from ambient temperature up to 325°C.
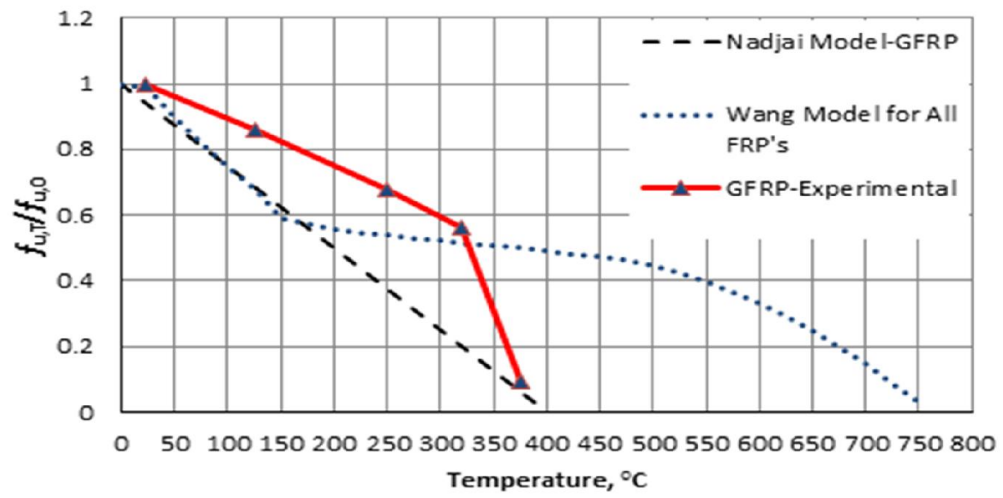
(a)
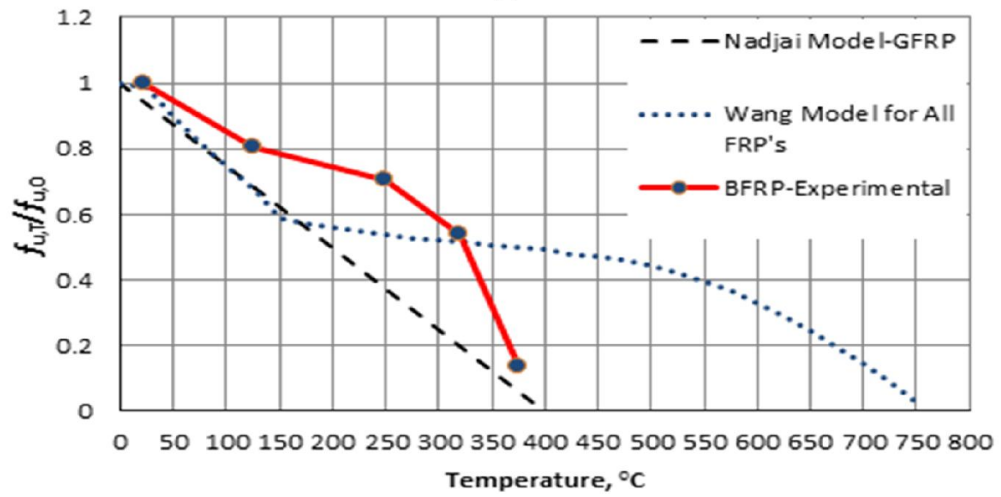
(b)
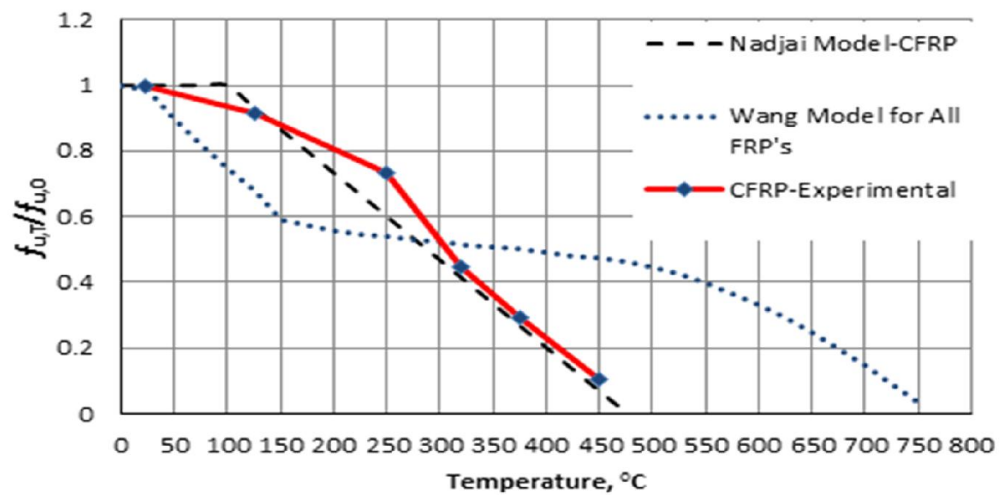
(c)

Figure 4.6: Residual tensile strength for FRP bars under elevated temperatures
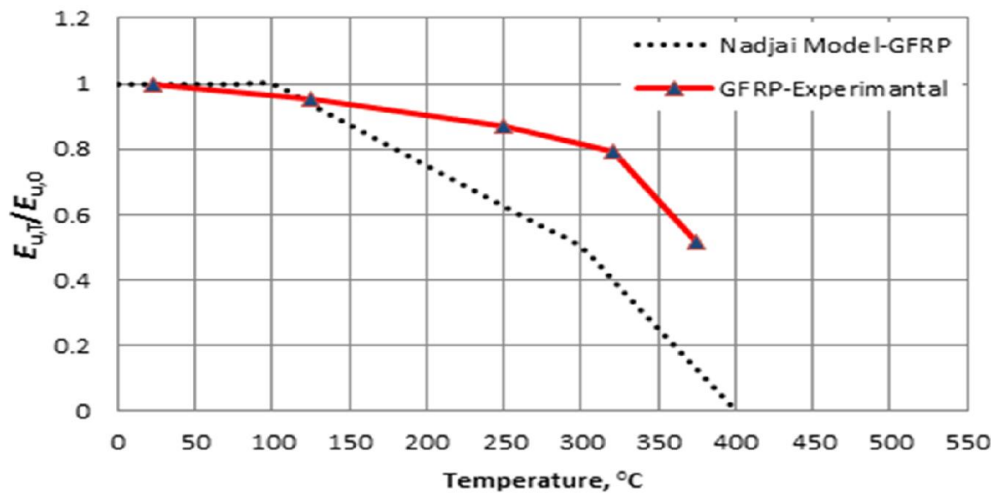
(a)
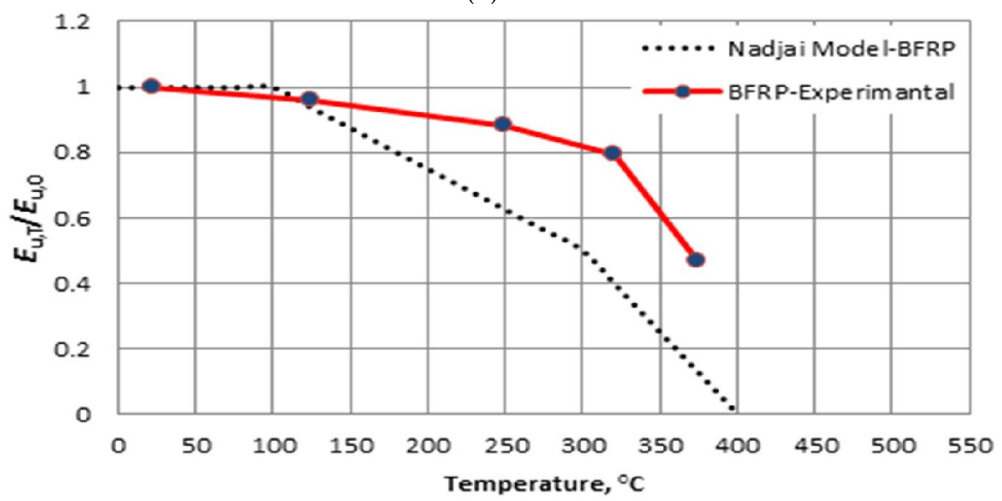
(b)
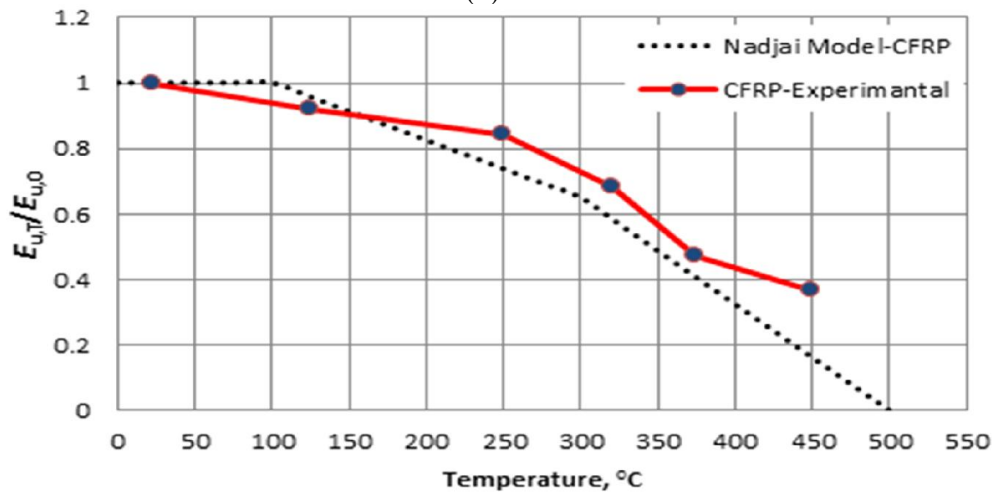
(c)

Figure 4.7: Residual elastic modulus for FRP bars under elevated temperatures

4.3.2 Characteristics of steel bars at different temperature exposures

Tensile tests were carried out on steel specimens before and after exposure to different high temperatures such as 125°C, 250°C, 325°C, 375°C & 450°C. The stress-strain data of steel bars before and after exposure to the different high temperatures is illustrated in Fig. 4.8 with the recorded characteristics summarized in Table 4.2; the stress-strain diagrams and corresponding characteristics for triplicate bars are reported in Fig. A-4 and Table A-4 of Appendix A.

The results in Table 4.2 show that the average yield and ultimate strengths of steel bars at ambient temperature were 571.5 MPa and 638.3 MPa, respectively, whereas its measured average elastic modulus was 228.3 GPa. Exposure of steel bars to high temperatures up to 450°C had a minor effect on their mechanical properties as compared to that of FRP bars.

Steel bars preserved high portions of their yield strength and elastic modulus upon exposure to high temperatures from 125°C to 375°C. Upon exposure to 450°C, the yield strength and the elastic modulus lost 5.3% and 7.7% of their corresponding room values, respectively. The elongation of steel bars at failure increased by 11% after heating the steel bars to 125°C, then steadily decreased reaching 97.8% at 450°C.

The normalized yield tensile strength and normalized elastic modulus of steel bars were compared with reduction factors presented in Section 3.2.3 of Eurocode 4-Part 1.2 (EN 1994-1-2, 2005), as shown in Figures 4.9 and 4.10. As shown, the Eurocode equations assume that the yield strength is not affected by temperature of less than 300°C, disagreeing with the experimental results. Furthermore, the Eurocode equations tend to overestimate the reduction in the yield strength at temperatures greater than 300°C compared with the experimental results. According

to Eurocode equations, the elastic modulus is not affected by temperature less than 100°C whereas reductions in the range of 13% to 60% is predicted with heating from 200 °C to 500°C, respectively. Eurocode equations tend to overestimate the reduction in elastic modulus at temperatures greater than 150°C compared with the experimental results.

Table 4.2: Steel bars-tensile tests results (mean ± standard deviation)

Temp.	f_y MPa	f_u MPa	ε_{ult}	ε_R % mm/mm	E_s GPa	$f_{y,T}$ / $f_{y,23°C}$	$f_{u,T}$ / $f_{u,23°C}$	$E_{s,T}$ / $E_{s,23°C}$	$\varepsilon_{R,T}$ / $\varepsilon_{R,23°C}$
23°C	571.46 ± 20.20	638.24 ± 20.98	84800	10.54 ± 0.88	228.3± 18.93	100.0%	100.0%	100.0%	100.0%
125°C	513.01 ± 51.34	598.70 ± 34.04	97300	11.72 ± 1.12	203.9± 11.75	89.8%	93.8%	89.3%	111.2%
250°C	524.90 ± 34.94	619.74 ± 22.63	93400	11.16 ± 0.55	207.74 ± 5.09	91.9%	97.1%	91.0%	105.9%
325°C	547.32 ± 27.53	628.26 ± 17.09	92300	10.97 ± 1.38	209.21 ± 3.94	95.8%	98.4%	91.6%	104.1%
375°C	554.37 ± 26.74	638.97 ± 28.15	90700	10.72 ± 0.60	213.14 ± 1.77	97.0%	100.1%	93.3%	101.7%
450°C	541.12 ± 17.95	622.45 ± 9.61	89400	10.30 ± 0.55	210.72 ± 1.21	94.7%	97.5%	92.3%	97.8%

f_y: yield strength, f_u: ultimate tensile strength, ε_{ult}: strain at ultimate tensile strength,
ε_R: elongation at rupture, E_s: modulus of elasticity
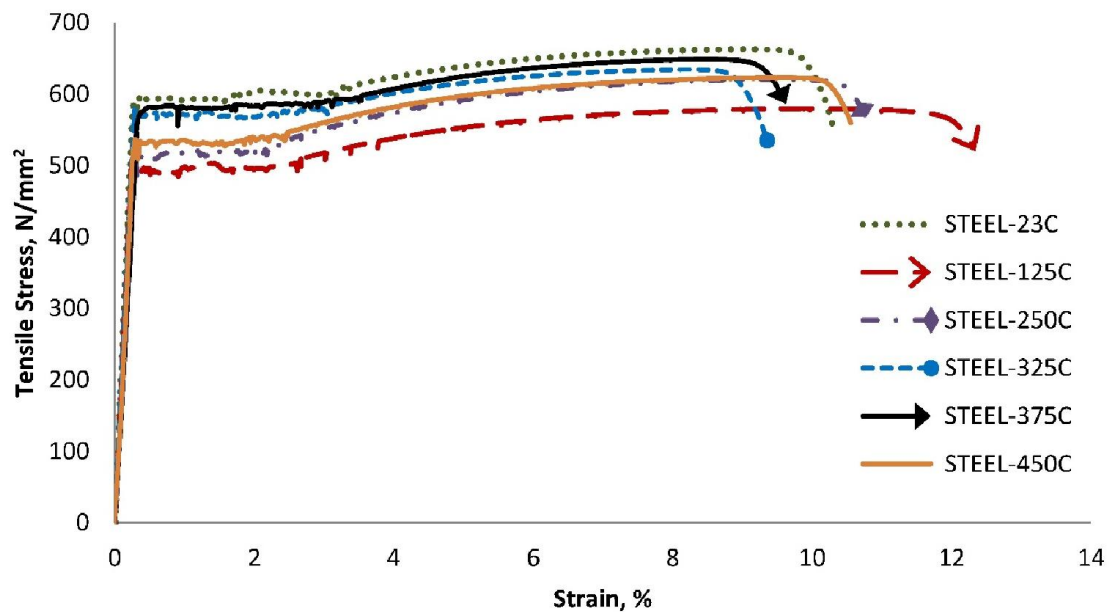
Figure 4.8: Typical stress-strain curves of steel bars at different temperatures
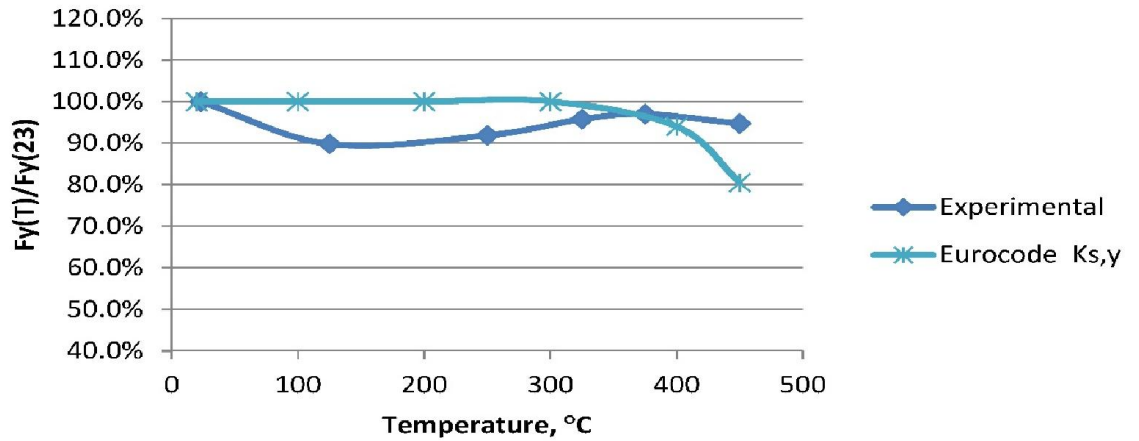
Figure 4.9: Normalized tensile strength of steel bars
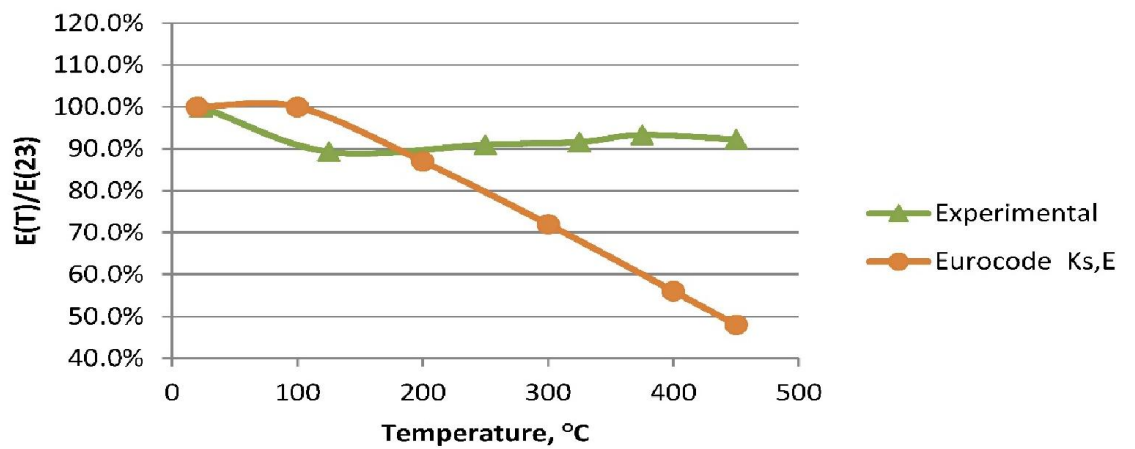
Figure 4.10: Normalized elastic modulus of steel bars

4.4 Residual mechanical properties of concrete

4.4.1 Compressive strength

Concrete compressive strength test was carried out on twelve concrete cylinders (Φ100×200 mm) and eighteen concrete cubes (100×100×100 mm), before and after exposure to a high temperature of 500°C for 90 minutes. Compressive stress-strain diagrams of the tested cylinders were obtained and illustrated in Fig. 4.11 while the average readings were summarized in Table 4.3. Readings and curves for triplicate concrete cylinders are presented in Table A-5 and Fig. A-5, respectively, of Appendix A.

According to Eurocode 2 (EN 1992-1-2, 2004), the reduced concrete compressive strength after heating to 500°C is approximately 60.5% of its unheated value (Refer to

106

eq 2-15), which is close to that of Zhang et *al.*, (2002) at 65%. In the present work, the experimental average cylinder compressive strength (fc') was found to be 34.0 MPa before exposure to heating but was reduced to 25.2 MPa after heating to 500°C at a residual value of 74%. The corresponding average cube compressive strength (f$_{cu}$) was 41.0 MPa as compared to 31.3 MPa after heating. The corresponding average strain at ultimate stress increased from 0.00260 before heating to 0.006489 after heating; readings for each specimens are reported in Table A.5, of Appendix A.
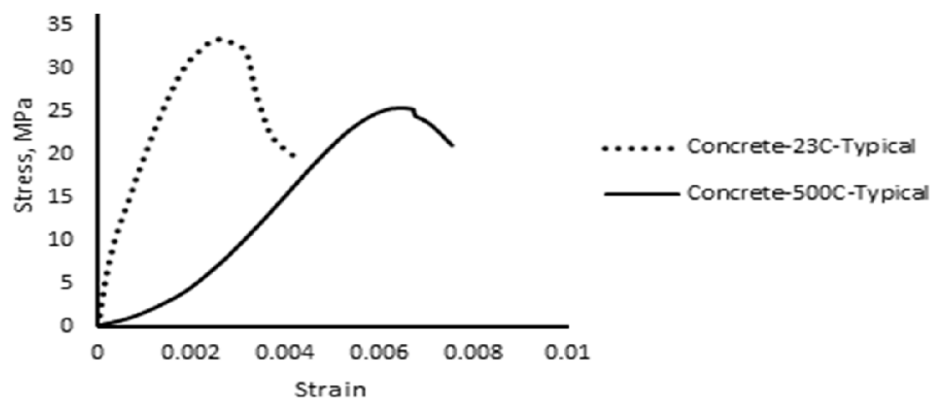
Fig. 4.11: Compressive stress versus strain for concrete before and after exposure to 500°C

4.4.2 Splitting tensile strength

Splitting tensile strength test were carried out on six concrete cylinders (Φ100X200mm) before and after exposure to high temperature of 500°C for 90 minutes. Average readings of the tested cylinders were obtained and presented in Table 4.3 while readings of individual specimens were summarized in Table A-5, Appendix A.

According to Eurocode 2 (EN 1992-1-2, 2004), the theoretical residual splitting tensile strength of concrete after exposure to 500°C is 20% as compared to 35% and 45% calculated by Zhang et al., (2002), and Noumowe et *al.*, (1996), respectively. The experimental average splitting tensile strength was 3.265 MPa before as compared to 1.706 MPa after heating with a residual value of 52%.

Table 4.3: Compressive and tensile strength of concrete at 23°C and 500°C (Mean ± standard deviation)

Temp.	P_C (kN)	f_c' (MPa)	ε_c %	P_T (kN)	f_{sp} (MPa)
23°C	266.9 ± 12.34	33.98 ± 1.57	0.2635 ± 0.0233	102.58 ± 22.34	3.265 ± 0.71
500°C	198.2 ± 21.70	25.24 ± 2.76	0.6489 ± 0.0451	53.60 ± 8.65	1.706 ± 0.27

P_C: maximum measured compression load, f_c': concrete cylinder compressive strength at 28 days, ε_c: Strain at f_c', P_T: maximum measured tensile load, f_{sp}: splitting tensile strength.

4.5   Bond strength test results

4.5.1   Bond between FRP/steel bars and concrete at ambient temperature

Results of bond versus slip of triplicate FRP bars were obtained and presented in Figs. A.6- A.9, Appendix A. Accordingly, typical bond slip curves representing different specimens and exposure temperatures were prepared to study the bond performance of each type of FRP bars with concrete under various exposure temperatures. Fig. 4.12 demonstrates bond versus slip between concrete and GFRP, BFRP, CFRP and steel bars for pullout specimens maintained at ambient temperature before testing. As shown, the bond slip curves consist mainly of three portions; linear followed by nonlinear portion; representing the ascending part of the curve then irregular descending portion of the curve which showed non-linear softening behavior reflecting the degradation of the bond.

The behavior obtained in Fig. 4.12 is in agreement with previous research which concluded that the bond strength between reinforcing bars and concrete is influenced by the bar's surface characteristics, elastic modulus; the surface of all FRP bars were damaged when observed after the pullout testing.

As expected the steel bars attained the highest bond with concrete at 11.31 MPa followed, in sequence, by CFRP, BFRP, and GFRP at 8.338, 2.628 and 2.014 MPa, respectively. On the other hand, the CFRP bars showed the highest bond stiffness yet the lowest slip at failure among other FRP bars due to better surface compared with the GFRP and BFRP bars.
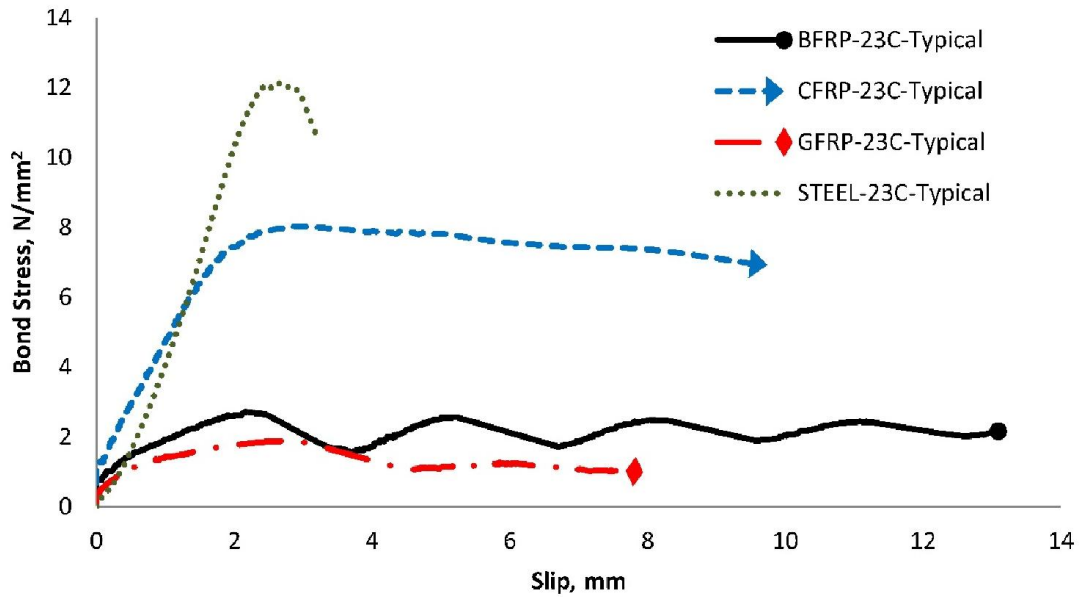
Figure 4.12: Typical bond-slip curves of FRP and steel bars at ambient temperature

4.5.2 Post-heating bond behaviour between FRP/steel bars and concrete

4.5.2(a) Introduction

Since FRP bars have high transverse coefficient of thermal expansion as compared to concrete, hence the surrounding concrete would be bursted at a relatively low exposure temperature; reducing bond strength between the bars and concrete. The reduction in bond is aggravated further due to the undesirable change in the mechanical properties of the surface polymer resin upon heating. Accordingly, two types of failure modes were noticed. The first was represented in pullout of the bar due to concrete splitting with radial cracking along the embedded length of the bar. When the bond strength is lower than the splitting tensile strength of concrete, pullout of the bars occurs due to the abrasion of the exterior surface of the bars that is rather weak. The first mode is expected to be predominant in pullout specimens subjected to temperatures lower than the glass transition temperature (T_g) of the FRP bar; whereas the second is most probably to happen in specimens subjected to temperatures higher

than the glass transition temperature (T_g) (Lublóy et al., 2005; Galati et al., 2006; Rafi et al., 2007; Bai et al., 2007b; Bellakehal et al., 2014).

4.5.2(b) Bond stress versus slip relationship

The above discussion explained the clear degradation in the bond characteristics of FRP bars upon exposure to varying exposure temperatures. Fig. 4.13 through Fig. 4.16 demonstrate that the change in the drawn bond stress versus slip curves was affected by both the type of the bar and exposure temperature. In general the curves of the bond stress versus slip pertaining to GFRP and BFRP experience limited linearity with noticeable softening at temperatures greater than 23°C. The slope of the ascending portion of the bond stress versus strain curves was reduced by exposure temperature, accompanied with reduction in maximum bond stress. As was expected, the CFRP and steel bars maintained high bond with concrete up to 250°C and 325°C, respectively, beyond which the corresponding bond stress versus slip curves tend to show noticeable softening, as shown in Fig 4.16.
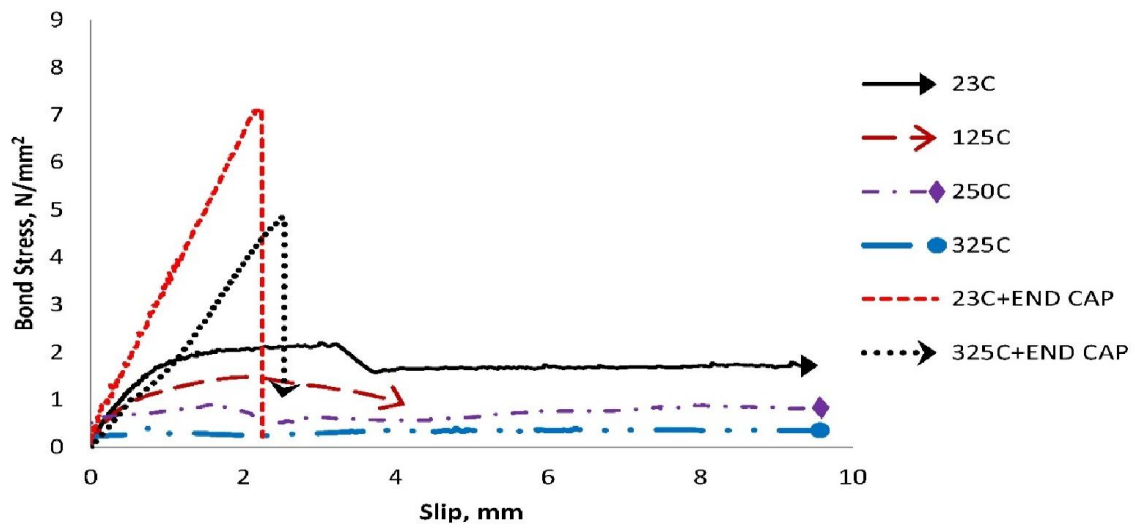
Figure 4.13: Typical bond stress-slip curves of pullout specimens with GFRP bars subjected to different temperatures
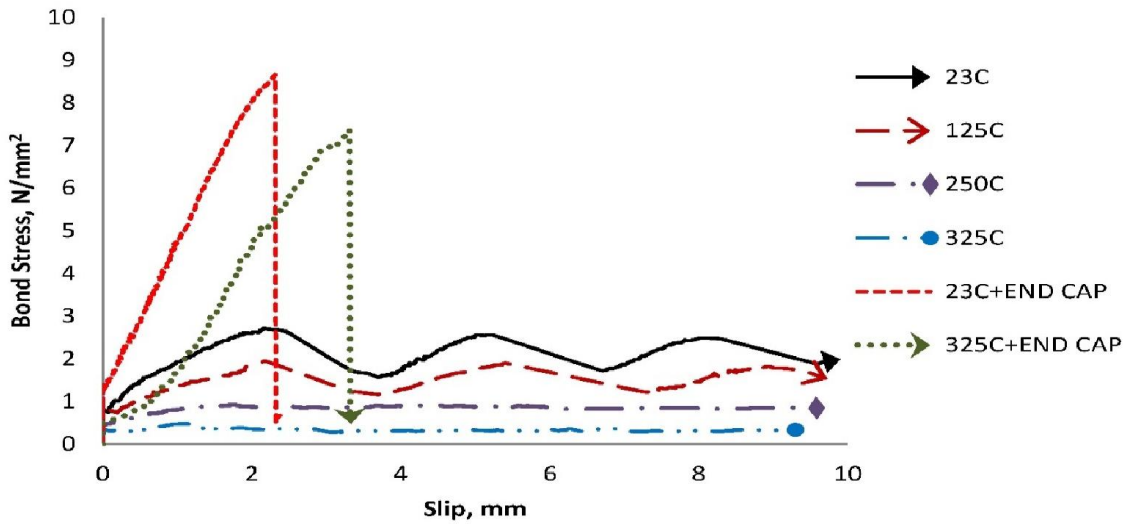
Figure 4.14: Typical bond stress-slip curves of pullout specimens with BFRP bars subjected to different temperatures
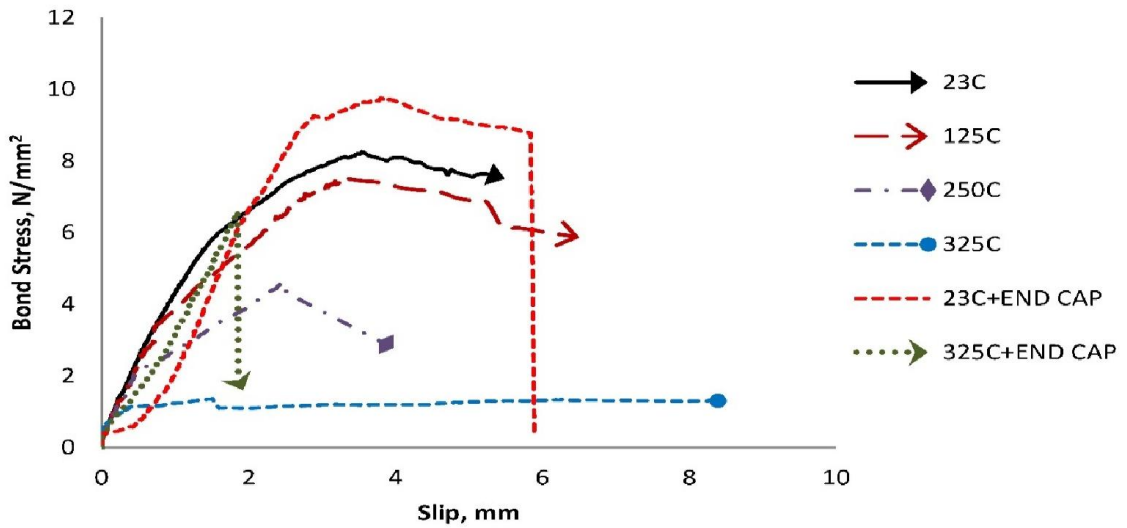
Figure 4.15: Typical bond stress-slip curves of pullout specimens with CFRP bars subjected to different temperatures
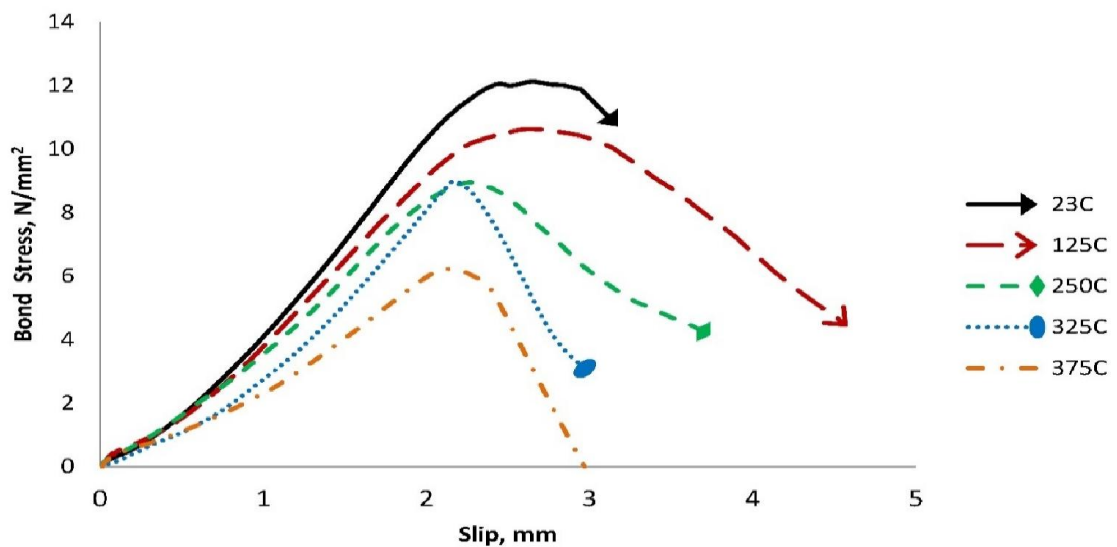
Figure 4.16: Typical bond stress- slip curves of pullout specimens with steel bars subjected to different temperatures

4.5.2(c) Characteristics of bond stress versus slip curves

The bond characteristics of the different pullout specimens are summarized in Table 4.4; representing the average of three specimens while the bond characteristics of all triplicate pullout specimens were summarized in Tables A-6 through A-9, of Appendix A. As indicated earlier, the different characteristics were affected by both the type of reinforcement bar as well as the exposure temperature.

Among the FRP bars pullout specimens, the CFRP ones showed the highest residual bond strengths with concrete when exposed to temperatures of (125, 250 and 325°C) at values of (84%, 56.4% and 18.5%) followed by those of BFRP and GFRP at (78.2%, 39.1%, 21.1) and (72.6%, 49.8%, 20.8), respectively. The corresponding slip values at maximum bond stress were the highest for pullout specimens with CFRP bars followed, in sequence, by BFRP and GFRP at (3.028, 2.224, and 1.607 mm), (2.158, 1.962, and 0.909 mm), and (2.060, 1.892, and 1.048 mm), respectively.

As expected, the steel bars showed the best performance among all bars and sustained higher temperature exposures while maintaining satisfactory bond. The residual bond strengths of pullout specimens with steel bars were (94.5%, 80%, 72.8% and 69.2%) at exposure temperatures of (125, 250, 325 and 375°C), respectively. The corresponding slip at maximum stress showed close values to those of the CFRP bars with values of (2.74, 2.28, 1.93 and 2.62 mm), respectively. The slip values of steel bars were lower than those of GFRP and BFRP at the same load level due to stronger bond behavior of specimens with steel bars.

4.5.2(d) Bond stress versus slip relationship of FRP bars with end cap anchorage

Figures 4.13 through 4.15 show that the use of end cap to anchor different FRP bars had contributed towards improving the bond characteristics substantially. The

curves show linear behaviour without a softening pattern up till failure contrary to the

case without end cap anchorage. This suggests that the applied anchorage technique

was very effective in promoting bond strength.

Table 4.4: Characteristics of bond stress versus strain curves for pullout specimens
with different bars and exposure temperatures

Bar Type	Temp.	F_u	SAF	BE	UBS	SABS	RUBS/UBS
	°C	kN	mm	mm	MPa	mm	
GFRP	23	6.328	4.022	1.282	2.014	2.740	100%
	125	4.593	3.038	0.977	1.462	2.060	72.6%
	250	3.150	2.627	0.735	1.003	1.892	49.8%
	325	1.316	1.384	0.336	0.419	1.048	20.8%
	23+EC	21.055	6.753	4.265	6.702	2.488	332%
	325+EC	15.654	6.438	3.997	4.983	2.441	247%
BFRP	23	8.256	3.635	1.197	2.628	2.438	100%
	125	6.453	3.136	0.978	2.054	2.158	78.2%
	250	3.227	2.496	0.534	1.027	1.962	39.1%
	325	1.741	1.319	0.320	0.554	0.999	21.1%
	23+EC	27.062	6.332	3.924	8.614	2.407	328%
	325+EC	21.016	7.472	3.868	6.690	3.605	255%
CFRP	23	26.198	5.380	2.101	8.339	3.279	100%
	125	22.007	4.943	1.915	7.005	3.028	84%
	250	14.765	3.626	1.402	4.700	2.224	56.4%
	325	4.844	2.177	0.570	1.542	1.607	18.5%
	375	2.719	2.729	0.462	0.865	2.267	10.4%
	23+EC	28.079	6.056	2.252	8.938	3.805	107.2%
	325+EC	21.830	4.513	2.570	6.949	1.943	83.3%
Steel	23	35.54	4.45	0.99	11.31	2.85	100%
	125	33.59	3.79	1.05	10.69	2.74	94.5%
	250	28.45	3.16	0.87	9.06	2.28	80.0%
	325	25.87	2.71	0.79	8.24	1.93	72.8%
	375	24.59	3.35	0.73	7.83	2.62	69.2%

F_u: maximum measured force, SAF: stroke at maximum force, BE: bar elongation, UBS: bond
strength, SABS: slip at maximum bond strength, RUBS: residual ultimate bond strength, EC:
end cap

4.5.2(e) Characteristics of bond stress versus slip curves for FRP bars with end cap anchorage

The bond characteristics provided in Table 4.4 show that the benefit from using end cap anchorage was the highest in pullout specimens with GFRP followed by BFRP and CFRP. Upon the use of end cap anchorage, the corresponding residual bond strengths at (23°C and 325°C) were (332% and 247%), (328% and 255%) and (107%, 83%), respectively. The slip at maximum stress showed limited changes at room temperature upon the use of the end caps yet was significantly increased when anchorage was applied to pullout specimens heated to 325°C. Upon the use of end cap anchorage, the percentage increase in slip at maximum stress for heated pullout specimens with GFRP, BFRP and CFRP were (133%, 260% and 21%), respectively.

4.5.3 Failure modes of pull-out specimens

The pullout specimens with GFRP and BFRP failed due to the damage and shearing-off of the surface matrix layer from the core of the slipped bars as shown in Fig 4.17a. After breaking the pullout specimens, the residue of the rebar's surface polymers was seen on the concrete whereas no residue of concrete was seen on the bar's surface. The pullout specimens, tested after exposure to 325°C, showed a high slip value at a low load level indicating that the bond between the FRP bars and concrete was almost damaged whereas the pullout specimens with GFRP and BFRP, which were heated to 375°C, were totally damaged, hence were not tested.

Pullout failure of unheated specimens with CFRP bars was accompanied by cone failure as shown in Fig. 4.17b. Upon heating, the sand-coating layer of the carbon bar peeled off when the shear strength at the interface between the coating layer and bar core was less than the shear strength of the concrete cover, causing a damage in the bond between the carbon bars and the surrounding concrete.

A sudden splitting concrete failure was noticed in the pullout specimens with steel bars accompanied with the formation of 2 to 4 splitting cracks along the embedded length where the steel bar ribs remain un-damaged. This splitting failure occurred because the bond strength exceeded the splitting tensile strength of the concrete which was clearer in the case of heated specimens due to effect of high temperatures in reducing the splitting tensile strength of concrete

After reaching the maximum bond stress for pullout specimens with FRP/steel bars, the slip continued with gradual reduction in the bond stress whereas a sudden failure was noticed in the case of specimens with end capped FRP bars.

| (a) Pullout slip failure mode | (b) Concrete cone failure mode |

(c) Concrete splitting with radial cracks failure mode

Figure 4.17: Different failure modes of pullout tests

4.6 Flexural Performance of FRP-RC and steel-RC beams

The flexural behavior and the characteristics of load versus mid-span deflection of concrete beams, reinforced with FRP and steel bars and tested before and after exposure to 500°C, are discussed in details in the following sections.

4.6.1 Load deflection diagram of RC beams with FRP bars

Due to the linear elastic nature of FRP bars, the experimental load deflection curves of FRP-RC beams consist mainly of two main linear segments followed by a nonlinear segment prior to failure as shown in Fig.4.18. The first linear segment represents the un-cracked concrete section where the behavior of the concrete is still linear. The second linear segment of the curve starts exactly after the first cracking of concrete where it transforms from the linearity to non-linearity while the FRP bars still in linear behavior. At certain point prior to ultimate load, cracked concrete shows unreasonable nonlinear behavior which reflects on the behavior of the FRP-RC beams and the nonlinearity become more visible up to failure.
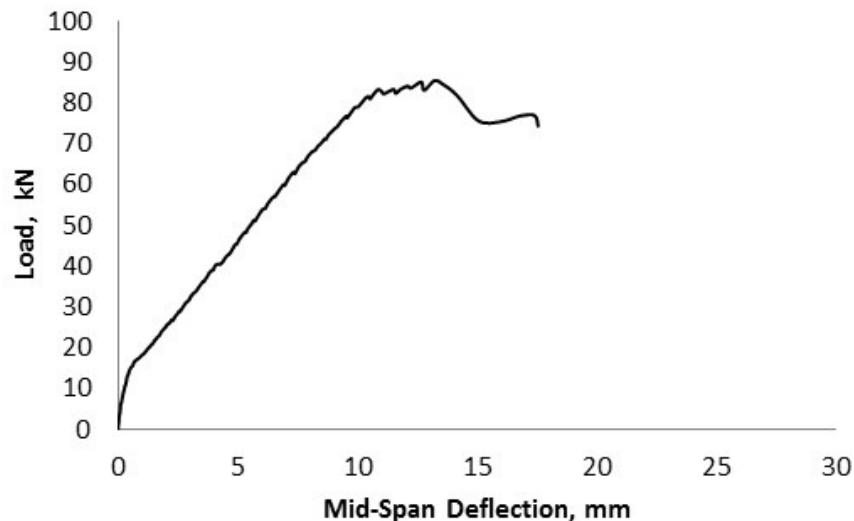
Fig. 4.18: Typical load-deflection behavior of FRP-RC beams

Below the cracking load, the beam's deflection is related directly to the beam's gross moment of inertia which depends on the beam's overall cross sectional

dimensions (width and height) therefore, all beams of similar size and reinforcement should have similar first linear part of the curve.

Results of load versus mid-span deflection response of triplicate beams with different FRP bars, with and without end cap anchorage, before and after exposure to 500°C were obtained and presented in Figs. A.10 through A.12, Appendix A. Accordingly, typical load versus mid-span deflection diagrams representing beams with different FRP bars at similar exposure conditions were prepared to study and compare their flexural performance. Fig. 4.19 presents the typical load-deflection response of GFRP, BFRP, and CFRP reinforced concrete beams with and without end caps before and after exposure to 500°C.

The experimental load-deflection diagrams of FRP-RC beams without end cap anchorage showed a relatively high initial deflection value at low level of applied load, occurred due to expected initial slippage of the FRP bars leading to reduce the beam's stiffness and increase the deflection. Sudden drops in the applied load, accompanied with increase in the mid-span deflection, were noticed concurrent with the initiation of each new crack. These drops in load were more visible in the case of GFRP and BFRP than CFRP.

Upon exposure to 500°C, the FRP reinforced concrete beams suffered from a non-linear load-deflection response accompanied with a dramatic increase in mid-span deflection at low load levels due to the loss of bond between the FRP bars and the surrounding concrete. The effect of high temperature on the behavior of FRP-RC beams was much clearer in the GFRP and BFRP-RC beams compared with the CFRP-RC beams due higher negative effect of temperature on the bond strength of the GFRP and BFRP bars.
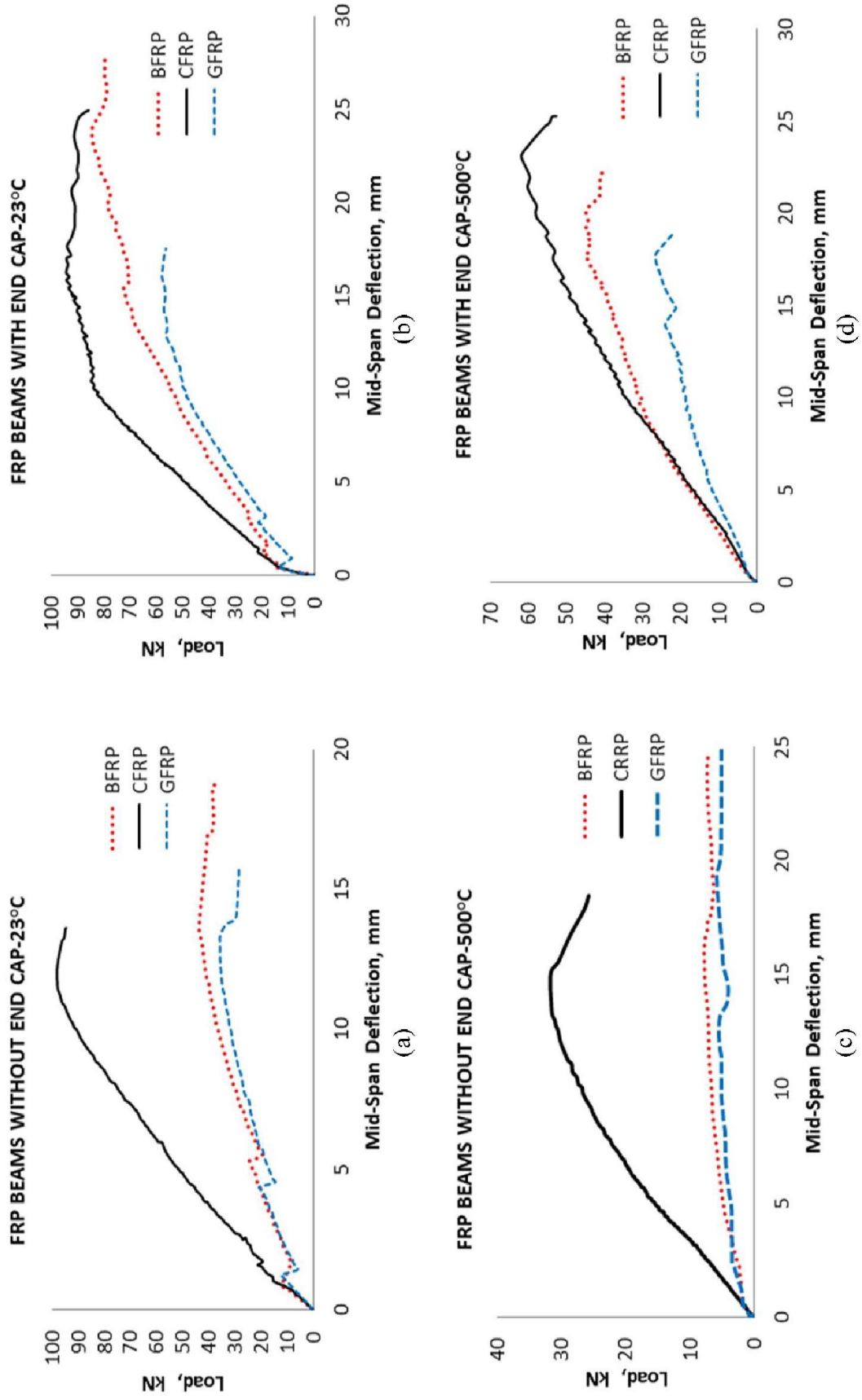
Fig.4.19: Typical load-deflection response of FRP beams with and without end caps before and after exposure to 500°C

By using end cap anchorage, the linearity of load-deflection behavior of FRP-RC beams was improved with higher load capacity and lower number of load drops. The use of end cap anchorage had prevented the occurrence of initial slippage, hence increasing the beams stiffness and reducing the expected initial mid-span deflection especially in the cases of end capped BFRP and CFRP reinforced concrete beams. Under high temperature exposure, the use of end cap anchorage in the FRP-RC beams had improved their load-deflection behavior with higher load capacity and better linearity.

4.6.2   Load deflection diagram of RC beams with steel bars

Typical load-deflection curves of steel-RC beams tested before and after exposure to 500°C are shown in Fig. 4.20. Load versus mid-span deflection diagrams of triplicate steel reinforced concrete beams, before and after exposure to 500°C, were obtained and presented in Figs. A.13, of Appendix A. Characteristics of load-deflection curves of the steel-RC beams are discussed and compared with that of the FRP-RC beams in the following section.
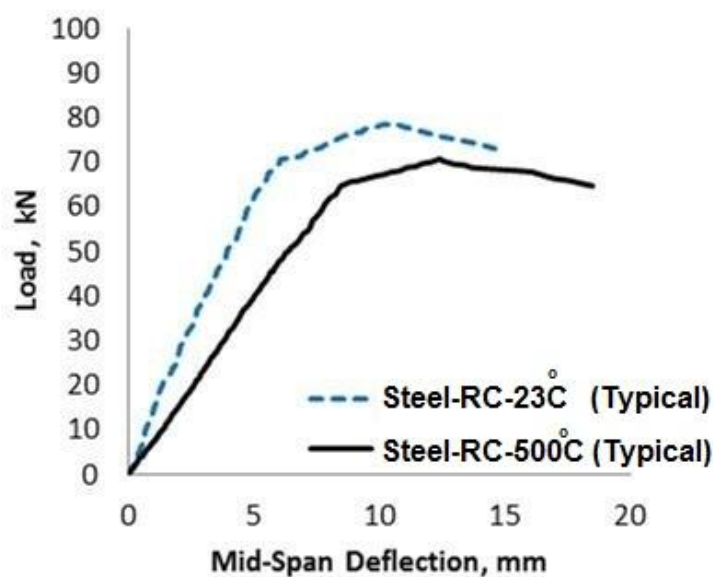
Fig.4.20: Typical load-deflection curve of steel-RC beams before and after exposure to 500°C

4.6.3 Characteristics of load deflection diagram of RC beams with different bars

The characteristics of load versus mid-span deflection of beams with different bars at different exposure conditions are summarized in Table 4.5; representing the average of three specimens while the characteristics of all triplicate beams are presented in Tables A-10 through A-12, of Appendix A. These characteristics, including ultimate load capacity, stiffness, mid-span deflection and ductility, were affected by different factors such as type of reinforcement bar, exposure temperature and usage of end cap anchorage. Discussions are presented in the following sections.

4.6.3(a) Ultimate load capacity

Pullout test results showed that the CFRP bars had the highest bond strength with concrete compared with that of the other reinforcement types which reflected positively on their flexural performance. Hence, concrete beams with CFRP bars, tested at ambient temperature, had the highest ultimate load capacity followed, in sequence, by beams with steel, BFRP and GFRP bars where the measured ultimate load capacity of beams with CFRP, steel, BFRP, and GFRP bars was 89.9, 76.1, 38.6 and 32.6 kN, respectively.

The measured ultimate load capacity was improved upon the use of bonded end caps in BFRP, and GFRP reinforced concrete beams, hence these beams carried much higher loads than similar beams without end caps whereas no change was noticed in the case of CFRP beams due to the primary good bond between CFRP bars and concrete. The measured ultimate load capacity of BFRP, GFRP and CFRP beams with end caps was 80.2, 58.4, and 89.8 kN, which represent 207.7%, 179%, and 100% of that of corresponding beams without end caps, respectively.

Upon exposure to high temperatures, the mechanical properties of FRP bars and their bond with concrete were deteriorated dramatically, especially in the case of GFRP and BFRP bars, which reflected negatively on the flexural performance of concrete beams with FRP bars when exposed to 500°C. The degradation of the GFRP and BFRP beams' load capacity was more pronounced than that of the CFRP beams where the average measured ultimate load capacity of the BFRP, GFRP and CFRP beams, exposed to 500°C, were reduced to 7.26, 6.85, and 31.9 kN, which represent 18.8%, 20.9%, and 35.5% of that of the control beams, respectively. Due to minor effect of heating on the tensile strength of steel bars and bond between steel bars and concrete, minor reduction of 8.8% in the ultimate load capacity from 76.1 to 69.4 kN was measured upon heating to 500°C.

With the use of the bonded end caps, the performance of the heated FRP beams was improved noticeably where the ultimate load capacity of the heated BFRP, GFRP and CFRP beams was increased to 47.3, 27.8, and 60.8 kN, respectively, which is approximately 122.6%, 85.1%, and 67.6% of that of control beams tested at ambient temperature without end caps. By comparing the results of heated FRP beam before and after using end cap anchorage, the ultimate load capacity of the end-capped BFRP, GFRP, and CFRP was increased very significantly to 652%, 405%, and 190% of that of heated beams without end caps, respectively. This can be explained that, at early stage, the bond between heated FRP bars and concrete exceeded its deteriorated maximum bond strength value, hence the tensile forces were not transferred between the concrete and reinforcement leading to early failure. By using steel end caps, the caps started their role in transferring these tensile forces immediately after losing the bond between the bars and concrete. When the tensile forces in the bars reached the allowable bond forces capacity of the bonded end caps,

bond failure happened leading to the failure of the beams. Comparison between load-deflection diagrams for different cases of concrete beams with similar reinforcement bars is presented graphically in Fig. 4.21.
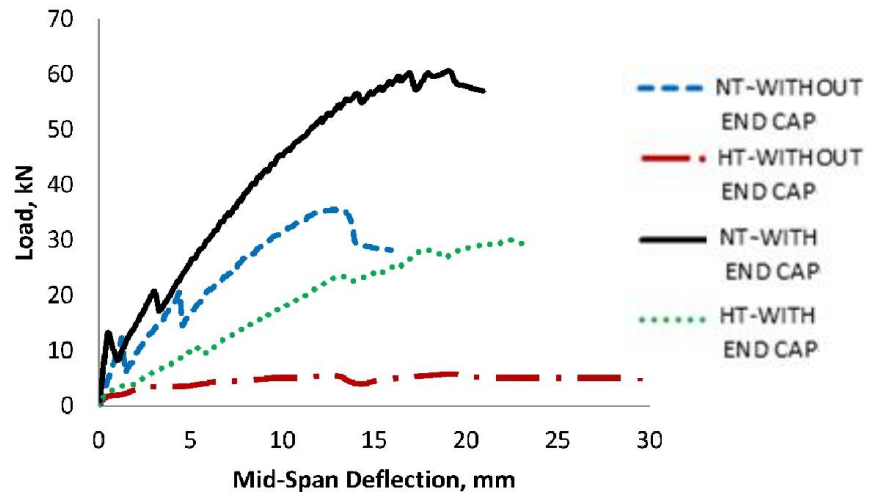
(a) GFRP beams
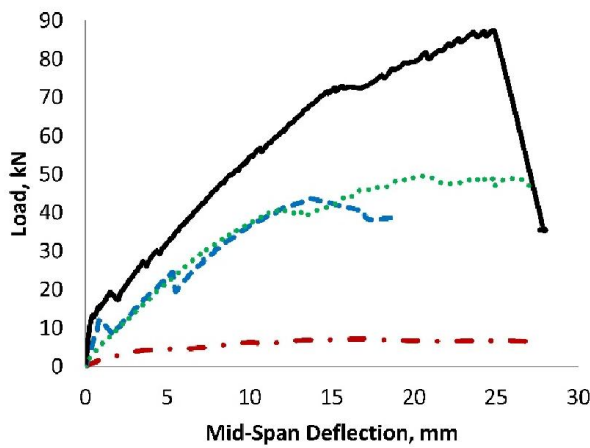
(b) BFRP beams
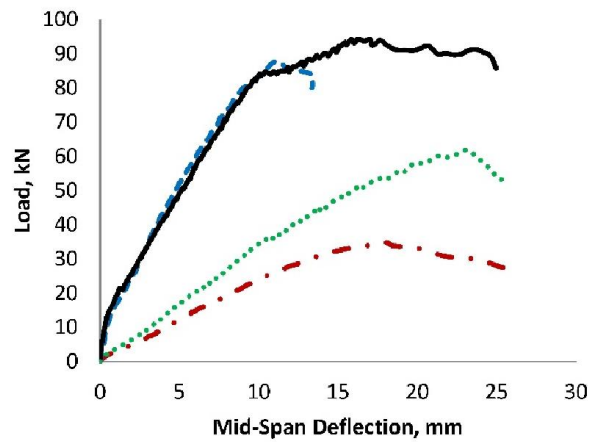
(c) CFRP beams

Fig.4.21: Typical load-deflection curves pertaining to different FRP-RC beams (with and without steel end caps) tested in flexure before and after exposure to 500°C

Table 4.5: Characteristics of load-deflection diagram for RC beams with different FRP bars, without and with end caps, before and after heating to 500°C

	$P_{exp-ult}$	$\Delta_{exp-ult}$	P_{exp-cr}	Δ_{exp-cr}	Δ_{exp-s}	I.S.	$S.2^{nd}$	S.R	E_{total}	μ	ODF
GFRP-N.T.-Without End Cap	32.638	13.280	10.762	0.804	6.554	12543	4370	65%	285.6	2.430	3.14
GFRP-N.T.-With End Cap	58.438	18.244	13.297	0.474	4.238	28119	5601	80%	711.7	3.010	8.91
GFRP-H.T.-Without End Cap	6.853	19.969	1.501	0.376	N.A.	4071	853	79%	90.80	4.708	N.A.
GFRP-H.T.-With End Cap	27.786	19.802	3.596	0.496	6.196	7270	2056	72%	334.0	1.558	6.30
BFRP-N.T.-Without End Cap	38.569	11.983	11.938	0.923	6.860	13440	3892	71%	279.8	1.954	3.01
BFRP-N.T.-With End Cap	80.207	23.533	13.990	0.462	3.300	30304	6011	80%	1266.5	2.781	8.13
BFRP-H.T.-Without End Cap	7.262	15.860	1.620	0.490	N.A.	3277	1428	56%	84.70	3.489	N.A.
BFRP-H.T.-With End Cap	47.348	20.430	2.709	0.391	4.020	7134	3613	49%	602.0	1.547	8.72
CFRP-N.T.-Without End Cap	89.973	11.437	13.667	0.802	2.728	18147	9260	48%	609.7	1.291	8.99
CFRP-N.T.-With End Cap	89.748	15.679	13.946	0.536	2.736	32159	7370	76%	955.0	1.886	9.28
CFRP-H.T.-Without End Cap	31.969	16.418	1.584	0.413	9.513	3851	2087	46%	312.3	1.265	3.17
CFRP-H.T.-With End Cap	60.805	24.647	2.705	0.714	7.505	4678	2665	43%	859.3	1.282	7.96
Steel N.T.	76.137	11.123	20.667	1.376	1.587	15888	11496	26.55%	625.5	N.A.	1.897*
Steel H.T.	69.420	13.686	2.919	0.321	2.730	9990	8247	15.79%	632.5	N.A.	1.713*

$P_{exp-ult}$, experimental ultimate load, $\Delta_{exp-ult}$, measured mid-span deflection at ultimate load, P_{exp-cr}, experimental cracking load, Δ_{exp-cr}, measured mid-span deflection at cracking load, I.S., initial stiffness, S.2nd, stiffness after cracking, S.R. Reduction in stiffness, Δ_{exp-s}, mid-span deflection at theoretical service load, E_{total}, total absorbed energy, μ, ductility index, ODF, overall ductility factor, * based on deflection only, N.A., not available

4.6.3(b) Stiffness

As mentioned previously, the load deflection curves of FRP-RC beams consist mainly of two main linear segments followed by a nonlinear segment prior to failure. The slope of the first linear segment of the load-deflection curve represents the initial stiffness of the RC beam (k). After cracking, the slope of the second linear portion of the curve was reduced indicating that the stiffness of the RC beams reduced after cracking. The initial stiffness, stiffness after cracking and the stiffness reduction percent after cracking were summarized in Table 4.5; representing the average of three specimens.

The highest initial stiffness of control FRP beams (without end caps), tested at ambient temperature, was noticed in CFRP beams followed, in sequence, by BFRP and GFRP beams at 18147, 13440, and 12543 kN/m which were reduced after first cracking by 48%, 71% and 65%, to 9260, 3892 and 4370 kN/m, respectively. The lowest reduction in stiffness after first cracking was found in steel-RC beams with 27% reduction from 15888 kN/m to 11496 kN/m.

Adding steel end caps to the ends of FRP bars had improved the initial stiffness of the GFRP, BFRP and CFRP RC beams to 28119, 30304 and 32154 kN/m which represents 224%, 225% and 177% of that of the corresponding control beams, respectively. The improved initial stiffness of the FRP-RC beams with end was approximately in the range of 28,000 to 32000 kN/m. However, the CFRP-RC beams had the highest initial stiffness, they had the lowest increase in stiffness after using the end caps. However the use of end cap anchorage had improved the initial stiffness of the GFRP, BFRP and CFRP beam, their stiffness after cracking was reduced by 80%, 80% and 77%, to 5601, 6011, and 7370 kN.m, respectively.

Upon exposure to 500°C, all RC beams suffered from degradation in their stiffness, where the initial stiffness of the heated GFRP, BFRP, CFRP and steel -RC beams was 4071, 3277, 3851 and 9990 kN.m representing 32.5%, 24.4%, 21.2%, and 62.8% of their control beam's stiffness, respectively. After cracking, they suffered from 79%, 56%, 46% and 16% reduction in their stiffness to values of 853, 1428, 2087 and 8247 kN.m, respectively.

Effect of using steel end caps on the stiffness of the heated FRP-RC bars was highly clear in both GFRP and BFRP-RC beams with smaller effect on the CFRP-RC beams. Using end cap anchorage had increased the stiffness of the heated GFRP, BFRP, and CFRP RC beams from 32.5% to 58%, 24.4% to 53%, and 21.2% to 26% of their control beam's stiffness, respectively. After cracking, the stiffness of the heated GFRP, BFRP, and CFRP beams with end cap anchorage had decreased from 7270 to 2056, 7134 to 3613, 4678 to 2665 kN/m, representing reduction percentages of 72%, 49% and 43%, respectively.

4.6.3(c) Mid-span deflection at ultimate load

According to the load-deflection curves presented in Fig. 4.20 and their characteristics summarized in Table 4.5, the FRP reinforced concrete beams showed larger mid-span deflections than that of the steel reinforced concrete beams at same load level due to the lower modulus of elasticity and bond strength of the FRP bars compared with that of the steel bars. The mid-span deflections of the GFRP, BFRP, CFRP and steel reinforced concrete beams, measured at ultimate load capacities of 32.64, 38.6, 89.97 and 76.13 kN were 13.28, 11.98, 11.44 and 11.13 mm, respectively.

The effect of adding steel end caps to the ends of the FRP bars was more pronounced in beams with GFRP and BFRP bar where both of ultimate load capacity

and its corresponding mid-span deflection were significantly increased. The mid-span deflection of the GFRP, BFRP, and CFRP beams was increased by 37.5%, 96.4%, and 37% to reach 18.25, 23.53, and 15.68 mm measured at ultimate load capacities of 58.4, 80.2 and 89.8 kN, respectively.

Upon exposure to high temperature, the FRP bar's modulus of elasticity and the bond between FRP bars and concrete were affected negatively, resulting in reducing the stiffness of the beams and thus increasing the mid-span deflection at low load levels. All heated beams failed at small loads simultaneous with large deflections. Upon exposure to 500°C, mid-span deflection of the GFRP, BFRP, and CFRP beams was increased by 50.4%, 32.4%, and 43.5% to reach 19.97, 15.86, and 16.42 mm measured at low load capacities of 6.85, 7.26 and 31.97 kN, respectively.

Adding steel end caps to the ends of FRP bars showed a similar effect on the flexural performance for both beams tested before and after exposure to 500°C. The ultimate load capacity of the heated GFRP, BFRP and CFRP-RC beams and its corresponding mid-span deflection of were increased to (27.79, 47.35 and 60.8 kN) and (19.8, 20.43 and 24.65 mm), respectively, after using the end cap anchorage.

4.6.3(d) Mid-span deflection at service load (serviceability)

Serviceability is defined as the ability of the structure to be remain useful. Serviceability includes criteria's such as deflection, cracking width and fire resistance. Common international codes defined the serviceable deflection limit of ordinary usage floor beams as L/240. As per Veysey and Bischoff, (2011), FRP-RC beams satisfy the deflection limit of L/240 at service load levels range between 35 to 45% of the member capacity. Therefore, in the present study, the service load P_s was taken as 35% of the theoretical member capacity. The mid-span deflections, at

service load of 35% of theoretical ultimate load of each beam, were measured and presented in Table 4.5.

Beams with CFRP bars showed a lower serviceable mid-span deflection than BFRP and GFRP beams due to higher stiffness of CFRP bars than the others. Adding steel end caps to the ends of the CFRP bars had a negligible effect on the serviceable mid-span deflection of the CFRP-RC beams whereas significant reductions of 35.3% and 51.9% was noticed in that of the BFRP and GFRP beams, respectively, upon using the end cap anchorage. The mid-span deflections at service load of control GFRP, BFRP, and CFRP-RC beams were 6.55, 6.86, and 2.728 mm, which were decreased to 4.238, 3.30, and 2.736 mm by adding the end caps, respectively.

Upon exposure to 500°C, the maximum load capacities of GFRP and BFRP-RC beams were quite significantly decreased to levels lower than the defined service loads, therefore their serviceable mid-span deflection could not be measured. Adding steel end caps to the ends of the GFRP and BFRP bars had improved the maximum load capacities of their heated beams to values greater than the defined service load, yet decreased their serviceable mid-span deflections to 6.19 and 4.02 mm which represents 94.5% and 58.6% of their control beam's deflections, respectively. Upon exposure to 500°C, the serviceable mid-span deflection of the CFRP beams was highly increased by 250% to reach 9.51 mm which was decreased to 7.51 mm upon using steel end caps. Although the CFRP-RC beams showed a stiffer response than other the FRP-RC beams, the CFRP beams with end caps showed the highest mid-span deflection at service load, due to the higher defined service load of the CFRP beams compared with the other FRP beams.

Beams with steel bars, tested before and after exposure to 500°C, showed lower serviceable mid span deflections than that of the FRP-RC beams due to the higher

127

stiffness of the steel RC beams. Upon exposure to 500°C, the measured serviceable mid-span deflection of the steel-RC beams was increased from 1.587 to 2.73 mm due to the effect of heating on reducing beam's stiffness.

4.6.3(e) Ductility

Ductility is the term used to describe the ability of a material to deform plastically and absorb energy during deformation. Several forms of ductility are available like curvature, energy ductility, rotational and deformation ductility. In this research the energy ductility and deformation ductility are reported.

The traditional ductility definition of steel-RC elements is the ratio of post yield deformation to the yield deformations which can't be applied to FRP-RC elements due to the linear elasticity of the FRP bars. Energy based approach and overall ductility factor approach are used to describe the ductility of FRP-RC beams.

Energy based approach, defined the ductility index, μ, for FRP-RC beams as the ability to absorb the inelastic energy without losing the load capacity and it can be calculated according to Eq. 2.1 using the elastic and total absorbed energy, defined by Naaman and Jeong , (1995) as shown in Chapter 2- Fig.2.1; the total energy is the total area under the load-deflection curve while the elastic energy is the area of right triangle formed at failure load with hypotenuse slope equal to weighted average slope of the two initial straight lines of the load deflection curve. The hypotenuse slope (S) depends on the selection of P1 and P2 and the slopes S1 and S2. In some cases, it was difficult to idealize the load-deflection curves into three segments as per the typical curve presented by Naaman and Jeong, (1995), therefore some errors were expected in finding the points P1 and P2 and their corresponding slopes S1 and S2.

The overall ductility factor was defined by Mufti et. al, (1996) as the product of the strength factor and the deformability factor; where the deformability factor is the

ratio of ultimate deflection to the deflection when the maximum concrete compressive strain equal 0.001 while the strength factor is the ratio of the ultimate moment to the moment when the maximum concrete compressive strain equal 0.001.

Mufti et. al, (1996) considered the concrete compressive strain of 0.001 as the strain at which the inelastic deformation of concrete starts. Service strain limit of 0.001 is accepted for intact concrete, while the strain value at which heat-damaged concrete starts its inelastic deformation is much higher than 0.001. The applied load corresponded to 0.001 concrete compressive strain was found experimentally to be 40-50% of the theoretical ultimate load capacity of unheated beams while the concrete compressive strain of heated beams corresponds to 40-50% of its theoretical ultimate load capacity was found in the range of 0.0016 to 0.0026. An average strain value of 0.0021 was used instead of 0.001 as strain limit in the case of the heated beams. Overall ductility factors are given by Eq. 2-3 for the control beams and Eq. 4-1 for the heated beams

$$\text{Modified Overall Ductility Factor of Heated Beams} = \frac{\Delta_{ult}}{\Delta_{\varepsilon_c=0.0021}} \times \frac{M_{ult.}}{M_{\varepsilon_c=0.0021}} \quad (4.1)$$

The results of the two methods were summarized in Table 4.5; representing the average of three specimens, while ductility results of all triplicate beams were presented in Tables A-15 through A-18, Appendix A. The two methods are widely different where the ductility indices computed using the energy methods were much lower than the overall ductility factors calculated using Mufti's method.

Minimum ductility index value of 4 is considered enough to have ductile failure mode as per Canadian Highways Bridge Design Code, while the New Zealand standards (NZS3101:2006) defined the perfect ductile failure mode occurred when a ductility index of more than 6 is obtained. Lower ductility means brittle performance at failure (sudden failure).

Energy method showed that the ductility indices for all FRP-RC beams tested at normal temperature were less than the lower limit of ductility (minimum 4) indicating that these FRP-RC beams failed in non-ductile mode. The GFRP -RC beams failed in a more ductile mode than the other FRP-RC beams where ductility indices of the GFRP, BFRP and CFRP-RC beams were 2.43, 1.954, and 1.291, respectively. Although the CFRP-RC beams have the lowest ductility index, they showed the highest absorbed total energy up to failure among the FRP beams where the average total absorbed energy for the GFRP, BFRP and CFRP-RC beams were 286, 280, and 610 kN.mm, respectively.

Adding end caps to the ends of FRP bars has improved significantly both the ductility indices and absorbed total energies of the GFRP, BFRP and CFRP beams to (3.01, 2.781 and 1.886) and (711.7, 1266.5 and 955.7 kN.mm), which represents (124%, 142%, and 146%) and (249%, 453%, and 157%) of that of the control beams, respectively. However the highest effect of using end caps on ductility index was noticed in CFRP-RC beams, they showed the lowest change in total absorbed energy.

Generally, upon exposure to high temperature, concrete suffers from a decrease in compressive strength accompanying with an increase in ductility, therefore a significant effect of high temperature on the ductility of FRP-RC beams was noticed. Upon exposure to 500°C, the ductility indices of the GFRP and BFRP were increased by 94% and 79% to reach 4.708 and 3.489, respectively, while a slight change from 1.291 to 1.265 was noticed in the case of the CFRP beams. Due to the major reduction in the load capacity of heated FRP beams, the total absorbed energy of the GFRP, BFRP and CFRP-RC beams had dropped to 90.8, 84.7, and 312.3 kN.mm, respectively, which represents 32%, 30%, and 51% of that of the control FRP-RC beams, respectively.

Using end caps in heated FRP-RC beams had improved their ultimate load capacity which in turn had increased the total absorbed energy, yet reduced their ductility indices due to the change of failure mode into sudden combined bond slip-shear failure. Upon using steel end caps, the ductility index of the heated GFRP, BFRP and CFRP beams were reduced to 1.558, 1.547 and 1.282 which represent 64%, 79% and 99% of that of the control FRP-RC beams while the total absorbed energies were increased by 17%, 115%, and 41% to reach 334.0, 602, and 859.3 kN.mm, respectively.

Based on energy method, the total absorbed energy of steel-RC beams was increased from 625.5 to 632.5 kN.mm upon exposure to 500°C due to the significant increase in mid-span deflection accompanied by small reduction in load capacity after heating which indicated that the behavior of the steel-RC beams is more ductile than that of the FRP-RC beams.

The overall ductility factor is more reasonable than the ductility index because it considered both the effect of load and deformation at ultimate condition. Also, the effect of using steel end caps on the ductility of FRP-RC beams were clearer in overall factor method than in energy method. The overall ductility factor method has confirmed the improvement of ductility of FRP-RC beams after using the steel end caps where the overall ductility factor of the control GFRP, BFRP and CFRP-RC beams was increased from (3.14, 3.01 and 8.99) to (8.91, 8.13 and 9.28) upon adding the end caps, respectively.

The overall ductility factor of the heated GFRP and BFRP-RC beams could not be calculated because the measured strain of concrete at failure was less than the defined strain limit of 0.0021 whereas that of the CFRP-RC beams was reduced by 65% from 8.99 to 3.17 upon heating to 500°C.

Contrary to the energy method, a significant improvement was noticed in the overall ductility factor of the heated GFRP and BFRP-RC beams upon using the steel end caps where the overall ductility factors increased to 201% and 290% of that of the control beams at 6.30 and 8.72, respectively. Upon using steel caps, the overall ductility factor of the heated CFRP-RC beams was increased from 3.17 to 7.96 which represents 89% of that of the normal temperature CFRP-RC beams without end caps.

Ductility indices of steel-RC beams, calculated according to the traditional displacement ductility method before and after exposure to 500°C, were 1.897 and 1.713, respectively, which are lower than 4, minimum limit of ductile behavior as per Canadian Highways Bridge Design code, which means that these steel-RC beams lacked the adequate ductility to resist larger displacement although these steel-RC beams have better ductility than FRP-RC beams. The ductility indices of both FRP and steel -RC beams can't be compared due to different methods of calculations.

4.6.4   Modes of failure, strains and cracking patterns

Tensile forces are transferred from the concrete to the rebar upon first cracking, which initiates in locations of higher tensile stress than concrete tensile strength, followed by a formation of additional cracks in other locations due to continues increase of stresses up to failure.

The Control beams with GFRP and BFRP bars failed due the breakdown of bond between FRP bars and concrete while the CFRP beams failed by shear. Upon bonding the ends of FRP bars with steel caps, the GFRP beams failed by concrete crushing while the BFRP and CFRP-RC beams failed in shear, at higher load capacities, due to the high concentration of concrete shear stresses at locations of loaded end caps which led to shear failure at the beam's ends.

When exposed to 500°C, all FRP beams failed at low load levels due to loss of bonds between the FRP bars and the surrounding concrete. Upon using steel end anchorage in heated FRP beams, load capacity was increased to higher levels followed by a sudden breakdown of bonds between bars and concrete in the case of the GFRP beams while a combined bond-shear failure was noticed in the BFRP and CFRP beams.

The steel-RC beams, before and after exposure to 500°C, suffered from steel bar's yielding before failing by concrete crushing.

The observed experimental failure modes are summarized in the Table 4.6 while detailed cracking patterns and failure modes for all beams are presented in the following sections.

Table 4.6: Observed modes of failure

Temp	End Cap	Observed Failure Mode			
		GFRP	BFRP	CFRP	Steel
N.T.	Without	B.S	B.S	S	S.Y
N.T.	With	C.C	S	S	N.A.
H.T.	Without	B.S	B.S	B.S.	S.Y
H.T.	With	B.S	B.S+ S	B.S+ S	N.A.

B.S, bond slip, C.C, concrete crushing, S, shear, S.Y, Steel yielding followed by concrete crushing, N.T., normal temperature, H.T, high temperature, N.A., not available

Typical curves of the applied loads versus strains of concrete and FRP bars were illustrated graphically in Figs 4.22 whereas all curves of triplicate specimens were presented in Figs. A.14 through A.17 of Appendix A. Strain readings of concrete and reinforcement at ultimate load capacities were summarized in Table 4.7, representing the average of three specimens, whereas results of all triplicate beams were presented in Table A.14, Appendix-A.

Table 4.7: Strain readings of concrete and different reinforcing bars at ultimate loads

Temp	End Cap	GFRP		BFRP		CFRP		Steel			
		ε_c x 10^{-6}	ε_f x 10^{-6}	ε_c x 10^{-6}	ε_f x 10^{-6}	ε_c x 10^{-6}	ε_f x 10^{-6}	ε_c x 10^{-6} (ult)	ε_s x 10^{-6} (ult)	ε_c x 10^{-6} (yield)	ε_s x 10^{-6} (yield)
N.T.	Without	1412	5419	1707	5075	2740	7144	5418	6910	2885	2996
N.T.	With	3346	10911	2689	10362	2805	6702	N.A			
H.T.	Without	1075	1644	1443	1869	3255	2835	6201	N.A	3279	2360
H.T.	With	4093	6103	3997	7556	4559	6952	N.A			

ε_f, FRP strain at ultimate load, ε_c, concrete strain at ultimate or yield load, ε_s, steel strain at yield or ultimate load N.T., normal temperature, H.T, high temperature

In control FRP-RC beams, a significant increase in reinforcement tensile strain was noticed at first cracking followed by an almost linear response up to failure; at which the measured tensile strain of FRP bars and concrete compressive strain were less than the FRP bar's ultimate tensile strain and concrete crushing strain, respectively, which confirmed that bond slip failure happened before reaching either concrete crushing or FRP rupture.

Adding the end caps to the ends had improved the bond between bars and concrete; hence improved the linearity of load versus tensile strain curves and increased the maximum tensile strain at failure. Upon exposure to 500°C, bonds between FRP bars and concrete were weakened, hence load versus tensile strain curves of the GFRP and BFRP beams suffered from high nonlinearity which was improved by adding steel end caps to the ends of the FRP bars. Contrary to the GFRP and BFRP beams, load-tensile strain relationship of the heated CFRP-RC beams showed good linear behavior up to failure.
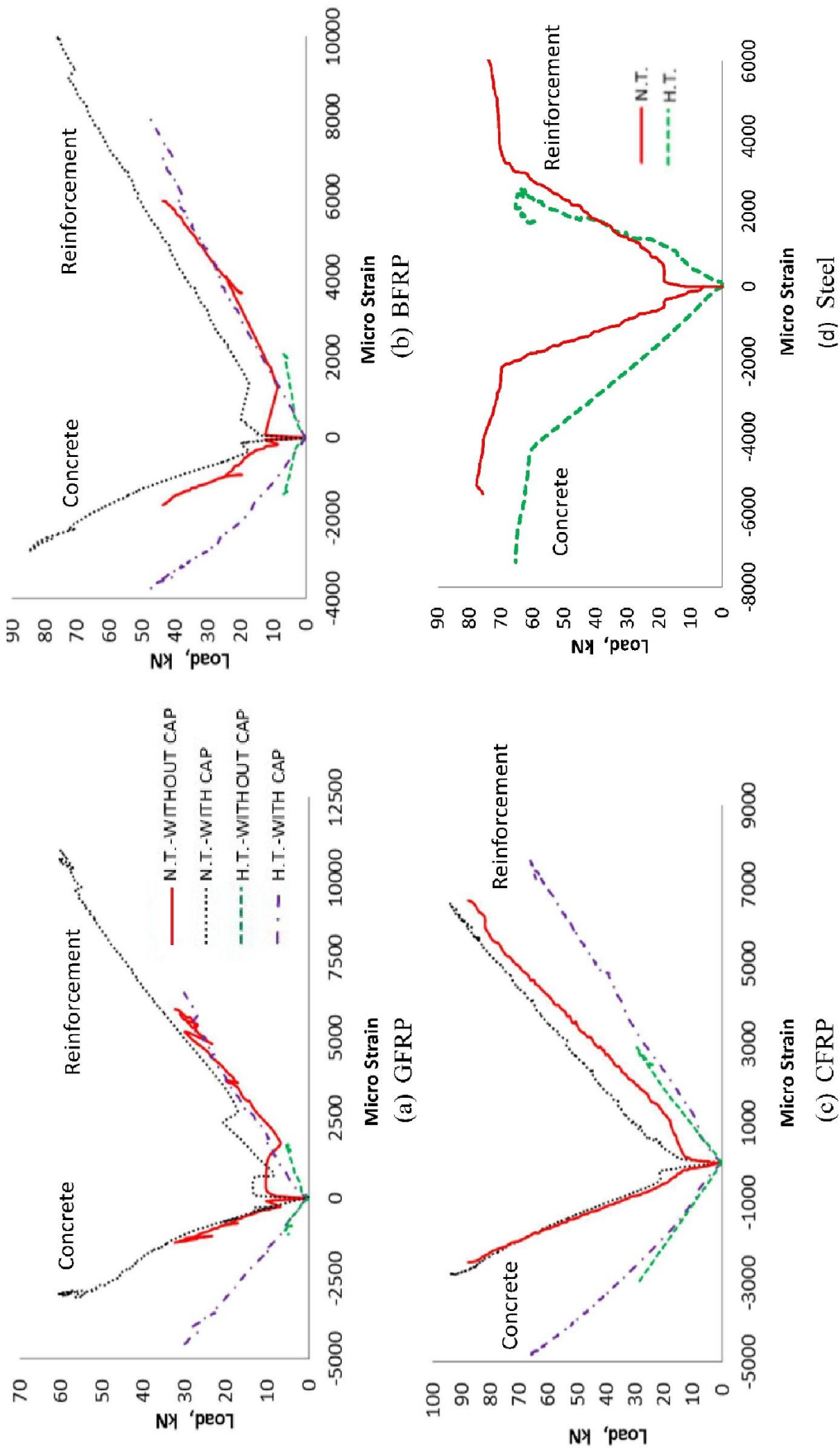
Fig 4.22: Typical curves of load versus strain in concrete/reinforcement in different RC beams, with and without end caps, tested under flexural before and after exposure to 500°C

135

4.6.4(a) Failure mode and cracking pattern of GFRP beam

    a) Control GFRP beams

As shown in Fig.4.23, the first flexural crack of the control GFRP beams initiated in the maximum tension zone, the middle third of the beam, at average cracking load of 10.7 kN, which was extended towards the compression zone upon increasing of the applied load, followed by the formation of two or three new main flexural cracks. A sudden drop in load was noticed concurrently with the formation of further new flexural crack. Before reaching the ultimate load, the cracks were widening rapidly with small increase in load up to failure, which then the cracks width and deflection increased with no increase in load.

The average measured strain of concrete and reinforcement at ultimate load was 1412×10^{-6} and 5419×10^{-6}, respectively, indicating that a bond slip failure happened before reaching the concrete crushing strain (3000×10^{-6}) or the GFRP bars rupture strain (21500×10^{-6}).

    b) GFRP Beams with end caps at normal temperature

With the use of steel end caps, the cracking load was increased by 23.3% to 13.2 kN. With increasing load, the beams with end-capped GFRP bars were initially cracked in the middle third zone then the crack extended towards the compression zone accompanied with the formation of a new flexural crack. The two main flexural cracks extended deeply towards the top compression zone until the occurrence of concrete crushing failure. Failure mode was purely flexural failure as shown in Fig. 4.24. The average measured strain of concrete and reinforcement at ultimate load was 3346×10^{-6} and 10911×10^{-6}, respectively, which confirmed that the failure happened

after exceeding the concrete crushing strain (3000×10^{-6}) and before reaching the GFRP bars rupture strain (21500×10^{-6}).

c) GFRP beams, exposed to 500°C

When heated to 500°C, the cracking load was dramatically decreased by 86% where cracking was initially formed in the middle third zone at low load of 1.5 kN, immediately followed by the formation of two new flexural cracks, located below the loading points, at approximate load of 3.0 kN. These locations were mainly considered the weak points at which bond failure starts, refer to Fig. 4.25. A sudden drop in load was noticed concurrently with the formation of any new flexural crack. The cracks were widening rapidly with a small increase in load until failure due to the slip of the GFRP bars from concrete. The average measured strain of concrete and reinforcement at ultimate load was 1075×10^{-6} and 1644×10^{-6}, respectively, which confirm the bond loss failure mode.

d) GFRP beams with end cap, exposed to 500°C

The use of steel end caps in the GFRP beams exposed to 500°C, had improved the cracking load from 1.5 to 3.6 kN which represents 33.7% of that of the control GFRP beam. The first flexural crack initiated in the middle zone. By increasing the applied load, only two specimens showed additional two flexural cracks at locations below the loading points, as shown in Fig. 4.26, which were extended more towards the compression zone until a sudden failure with explosive sound occurred due to the breakdown of bond between the GFRP bar and the steel end cap. At failure load, the measured concrete and reinforcement strain was 4093×10^{-6} and 6103×10^{-6}, respectively, which confirms that the bond failure took place before reaching the heat-damaged concrete crushing strain (15000×10^{-6}) or the heated GFRP bars rupture strain (14800×10^{-6}).
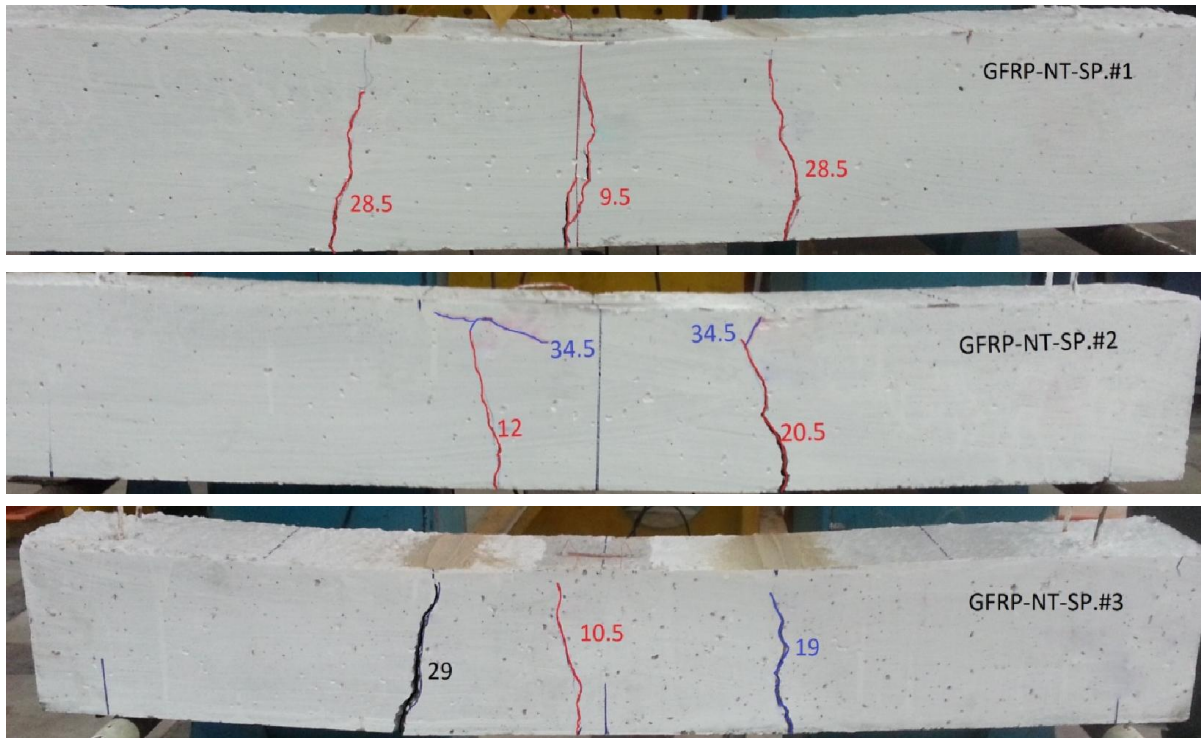
Fig. 4.23: Cracking pattern of beams with GFRP bars, without end caps, tested at 23°C
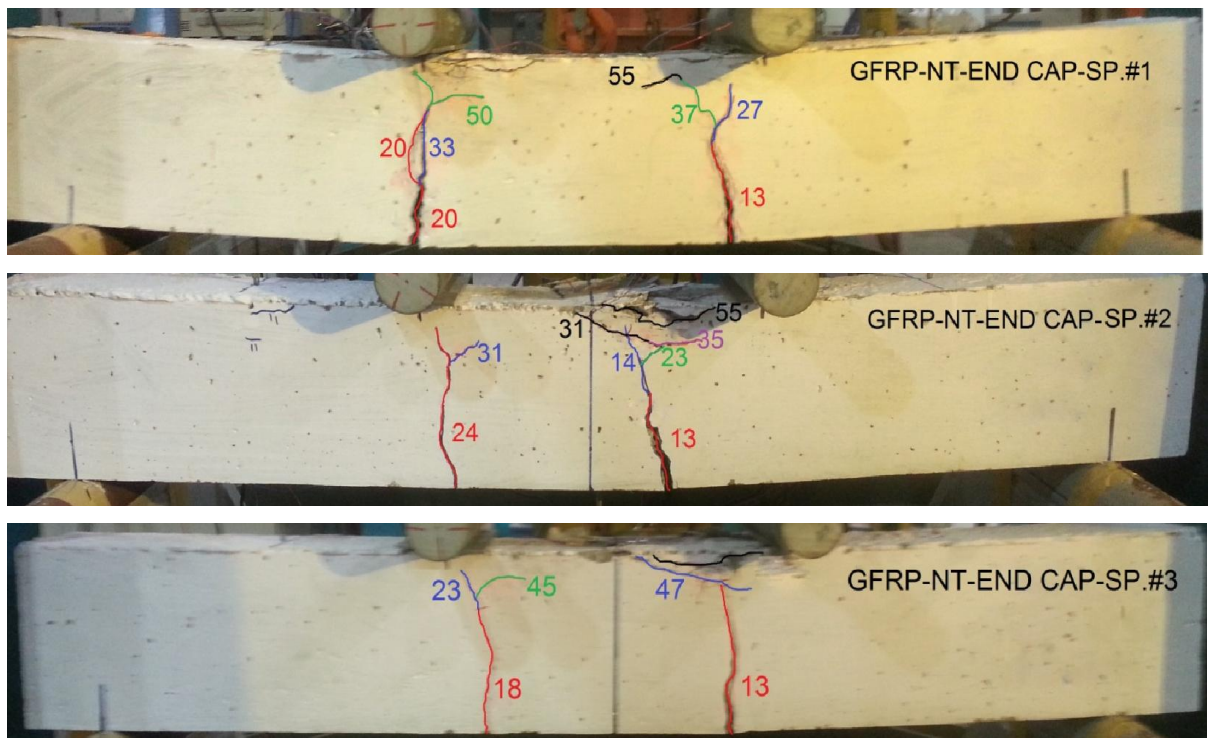
Fig. 4.24: Cracking pattern of beams with GFRP bars, with end caps, tested at 23°C
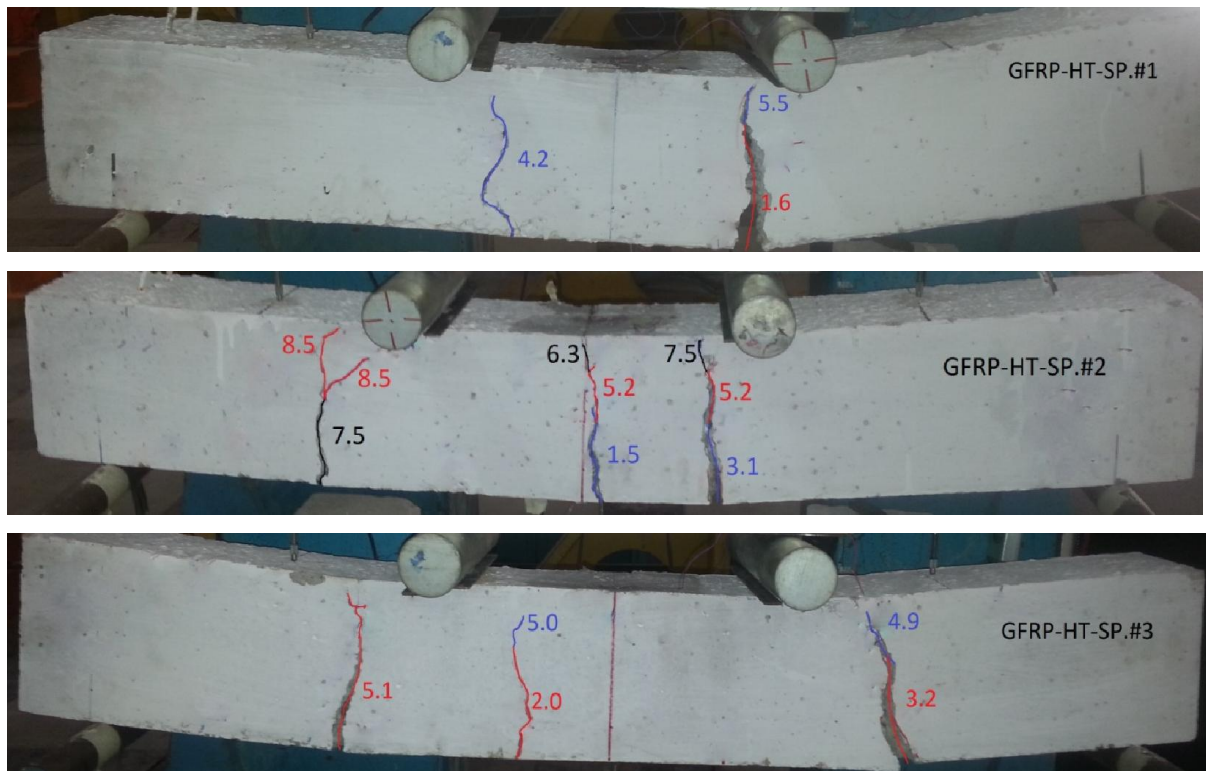
Fig. 4.25: Cracking pattern of beams with GFRP bars, without end caps, tested after exposure to 500°C
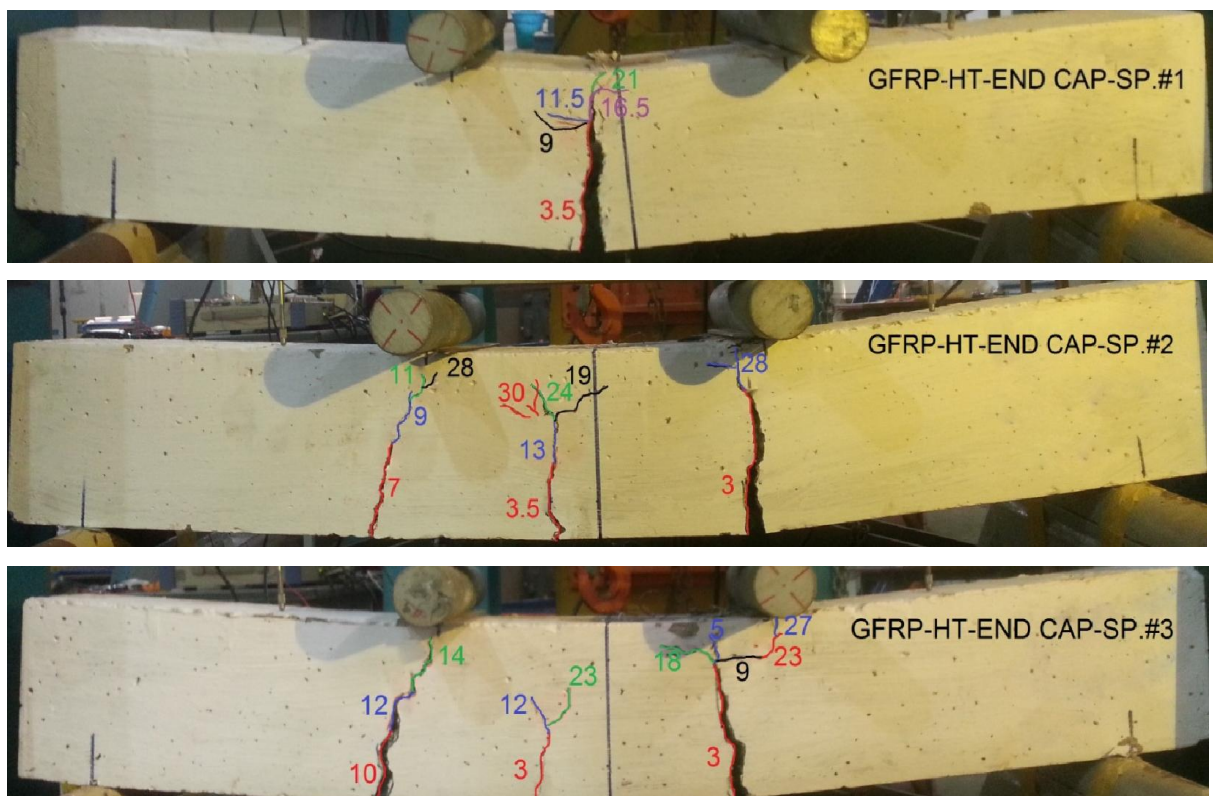
Fig. 4.26: Cracking pattern of beams with GFRP bars, with end caps, tested after exposure to 500°C

4.6.4(b) Failure mode and cracking pattern of BFRP beam

a) Control BFRP beams

Fig. 4.27 showed that cracking was initially formed in the middle third of the beam at average cracking load of 11.94 kN, then extended towards the compression zone with increasing load. At load of double cracking load, maximum of two additional flexural cracks were formed below the loading points; the cracks were widening rapidly with slight increase in load up to failure due to the loss of bond between the BFRP bars and concrete. Bond loss failure occurred at maximum concrete and reinforcement strains of 1707×10^{-6} and 5075×10^{-6}, respectively, which are less than the concrete crushing strain (3000×10^{-6}) and the BFRP bars rupture strain (20600×10^{-6}).

b) BFRP Beams with end caps at normal temperature

Adding steel end caps to the ends of the BFRP bars had increased the cracking load to 14 kN which represent 117.3% of that of the control beams. Similar to the control beams, vertical flexural crack initiated in the middle third zone followed by formation of additional vertical cracks in the maximum tension zone with increasing load. By increasing the applied load, inclined shear cracks were branched from the existing vertical cracks, located below the loading point, and new inclined cracks were formed in the nearby zones of the beam which extended towards the compression zone until a sudden shear failure happened due the high concentration of shear stresses at locations of the loaded end caps. The measured strain of the concrete and reinforcement at ultimate load was 2689×10^{-6} and 10362×10^{-6}, respectively indicating that failure happened just before reaching the concrete crushing strain (3000×10^{-6}). Adding end caps to the BFRP bars had increased number of cracks and reduced the visible crack widths as shown in Fig. 4.28.

c) BFRP beams, exposed to 500°C

Upon exposure to 500°C, the beams with BFRP bars cracked initially in the middle third zone at low load of 1.62 kN, as shown in Fig. 4.29, followed by the formation of additional vertical cracks in the nearby zone which were widening rapidly with a small increase in load up to failure due to the loss of bond between the BFRP bars and concrete. At failure load, the measured strains of concrete and reinforcement were 1443×10^{-6} and 1869×10^{-6}, respectively, which confirm our expectation of bond breakdown at low load.

d) BFRP beams with end caps, exposed to 500°C

Cracking load of the heated beams with BFRP bars had increased, upon using end caps, from 1.62 to 2.71 kN which is 22.7% of that of the control beams. First crack initiated in the middle third zone followed by the formation of multiple vertical cracks distributed along the beam which were extended towards the compression zone with increasing load. Vertical cracks in the high shear zone grew up in the shape of inclined shear cracks accompanied with the development of new inclined shear cracks until the breakdown of the end cap bonding resulting in a sudden explosive failure. The measured strains of concrete and reinforcement at ultimate load was 3997×10^{-6} and 7556×10^{-6}, respectively. A combined shear–bond loss failure with increasing number and reducing widths of cracks was observed in the heated beams with BFRP end-capped bars as shown in Fig.4.30.
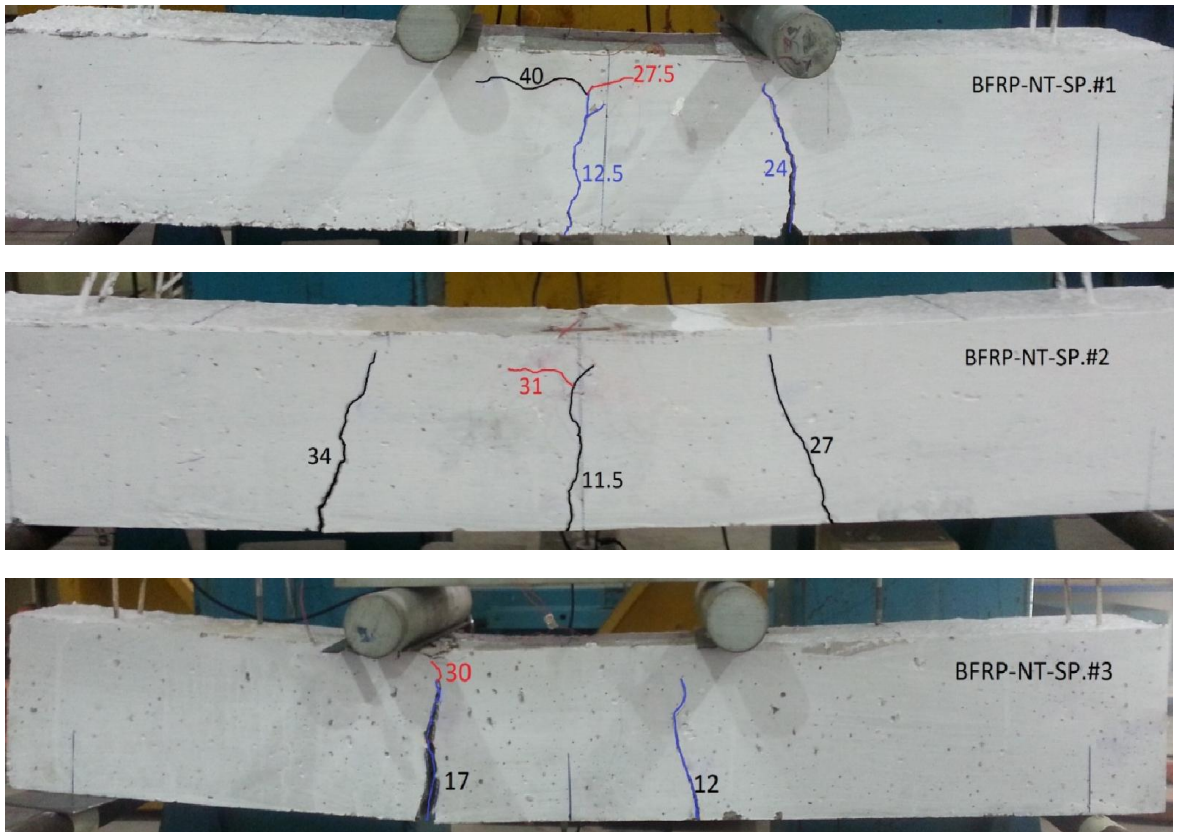
Fig. 4.27: Cracking pattern of beams with BFRP bars, without end caps, tested at 23°C
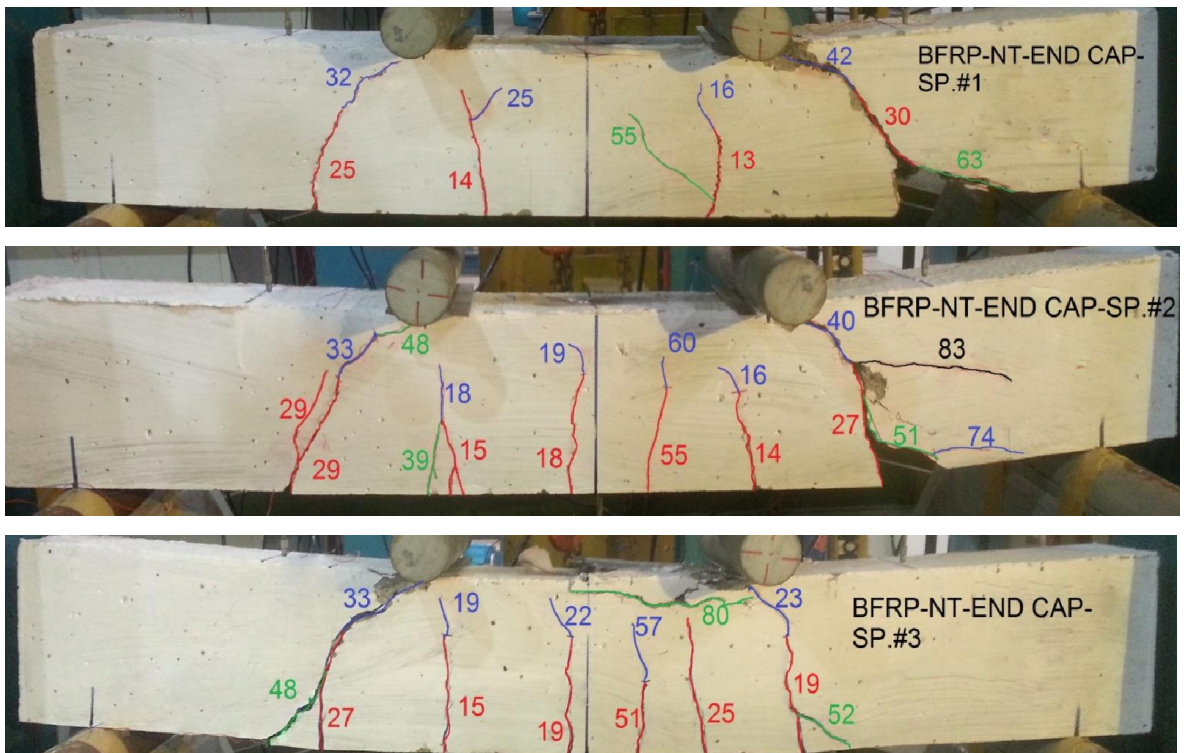
Fig. 4.28: Cracking pattern of beams with BFRP bars, with end caps, tested at 23°C
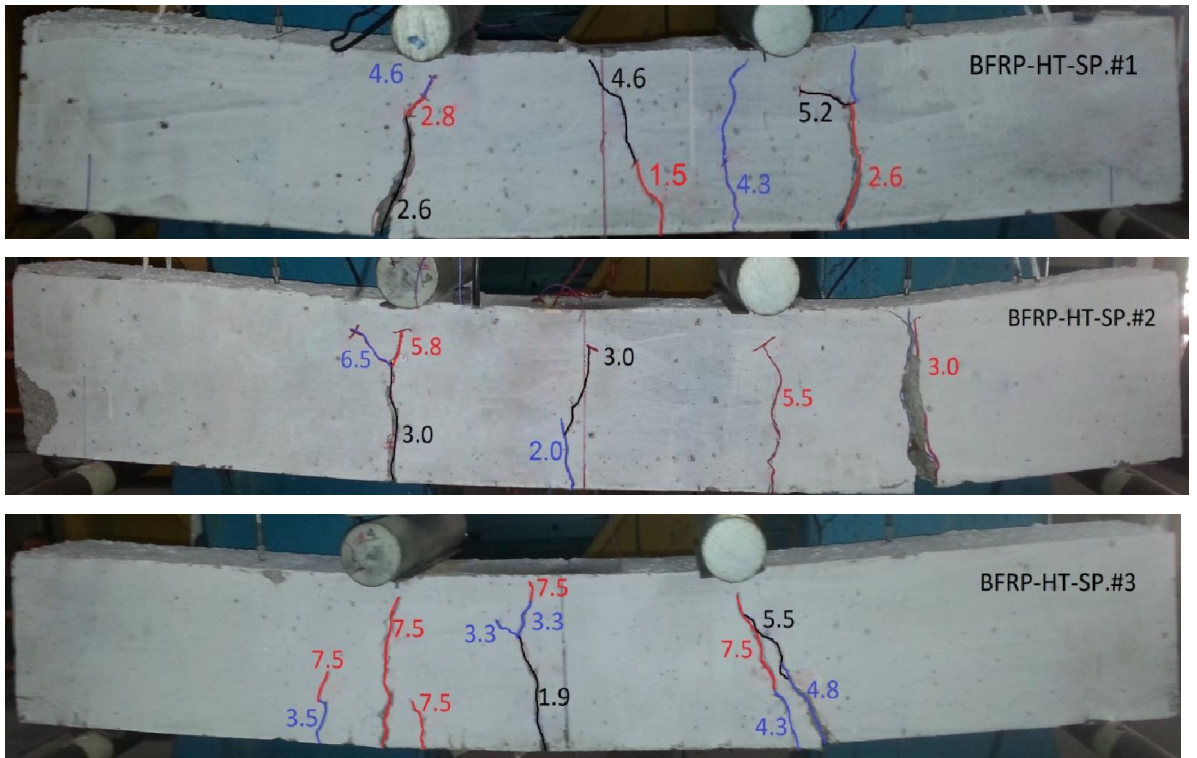
Fig. 4.29: Cracking pattern of beams with BFRP bars, without end caps, tested after exposure to 500°C
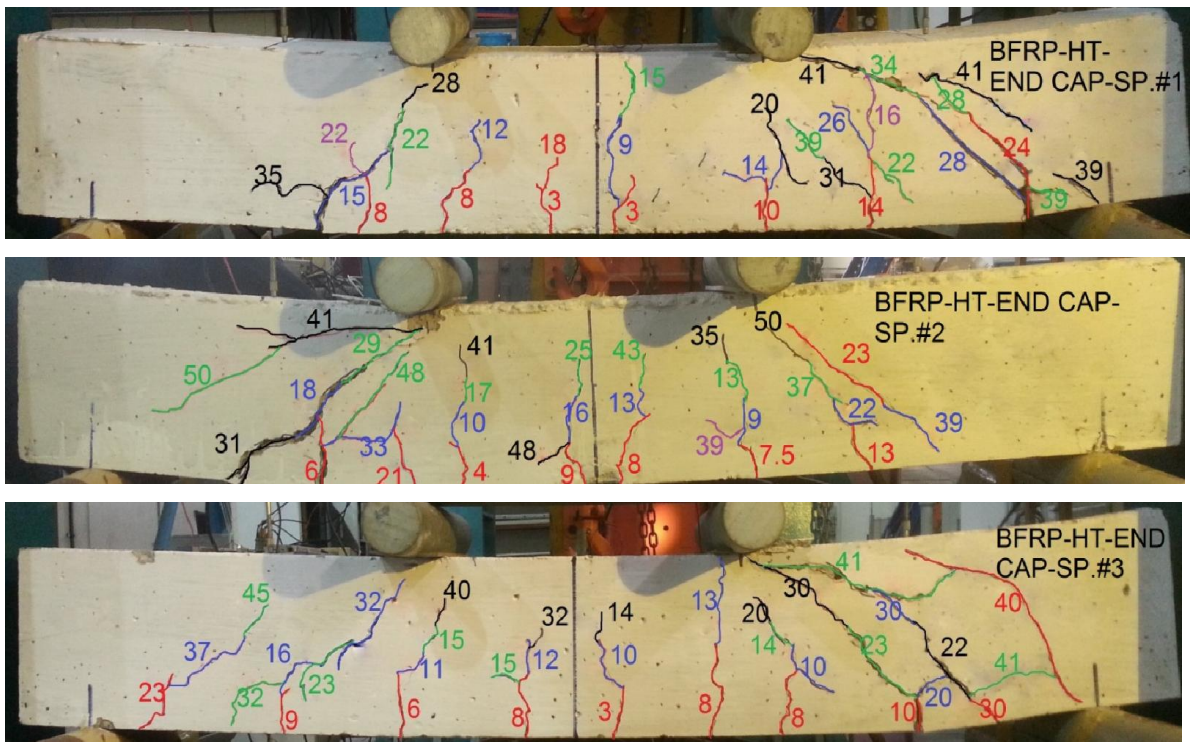
Fig. 4.30: Cracking pattern of beams with BFRP bars, with end caps, tested after exposure to 500°C

4.6.4(c) Failure mode and cracking pattern of CFRP beam

a) Control CFRP beams

At average load of 13.7 kN, first crack had appeared in the middle third zone of the beams with CFRP bars which grew towards the compression zone by increasing load, followed by the development of new vertical cracks that branched and propagated deeply towards the top compression zone. At approximately 60% of the measured maximum load, new inclined shear cracks were developed near the supports of the beams and extended diagonally towards the top loading points until a sudden shear failure happened. At failure, number of cracks was higher than that of similar beams with GFRP and BFRP bars as shown in Fig. 4.31. At ultimate load, the maximum strains of concrete and reinforcement were 2740×10^{-6} and 7144×10^{-6}, respectively, indicating that the shear failure happened just before reaching the concrete crushing strain (3000×10^{-6}).

b) CFRP beams with end caps at normal temperature

Using steel end caps in the beams with CFRP bars had a slight effect on their behavior where the cracking load had changed from 13.67 to 13.95 kN. Similar to the CFRP-RC beams, the vertical cracks had initiated and grown in the middle third of the beam, as shown in Fig. 4.32. With increasing load, cracks located below the loading points had been branched to diagonal shear cracks followed by the formation of new inclined cracks near the supports of the beam. All inclined cracks were grown diagonally towards the top compression zone by increasing load until a sudden shear failure occurred at concrete and reinforcement strains of 2805×10^{-6} and 6702×10^{-6}, respectively, just before reaching the concrete crushing strain (3000×10^{-6}).

c) CFRP beams, exposed to 500°C

Similar to the heated beams with BFRP and GFRP bars, the beams with CFRP bars, exposed to 500°C, were initially cracked at their middle third zone at low load of 1.59 kN, as shown in Fig 4.33. With increasing load, additional vertical cracks were formed below the loading points, branched and extended towards the compression zone, then widened rapidly with a small load increase up to failure which then the cracks width and deflection were increasing quickly without any increase in load due to the loss of bond between the CFRP bars and concrete. At failure load, strains of concrete and reinforcement were 3255×10^{-6} and 2835×10^{-6}, respectively, indicating that bond-slip failure had occurred before reaching the heated-concrete crushing strain (15000×10^{-6}) or the heated-CFRP bars rupture strain (9400×10^{-6}).

d) CFRP beams with end caps, exposed to 500°C

As in the case of the heated beams with BFRP and GFRP bars, adding steel caps to the ends of CFRP bars in beams exposed to 500°C, had increased the average cracking load from 1.59 to 2.7 kN. First crack initiated in the middle third zone followed by the formation of multiple vertical cracks which were distributed along the beam with more concentration in the middle third zone. With further increase in load, the vertical flexural cracks located in the maximum tension zone extended vertically towards the compression zone whereas cracks located in the high shear zone were branched and grown diagonally followed by the formation of new inclined shear cracks near to the supports which were expanded towards the loading points until the breakdown of the end caps bonding resulting in an explosive sudden failure as shown in Fig. 4.34. The strains of concrete and bars at ultimate load were 4559×10^{-6} and 6952×10^{-6}, respectively, indicating that bond breakdown failure happened before reaching the concrete crushing strain or the CFRP bars rupture strain.
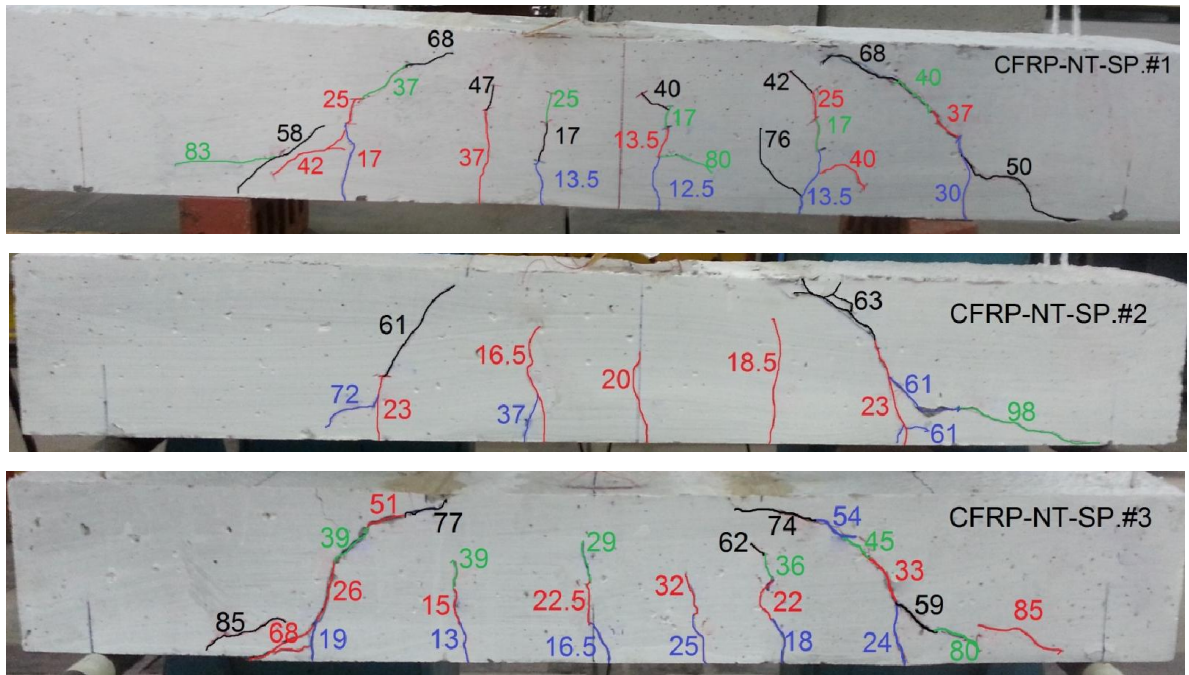
Fig. 4.31: Cracking pattern of beams with CFRP bars, without end caps, tested at 23°C
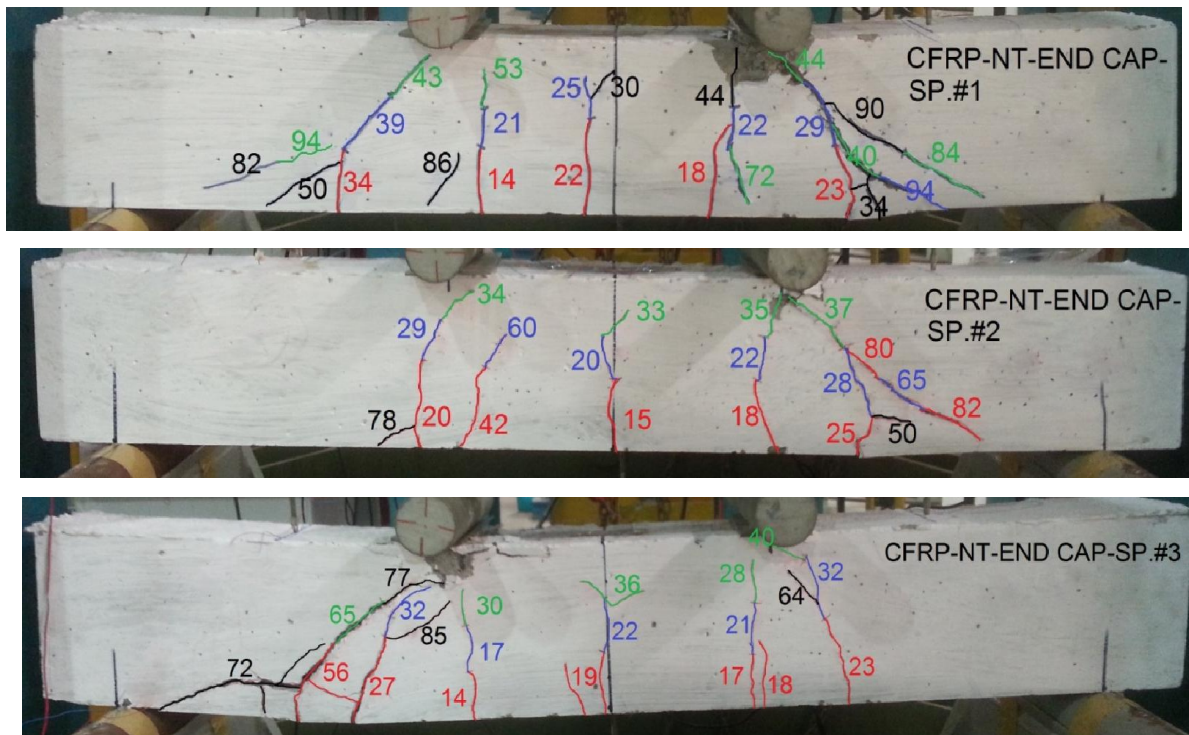
Fig. 4.32: Cracking pattern of beams with CFRP bars, with end caps, tested at 23°C
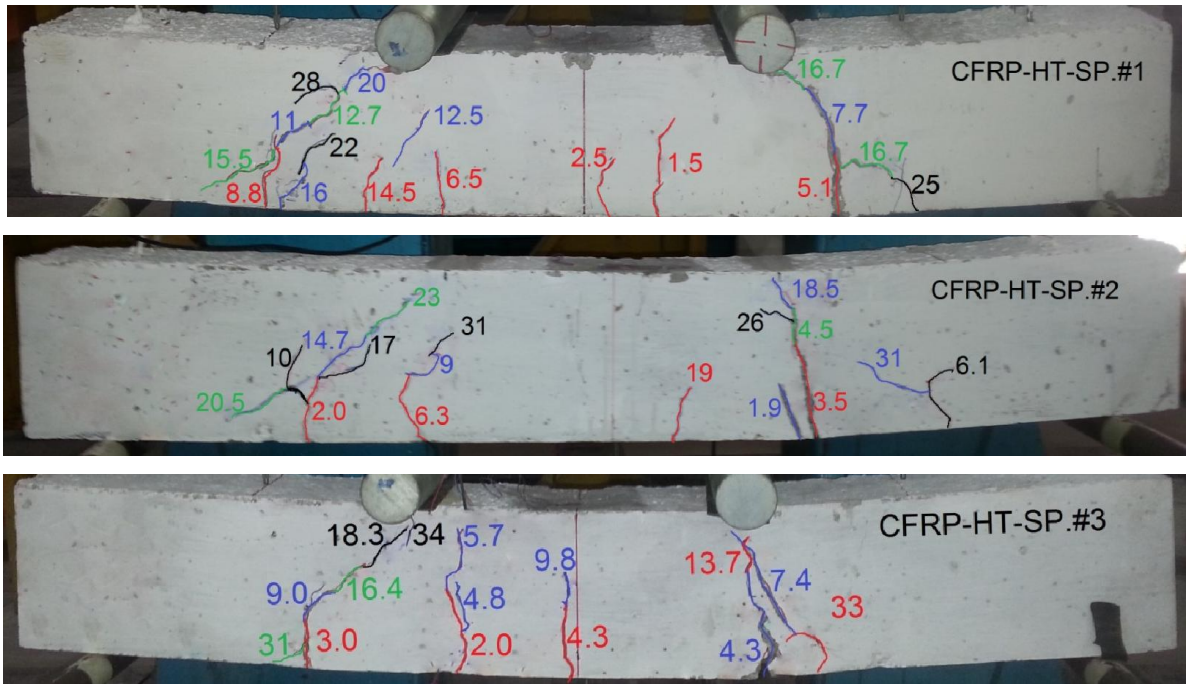
Fig. 4.33: Cracking pattern of beams with CFRP bars, without end caps, tested after exposure to 500°C
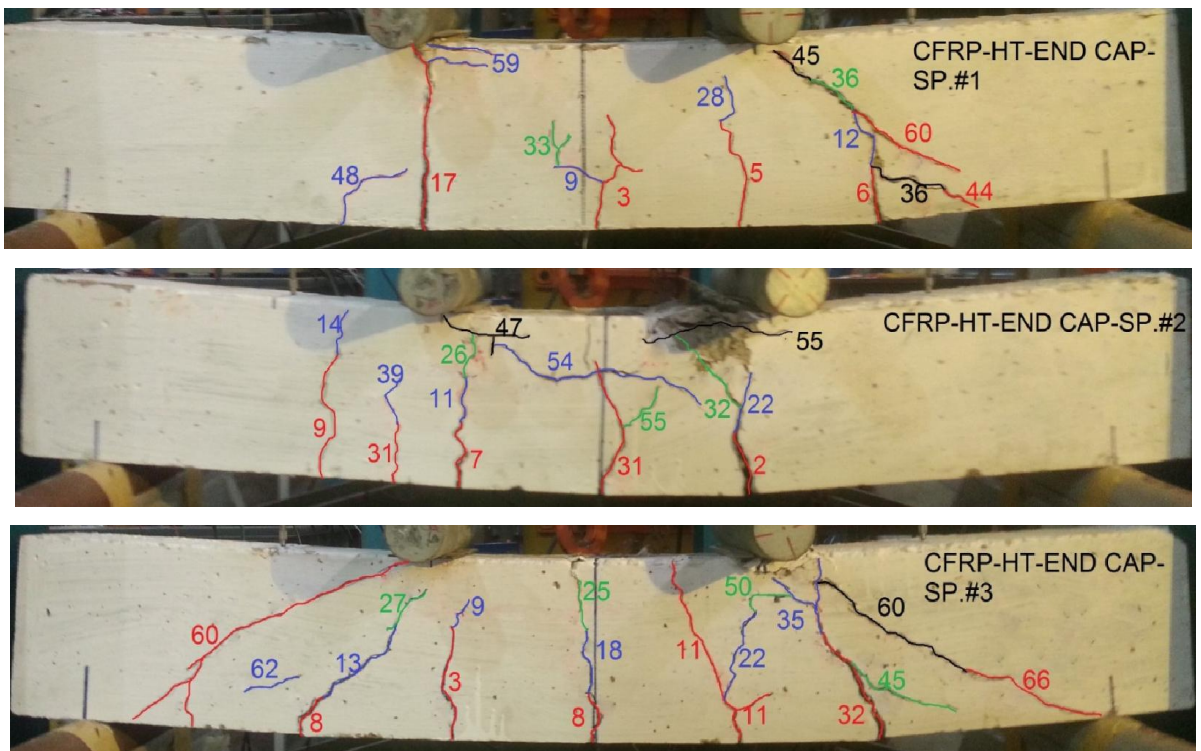
Fig. 4.34: Cracking pattern of beams with CFRP bars, with end caps, tested after exposure to 500°C

4.6.4(d) Failure mode and cracking pattern of steel-RC beam

a) Control steel-RC beams

The first flexural crack of the beams with steel bars initiated in the middle zone at average cracking load of 20.67 kN which extended towards the compression zone, by increasing load, accompanied by the formation of new vertical flexural cracks along the beam with more concentration in the maximum tension zone (six to eight main flexural cracks in total). At higher loads, flexural cracks in the maximum tension zone were branched and grown towards the compression zone while cracks in the high shear zone were developed with inclined branches that extended diagonally towards the loading points until occurrence of concrete crushing failure at strain of 5418×10^{-6} with a reinforcement strain of 6910×10^{-6}. The strains of concrete and steel measured at yielding load was 2885×10^{-6} and 2996×10^{-6}, respectively, then increased up to failure confirming that concrete crushing happened after steel yielding. As shown in Fig. 4.35, the total number of cracks in steel-RC beams was higher than that of similar beams with FRP bars, yet with smaller visible cracks widths.

b) Steel-RC Beams, exposed to 500°C

The cracking pattern of steel-RC beams, tested after exposure to 500°C, was similar to that of control steel-RC beams but with a lower cracking load of 2.92 kN which represents 14.1% of that of the control beams. Six to eight main flexural cracks were formed along the beam extended towards the compression zone with increasing load. At higher loads, additional inclined shear cracks were formed near the supports, due to the reduction in concrete shear strength upon heating, and extended diagonally towards the loading points up to failure as shown in Fig. 4.36. The strains of concrete and steel measured at yielding load were 3279×10^{-6} and 2360×10^{-6}, respectively. After yielding point, the strain gauges used to measure the reinforcement strain

stopped giving correct readings and the recorded readings were ignored whereas the

average measured concrete strain at ultimate load was 6201×10^{-6}.

Fig. 4.35: Cracking pattern of beams with steel bars, tested at 23°C

Fig. 4.36: Cracking pattern of beams with steel bars, tested after exposure to 500°C

4.7 Summary

In this Chapter, the results of all experimental works performed were presented and discussed in details. In Section 4.2, the temperature distribution profile for the RC beams heated to 500°C for four hours was presented. The main reinforcement bar's temperature during the heating process was monitored, and the minimum concrete cover needed to maintain the bar's temperature below the critical temperature was determined. The mechanical properties of the different reinforcing bars, such as ultimate tensile strength, ultimate strain and elastic modulus, tested before and after exposure to different high temperatures, were presented and discussed in Section 4.3. In Section 4.4, the different properties of concrete such as compressive and tensile strengths were presented and the effect of heating to 500°C on the concrete's mechanical properties was discussed. The effect of exposure to different high temperatures on the FRP/steel bars to concrete bond-slip behavior and their pullout failure modes was presented and discussed in Section 4.5. The effect of using steel end caps in improving the pre- and post-heating bond between FRP bars and concrete was presented also in Section 4.5. In Section 4.6, the flexural performance, cracking patterns and modes of failure of concrete beams with FRP/steel bars, before and after exposure to 500°C, were presented. The load-deflection characteristics of the tested beam specimens including the ultimate load capacity, mid-span deflection, stiffness, serviceability and ductility were discussed in details. The effect of using steel end caps in improving the pre- and post-heating flexural performance of FRP-RC beams was quantified.

CHAPTER FIVE
THEORETICAL STUDY

5.1   Introduction

Different theoretical studies were performed and presented in this chapter including the empirical prediction of post-heating bond behaviour between FRP bars and concrete, presented in Section 5.2. The theoretical prediction of the load carrying capacity, mid-span deflection and cracking load for beams with FRP/steel bars without and with end anchorage, before and after exposure to 500°C, which is presented in details in Section 5.3. The comparisons between the theoretical and experimental results were presented in Section 5.4.

5.2   FRP to concrete bond empirical modelling

Different models were analytically developed to predict the the ascending branch of the bond stress versus slip diagram; among which was the model proposed by Ciampi et al., (1982).

Ciampi et al., (1982) provided the following general equation for bond-slip relation of any reinforcing bars type:

$$\tau_{(s)} = \tau_{max} \left(\frac{s}{s_{max}} \right)^{\beta} \tag{5.1}$$

where:

$\tau_{(s)}$ is the local bond stress at local slip (s);

τ_{max} and s_{max} are the maximum bond stress and its corresponding slip, respectively; and

β is a parameter derived from curve fitting process.

Equation (5-1) was applied to the present results after a new parameter (α_T) that accounts for the temperature effect was introduced. The modified form of Ciampi's equation is written as follows:

$$\tau_{(s,T)} = \alpha_T \times \tau_{max,23°} \times (s)^{\beta_T} \tag{5.2}$$

Where:

$\tau_{(s,T)}$ is the local bond stress of a FRP specimen that was exposed to temperature (T) at corresponding local slip (s);

$\tau_{max,23°}$ is the bond strength of the FRP bar measured at normal temperature (23°C);

(s) is the local slip which must not exceed the expected maximum slip value ($s_{max,T}$) for each exposure temperature T.

The present results were used to develop a new equation for maximum slip value of FRP specimen exposed to high temperature (T). The equation is given as:

$$s_{max,T} = s_{max,23} \times \left(1 - \frac{T^{2.287}}{10^6}\right) \tag{5.3}$$

α_T and β_T are parameters that depend on the exposure temperature (T) and given by the following equations:

$$\alpha_T = A \times |0.672 - B - 5.285\,T \times 10^{-4} - 2.983\,T^2 \times 10^{-6}|^C \tag{5.4}$$

$$\beta_T = D\left[0.507 - \left(\frac{T}{1314}\right)^{0.856}\right]^E + F \tag{5.5}$$

where A, B, C, D, E and F are constants estimated based upon curve fitting process of each type of FRP bars; The results are summarized in Table 5.1.

Table 5.1: Regression constants for predicting α_T and β_T (Eq. 5.4 and Eq. 5.5)

FRP Type	A	B	C	D	E	F
BFRP	1.0	0.0	1.0	1.0	1.0	0.0
GFRP	1.054	0.115	0.656	3.135	3.590	0.169
CFRP	0.564	0.184	0.186	1.047	0.582	0.0

Based upon Eqs. 5.2 through 5.5 and constants of Table 5.1, predictions of the maximum bond stress were made. A sample calculations for a certain case is explained in the following section. Results representing different FRP bars and exposure temperature were then obtained and summarized in Table 5.2, before the data were graphically presented in Figs. 5.1 through 5.3 along with the triplicate readings obtained experimentally. More curves were drawn to show the trend behavior of analytical predictions considering the FRP bar type and exposure temperature as shown in Figs. 5.4 through 5.6.

Comparison between the fit of the present model with the experimental data revealed a very good fit in terms of the experimental data scattering around the empirical curve or their trend versus that of the model, Figs. 5.1 through 5.3. Furthermore, the predictions of the model of post-heating bond strength at various temperatures for pullout specimens with FRP bars were consistent with the behavior observed in the laboratory (Figs. 5.4-5.6).

Example:

To find the analytical equation that represent the ascending part of the CFRP bar's bond-slip curve after exposure to 125°C, parameters A =0.564, B= 0.184, C = 0.186, D= 1.047, E = 0.582, F=0.0 were used to calculate the variables α and β.

$$\alpha_{125} = 0.564 \times |0.672 - 0.184 - (5.285 \times 125 \times 10^{-4}) - (2.983 \times 125^2 \times 10^{-6})|^{0.186}$$

$$= 0.4700$$

$$\beta_{125} = \left\{ 1.047 \times \left[0.507 - \left(\frac{125}{1314} \right)^{0.856} \right]^{0.582} \right\} + 0.0 = 0.5902$$

$Therefore, \quad For\ CFRP\ bars\ @125C \quad \tau_{(s,125)} = 0.47 \times \tau_{m,23°} \times (s)^{0.5902}$

$For\ CFRP\ bars\ @125C \quad s_{max,125} = s_{max,23} \times \left(1 - \frac{125^{2.287}}{10^6} \right)$

$$= 0.9375 \times s_{max,23}$$

The experimental pullout tests of CFRP bars at 23°C showed that maximum bond strength $\tau_{m,23°}$ was 8.338 MPa at corresponding slip $s_{max,23°}$ of 3.278 mm.

$$For\ CFRP \quad s_{max,125} = 0.9375×3.278 = 3.073\ mm$$

$$\tau_{(s,125)} = 0.470×8.338×(s)^{0.5902} = 3.919×(s)^{0.5902}$$

$$\tau_{(max,125)} = 0.470×8.338×(3.073)^{0.5902} = 7.6\ MPa$$

Table 5.2: Experimental and analytical FRP's maximum bond stress and corresponding slip at different temperatures

FRP Type	Temp.	τ_{exp}	s_{exp}	τ_{emp}	s_{emp}	Error in Bond Strength	Error in Slip
	°C	MPa	mm	MPa	mm	100%	100%
GFRP	23	2.014	2.740	2.100	2.736	4.2%	0.2%
	125	1.462	2.060	1.594	2.568	9.0%	24.7%
	250	1.003	1.892	0.940	1.904	6.2%	0.7%
	325	0.411	1.048	0.385	1.218	6.3%	16.2%
BFRP	23	2.628	2.438	2.642	2.435	0.5%	0.1%
	125	2.054	2.158	2.002	2.286	2.5%	5.9%
	250	1.027	1.942	1.068	1.695	4.0%	12.7%
	325	0.554	0.999	0.495	1.084	10.7%	8.5%
CFRP	23	8.339	3.279	9.163	3.274	9.9%	0.1%
	125	7.005	3.028	7.604	3.074	8.5%	1.5%
	250	4.700	2.224	5.035	2.279	7.1%	2.5%
	325	1.542	1.607	1.564	1.457	1.4%	9.3%
Average Error						5.9%	6.9%

τ_{exp}: experimental bond strength, s_{exp}: experimental slip at maximum bond stress, τ_{emp}: empirical bond strength, s_{emp}: empirical slip at maximum bond stress.
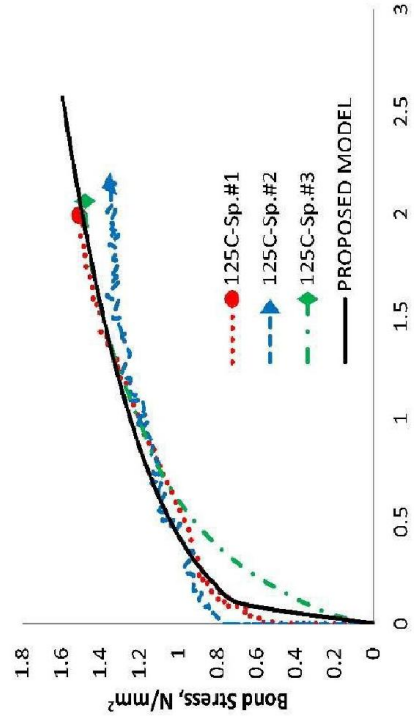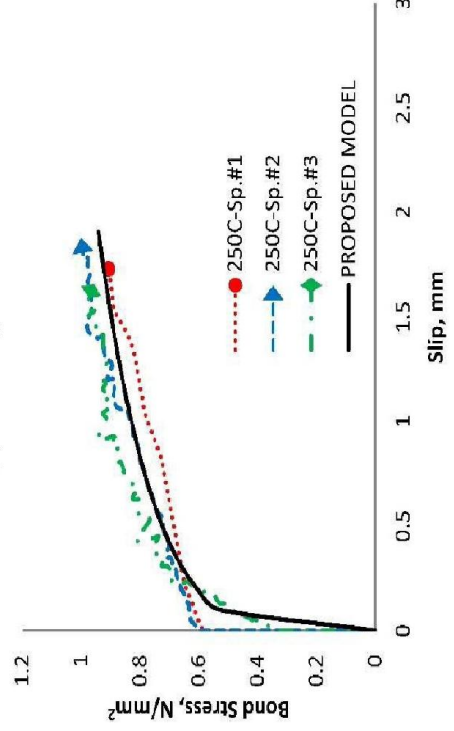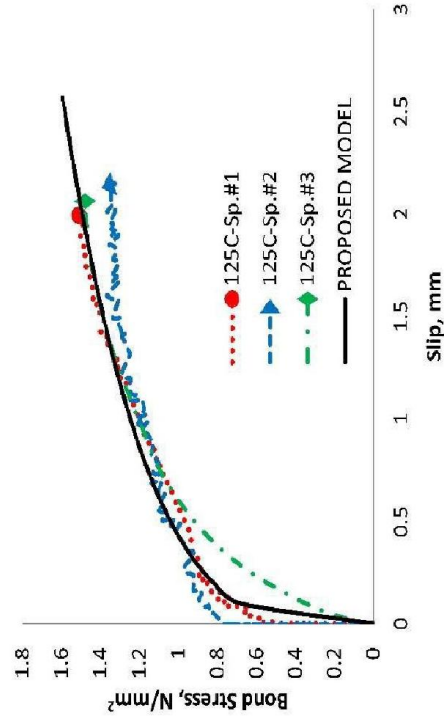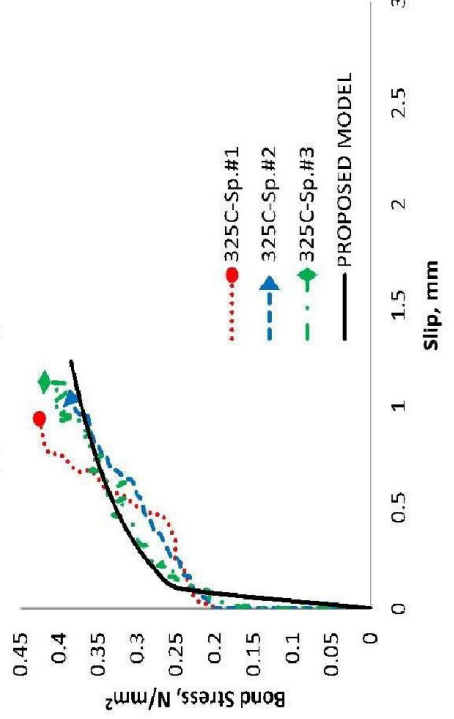
Fig. 5.1: Experimental and empirical ascending portion of bond-slip curves for pullout specimens with GFRP bars exposed to different temperatures
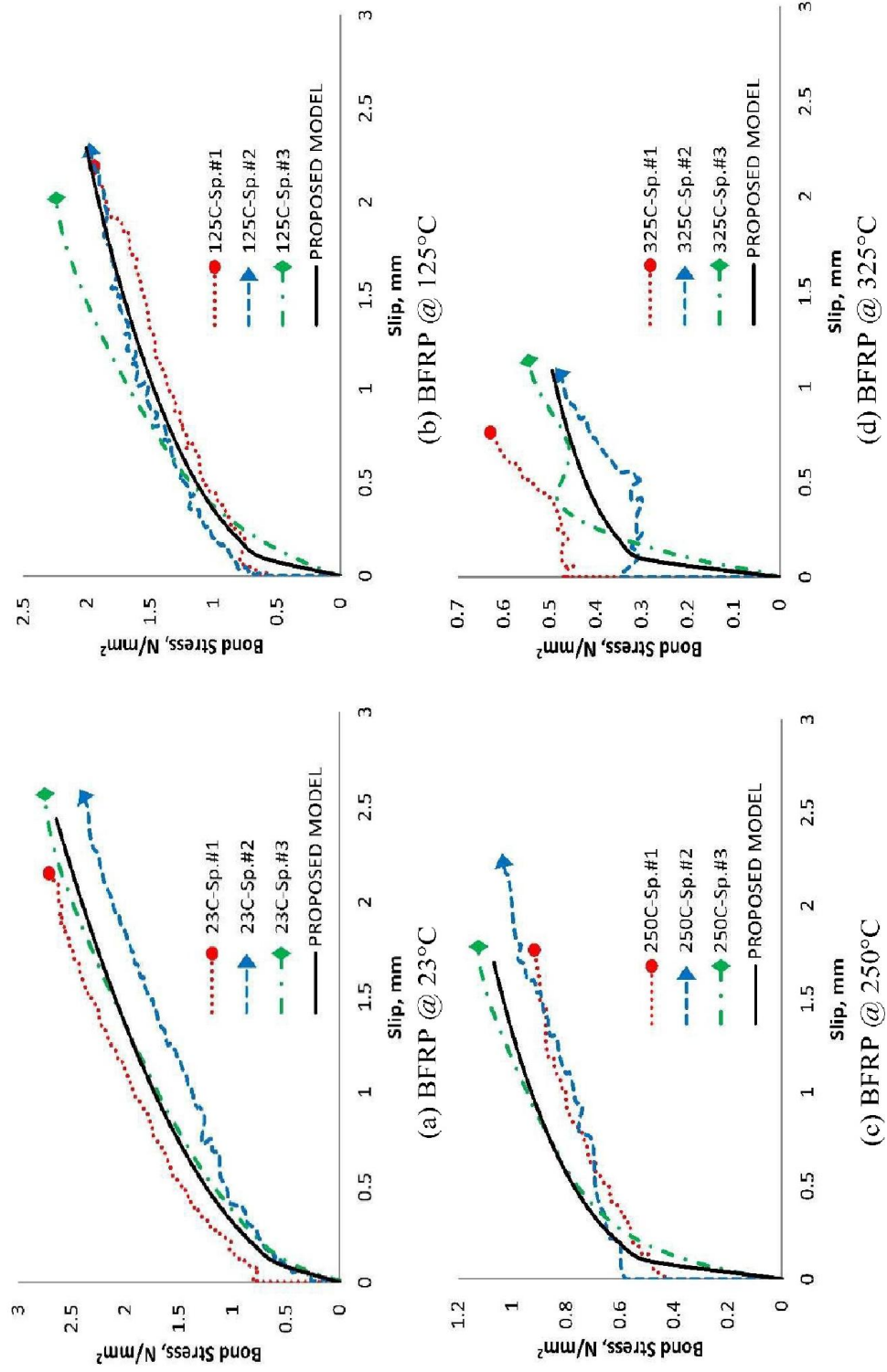
Fig. 5.2: Experimental and empirical ascending portion of bond-slip curves for pullout specimens with BFRP bars exposed to different temperatures
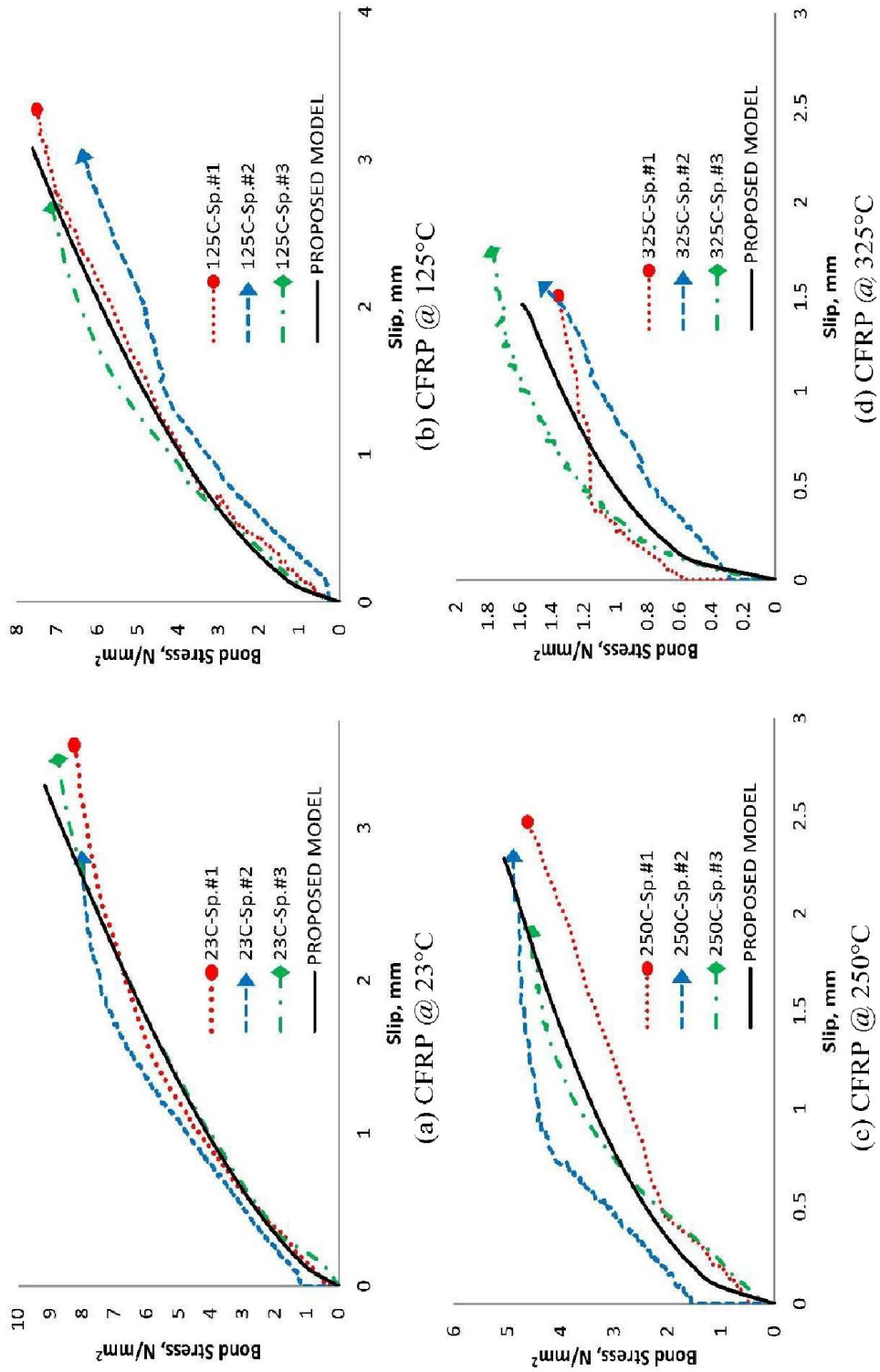
Fig. 5.3: Experimental and empirical ascending portion of bond-slip curves for pullout specimens with CFRP bars exposed to different temperatures
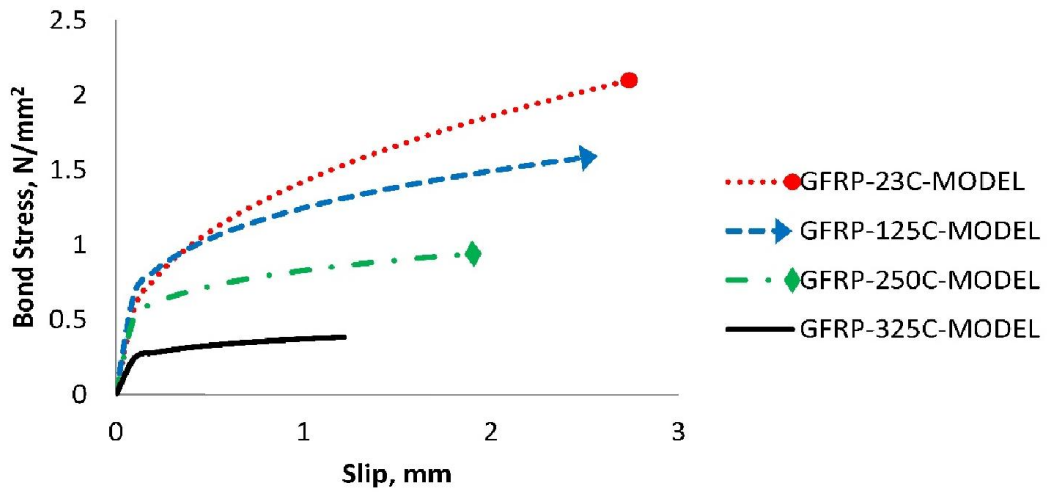
Figure 5.4: Empirical ascending portion of bond-slip curves for pullout specimens with GFRP bars exposed to different temperatures
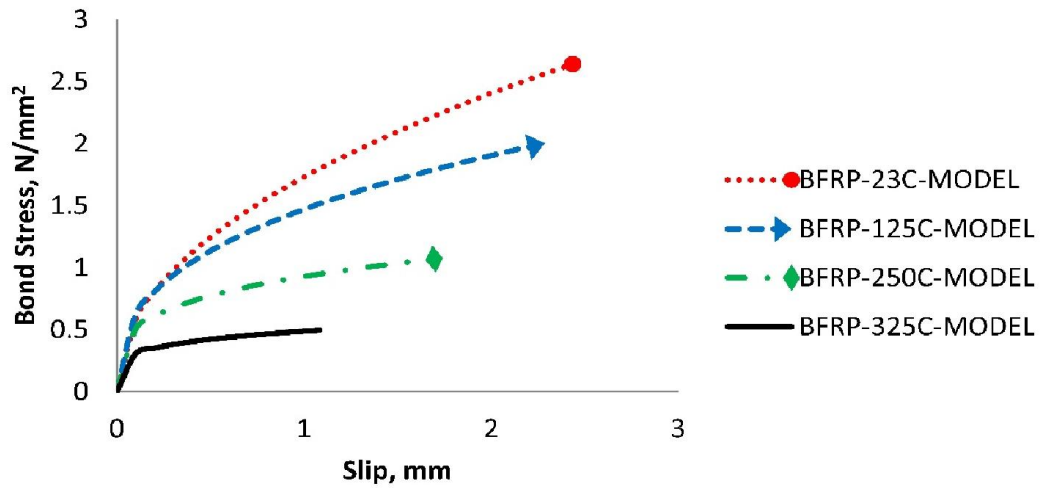
Figure 5.5: Empirical ascending portion of bond-slip curves for pullout specimens with BFRP bars exposed to different temperatures
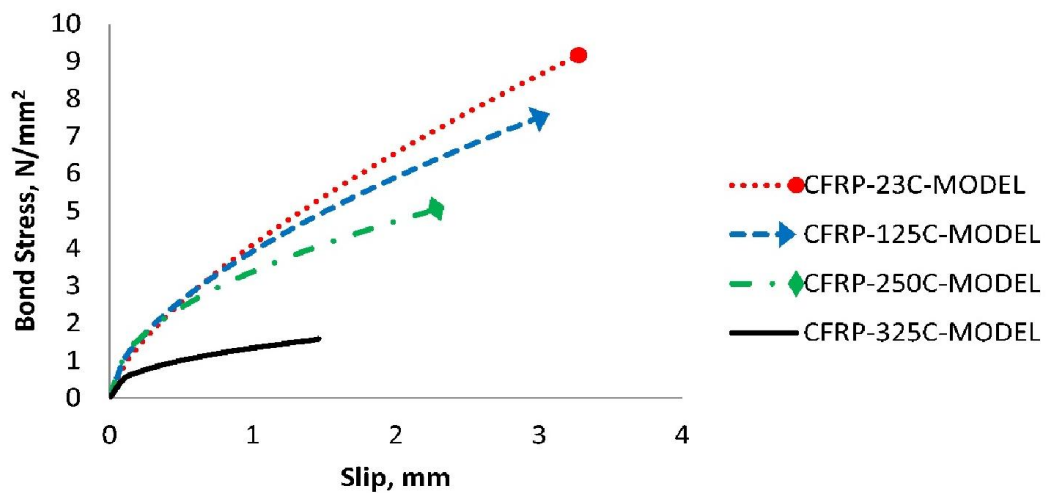
Figure 5.6: Empirical ascending portion of bond-slip curves for pullout specimens with CFRP bars exposed to different temperatures

5.3 Theoretical prediction of shear and flexural behaviour of concrete beams with FRP or steel bars

In this part, both shear and flexural capacity of the present beams are estimated based on ACI, 2006 (ACI 440.1R) for FRP-reinforced concrete beams and ACI, 2005 (ACI 318R) for steel RC beams; considering behavior of concrete in compression, bond behavior between bars and concrete and mechanical properties of the bars used as obtained experimentally, prediction from ACI formulae (ACI 440.1R, 2006 and ACI 318R, 2005) are compared with the experimental results obtained from direct testing of beams under four-point loading.

5.3.1 Theoretical shear strength of FRP-RC beams

As per ACI440.1R, shear capacity of FRP-RC beam's V_n can be calculated from

$$V_n = V_c + V_s \qquad (5.6)$$

Where V_c is concrete shear capacity and can be evaluated from the following equations:

$$V_c = \frac{2}{5}\sqrt{f_c'}bkd \qquad (5.7)$$

$$k = \sqrt{(2\rho_f n) + (\rho_f n)^2} - (\rho_f n) \qquad (5.8)$$

$$\rho_f \ (reinforcement\ ration) \ = \frac{A_f}{bd} \qquad (5.9)$$

$$n = \frac{E_f}{E_c} \qquad (5.10)$$

While V_s is shear resistance of stirrups perpendicular to the member axis can be calculated as per ACI318-05 code:

$$V_s = \frac{A_v f_y d}{S} \qquad (5.11)$$

Where b = concrete section width =130 mm,

d= beam's effective depth =144 mm,

A_f = Area of FRP bars in tension region=157.08 mm^2,

k_d = cracked transformed section neutral axis depth, mm,

E_c = Concrete modulus of elasticity =4700 $\sqrt{f_c'}$, GPa at $ambient$ $temperature$,

(Note: at 500°C, E_c=4700 $\sqrt{f_c'}\big/6$, GPa)

E_f = FRP modulus of elasticity, GPa,

S= Stirrups spacing =70 mm and stirrups diameter =6 mm,

f_c' = compressive strength of concrete, MPa,

A_v = cross-sectional area of each stirrup (2 legs) = 56.55 mm^2, and

f_y = stirrups yield strength =280 MPa (note: f_y at 300-350°C = 0.8f_y at 23°C).

5.3.2 Theoretical shear strength of steel-RC beams

According to ACI-318, Steel-RC Beam's total shear capacity $V_n = V_c + V_s$ where concrete shear capacity V_c and shear resistance of stirrups V_s can be evaluated from the following equations

$$V_c = \frac{\sqrt{f_c'}\,bd}{6} \tag{5.12}$$

$$V_s = \frac{A_v f_y d}{S} \tag{5.11}$$
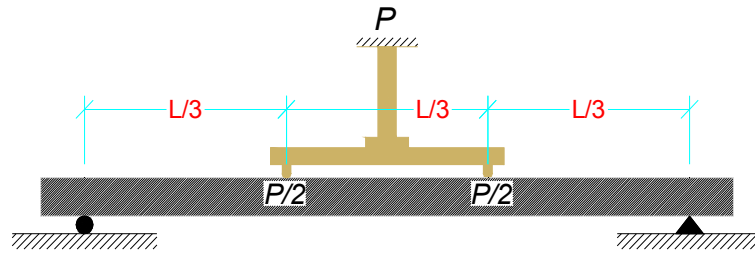
Figure 5.7: Schematic of tested beams loading

For four point loading beams, beam's shear capacity $P_n = 2V_n$

The theoretical shear capacities of the concrete beams with different reinforcing bars were calculated using Eqs. 5.6 through 5.11 and summarized in Table 5.3.

Table 5.3: Theoretical shear capacity of RC beams at different conditions

Reinf. Type	Exposure Temp.	f_c' MPa	E_c GPa	E_f or Es GPa	n	k	V_c kN	V_s kN	V_n kN	P_n kN
CFRP	Ambient Temp. 23°C	34	27.4	119	4.34	0.236	10.30	32.57	42.87	85.74
GFRP		34	27.4	47.14	1.72	0.156	6.82	32.57	39.39	78.78
BFRP		34	27.4	65.85	2.40	0.182	7.93	32.57	40.50	81.00
Steel		34	27.4	200	N.A	N.A	18.19	32.57	50.76	101.5
CFRP	Exposure to 500°C for 90 minutes	25.2	4.6	80.41	17.6	0.415	15.62	26.06	41.68	83.36
GFRP		25.2	4.6	37.39	8.19	0.308	11.58	26.06	37.64	5.28
BFRP		25.2	4.6	51.89	11.4	0.351	13.21	26.06	39.27	78.54
Steel		25.2	4.6	200	N.A	N.A	15.66	26.06	48.23	96.46

f_c', concrete compressive strength, E_c, concrete modulus of elasticity, E_f, FRP bars's modulus of elasticity, E_s, steel modulus of elasticity, n, elastic moduli ratio, V_c, concrete shear capacity, V_s, stirrup shear capacity, V_n, beam total shear capacity, P_n, Load shear capacity, N.A., not available

5.3.3 Theoretical flexural strength of FRP-RC beams according to ACI440.1R

Flexural concrete sections reinforced with FRP is designed or analyzed as over-reinforced where the failure mode is detected by concrete crushing.

High strength concrete is recommended with high-strength FRP bars as it increases the stiffness of the concrete cracked section and reduces the overall deformability of the flexural members (ACI 440.1R, 2006). For this, the upper limit of typical normal concrete strength should be used. As per ACI codes, upper limit for normal weight concrete is 41 MPa and 35 Mpa for light weight concrete. Concrete mix design was proportioned to obtain the required concrete strengths; the experimental tests on concrete cubes and cylinders showed an average concrete strengths of 42.5 MPa and 34 MPa, respectively. (Refer section 4.4.1)

To minimize the possibility of FRP rupture failure, ACI 2006 (ACI 440.1R).recommended reducing the ultimate tensile strength of the FRP bars by 10% to 30%. In addition, the material properties of FRP given by manufacturer or obtained

by direct testing were reduced by environmental reduction factor as per ACI 440.1R to include the effect of long-term exposure to the environment.

The design tensile strength and strain of FRP were calculated from the following equations:

$$f_{uf} = C_E \, f_{ult-f}^*$$ (5.13)

$$\varepsilon_{uf} = C_E \, \varepsilon_{ult-f}^*$$ (5.14)

where

f_{ult-f} = design tensile strength of FRP, considering reductions for service environment, (MPa);

f_{ult-f}^* = Ultimate tensile strength of an FRP bar (MPa);

ε_{ult-f} = design strain of FRP reinforcement at ultimate strength;

ε_{ult-f}^* = Ultimate tensile strain of FRP reinforcement at ultimate strength;

CE = environmental reduction factor, given in Table 7.1 of ACI440.1R, 2006 for various fiber type and exposure conditions; (0.9 for carbon, 0.7 for glass, 0.8 for basalt); and

E_f = design modulus of elasticity of FRP, reported by the manufacturer.

The nominal flexural strength of FRP-reinforced concrete section, M_n, is calculated using strain compatibility, internal forces equilibrium and the controlling mode of failure.

ACI440 Code assumptions: Code assumptions were used, as follows:

1. Plain section before loading remains plain after loading, therefore strain in concrete and reinforcement is proportional to the distance from neutral axis.

2. Maximum usable concrete compressive strain ε_{cu} to be assumed as 0.003.

3. Tensile strength of concrete is ignored

4. Perfect bond between concrete and FRP reinforcement.

<u>Additional assumptions</u>: the following two additional assumptions were used.

1. Stress-strain relationship for concrete at normal temperature

   Concrete compressive stress f_c at any strain level can be evaluated using concrete stress-strain curve proposed by Hognestad 1955, which consists of two parts, parabolic shape curve up to peak stress then linear curve from peak stress to 85% of the peak stress at crushing strain, as shown in Fig. 5.8.
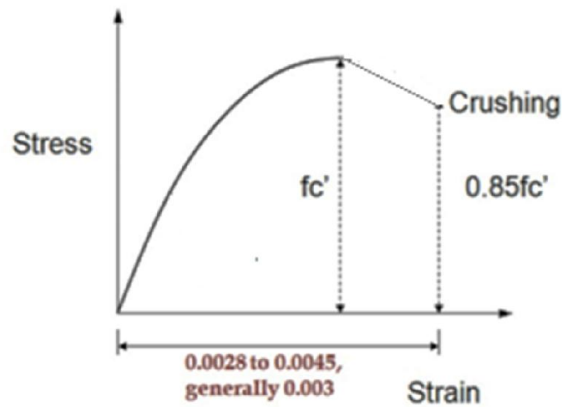
Fig. 5.8: Hognestad's model for concrete stress-strain relationship

The stress in concrete at room temperature is computed using Hognestad's equations:

$$f_c = \begin{cases} f_c'\left(\dfrac{\varepsilon_c}{\varepsilon_o}\right)\left(2 - \dfrac{\varepsilon_c}{\varepsilon_o}\right) & \text{if } \varepsilon_c \leq \varepsilon_o \\[2mm] f_c'\left[1 - \left(0.15 \times \dfrac{\varepsilon_c - \varepsilon_o}{\varepsilon_{cu} - \varepsilon_o}\right)\right] & \text{if } \varepsilon_o < \varepsilon_c \leq \varepsilon_{cu} \end{cases} \tag{5.15}$$

$$\text{where } \varepsilon_o \text{ strain at peak stress } = \frac{1.8 f_c'}{E_c} = \frac{1.8 f_c'}{4700\sqrt{f_c'}} \tag{5.16}$$

2. Stress-strain relationship for concrete at high temperature

   Concrete compressive stress f_c at any strain level can be evaluated using concrete stress-strain curve proposed by Eurocode EN1992-1-2:2004, which consists of two parts, parabolic shape curve up to peak stress then descending linear branch up to crushing strain, as shown in Fig 5.9.
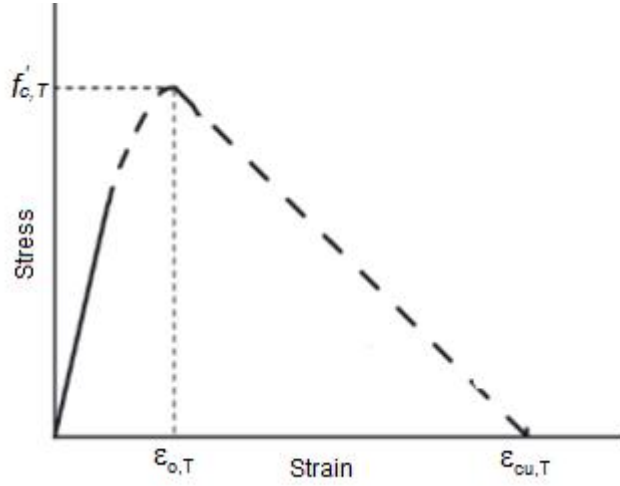
Fig. 5.9: Eurocode's model for concrete stress-strain relationship at high temperatures

The stress in concrete, exposed to 500°C, is computed using the following equation where $\varepsilon_o = 0.015$ and $\varepsilon_{cu} = 0.025$ for concrete exposed to 500°C per EN1992 code:

$$f_{c,T} = \left(\frac{3\varepsilon_{c,T}f'_{c,T}}{\varepsilon_{o,T}\left[2 + \left(\frac{\varepsilon_{c,T}}{\varepsilon_{o,T}}\right)^3\right]}\right) \rightarrow f_{c,500} = \left(\frac{3\varepsilon_{c,T}f'_{c,500}}{0.015\left[2 + \left(\frac{\varepsilon_{c,T}}{0.015}\right)^3\right]}\right) \quad (5.17)$$

In the present study, three types of failure modes were expected including:

1. **Concrete crushing failure mode** which occurs when the reinforcement ratio (ρ_f) is higher than balance reinforcement ratio (ρ_b) and the bond between FRP bars and concrete is good enough to reach the crushing strain of concrete (ε_{cu}); the reinforcement ratio and balance reinforcement ratio can be computed using Eq. 5.9 and Eq. 5.18, respectively.

$$\rho_b = 0.85\beta_1 \frac{f'_c}{f_{ult-f}} \frac{E_f\varepsilon_{cu}}{E_f\varepsilon_{cu} + f_{ult-f}} \quad (5.18)$$

$$\text{where} \quad \beta_1 = \begin{cases} 0.85 - 0.05\left(\dfrac{f'_c - 28}{7}\right) & \text{for } f'_c > 28MPa \\ 0.85 & \text{for } f'_c < 28MPa \end{cases} \quad (5.19)$$

164

2. **FRP bars rupture failure mode** which occurs when the reinforcement ratio (ρ_f) is lower than balance reinforcement ratio (ρ_b) and the bond between FRP bars and concrete is good enough to reach the FRP bar's ultimate tensile strength (f_{fu}) before reaching the crushing strain of concrete (ε_{cu}).

3. **Bond failure mode** which occurs when the bond stress between FRP bars and concrete reaches it maximum value before reaching either concrete crushing or FRP rupture.

Separate procedures for calculations of flexural capacity for each of the three cases are presented in the following sections.

5.3.3(a) Calculations steps for flexural capacity of beams with FRP bars - concrete crushing failure case ($\rho f > \rho b$)

1. Calculate FRP bar's tensile stress at time of concrete crushing f_f from

$$f_f = \sqrt{\left(\frac{E_f \varepsilon_{cu}}{2}\right)^2 + \left(\frac{0.85\beta_1 f_c' E_f \varepsilon_{cu}}{\rho_f}\right)} - \frac{E_f \varepsilon_{cu}}{2} \leq f_{uf} \qquad (5.20)$$

2. Calculate the maximum tensile force in FRP reinforcement (T_m) from

$$T_m = A_f f_f \qquad (5.21)$$

Fig. 5.10 illustrates the strains, stresses and internal forces of FRP-RC rectangular section:
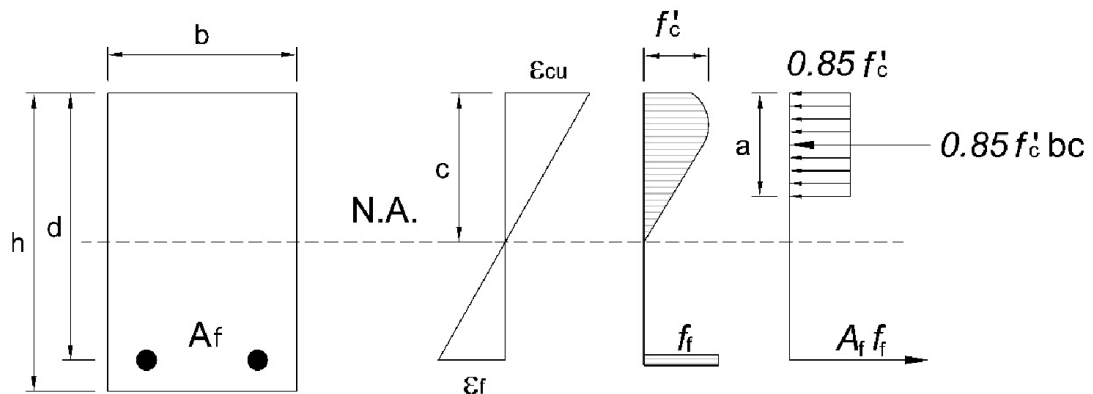
Fig. 5.10: Stresses and internal forces of FRP-RC rectangular section-case1

3. Calculate nominal moment capacity (M_n) from

$$M_n = T_m\, d\left(1 - \frac{0.59\rho_f f_f}{f_c'}\right)$$

(5.22)

4. Calculate nominal load capacity (P_n), for four point loading beams, from

$$P_n = \frac{6M_n}{L} \quad where\ L = beam's\ pure\ bending\ span$$

(5.23)

5.3.3(b) Calculations steps for flexural capacity of beams with FRP bars –FRP rupture failure case (ρf<ρb)

1. Calculate maximum FRP tensile force (T_m) from

$$T_m = A_f f_{ult-f}$$

(5.24)

2. Calculate maximum FRP strain from

$$\varepsilon_{ult-f} = \frac{f_{ult-f}}{E_f}$$

(5.25)

3. Assume that concrete stress is less than its peak. The ACI compression stress block is not applicable because the maximum concrete strain didn't reach its ultimate value of 0.003 therefore an approximate stress distribution of concrete using Hognestad or Eurocode model is used based on the calculated strain value. Parabolic distribution of concrete compressive stress with maximum value f_c is assumed as shown in Fig. 5.11. (note: parabolic area = 2/3 x f_c x c)
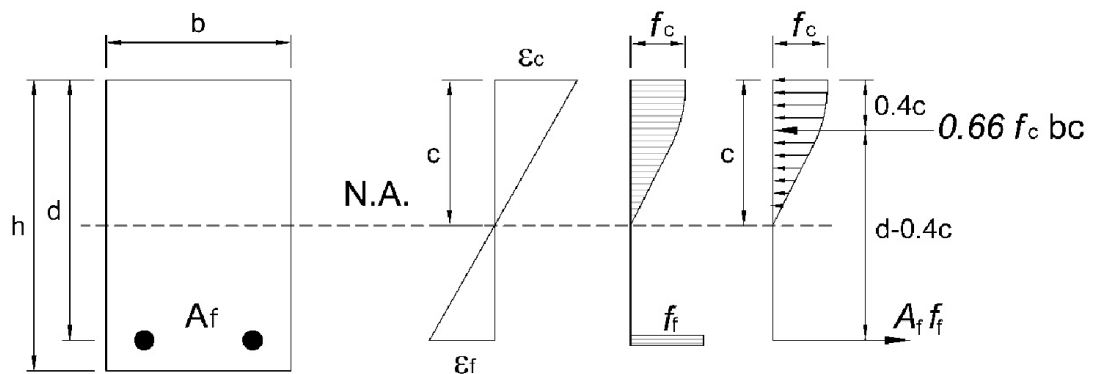
Fig. 5.11: Stresses and internal forces of FRP-RC rectangular section-case2

4. First trial, assume $f_c = f_c'$ and calculate compression force (C) from

$$C = \frac{2}{3} f_c cb \qquad (5.26)$$

5. Using internal forces equilibrium, $C = T_m$, find c

$$c = \frac{3T_m}{2f_c b} \qquad (5.27)$$

6. Calculate concrete strain (ε_c) from

$$\varepsilon_c = \frac{c \, \varepsilon_{ult-f}}{d - c} \qquad (5.28)$$

7. Use Eq. 5.15 proposed by Hognestad. 1955 or Eq. 5.17 proposed by Eurocode to calculate concrete strain new compressive strength (f_c) based on (ε_c) calculated in step # 6.

8. By trial and error, previous steps were repeated using the new (f_c) value until getting the correct (f_c) value

9. Calculate the correct (c) using the maximum FRP tensile force (T_m) and the correct (f_c) calculated in step # 8 ;

$$c = \frac{3T_m}{2f_c b} \qquad (5.27)$$

10. Calculate nominal moment capacity (M_n) from

$$M_n = T_m(d - 0.4c) \qquad (5.29)$$

11. Calculate nominal load capacity (P_n), for four point loading beams, from

$$P_n = \frac{6M_n}{L} \qquad (5.23)$$

5.3.3(c) Calculations steps for flexural capacity of beam with FRP bars –bond failure case

1. Calculate the ultimate tensile force (F) based on the maximum bond capacity

The tensile force is transferred to the bars through bar-concrete bond. The bond stress distributions are not constant along the reinforcement bars so the average mean

values of the bond will be used to indicate the bond strength between the bars and concrete. Average bond strength capacity between different FRP and concrete at normal and high temperature are taken from the present pullout test results.
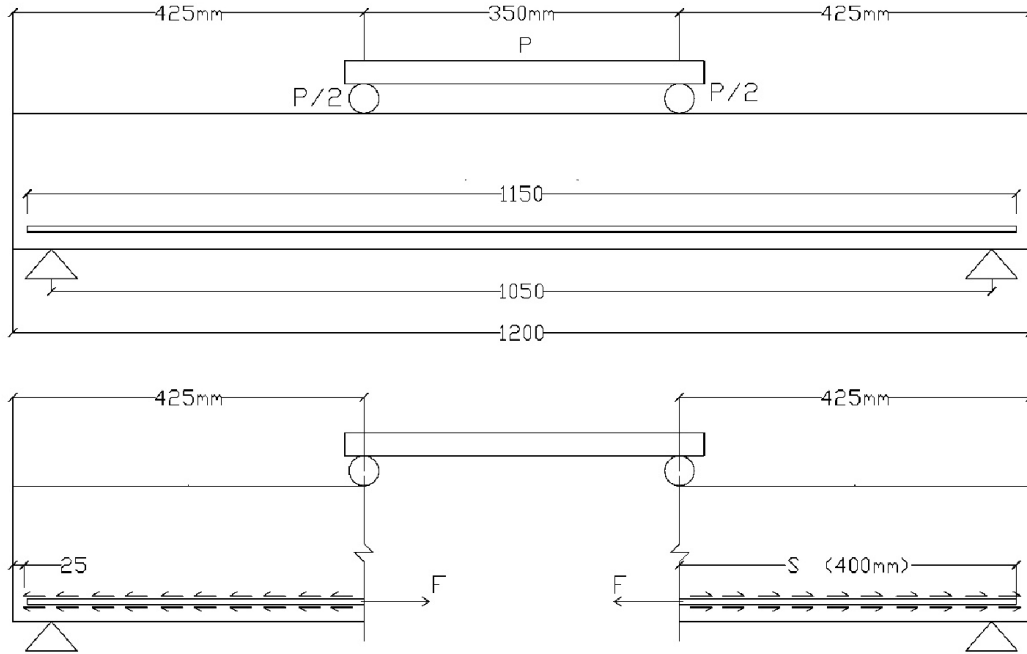
Fig. 5.12: Critical section for bonding failure

$$For\ FRP\ bar, ultimate\ bond\ force\ (Fig\ 5.12)\ = \pi\ \tau_{max} d_b\ S$$

$$For\ two\ FRP\ bars, ultimate\ bond\ force(F) = 2{\times}\pi\ \tau_{max} d_b\ S \qquad (5.30)$$

2. If the maximum bond force capacity (F) is lower than the maximum tensile force capacity (T_m), calculated using Eq. 5.21 or Eq. 5.24, therefore bond failure between FRP and concrete is expected before reaching either concrete crushing or FRP rupture.

3. Calculate maximum FRP strain (ε_f) from

$$\varepsilon_f = \frac{F}{A_f E_f} \qquad (5.31)$$

4. Assume that the concrete stress is less than its peak. Parabolic distribution of concrete compressive stress of maximum value (f_c) is used as shown in Fig. 5.11.

168

First trial, assume $f_c = f_c'$ and calculate compression force (C) from

$$C = \frac{2}{3} f_c c b \qquad (5.26)$$

5. Using internal forces equilibrium, C = F, find c

$$c = \frac{3F}{2 f_c b} \qquad (5.32)$$

6. Calculate concrete strain (ε_c) from

$$\varepsilon_c = \frac{c \, \varepsilon_f}{d - c} \qquad (5.33)$$

7. Use Eq. 5.15 proposed by Hognestad. 1955 or Eq. 5.17 proposed by Eurocode to calculate concrete strain new compressive strength (fc) based on (ε_c) calculated in step # 6.

8. By trial and error, repeat previous steps using the new (f_c) value until getting the correct (f_c) value

9. Calculate the correct (c) using the maximum bond force (F) and the correct (f_c) calculated in step # 8 ;

$$c = \frac{3F}{2 f_c b} \qquad (5.34)$$

10. Calculate nominal moment capacity (M_n) from

$$M_n = F(d - 0.4c) \qquad (5.35)$$

11. Calculate nominal load capacity (P_n), for four point loading beams, from

$$P_n = \frac{6 M_n}{L} \qquad (5.23)$$

Properties of FRP bars before and after exposure to high temperature, summarized in Table 5.4, were used to calculate the theoretical flexural capacity of the FRP-RC beams based on the previous calculations steps.

Table 5.4: FRP properties at 23°C and 325°C

Temp.	FRP Type	CE	E_f MPa	$f_{ult-f}*$ MPa	f_{ult-f} MPa	$\varepsilon_{ult-f}*$	ε_{ult-f}
23 °C	Carbon	0.9	119,000	1572	1414	0.0167	0.01503
	Glass	0.7	47,140	816	571	0.0215	0.01505
	Basalt	0.8	65,850	940	752	0.0206	0.01648
325 °C	Carbon	0.9	80,410	700	630	0.0094	0.00846
	Glass	0.7	37,390	452	316	0.0148	0.01036
	Basalt	0.8	51,890	510	408	0.0141	0.01128

CE, environmental reduction factor, E_f, FRP modulus of elasticity, $f_{ult-f}*$ = FRP ultimate tensile strength, f_{ult-f} = design tensile strength of FRP, $\varepsilon_{ult-f}*$ = FRP ultimate tensile strain, ε_{ult-f} = FRP design strain, fc', concrete compressive strength

Detailed calculations for flexural capacity of each beams with different FRP bars and different exposure temperature were presented in detailed in Appendix B. Reinforcement ratios based on ACI codes were summarized in Table 5.5 while the reinforcement's maximum bond force based on bond strength tests results were summarized in Table 5.6. A summary of the theoretical flexural capacities of all FRP-RC beams calculated according to ACI440 (assuming perfect bond up to failure either concrete crushing or FRP rupture) and a summary of the theoretical predicted flexural capacities of all FRP-RC beams based on the experimental bond strength results was presented in Table 5.7.

Design calculations of steel-RC beams at normal and high temperature exposure were presented in Appendix C, concrete compressive strength of 34 MPa and 25.2 MPa at 23°C and 500°C, respectively, were used in the detailed design calculations.

Table 5.5: Reinforcement ratio for FRP-RC beams

FRP Type	Temp. °C	f_c' MPa	f_{ult-f} MPa	E_f MPa	ρ_f	ρ_b	ρ_f / ρ_b	EFM
Carbon		34	1414.8	119,000	0.008391	0.003324	2.525	S
Glass	23	34	571.2	47,140	0.008391	0.008104	1.035	CC
Basalt		34	752	65,850	0.008391	0.006453	1.300	CC

Table 5.5: continued

FRP Type	Temp. °C	f_c' MPa	f_{ult-f} MPa	E_f MPa	ρ_f	ρ_b	ρ_f / ρ_b	EFM
Carbon		25.2	630	80,410	0.008391	0.008001	1.049	CC
Glass	325	25.2	316	37,390	0.008391	0.015061	0.557	FR
Basalt		25.2	408	51,890	0.008391	0.012324	0.681	FR

f_c', concrete compressive strength, E_f, FRP modulus of elasticity, f_{ult-f} = FRP designs tensile strength, ρ_f reinforcement ratio, ρ_b balance reinforcement ratio, EFM, expected failure mode

Table 5.6: Maximum bond forces for FRP-RC beams based on bond strength results

FRP Type	Temp. °C	T_m kN	F kN Without EC	F kN With EC
Carbon		130.97	209.5	213.21
Glass	23	88.0	50.62	80.08
Basalt		101.92	66.05	103.92
Carbon		98.96	38.53	72.55
Glass	325	49.7	10.53	39.2
Basalt		64.09	13.95	52.5

T_m, reinforcement's maximum theoretical tension force, F, reinforcement's maximum bond force based on bond tests results, EC, end cap

Table 5.7: Theoretical flexural capacities of all RC beams as per ACI codes and predicted flexural capacities based on bond strength results

	P	GFRP Without EC	GFRP With EC	BFRP Without EC	BFRP With EC	CFRP Without EC	CFRP With EC	Steel
Unheated Beams	P_{th-ult}	66.51		75.94		94.69		67.66
	$P_{pred-ult}$	39.14	61.0	50.42	75.94	85.74*	85.74*	
Heated Beams	P_{th-ult}	35.16		44.32		66.05		63.1
	$P_{pred-ult}$	7.46	27.74	9.66	36.33	25.81	48.55	

P, ultimate load capacity, EC, end cap anchorage, P_{th-ult}, theoretical ultimate load capacity, $P_{pred-ult}$, predicted ultimate load capacity, *:load capacity is governed by shear

5.3.4 Theoretical prediction of cracking load

Cracks initiate when the tensile stress in the concrete exceeds the tensile strength of concrete, cracking load can be estimated using Eqs. 5.36 through 5.40. Calculated cracking loads for all RC beams are summarized in Table 5.8.

1. Calculate moment of inertia of un-cracked transformed section (gross section) (I_g) from:

$$I_g = \frac{bh^3}{12}$$

(5.36)

Where h= overall height of the beam =180 mm and b = cross section width =130 mm

2. Calculate modulus of rupture of concrete (f_{cr}) using

$$f_{cr} = 0.62\sqrt{f_c'} \qquad (ACI318\ Code)$$

(5.37)

3. Calculate the cracking moment (M_n) using

$$M_{cr} = cracking\ moment = \frac{2f_{cr}I_g}{h}$$

(5.38)

4. Calculate the cracking load (P_{cr}) using

$$P_{cr} = \frac{6M_{cr}}{L}$$

(5.39)

5. For concrete exposed to 500°C, tensile strength is 20% of its normal temperature strength as per EuroCode EN 1992-1-2:2004, therefore cracking load can be calculated using modulus of rupture of 0.2 f_{cr}.

Table 5.8: Theoretical cracking load of all RC beams, kN

GFRP		BFRP		CFRP		Steel	
Normal Temp.	High Temp.	Normal Temp.	High Temp.	Normal Temp.	High Temp.	Normal Temp.	High Temp.
14.5	2.9	14.5	2.9	14.5	2.9	14.5	2.9

5.3.5 Theoretical prediction of moment of inertia of the cracked section

The moment of inertia of the cracked transformed section (I_{cr}) can be calculated using Eq. 5.40, cracked moment of inertia for different beams are as summarized in Table 5.9.

$$I_{cr} = \left[\frac{bd^3k^3}{3}\right] + \left[(n_f A_f)d^2(1-k)^2\right]$$

(5.40)

where

d = beam's effective depth;

k, n and ρ_f can be calculated using Eqs. 5-8 through 5-10

$$E_C = 4700\sqrt{f_c'} \text{ for normal concrete and}$$

$$E_C \text{ at } 500°C = \frac{1}{6} \times E_C \text{ at } 23°C, \text{ as per Eurocode, EN } 1992 - 1 - 2: 2004$$

Table 5.9: Cracked moment of inertia for different RC beams

Beam Type	Exposure Type	f_c' MPa	E_c GPa	E_f or E_s GPa	n	k	I_{cr} mm^4	M_{cr} kN.m
CFRP	N.T	34	27.4	119	4.34	0.236	9956228	2.538
GFRP	N.T	34	27.4	47.14	1.72	0.156	4482230	2.538
BFRP	N.T	34	27.4	65.85	2.40	0.182	6016890	2.538
Steel	N.T	34	27.4	228	8.32	0.310	16757029	2.538
CFRP	H.T	25.2	4.6	80.41	17,6	0.415	28871751	0.508
GFRP	H.T	25.2	4.6	37.39	8.19	0.308	16548703	0.508
BFRP	H.T	25.2	4.6	51.89	11.36	0.351	21181234	0.508
Steel	H.T	25.2	4.6	210	45.66	0.572	51459577	0.508

N.T., normal temperature exposure, H.T., high temperature exposure, E_c, concrete modulus of elasticity, E_f, FRP modulus of elasticity, E_s, steel modulus of elasticity, I_{cr}, cracked moment of inertia, M_{cr}, cracking moment, fc', concrete compressive strength.

5.3.6 Theoretical prediction of mid-span deflection of FRP-RC beams

For simply supported beam of span L, loaded with two equal concentrated load (P/2) applied at a distance L/3 from the support, as shown in Fig. 5.7, short term mid-span deflection (Δ) can be calculated using :

$$\Delta = \frac{23PL^3}{1296 \, E_c \, I_e} \tag{5.41}$$

According to Eq. 5.41, the mid span deflection of RC beams depends mainly on the beam's effective moment of inertial (I_e). Many research works were performed to

predict the FRP-RC beam's effective moment of inertia (I_e) which led to modify or develop new empirical equations as summarized below:.

1. Branson, 1977, proposed a method for calculating the effective moment of inertia, I_e, of steel-RC beams and this method was adopted by ACI-318 code.

$$I_e = I_g \left(\frac{M_{cr}}{M_a}\right)^3 + I_{cr}\left[1 - \left(\frac{M_{cr}}{M_a}\right)^3\right] \leq I_g \tag{5.42}$$

Where, M_a = the maximum service moment at the required stage,

M_{cr} = cracking moment, and

I_{cr} = the moment of inertia of the cracked transformed section,

I_g = the moment of inertia of the gross section,

This model underestimates the deflection if applied to FRP-RC beams.

2. **Alsayed and Alsalloum, 2000, proposed a modified ACI-318 equation, as follows:**

$$\boldsymbol{I_e} = I_g \left(\frac{M_{cr}}{M_a}\right)^{5.5} + I_{cr}\left[1 - \left(\frac{M_{cr}}{M_a}\right)^{5.5}\right] \leq I_g \tag{5.43}$$

3. ACI 440.1R, 2003, modified ACI-318 equation with new factors were introduced to account for the reduced area of the compression after exceeding the cracking moment.

$$I_e = \frac{I_g}{\beta} \left(\frac{M_{cr}}{M_a}\right)^3 + \alpha I_{cr}\left[1 - \left(\frac{M_{cr}}{M_a}\right)^3\right] \leq I_g \tag{5.44}$$

$\text{where } \alpha = 0.84 \text{ and } \beta = 7$

In the third revision of ACI 440.1R, 2003, the previous equation was modified:

$$I_e = \beta_d I_g \left(\frac{M_{cr}}{M_a}\right)^3 + I_{cr}\left[1 - \left(\frac{M_{cr}}{M_a}\right)^3\right] \leq I_g \text{ when } M_a > M_{cr} \tag{5.45}$$

where β_d is a reduction coefficient related to the reduced tension stiffening exhibited by FRP-reinforced members and can be calculated as follows.

$$\beta_d = \alpha_b \left(\frac{E_f}{E_s} + 1\right) \tag{5.46}$$

$\qquad$ where $\alpha_b = 0.5$ is recommended by ACI 440 for all types of FR bars.

In ACI 440.1R, 2006, β_d was modified as follows:

$$\beta_d = \frac{1}{5}\left(\frac{\rho_f}{\rho_b}\right) \leq 1.0 \tag{5.47}$$

4. Alsayed and Alsalloum, 2000, proposed a new method based on their experimental

    results as follows:

$$I_e = \left[1.4 - \left(\frac{2\times M_a}{15\times M_{cr}}\right)\right] I_{cr} \geq I_{cr} \tag{5.48}$$

5. According to Faza and Ganga, 1992, an assumption of a fully cracked section

    between the two point loads and partially cracked section in the remaining parts of

    the beam was used to develop the modified moment of inertia, I_m, formula as

    follows:

$$I_m = \frac{23 I_e I_{cr}}{8 I_{cr} + 15 I_e} \tag{5.49}$$

$\qquad$ where I_e is calculated according to ACI318 (Branson equation)

6. Bischoff, 2007, proposed the following equation:

$$I_e = \frac{I_{cr}}{1 - \left[\left(1 - \frac{I_{cr}}{I_g}\right)\left(\frac{M_{cr}}{M_a}\right)^2\right]} \leq I_g \tag{5.50}$$

Mid-span deflection of different beams at different load stages such as theoretical cracking load, theoretical ultimate load and theoretical service load is calculated using Eqs. 5.36 through 5.50 and summarized in the Table 5.10. Theoretical mid-span deflections of steel-RC beams were calculated according to ACI318 and summarized in Table 5.11. From Table 5.10, it can be noticed that the last five methods gave approximately equal results, therefore the deflections calculated according to ACI440 were used for comparison purposes with the experimental results.

Table 5.10: Theoretical mid-span deflection of FRP-RC beams at different load stages

Beam		Theoretical Load kN	Theoretical Mid-Span Deflection, mm					
			ACI-318	ACI-318 Modified	**ACI440**	AlSayed , AlSalloum	Faza , Ganga	Bischoff
GFRP N.T.	Δ_{th-cr}	14.5	0.1720	0.1720	**0.1720**	0.1720	0.1720	0.1720
	Δ_{th-s}	23.28	0.9345	1.9763	**2.6594**	3.2828	2.8641	2.4895
	Δ_{th-ult}	66.51	9.7940	11.0902	**10.9067**	11.1236	10.661	10.6323
GFRP H.T.	Δ_{th-cr}	2.9	0.2065	0.2065	**0.2065**	0.2065	0.2065	0.2065
	Δ_{th-s}	12.31	3.2257	3.3414	**3.3701**	3.3447	3.3033	3.2076
	Δ_{th-ult}	35.16	9.5412	9.5563	**9.5594**	9.5563	9.5510	9.5083
BFRP N.T.	Δ_{th-cr}	14.5	0.1720	0.1720	**0.1720**	0.1720	0.1720	0.1720
	Δ_{th-s}	26.58	1.3021	2.4724	**2.5848**	2.8655	2.6126	2.4195
	Δ_{th-ult}	75.94	8.8742	9.4514	**9.3486**	9.4613	9.2571	9.1491
BFRP H.T.	Δ_{th-cr}	2.9	0.2065	0.2065	**0.2065**	0.2065	0.2065	0.2065
	Δ_{th-s}	15.51	3.2518	3.2933	**3.3068**	3.2940	3.2793	3.2174
	Δ_{th-ult}	44.32	9.4061	9.4114	**9.4129**	9.4114	9.4096	9.3846
CFRP N.T.	Δ_{th-cr}	14.5	0.1720	0.1720	**0.1720**	0.1720	0.1720	0.1720
	Δ_{th-s}	30.01	1.4093	2.0579	**1.8091**	2.0101	1.9638	1.8150
	Δ_{th-ult}	85.74	6.2929	6.4537	**6.3875**	6.4557	6.3991	6.3001
CFRP H.T.	Δ_{th-cr}	2.9	0.2065	0.2065	**0.2065**	0.2065	0.2065	0.2065
	Δ_{th-s}	23.12	3.5930	3.6014	**3.6053**	3.6014	3.5985	3.5706
	Δ_{th-ult}	66.05	10.288	10.2897	**10.2902**	10.2897	10.289	10.2790

Δ_{th-cr}, theoretical deflection at theoretical cracking load, Δ_{th-ult}, theoretical deflection at theoretical ultimate load, Δ_{th-s}, theoretical deflection at theoretical service load

Table 5.11: Theoretical mid-span deflection of steel-RC beams as per ACI-318

Beam		Theoretical Load kN		Theoretical Mid-Span Deflection, mm	
		Normal Temp.	High Temp.	Normal Temp.	High Temp.
Steel	Cracking	14.5	2.90	0.172	0.2065
	Serviceable	23.68	22.08	0.648	1.922
	Ultimate	67.66	63.10	2.947	5.495

5.4 Comparison between theory and experiments

5.4.1 Ultimate load capacity

Theoretical flexural capacities of FRP-RC beams (P_{th-ult}), calculated according to ACI440 assuming a perfect bond between bars and concrete up to failure, were compared with both the predicted flexural capacities based on the experimental bond

test results ($P_{pre-ult}$) and the experimental load capacities ($P_{exp-ult}$) as illustrated in Table 5.12.

Table 5.12: Comparison between beams' theoretical and experimental load capacities

Beam Type	P_{th-ult} kN	$P_{pre-ult}$ kN	$P_{exp-ult}$ kN	$P_{exp-ult}$ / $P_{pre-ult}$	$P_{exp-ult}$ / P_{th-ult}	$P_{pre-ult}$ / P_{th-ult}
GFRP- N.T.	66.51	39.14	32.64	0.83	0.49	0.59
GFRP- N.T- End Cap		61.0	58.44	0.96	0.88	0.92
GFRP- H.T.	35.16	7.46	6.85	0.92	0.19	0.21
GFRP - H.T- End Cap		27.74	27.79	1.00	0.79	0.79
BFRP- N.T.	75.94	50.42	38.6	0.77	0.51	0.66
BFRP- N.T- End Cap		75.94	80.2	1.06	1.06	1.00
BFRP- H.T.	44.32	9.66	7.26	0.75	0.16	0.22
BFRP - H.T- End Cap		36.33	47.35	1.30	1.07	0.82
CFRP- N.T.	85.74 (Shear)	85.74	89.97	1.05	1.05	1.00
CFRP- N.T- End Cap		85.74	89.75	1.05	1.05	1.00
CFRP- H.T.	66.05	25.81	31.97	1.24	0.48	0.39
CFRP - H.T- End Cap		48.55	60.8	1.25	0.92	0.74
Steel- N.T.	67.66		76.14	1.13		-
Steel- H.T.	63.1		69.42	1.10		-

P_{th-ult}, theoretical ultimate load capacity based on ACI440 assumptions, $P_{pred-ult}$, predicted ultimate load capacity based on actual bond test result, $P_{exp-ult}$, experimental ultimate load capacity

Based on Table 5.12, the experimental load capacities of control beams with GFRP, BFRP and CFRP bars were (49.1%, 50.8% and 104.7% of their theoretical load capacities) and (83.4%, 76.6% and 104.7% of the predicted load capacities based on actual bond strength results), respectively, indicating that a bond loss failure had happened in GFRP and BFRP beams before reaching either concrete crushing or FRP bar's rupture. Upon adding steel end caps to the ends of the FRP bar's, the experimental load capacities of beams with GFRP, BFRP and CFRP bars had increased to (87.9%, 105.6% and 104.7% of their theoretical load capacities) and (95.8%, 105.6% and 104.7% of the predicted load capacities), respectively.

Upon exposure to 500°C, the experimental load capacities of beams with GFRP, BFRP and CFRP bars were highly decreased to 19.5%, 16.4% and 48.4% of their theoretical load capacities, respectively, indicating that the theoretical values, based on assumption of perfect bond, were no more correct after heating. Upon using the actual bond results in the proposed prediction model, the experimental load capacities of heated GFRP, BFRP and CFRP beam were found at 91.8%, 75.2% and 123.8% of the predicted load capacities. Using steel end caps in GFRP, BFRP and CFRP beam, exposed to 500°C, had increased the experimental load capacities to (79%, 106% and 92% of their theoretical load capacities) and (100.2%, 130.3% and 125.2% of the predicted load capacities) respectively.

Based on the above results, the proposed model for predicting the flexural load capacities of FRP-RC beams, based on actual bond strength results, were reasonably well and showed a good agreement with the experimental results, therefore can be used as a trusted method for prediction of flexural load capacities. Also, it was found that using steel end caps in FRP-RC beams had improved their measured load carrying capacity, before and after exposure to high temperature, to a limit close to the theoretical values.

The experimental load carrying capacity of beams with steel bars, tested before and after exposure to 500°C, were 112.5% and 100% of their theoretical values, respectively, which confirmed that the bond between steel bars and surrounding concrete was strong enough to reach the calculated theoretical capacities.

5.4.2 Mid-span deflection

The comparison between the theoretical and experimental mid-span deflection at cracking and ultimate load was summarized in Table 5.13. The theoretical prediction of deflection of FRP-beams under-estimated the actual deflections due to two reasons;

firstly, the available deflection formulas are based on the assumption of linear behavior of the concrete which is correct only for un-cracked concrete sections, and secondly, most of the current theoretical prediction methods do not take into consideration the effect of bond-slip on inducing more deflections and therefore under-estimate the actual deflection. Some nonlinearity in the beams' behavior had taken place, at high load levels, resulting in more errors in deflection prediction.

The mid-span deflections of control beams with GFRP, BFRP and CFRP bars at cracking and ultimate load were (467%, 537% and 466%) and (122%, 128% and 179%) of the corresponding theoretical values, respectively. Upon using steel end caps, the mid-span deflections at cracking load of GFRP, BFRP and CFRP beam were reduced to 276%, 269% and 312% of their theoretical values due to effect of these caps in improving the beam's stiffness, whereas the deflections at ultimate load were increased to 167%, 252% and 245% of the theoretical ones, respectively, due to the effect of these caps on increasing the non-linear portion of the beam's load-deflection response prior to failure.

After exposure to 500°C, the mid-span deflections of beams with GFRP, BFRP and CFRP bars at cracking and ultimate load were (182%, 237% and 200%) and (209%, 168% and 160%) of the corresponding theoretical values, respectively. Generally, adding the steel caps to beams with GFRP, BFRP and CFRP bars, exposed to 500°C, had increased the ratio between experimental to theoretical mid-span deflection at both cracking and ultimate loads to (240%, 189% and 345) and (207%, 217%, and 240%), respectively.

Beam Type	$\Delta_{\text{th-ult}}$	$\Delta_{\text{th-cr}}$	$\Delta_{\text{th-s}}$	$\Delta_{\text{exp-ult}}$	$\Delta_{\text{exp-cr}}$	$\Delta_{\text{exp-s}}$	$\Delta_{\text{exp-ult}}$ / $\Delta_{\text{th-ult}}$	$\Delta_{\text{exp-cr}}$ / $\Delta_{\text{th-cr}}$	$\Delta_{\text{exp-s}}$ / $\Delta_{\text{th-s}}$
GFRP- N.T.	10.91	0.172	2.66	13.28	0.804	6.55	1.22	4.67	2.46
GFRP- N.T+ E.C				18.25	0.474	4.24	1.67	2.76	1.59
GFRP- H.T.	9.56	0.207	3.37	19.97	0.376	N.A.	2.09	1.82	N.A.
GFRP - H.T+ E.C				19.80	0.496	6.19	2.07	2.4	1.84
BFRP- N.T.	9.35	0.172	2.58	11.98	0.923	6.86	1.28	5.37	2.66
BFRP- N.T+ E.C				23.53	0.462	3.30	2.52	2.69	1.28
BFRP- H.T.	9.42	0.207	3.31	15.86	0.490	N.A.	1.68	2.37	N.A.
BFRP - H.T+ E.C				20.43	0.391	4.02	2.17	1.89	1.21
CFRP- N.T.	6.39	0.172	1.81	11.44	0.802	2.73	1.79	4.66	1.51
CFRP- N.T+ E.C				15.68	0.536	2.74	2.45	3.12	1.51
CFRP- H.T.	10.29	0.207	3.61	16.42	0.413	9.53	1.60	2.0	2.64
CFRP - H.T+ E.C				24.65	0.714	7.51	2.40	3.45	2.08
STEEL-RC - N.T.	2.95	0.172	0.65	11.13	1.376	1.59	3.77	8.00	2.45
STEEL-RC - H.T.	5.50	0.207	1.92	13.68	0.321	2.73	2.49	1.55	1.42

$\Delta_{\text{exp-ult}}$, measured deflection at measured ultimate load, $\Delta_{\text{th-ult}}$, theoretical deflection at theoretical ultimate load as per ACI, $\Delta_{\text{exp-cr}}$, measured deflection at measured cracking load, $\Delta_{\text{th-cr}}$, theoretical deflection at theoretical cracking load as per ACI, $\Delta_{\text{exp-s}}$, measured deflection at service load, $\Delta_{\text{th-s}}$, theoretical deflection at service load, N.A., not available, E.C, end cap

5.4.3 Cracking load

The experimental cracking load was compared with the theoretical values as shown in Table 5.14. The experimental cracking loads of the control beams with GFRP, BFRP and CFRP bars were 74.2%, 82.3% and 94.2% of their theoretical values and were increased to 91.7%, 96.5%, and 96.2% of the theoretical ones, after adding steel end caps to the ends of the FRP bars, respectively. Upon exposure to 500°C, the experimental cracking loads were reduced to 51.7%, 55.8% and 54.6% of their theoretical values then were increased to 124%, 93.4%, and 93.2% of the theoretical ones, after adding steel end caps to the ends of the FRP bars. The effect of using steel end caps in the control and heated FRP beams was clear, especially in the GFRP and

BFRP-RC beams, in improving their measured cracking load to be close to the theoretical cracking loads.

Contrary to beams with FRP bars, the average measured cracking load of beams with steel bars was higher than their theoretical cracking load and reduced to 100.6% of the theoretical cracking load after exposure to 500°C.

Table 5.14: Theoretical and experimental cracking load for different RC beams

Beam Type	P_{th-cr}	P_{exp-cr}	P_{exp-cr} / P_{th-cr}	Beam Type	P_{th-cr}	P_{exp-cr}	P_{exp-cr} / P_{th-cr}
GFRP- N.T.	14.5	10.762	74.22%	CFRP- N.T.	14.5	13.667	94.26%
GFRP- N.T+ E.C		13.297	91.70%	CFRP- N.T+ E.C		13.946	96.18%
GFRP- H.T.	2.9	1.501	51.76%	CFRP- H.T.	2.9	1.584	54.62%
GFRP - H.T+ E.C		3.596	124.0%	CFRP- H.T+ E.C		2.705	93.28%
BFRP- N.T.	14.5	11.938	82.33%	Steel-RC - N.T.	14.5	20.67	142.5%
BFRP- N.T+ E.C		13.990	96.48%	Steel-RC - H.T.	2.9	2.919	100.6%
BFRP- H.T.	2.9	1.620	55.86%				
BFRP - H.T+ E.C		2.709	93.41%				

P_{exp-cr}, measured cracking load, P_{th-cr}, theoretical cracking load as per ACI, E.C, end cap

5.4.4 Failure modes

Theoretically, over-reinforced FRP-RC beams, used in this study, should fail by concrete crushing whereas expected failure modes, based on bond tests results, showed that failure modes were mostly due to bond loss between the bars and concrete except in the control CFRP-RC beams where the shear failure were expected. Steel-RC beams were expected to fail due to steel yielding before reaching the concrete crushing strain.

The theoretical mode of failure, based on ACI assumption of perfect bond, and the expected failure mode, based on the bond tests results, were compared with the experimentally observed failure modes and summarized in Table 5.15.

Table 5.15: Theoretical, expected and observed failure modes

FRP Type	T °C	Theoretical FM		Expected FM		Observed FM	
		Without EC	With EC	Without EC	With EC	Without EC	With EC
Carbon	23	S		S	S	S	S
Glass		CC		BS	BS	BS	CC
Basalt		CC		BS	CC	BS	S
Carbon	325	CC		BS	BS	BS	BS+S
Glass		FR		BS	BS	BS	BS
Basalt		FR		BS	BS	BS	BS+S

FM, failure mode, CC, concrete crushing, FR, FRP rupture, S, shear failure, EC, end cap, BS, bond slip

From Table 5.15, it was noticed that most of the observed failure modes were matching with the expected failure modes except in the case of the beams reinforced with end-capped FRP bars, tested at normal temperature, where the end-capped BFRP and CFRP-RC beams failed in shear as explained earlier in Sections 4.6.4.2 and 4.6.4.3, while the end-capped GFRP-RC beam failed due to concrete crushing and not as expected by bond loss, which means that the concrete reaches it crushing strain while the bond between the end-capped GFRP bars and concrete was still working. In the case of steel-RC beams, the observed failure mode was the same as the theoretical expected mode where steel yielded before concrete crushing.

5.4.5 Strains of concrete and reinforcement at failure

The experimental and theoretical strains of concrete and reinforcement are summarized in Table 5.16. As shown, maximum measured strain results were little different than the theoretical calculated strain values which can be explained that the assumption of linear strain distribution in FRP-RC beams is only accurate at low load level at which the bond is still perfect and cracking width is still minor while at ultimate load level, bonds become weaker and cracks become wider due to FRP's low modulus

of elasticity, hence the linear strain distribution becomes no more accurate. In the case of FRP-RC beams that carried high applied load, an interaction between shear and flexure occurred at the high load level resulting in diagonal tension cracks which leads to additional rebars strain therefore, higher measured reinforcement strain than the theoretical values were noticed in the CFRP-RC beams and the end-capped BFRP-RC beams which failed due to shear.

In the case of GFRP and BFRP-RC beams that failed at low load levels, the low modulus of elasticity of these GFRP and BFRP bars causes wider cracks that extended deeply towards the compression zone resulting in higher concrete compressive strain than predicted strains and therefore lower ultimate measured loads than expected loads.

Table 5.16: Experimental and theoretical strains of concrete and reinforcement at ultimate load

	Experimental		Theoretical	
	ε_c x10^{-6}	ε_r x10^{-6}	ε_c x10^{-6}	ε_r x10^{-6}
GFRP- N.T.	1412	5419	1213	6835
GFRP- N.T- End Cap	3346	10911	2410	10815
GFRP- H.T.	1075	1644	960	1793
GFRP - H.T- End Cap	4093	6103	3589	6676
BFRP- N.T.	1707	5075	1406	6390
BFRP- N.T- End Cap	2689	10362	3000	9853
BFRP- H.T.	1443	1869	1121	1923
BFRP - H.T- End Cap	3997	7556	4248	6441
CFRP- N.T.	2740	7144	2317	6248
CFRP- N.T- End Cap	2805	6702	2317	6248
CFRP- H.T.	3255	2835	2645	3051
CFRP - H.T- End Cap	4559	6952	5033	5744
Steel- N.T.	5418	6910	3000	11900
Steel- H.T.	6201	N.A.	3000	9290

ε_c, concrete strain at ultimate load, ε_r, reinforcement strain at ultimate load, N.A., not available

CHAPTER SIX
CONCLUSIONS AND RECOMMENDATIONS

6.1. Introduction

In this thesis, the post-heating performance of three types of FRP bars in concrete was evaluated. For that, three tracks of testing were followed. In the first, the mechanical performance of FRP bars under elevated temperatures in the range of 125 to 375°C was evaluated, whereas the post-heating bond behavior between FRP bars and concrete under the same temperature spectrum was evaluated using conventional pullout specimens. In the third track, post-heating flexural response of FRP reinforced concrete beams (130×180×1200 mm) was studied under four-point loading configuration. The FRP reinforcement bars in the beams were placed on the tension side, with or without end anchorage using special steel caps. For the purpose of comparison, identical pullout and beam specimens were prepared using conventional steel reinforcement of the same bar size and numbers with those of the FRP bars.

6.2. Conclusions

The following findings are based upon the discussion of chapters 4 and 5 of this thesis:

1. Effect of high temperatures on mechanical properties of FRP/Steel bars and bond behavior between FRP/Steel bars and concrete

FRP suffered significant reduction in their mechanical properties due to exposure to high temperatures. This reduction is almost linear up to a critical temperature of 325°C at which significant degradation in the tensile strength and elastic modulus of FRP bars in the ranges of (45 ~ 55%) and (20~30%), respectively. This reduction increased with exposure to temperature of up to 450°C at which GFRP and BFRP bars

184

melted and lost their total tensile strength capacity. The impact of heating on tensile strength and elastic modulus of steel bars was minor.

Steel bars attained the highest bond strength with concrete followed, in sequence, by CFRP, BFRP and GFRP because of their better surface characteristics. Three types of failure modes were noticed; pullout failure, concrete splitting failure and concrete cone failure. The percentage reduction in bond strength and stiffness was more pronounced in pullout specimens with FRP bars than those with steel bars under elevated temperatures; the highest percentage reductions in bond strength between concrete and BFRP, GFRP, CFRP and steel bars after exposure up to 325°C were 79.9%, 79.2%, 81.5% and 27.2%, respectively.

2. Flexural behavior of FRP/Steel RC beams

RC beams with GFRP and BFRP bars tested at ambient temperature failed before reaching their theoretical maximum load capacity due to bond failure. Therefore, the measured load capacity values for these beams were less than the theoretical ones, computed according to ACI440 code. Contrariwise, the experimental load capacity for beams with CFRP bars at ambient temperature was very close to the theoretical values; owing to the satisfactory surface characteristics of CFRP bars which imparted satisfactory bond with concrete. Stiffness of all RC beams was reduced after cracking with the highest reduction noticed in the beams with BFRP bars, followed, in sequence, by the control beams with GFRP, CFRP and steel bars at 71%, 65%, 48% and 26.5%. Beams with steel bars showed pure flexural failure; confirming the assumption that perfect bond strength between steel and concrete existed. At failure, number of cracks in beams with steel bars was higher than that of similar beams with FRP bars yet the cracks visible width was smaller than that of those with FRP bars. The mid-span

185

deflection for beams with steel bars was smaller than that of those with FRP bars; owing to steel bars higher stiffness.

3. Effect of heating to 500°C on the flexural behavior of FRP/Steel RC beams

Upon exposure to 500°C for 90 minutes, RC beams with FRP bars failed at relatively low load levels due to degradation of bars' tensile strength and loss in bond between the FRP bars and the surrounding concrete. Hence, they experienced significant loss in load capacity, stiffness and total absorbed energy, yet showed increased deflection and ductility; the maximum percentage reduction in load capacity, stiffness, and total absorbed energy reached 81.2%, 78.8%, and 69.2% whereas the ductility index, and ultimate load's deflection increased by as high as 93.7% and 50.3%, respectively. The beams with CFRP bars showed superior flexural behavior as compared to those with GFRP and BFRP bars under elevated temperatures; owing to the former bars higher resistance to heating. The detrimental impact of heating to 500°C on RC beams with steel bars were minimal as compared to that on heated beams with FRP bars.

4. Effect of using end caps on the pre- and post-heating flexural behavior of FRP/Steel RC beams

Pre and post-heating bond strength between FRP bars and concrete was improved upon the use of end caps as an anchorage technique; the residual for bond reached as high as (332 and 255%) for exposure temperatures of 23 and 325°C, respectively. Using the end caps with FRP bars in reinforcing beams enhanced the load carrying capacity, cracking load, stiffness, total absorbed energy and ultimate load's deflection yet contributed to reducing ductility, except for the beams tested at normal temperature. The positive impact of using steel end caps on flexural behavior of FRP

beams was more pronounced at higher temperatures rather room temperature. The pre- and post-heating residual load capacity, stiffness, ductility index, total absorbed energy and deflection at ultimate load for FRP-RC beams with end capping reached as high as (207.9%, 225.4%, 146.0%, 452.6% and 196.3%) and (122.7%, 57.9%, 99.3%, 215.1% and 215.5%), respectively. Whenever its estimation was possible, the overall ductility factor was increased upon the use of steel end cap especially for specimens with FRP bars and subjected to an elevated temperature of 500°C. The installation of steel end caps to the BFRP and CFRP bars had changed the failure mode of corresponding beams from bond-slip failure or flexural failure to shear-flexural failure, increased the number of cracks and reduced the visible cracks widths.

5. The theoretical studies

The ACI analytical formulae for the prediction of ultimate load of beams with FRP bars were over-estimated whereas ACI formulae used for the prediction of mid-span deflections were under-estimated, compared to the corresponding measured values; because bond reduction and excessive slippage as well as post-cracking nonlinearity due to heating were not accounted for in ACI analytical formulae. Upon the use of steel end caps for anchorage purposes, predictions became much closer to measured values; because the anchorage system applied had allowed different FRP bars to have a higher contribution to load capacity.

The present proposed model for predicting post-heating bond stress-slip relationship showed an acceptable agreement with experimentally obtained curves. Furthermore, the method proposed for predicting load capacity of FRP-RC beams, based upon actual pre and post-heating mechanical properties for FRP bars and concrete and their bond characteristics, gave reasonably reliable results.

6.3. Recommendations

Some important recommendations for further studies on the fire-response of FRP-RC elements are listed below:

1. Fire endurance tests on loaded FRP-RC elements are required to investigate the structural behavior of these heated elements and define the proper failure criteria FRP-RC elements under fire.

2. Fire endurance tests on loaded end-capped FRP-RC elements are required to investigate the effect of using these caps on the structural behavior.

3. New insulation methods need to be proposed and examined to insulate the ends of the FRP-RC beams.

4. Minimum concrete cover thickness should be determined experimentally based upon concrete materials properties, reinforcement type and exposure temperature for beams with FRP bars. This is to provide enough bar insulation at that the FRP bars are capable of maintaining their mechanical properties and bond with concrete during and after exposure to high temperatures.

REFERENCES

Abbas, A., and Hogg, P., (2006), Fire Testing of Concrete Beams With Fibre Reinforced Plastic Rebar, Composites Part A: Applied Science and Manufacturing, Vol.37, No. 8, p.p. 1142-1150.

Abbasi, A , and Hogg, P., (2005b), A Model for Predicting the Properties of The Constituents of a Glass Fibre Rebar Reinforced Concrete Beam at Elevated Temperatures Simulating a Fire Test, Composites Part B: Engineering, Vol. 36, No. 5, p.p. 384–393.

Abbasi, A., Hogg, P., (2005a), Temperature and Environmental Effects on Glass Fibre Rebar: Modulus, Strength and Interfacial Bond Strength with Concrete, Composites: Part B, Vol. 36, p.p. 394-404.

ACI 2004: ACI 440.3R-04, Guide Test Methods for Fiber-Reinforced Polymers (FRPs) for Reinforcing or Strengthening Concrete Structures, American Concrete Institute.

ACI 2004: ACI 440.4R-04, Prestressing Concrete Structures with FRP Tendons,, American Concrete Institute.

ACI 2005: ACI 318R-05, Building Code Requirements for Structural Concrete and Commentary, American Concrete Institute.

ACI 2008: ACI 440.2R-08, Guide for the Design and Construction of Externally Bonded FRP Systems for Strengthening Concrete Structures, American Concrete Institute.

ACI 2015: ACI 440.1R-15, Guide for the Design and Construction of Structural Concrete Reinforced with Fiber-Reinforced Polymer (FRP) Bars, American Concrete Institute.

Adelzadeh, M., Hajiloo, H., and Green, M. F., (2014), Numerical Study of FRP Reinforced Concrete Slabs at Elevated Temperature, Polymers, Vol. 6, p.p. 408-422.

Aiello, M., and Ombres, L., (2002), Structural Performances of Concrete Beams with Hybrid (Fiber-Reinforced Polymer-Steel) Reinforcements, Journal of Composites for Construction, Vol. 6, No. 2, p.p. 133-140.

AISI: A Designers' Handbook Series No. 9004 , High Temperature Characteristics of Stainless Steels, American Iron and Steel Institute, 2011.

Alarcon-Ruiz, L., Platret, G., Massieu, E., and Ehrlacher, A., (2005), The Use of Thermal Analysis In Assessing The Effect of Temperature on A Cement Paste, Cement And Concrete Research, V. 35, p.p. 609–613.

Alsayed, S. H., Al-Salloum, Y. A., and Almusallam, T. H., (2000) , Performance of Glass Fiber Reinforced Plastic Bars as A Reinforcing Material for Concrete Structures, Composites Part B: Engineering, Volume 31, Issues 6-7, p.p. 555-567.

Al-Sunna, R., Pilakoutas, K., Hajirasouliha, I., and Guadagnini, M., (2012), Deflection Behaviour of FRP Reinforced Concrete Beams and Slabs: An Experimental Investigation, Composites Part B: Engineering, Volume 43, No. 5, p.p. 2125-2134.

Al-Sunna, R., Pilakoutas, K., Waldron, P., and Al-Hadeed, T., (2005), Deflection of FRP reinforced concrete beams, in: 4th Middle East Symposium on Structural Composites for Infrastructure Applications (MESC-4), Alexandria, Egypt.

ASTM: C127-15, (2015), Standard Test Method for Relative Density (Specific Gravity) and Absorption of Coarse Aggregate, ASTM International, West Conshohocken, PA.

ASTM: C128-15, (2015), Standard Test Method for Relative Density (Specific Gravity) and Absorption of Fine Aggregate, ASTM International, West Conshohocken, PA.

ASTM: C136/C136M-14, (2014), Standard Test Method for Sieve Analysis of Fine and Coarse Aggregates, ASTM International, West Conshohocken, PA.

ASTM: C143 / C143M-15a, (2015), Standard Test Method for Slump of Hydraulic-Cement Concrete, ASTM International, West Conshohocken, PA.

ASTM: C192 / C192M-16a, (2016), Standard Practice for Making and Curing Concrete Test Specimens in the Laboratory, ASTM International, West Conshohocken, PA.

ASTM: C39 / C39M-16b, (2016), Standard Test Method for Compressive Strength of Cylindrical Concrete Specimens, ASTM International, West Conshohocken, PA.

ASTM : C496 / C496M-11, (2004), Standard Test Method for Splitting Tensile Strength of Cylindrical Concrete Specimens, ASTM International, West Conshohocken, PA.

ASTM: C617 / C617M-15, (2015), Standard Practice for Capping Cylindrical Concrete Specimens, ASTM International, West Conshohocken, PA.

ASTM: D7205 / D7205M-06, (2011), Standard Test Method for Tensile Properties of Fiber Reinforced Polymer Matrix Composite Bars, ASTM International, West Conshohocken, PA.

Baena, M., Torres, L., Turon, A., and Barris, C., (2009), Experimental Study of Bond Behaviour between Concrete and FRP Cars Using a Pull-out Test, Composites: Part B, Vol. 40, No. 8, p.p. 784–797.

Bai, Y., and Keller, T., (2009), Time Dependence of Material Properties of FRP Composites in Fire. Journal of Composite Materials, Vol. 43, No. 21, p.p. 2469-2484.

Bai, Y., Keller, T., and Valle´e, T., (2007b), Modeling of Thermo-Physical Properties and Thermal Response for FRP Composites in Fire, Asia-Pacific Conference on FRP in Structures (APFIS), p.p. 645-650.

Bai, Y., Valle´e, T., and Keller, T., (2007a), Modeling of Thermo-Physical Properties for FRP Composites Under Elevated and High Temperature, Composites Science and Technology, Vol. 67, No. 15-16, p.p. 3098–3109.

Bai, Y., Valle´e, T., and Keller, T., (2008), Modeling of Thermal Responses for FRP Composites under Elevated and High Temperatures, Composites Science and Technology, Vol. 68, p.p. 47–56.

Belarbi, A., and Wang, H., (2004), Bond–Slip Response of FRP Reinforcing Bars in Fiber Reinforced Concrete under Direct Pullout, In: Proceedings of ICFRC international conference on fiber composites, high performance concretes and smart materials, Chennai, India, p.p. 409–19.

Bellakehal, H., Zaidi, A., Masmoudi, R. and Bouhicha, M., (2014), Behavior of FRP Bars-Reinforced Concrete Slabs under Temperature and Sustained Load Effects, Polymers, Vol. 6, 873-889.

Bisby, L. A., Green, M., and Kodur, V. R., (2005a), Response to Fire of Concrete Structures That Incorporate FRP., Progress in Structural Engineering and Materials, Vol. 7, No. 3, p.p. 136–149.

Bisby, L.A, Williams, B.K, Kodur, V.R., Green, M.F., and Chowdhury, E., (2005b), Fire Performance of FRP Systems For Infrastructure: A State-of-the-Art Report , Research Report 179, Queen's University, Kingston and National Research Council, Ottawa.

Bischoff, P.H., (2007) , Deflection Calculation of FRP Reinforced Concrete Beams Based on Modifications to the Existing Branson Equation, Journal of Composite for Construction, Vol. 11, No. 3, p.p. 4–14.

Branson, D.E., (1977), Deformation of Concrete Structures, McGraw-Hill Book Company, New York, 1977, 546 pp.

Brik, V. B., (2003), Advanced Concept Concrete Using Basalt Fiber/BF Composite Rebar Reinforcement, Final Report for Highway-IDEA Project 86, Research & Technology Corp.

British Standards Institution (BSI), (1987), BS 476-20:1987, Fire tests on building materials and structures. Method for determination of the fire resistance of elements of construction, BSI, London.

British Standards Institution (BSI), (2009), BS EN 12390-3:2009, Testing hardened concrete. Compressive strength of test specimens, BSI, London.

Brown, V.L., and Bartholomew, C.L., (1996), Long-term deflections of GFRP-reinforced concrete beams, In ICCI'96: Proceedings of the 1st International Conference on Composites in Infrastructures, Tucson, Ariz., 15–17 January 1996.

Edited by H. Saadatmanesh and M.R. Ehsani. University of Arizona, Tucson, Ariz. pp. 389–400.

Cao, S., and Wu, Z., (2008), Tensile Properties of FRP Composites at Elevated and High Temperatures, Journal of Applied Mechanics Vol.11, pp. 963-970.

Carvelli, V., Pisani, M.A., and Poggi, C., (2011), High Temperature Effects On The Mechanical Response Of GFRP Reinforced Concrete Members, 16th International Conference on Composite Structures ICCS 16, University of Porto, Faculty of Engineering, Porto.

Chan, Y.N., Luo, X., and Sun, W., (2000), Compressive Strength and Pore Structure of High-Performance Concrete after Exposure to High Temperature Up to 800, Cement And Concrete Research, V. 30 ,No. 2, Pp. 247–251.

Chan, Y.N., Peng, G.F., and Anson, M., (1999), Residual Strength and Pore Structure of High Strength Concrete and Normal Strength Concrete After Exposure to High Temperatures, Cement and Concrete Research, V. 21, No. 1, p.p. 23-27.

Chen, B., and Liu, J., (2004), Residual Strength of Hybrid-Fiber-Reinforced High-Strength Concrete after Exposure to High Temperatures, Cement and Concrete Research, Vol. 34, Nol. 6, p.p.1065–1069.

Chin, J. W., Aouadi, K., and Nguyen, T., (1997), Effects of Environmental Exposure on Fiber-Reinforced Plastic. (FRP) Materials Used in Construction, Journal of Composites Technology and Research, Vol. 19, No. 4, pp. 205-213.

Chowdhury, E. U., Green, M. F., Bisby, L. A., Bénichou, N., and Kodur, V. K. R., (2007), Thermal and Mechanical Characterization of Fibre Reinforced Polymers, Concrete, Steel, and Insulation Materials for use in Numerical Fire Endurance Modelling, Structures under Extreme Loading, Proceedings of Protect 2007, Whistler, B.C. , pp. 1-10.

Chowdhury, E.U., Eedson, R., Bisby, L.A., Green, M.F., and Bénichou, N., (2011), Mechanical Characterization of Fibre Reinforced Polymers Materials at High Temperature, Fire Technology, Vol. 47, No. 4, pp 1063–1080.

Ciampi, V., Eligehausen, R., Bertero, V., and Popov, E., (1982), Analytical model for concrete anchorages of reinforcing bars under generalized excitations, Report of Earthquake Engineering Research Center NO. UCB/EERC-82/23, University Of California, Berkeley.

Concrete Society, (2012), Technical Report TR55, Design Guidance for Strengthening Concrete Structures using Fibre Composite Materials.

Cosenza, E., Manfredi, G., Pecce, M., and Realfonzo, R., (1999), Bond between Glass Fiber Reinforced Plastic Reinforcing Bars and Concrete Experimental Analysis, ACI Special Publication 188, P.P. 347-358.

Cosenza E., Manfredi G., Realfonzo R., (1995), Analytical modelling of bond between FRP reinforcing bars and concrete. In: Taerwe L, editor. Nonmetallic (FRP) reinforcement for concrete structures. London: E & FN Spon; p. 164–71.

Crea F., Porco G., and Zinno R., (1997), Experimental Evaluation of Thermal Effects on the Tensile Mechanical Properties of Pultruded GFRP Rods. Applied Composite Materials, Vol. 4, No. 3, pp 133–143.

CSA, (2002): CAN/CSA-S806-02 (R2007), Design and Construction of Building Components with Fibre-Reinforced Polymers, Canadian Standards Association International, Ottawa, Canada.

CSA, (2014): CAN/CSA-S6: Canadian Highway Bridge Design Code, Canadian Standards Association, Ottawa, Canada.

Dias, W. P., Khoury, G. A., and Sullivan, P. J., (1990), Mechanical Properties of Hardened Cement Paste Exposed to Temperatures up to 700 °C (1292F) , ACI Materials Journal, Vol. 87, No. 2, pp. 160-166.

Darby, A., Ibell, T. and Clarke, J., (2004), TR55 Design guidance for strengthening concrete structures using fibre composite materials. The Concrete Society.

Ehsani, M. R., and Saadatmanesh, H., (1996), Design Recommendations for Bond of GFRP Rebars to Concrete, Journal of Structural Engineering, Vol. 122, No.3, Page 247-254.

El-Gamal, S., AbdulRahman, B., and Benmokrane, B., (2010), Deflection Behaviour of Concrete Beams Reinforced with Different Types of GFRP Bars, Proceedings of the 5th International Conference on FRP Composites in Civil Engineering (CICE 2010) , Beijing, China.

Eligehausen R., Popov E.P., and Bertero V.V., (1983), Local bond stress-slip relationships of deformed bars under generalized excitations: experimental results and analytical model. Berkeley: Earthquake Engineering Research Center, University of California.

Ellis, Devon S., (2009), Evaluation of Post-Fire Strength of Concrete Flexural Members Reinforced with Glass Fiber Reinforced Polymer (GFRP) bars, Thesis (Ph.D.), The University of Wisconsin Milwaukee, 170 pages; Publication Number 3438489.

El-Refai, A., Ammar, M., and Masmoudi, R., (2014), Bond Performance of Basalt Fiber-Reinforced Polymer Bars to Concrete, Journal of Composites for Construction, Vol. 19, No. 3, p.p. 04014078-1 to 04014078-11.

El-Sayed, A. K., El-Salakawy, E. F., and Benmokrane, B., (2005), Shear Strength of Concrete Beams Reinforced with FRP Bars: Design Method, ACI Special Publications 230-54, p.p.955-974.

EN 1992-1-2, (2004), Eurocode 2: Design of concrete structures - Part 1-2: General rules - Structural fire design [Authority: The European Union Per Regulation 305/2011, Directive 98/34/EC, Directive 2004/18/EC].

EN 1994-1-2, (2005), Eurocode 4: Design of composite steel and concrete structures - Part 1-2: General rules - Structural fire design [Authority: The European Union Per Regulation 305/2011, Directive 98/34/EC, Directive 2004/18/EC].

Ezzeldin, S. A., and Shrive, N. G., (1999), Smart FRP Prestressing Tendons: Properties and Prospects, Proceedings to the Second Middle East Symposium on Structural Composites for Infrastructure Applications, p.p. 90-93.

Faiyadh, F. I., and Al-Ausi, M. A., (1986), Effect of Elevated Temperatures on Splitting Tensile strength of Fiber Concrete, The International Journal of Cement Composites and Lightweight Concrete, Vol. 11, No.3, p.p. 175-178.

Faza, S. S., and Ganga Rao, H. V. S., (1992), Pre- and post-cracking deflection behavior of concrete beams reinforced by fiber reinforced plastic rebars., Proc., First International Conference on the Use of Advanced Composite Materials in Bridges and Structures, Canadian Society for Civil Engineering, Montreal, 151–160.

Fu, Y. N., Zhao, J., and Li, Y. L., (2011), Research on Tensile Mechanical Properties of GFRP Rebar after High Temperature", Advanced Materials Research, Vol. 181-182, pp. 349-354.

FHWA Report, (2007), Thermal coefficient of Portland cement concrete." United States department of transportation- Federal Highway Administration. www.fhwa.dot.gov/pavement /pccp/thermal.cfm, USA.

Galati, N., Nannia, A., Dharanib, L. R., Focaccic, F., and Aiello, M. A., (2006), Thermal Effects on Bond between FRP Rebars and Concrete, Composites Part A: Applied Science and Manufacturing, Vol. 37, No. 8, p.p. 1223-1230.

Gates, T. S., (1991), Effects of Elevated Temperature on the Viscoelastic Modeling of Graphite Polymeric Composites, NASA Technical Memorandum 104160, National Aeronautics and Space Administration, Langley Research Center.

Georgali, B., and Tsakiridis, P.E., (2005), Microstructure of Fire-Damaged Concrete. A Case Study, Cement and Concrete Composites, V.27, No. 2, p.p. 255–259.

Goraya, R.A., Ahmed, K., and Tahir, M. A., (2011), Effect of Surface Texture on Bond Strength of GFRP Rebar in Concrete, Mehran University Research Journal of Engineering and Technology, Vol. 30, No. 1, p.p. 45-52.

Harries, K. A., Porter, M. L., and Busel, J., (2003), FRP Materials and Concrete - Research Needs, Concrete International, Vol. 25, No 10. p.p. 69-74.

Hertz, K. D., (1992), Danish Investigation on Silica Fume Concrete at Elevated Temperatures, ACI Materials Journal, Vol. 89, No. 4, pp. 345-347.

Hognestad, E., Hanson N. W., and McHenry, D. (1955), Concrete stress distribution in ultimate strength design, ACI Journal Proceedings, Vol. 52, No. 4, pp. 455-480.

Hulin, T., Hodicky, K., Schmidt, J. W., Nielsen, J. H., and Stang, H., (2013), Fire Performance of Basalt FRP Mesh Reinforced HPC Thin Plates. In Proceedings of the 4th Asia-Pacific Conference on FRP in Structures (APFIS 2013). Swinburne University of Technology.

ISIS, (2001): Design Manual No. 4 – Strengthening Reinforced Concrete Structures with Externally—Bonded Fibre Reinforced Polymers (FRPs), ISIS Canada, Intelligent Sensing for Innovative Structures, University of Manitoba, Canada.

ISIS, (2006): Design Manual No. 3 – Reinforcing Concrete Structures with Fibre Reinforced Polymers (FRPs), ISIS Canada, Intelligent Sensing for Innovative Structures, University of Manitoba, Canada.

Ismail, M., Ismail, E. M., and Muhammad, B., (2011), Influence of Elevated Temperatures on Physical and Compressive Strength Properties of Concrete Containing Palm Oil Fuel Ash, Construction and Building Materials, Vol. 25, No. 5, p.p. 2358–2364.

ISO 834-10, (2014), Fire resistance tests -Elements of building construction- Part 10: Specific requirements to determine the contribution of applied fire protection materials to structural steel elements.

Issa, M. S. and Elzeiny, S. M., (2011), Flexural Behavior of Cantilever Concrete Beams Reinforced With Glass Fiber Reinforced Polymers (GFRP) Bars, Journal of Civil Engineering and Construction Technology, Vol. 2, No.2, p.p. 33-44.

Karbhari, V. M., Chin, J. W., Hunston, D., Benmokrane, B., Juska, T., Morgan, R., Lesko, J. J., Sorathia, U., and Reynaud, D., (2003), Durability Gap Analysis for Fiber-Reinforced Composites in Civil Infrastructure, Journal of Composites for Construction, Vol. 7, No. 3, p.p. 238-247.

Katz, A., (2001), Bond to Concrete of FRP Rebars and Tendons, Composites in Construction, pp. 121-129.

Katz, A., Berman, N., and Bank, L., (1999), Effect of High Temperature on Bond Strength of FRP Rebars, Journal of Composites for Construction, Vol. 3, No. 2, p.p.73-81.

Koch G. H., Michiel P. H., Virmani Y. P., and Payer J. H., (2002), Corrosion Costs and Preventive Strategies in the United States, Publication No. FHWA-RD-01-156, Department of Transportation, U.S. Federal Highway Administration.

Kodur, V., Baingo, D., (1998), Fire Resistance of FRP Reinforced Concrete Slabs, Internal Report No. 758, Institute for Research in Construction, National Research Council Canada.

Kodur, V., Bisby, L. and Green, M., (2007), Preliminary Guidance for the Design of FRP Strengthened Concrete Members Exposed to Fire, Journal of Fire Protection Engineering, Vol. 17, No. 1, p.p. 5-26.

Kodur, V., Bisby, L., Foo, S., (2005), Thermal Behaviour of Fire-Exposed Concrete Slabs Reinforced With Fibre Reinforced Polymer Bars. ACI Structural Journal, Vol. 102, No. 6, p.p.799–808.

Kumahara, S., Masuda, Y., Tanano, H., and Shimizu, A., (1993), Tensile Strength Of Continuous Fiber Bar Under High Temperature, ACI Special Publication 138, p.p. 731-742.

Li, M., Qian, C., and Sun, W., (2004), Mechanical Properties of High-Strength Concrete After Fire, Cement and Concrete Research, V. 34, No. 6, p.p. 1001–1005.

Liao, W. C., Lin, H. Y., Lee, M. H., and Hung, P. H., (2009), The Pullout Test Of A FRP Rebar Within A Nanoclay/Concrete Block, Proceedings to Seventeenth International Conference on Composite Materials, A1-7, Edinburgh, Scotland.

Lie, T. T., (1992), Structural Fire Protection, ASCE Manuals and Reports on Engineering Practice No. 78, American Society of Civil Engineers, New York.

Lin, W.M., Lin, T.D., and Powers-Couche, L.J., (1996), Microstructures of Fire-Damaged Concrete, ACI Materials Journal, Vol. 93, No.3, p.p. 199-205.

Lublóy, E., Balázs, G. L., Borosnyói, A., Nehme, S. G., (2005), Bond of CFRP Wires Under Elevated Temperature, Proceedings of the International Symposium on Bond Behaviour of FRP in Structures (BBFS 2005), Hong Kong, China.

Mahdy, M., Speare, P. R., and Abdel-Reheem, A. H., (2002), Effect of Transient High Temperatures on Heavyweight, High Strength Concrete, 15th ASCE Engineering Mechanics Conference, Columbia University, New York .

Maluk, C., Bisby, L., Santa Maria, H., Terrasi, G., and Green, M., (2010), Effects of Elevated Temperatures and Fire on Bond Strength of Prestressed Steel and Carbon FRP Bars in High Performance Self-Consolidating Concrete. Proceedings of the 2nd Postgraduate Engineering Students' PUC Congress, May 28, 2010, Pontificia Universidad Católica de Chile, Santiago, Chile.

Maluk, C., Bisby, L., Terrasi, G., and Hugi, E., (2010) Bond Strength Degradation for Pre-Stressed Steel and Carbon FRP Bars in High-Performance Self-Consolidating Concrete at Elevated Temperatures and in Fire, Proceedings of the 6th International Conference on Structures in Fire (SiF 2010), June 02-04, 2010, Michigan State University, East Lansing, Michigan, USA, pp. 743-750. (Invited for a Special Publication in the Journal of Structural Fire Engineering).

Maluk, C., Bisby, L., Terrasi, G., Hugi, E. and Green, M., (2011), Bond Strength Degradation for CFRP and Steel Reinforcing Bars in Concrete at Elevated Temperature. American Concrete Institute Special Publication on Advances in Fire Design of Concrete Structures (ACI SP-297), pp. 2.1-2.36.

Maraveas, C., Miamis, K. and Vrakas, A. A., (2012), Fiber Reinforced Polymer - Strengthened / Reinforced Concrete Structures exposed to fire: A review, Structural Engineering International, Vol. 22, No. 4, pp. 500-513.

Masmoudi, A., Masmoudi, R., Ben Ouezdou, M., (2010), Thermal Effects on GFRP Rebars: Experimental Study and Analytical Analysis, Materials and Structures, Vol. 43, No. 6, p.p. 775–788.

Masmoudi, R., Masmoudi, A., Daoud, A., and Ben Ouezdou, M., (2010), Thermal Effects on Bond Properties of GFRP Rebars Embedded in Concrete, Journal of Civil Engineering and Architecture, Vol. 4, No.3 (Serial No.28).

Mazaheripour, H., Barros, J., Sena-Cruz, J. M., Pepe, M., and Martinelli, E., (2013), Experimental Study on Bond Performance of GFRP Bars in Self-Compacting Steel Fiber Reinforced Concrete, Composite Structures, Volume 95, Pages 202–212.

Mohamedbhai, G. T., (1986), Effect of Exposure Time and Rates of Heating and Cooling on Residual Strength of Heated Concrete, Magazine of Concrete Research, Vol. 38, No. 136, pp. 151-158.

MS EN 197-1, (2014): Malaysian Standard, Cement - Part 1: Composition, specifications and conformity criteria for common cements, Malaysia.

Mufti, A. A., Newhook, J. P., and Tadros, G., (1996), Deformability Versus Ductility in Concrete Beams with FRP Reinforcement, Proceedings of the second International conference on Advance Composite Materials in Bridges and Structures , ACMBS-II, Montreal, Canada, pp 189-199.

Munoz, M. B., (2010), Study of Bond Behavior between FRP Reinforcement and Concrete", PhD Thesis, Universitat de Girona, ISBN: 978-84-694-2484-1.

Naaman, A. E., and Jeong, S. M., (1995), Structural Ductility of Concrete Beams Prestressed with FRP Tendons, Proceedings of the 2nd International Symposium on Non-metallic Reinforcement for Concrete Structures (FRPRCS-2) , Ghent, Belgium, pp.379-386.

Nadjai, A., Talamona, D., and Ali, F., (2005), Fire Performance of Concrete Beams Reinforced with FRP Bars, Proceedings of the International Symposium on Bond Behaviour of FRP in Structures (BBFS 2005), p.p. 401-410.

Nanni, A., (2001), Relevant Applications of FRP Composites in Concrete Structures, Proceedings to CCC 2001, Composites in Construction, Porto, Portugal, J Figueiras, L. Juvandes and R. Furia, Eds., pp. 661-670.

Newman, J., and Choo, B. S., (2003), Advanced Concrete Technology 2 – Concrete Properties", Elsevier Science Publishers , Total Pages 352.

Nigro, E., Cefarelli, G., Bilotta, A., Manfredi, G., and Cosenza E., (2012), Performance under Fire Situations of Concrete Members Reinforced with FRP Rods: Bond Models and Design Nomograms, Journal of Composites for Construction, Vol. 16, No. 4, p.p. 395–406.

Nigro, E., Cefarelli, G., Bilotta, A., Manfredi, G., and Cosenza, E., (2011a), Fire resistance of concrete slabs reinforced with FRP bars Part I: Experimental

investigations on mechanical behavior, Composites: Part B, Vol. 42, p.p. 1739–1750.

Nigro, E., Cefarelli, G., Bilotta, A., Manfredi, G., and Cosenza, E., (2011b), Fire resistance of concrete slabs reinforced with FRP bars Part II: Experimental results and numerical simulations on the thermal field, Composites: Part B, Vol. 42, p.p.1751–1763.

Nigro, E., Cefarelli, G., Bilotta, A., Manfredi, G., and Cosenza, E., (2011c), Tests at High Temperatures on Concrete Slabs Reinforced With Bent FRP Bars, ACI Special Publication 275-50, p.p. 1-20.

Nor, N. M., Boestamam, M. H. A., and Yusof, M. A., (2013), Carbon Fiber Reinforced Polymer (CFRP) as Reinforcement for Concrete Beam, International Journal of Emerging Technology and Advanced Engineering, Vol. 3, No. 2, p.p. 6-10.

Noumowe, A. N., Clastres P., Debicki G., and Costaz J-L., (1996), Thermal Stresses and Water Vapor Pressure of High Performance Concrete at High Temperature, Proc. 4th International Symposium on Utilization of High-Strength/High-Performance Concrete, Paris.

NZS 3101-1, (2006): Concrete structures standard - The design of concrete structures, [By Authority of Development Sponsored by the Earthquake Commission (EQC) and Department of Building and Housing (DBH)].

Pawłowski, D., and Szumigała, M., (2015), Flexural Behaviour of Full-Scale Basalt FRP RC Beams Experimental and Numerical Studies, Procedia Engineering, Vol.108, p.p. 518 – 525.

Petkova, D., Donchev, T., and Benedetti, A., (2012), Effect of Elevated Temperatures on the Bond Strength of CFRP-to-Concrete Joints. Conference: 6th International Conference CICE 2012, Rome, Italy.

Pires, J.M. de Costa, (2012), Mechanical Behaviour at elevated temperature of GFRP pultruded composite profile, M.Sc. Thesis, Technical University of Lisbon, Portugal, Nov. 2012.

Poon, C. S., Azhar, S., Anson, M., Wong, Y. L., (2001), Comparison Of The Strength And Durability Performance Of Normal- And High-Strength Pozzolanic Concretes At Elevated Temperatures, Cement And Concrete Research, Vol. 31, No.9 ,p.p.1291–1300.

Poon, C. S., Azhar, S., Anson, M., Wong, Y. L., (2003), Performance of Metakaolin Concrete at Elevated Temperatures", Cement & Concrete Composites, V. 25, No. 1, p.p. 83–89.

Qu, W., Zhang, X., and Huang, H., (2009), Flexural Behavior of Concrete Beams Reinforced With Hybrid (GFRP and Steel) Bars, Journal of Composites for Construction, Vol. 13, No. 5, p.p. 350-359.

Rafi, M., and Nadjai, A., (2008), Experimental Behaviour of Carbon FRP Reinforced Concrete Beams at Ambient and Elevated Temperatures, Journal of Advanced Concrete Technology Vol. 6, No. 3, p.p.431-441.

Rafi, M., and Nadjai, A., (2011a), Behavior of hybrid (steel–CFRP) and CFRP bar-reinforced concrete beams in fire, Journal of Composite Materials, Vol. 45, No. 15, p.p. 1573-1584.

Rafi, M., and Nadjai, A., (2011b), Fire Test of Hybrid and Carbon Fiber-Reinforced Polymer Bar Reinforced Concrete Beams, ACI Materials Journal, Vol. 108, No. 3, p.p. 252-260.

Rafi, M., Nadjai, A., Ali, F., and O'Hare, P., (2011), Evaluation of Thermal Resistance of FRP Reinforced Concrete Beams in Fire, Journal of Structural Fire Engineering, Vol. 2 , No. 2, pp. 91 – 107.

Rafi, M., Nadjai, A., and Ali, F., (2007), Fire Resistance of Carbon FRP Reinforced-Concrete Beams, Magazine of Concrete Research, Vol. 59, No. 4, p.p. 245–255.

Robert, M., and Benmokrane, B., (2010), Behavior of GFRP Reinforcing Bars Subjected to Extreme Temperatures, Journal of Composites for Construction, Vol. 14, No. 4, p.p. 353-360.

Sarshar, R., and Khoury, G. A., (1993), Material and Environmental Factors Influencing the Compressive Strength of Unsealed Cement Paste and Concrete at High Temperatures", Magazine of Concrete Research, Vol. 45, No.162, pp.51-61.

Sumida, A, Fujisaki, T, Watanabe, K. and Kato, T., (2001), Heat Resistance of Continuous Fiber Reinforced Plastic Rods. Proceedings to the 5th Annual Symposium on Fibre-Reinforced-Plastic Reinforcement for Concrete Structures (FRPRCS-5), Fibre-reinforced plastics for reinforced concrete structures Volume 1, p.p. 557–565.

Tastani, S. P., and Pantazopoulou, S. J., (2006), Bond of GFRP Bars in Concrete: Experimental Study and Analytical Interpretation, Journal of Composites for Construction, Vol. 10, No. 5, p.p. 381–39.

Veysey, S., and Bischoff, P.H., (2011), Designing FRP Reinforced Concrete for Deflection Control, ACI Special Publication, Vol. 275, p.p. 1-24.

Wang, H., and Belarbi, A., (2005), Flexural Behavior of Fiber-Reinforced-Concrete Beams Reinforced with FRP Rebars, ACI Special Publications 230-51, p.p. 895-914.

Wang, H., Zha, X., and Ye, J., (2009), Fire Resistance Performance of FRP Rebar Reinforced Concrete Columns), International Journal of Concrete Structures and Materials, Vol.3, No.2, pp. 111-117.

Wang, K., Young, B., and Smith, S.T., (2011), Mechanical, Properties of Pultruded Carbon Fibre-Reinforced Polymer (CFRP) Plates at Elevated Temperatures, Engineering Structures, Vol. 33, No. 7, p.p. 2154-2161.

Wang, N., and Evans, J. T., (1995), Collapse of Continuous Fiber Composite Beam at Elevated Temperatures, Composites, Vol. 26, No. 1, pp.56-61.

Wang, X., and Zha, X., (2011), Experimental Research on Mechanical Behavior of GFRP Bars under High Temperature, Applied Mechanics and Materials, Vol. 71-78, pp. 3591-3594.

Wang, Y. C., Wong, P. M. H., and Kodur, V., (2007) , An Experimental Study of the Mechanical Properties of Fibre Reinforced Polymer (FRP) and Steel

Reinforcing Bars at Elevated Temperatures, Composite Structures, Vol. 80, No. 1, p.p. 131-140 .

Xiaoshan, L., and Zhang, Y. X., (2013), Bond–Slip Behaviour of FRP-Reinforced Concrete Beams, Construction and Building Materials, Vol. 44 , p.p. 110–117.

Xu, Y., Wong, Y. L., Poon, C. S., and Anson, M., (2001), Impact of High Temperature on PFA Concrete", Cement and Concrete Research, Vol. 31, No. 7, Pp. 1065–1073.

Zhang, B., Bicanic, N., Pearce, C. J., and Phillips, D. V., (2002), Relationship between Brittleness and Moisture Loss of Concrete Exposed to High Temperatures, Cement and Concrete Research, Vol.32, p.p. 363–371.

Zin, T., Mutsuyoshi, H., Sumida, A. and Tanabe, K., (2004), Investigation of Bond and Flexural Behavior of FRP Reinforced Concrete under High Temperature, Proceedings of the Japan Concrete Institute, Vol.26, No.2, pp.357-362.

APPENDICES

Appendix A: Tables and Figures

Table A.1: GFRP bars-tensile tests results

FRP Type	Sample #	Temp.	f_{ult-f} MPa	ε_{ult-f} % mm/mm	$\sigma_{0.001}$ MPa	$\sigma_{0.003}$ MPa	E_f GPa	$f_{ult-f,T}$ / f_{ult-f}	$E_{f,T}$ / E_f
GFRP	S1	23°C	841.173	2.121	49.66	142.45	46.40		
	S2		727.740	2.112	44.56	136.87	46.16		
	S3		880.564	2.433	53.05	150.78	48.87	1.00	1.00
	Average		816.49	2.22			47.14		
	S1	125°C	668.05	1.755	47.38	141.01	46.81		
	S2		715.71	1.901	47.42	135.29	43.93		
	S3		726.11	1.94	43.57	131.28	43.85	0.86	0.95
	Average		703.29	1.87			44.87		
	S1	250°C	540.22	1.566	40.68	123.38	41.35		
	S2		542.48	1.525	40.05	123.57	41.76		
	S3		574.04	1.667	39.37	118.63	39.63	0.68	0.87
	Average		552.25	1.59			40.91		
	S1	325°C	408.60	1.320	41.81	121.51	39.85		
	S2		449.12	1.529	37.35	106.70	34.68		
	S3		501.194	1.371	38.10	113.45	37.68		
	Average		452.97	1.41			37.40	0.55	0.79
	S1	375°C	59.78	0.380	20.29*	41.02*	21.83*		
	S2		81.63	0.487	33.10*	62.34*	24.00*		
	S3		88.79	0.328	23.15*	45.85*	27.68*		
	Average		76.74	0.40			24.50	0.09	0.52

f_{ult-f}: ultimate tensile strength, ε_{ult-f}: strain at ultimate tensile strength, E_f: tensile chord modulus of elasticity, $\sigma_{0.001}$, stress at 0.001 strain, $\sigma_{0.003}$, stress at 0.003 strain, * start and end points were $0.25\varepsilon_{ult}$ and $0.5\ \varepsilon_{ult}$

Table A.2: BFRP bars-tensile tests results

FRP Type	Sample #	Temp.	f_{ult-f} MPa	ε_{ult-f} % mm/mm	$\sigma_{0.001}$ MPa	$\sigma_{0.003}$ MPa	E_f GPa	$f_{ult-f,T}$ / f_{ult-f}	$E_{f,T}$ / E_f
BFRP	S1	23°C	892.36	1.964	68.70	202.30	66.80		
	S2		971.46	2.228	68.43	190.15	60.86	1.0	1.0
	S3		956.14	2.225	68.87	207.01	69.07		
	Average		939.99	2.14			65.58		
	S1	125°C	773.70	1.692	65.95	186.23	60.14		
	S2		733.45	1.370	66.10	197.76	65.83		
	S3		765.72	1.778	65.29	191.48	63.10	0.81	0.96
	Average		757.62	1.61			63.02		
	S1	250°C	654.69	1.728	59.64	175.00	57.68		
	S2		621.82	1.259	61.71	181.33	59.81		
	S3		710.59	1.446	56.13	167.59	55.73	0.70	0.88
	Average		662.37	1.48			57.74		
	S1	325°C	484.46	1.498	51.48	160.59	54.56		
	S2		536.80	1.30	51.02	150.20	49.59	0.55	0.79
	S3		521.59	1.11	49.26	152.28	51.51		
	Average		514.28	1.30			51.89		
	S1	375°C	122.28	0.791	31.15	84.77	26.81		
	S2		92.67	0.500	37.72*	82.61*	35.91*	0.13	0.47
	S3		159.00	0.635	31.25	90.17	29.46		
	Average		122.28	0.791			30.73		

f_{ult-f}: ultimate tensile strength, ε_{ult-f}: strain at ultimate tensile strength, E_f :tensile chord modulus of elasticity, $\sigma_{0.001}$, stress at 0.001 strain, $\sigma_{0.003}$, stress at 0.003 strain, * start and end points were $0.25\varepsilon_{ult}$ and $0.5 \varepsilon_{ult}$

Table A.3: CFRP bars-tensile tests results

FRP Type	Sample #	Temp.	f_{ult-f} MPa	ε_{ult-f} % mm/mm	$\sigma_{0.001}$ MPa	$\sigma_{0.003}$ MPa	E_f GPa	$f_{ult-f,T}$ / f_{ult-f}	$E_{f,T}$ / E_f
CFRP	S1	23°C	1595.00	1.75	111.76	346.66	117.45	1.0	1.0
	S2		1504.22	1.61	119.57	351.82	116.12		
	S3		1616.98	1.73	124.55	371.88	123.66		
	Average		1572.07	1.70	118.63	356.78	119.08		
	S1	125°C	1400.56	1.809	113.86	324.03	105.08	0.91	0.92
	S2		1413.66	1.722	113.35	328.26	107.45		
	S3		1500.78	1.478	116.74	350.22	116.74		
	Average		1438.33	1.67	114.65	334.17	109.76		
	S1	250°C	1215.03	1.49	125.28	334.51	104.62	0.73	0.84
	S2		1102.27	1.40	92.23	280.33	94.05		
	S3		1139.62	1.32	103.02	309.73	103.00		
	Average		1152.30	1.40	106.84	308.19	100.56		
	S1	325°C	670.16	0.85	102.50	264.60	81.05	0.45	0.68
	S2		642.86	0.91	110.07	269.61	79.77		
	S3		787.02	1.10	81.55	246.49	82.47		
	Average		700.02	0.95	98.04	260.23	81.10		
	S1	375°C	486.85	1.152	55.19	167.06	55.93	0.29	0.47
	S2		476.59	1.255	49.47	154.39	52.46		
	S3		399.80	1.029	61.39	181.99	60.30		
	Average		454.41	1.15	55.35	167.81	56.23		

Table A.3: Continued

	Sample #	Temp.	f_{ult-f} MPa	ε_{ult-f} % mm/mm	$\sigma_{0.001}$ MPa	$\sigma_{0.003}$ MPa	E_f GPa	$f_{ult-f,T}$ / f_{ult-f}	$E_{f,T}$ / E_f
CFRP	S1	450°C	165.01	0.436	58.37*	113.10*	50.16*	0.10	0.37
	S2		137.45	0.419	50.82*	102.09*	48.91*		
	S3		190.37	0.58	62.98*	109.95*	32.36*		
	Average		164.27	0.48			43.81		

f_{ult-f}: ultimate tensile strength, ε_{ult-f}: strain at ultimate tensile strength, E_f :tensile chord modulus of elasticity, $\sigma_{0.001}$, stress at 0.001 strain, $\sigma_{0.003}$, stress at 0.003 strain, * start and end points were $0.25\varepsilon_{ult}$ and $0.5\ \varepsilon_{ult}$

Table A.4: Steel bars-tensile tests results

Type	Sample #	Temp.	f_y MPa	f_u MPa	ε_{ult} % mm/mm	ε_R % mm/mm	E_s GPa	$f_{y,T}/f_{y,23°C}$	$f_{u,T}/f_{u,23°C}$	$E_{s,T}/E_{s,23°C}$	$E_{R,T}/E_{R,23°C}$
Steel	S1	23°C	563.10	627.03	9.29	11.41	240.54				
	S2		556.98	625.25	8.14	9.65	206.53				
	S3		594.30	662.44	8.02	10.55	237.94				
	Average		571.46	638.24	8.48	10.54	228.33	100.0%	100.0%	100.0%	100.0%
	S1	125°C	501.17	579.38	10.08	12.81	212.42				
	S2		468.62	578.71	9.99	11.77	190.52				
	S3		569.23	638.00	9.12	10.57	208.83				
	Average		513.01	598.70	9.73	11.72	203.92	89.8%	93.8%	89.3%	111.2%
	S1	250°C	500.72	596.58	8.89	10.59	209.04				
	S2		509.04	620.84	9.49	11.21	202.21				
	S3		564.96	641.80	9.63	11.69	211.98				
	Average		524.90	619.74	9.34	11.16	207.74	91.9%	97.1%	91.0%	105.9%

f_y: yield strength, f_u: ultimate tensile strength, ε_{ult}: strain at ultimate tensile strength, ε_R: elongation at rupture, E_s: modulus of elasticity

Table A.4: Continued

Type	Sample #	Temp.	f_y MPa	f_u MPa	ε_{ult} % mm/mm	ε_R % mm/mm	E_s GPa	$f_{y,T}$ / $f_{y,23°C}$	$f_{u,T}$ / $f_{u,23°C}$	$E_{s,T}$ / $E_{s,23°C}$	$E_{R,T}$/ $E_{R,23°C}$
	S1	325°C	526.02	608.92	9.36	10.86	208.29				
	S2		537.53	641.35	10.09	12.41	213.53				
	S3		578.40	634.50	8.25	9.65	205.82				
	Average		547.32	628.26	9.23	10.97	209.21	95.8%	98.4%	91.6%	104.1%
	S1	375°C	528.85	607.23	9.42	11.16	214.82				
	S2		552.08	660.91	9.37	10.95	211.30				
	S3		582.19	648.79	8.42	10.04	213.30				
	Average		554.37	638.97	9.07	10.72	213.14	97.0%	100.1%	93.3%	101.7%
	S1	450°C	525.97	612.68	8.40	9.83	211.83				
	S2		536.44	622.77	9.56	10.91	209.43				
	S3		560.95	631.90	8.88	10.17	210.90				
	Average		541.12	622.45	8.94	10.30	210.72	94.7%	97.5%	92.3%	97.8%

f_y: yield strength, f_u: ultimate tensile strength, ε_{ult}: strain at ultimate tensile strength, ε_R: elongation at rupture, E_s: modulus of elasticity

Table A.5: Compressive and Tensile strength of concrete at 23°C and 500°C

Sample	P_c kN	f_c' MPa	ε_c	P_T kN	f_{sp} MPa
S1-23°C	257.0	32.72	0.002527	127.88	4.070
S2-23°C	252.2	32.11	0.002687	94.35	3.003
S3-23°C	268.7	34.21	0.002586	85.53	2.723
S4-23°C	274.8	34.99	0.002615		
S5-23°C	286.0	36.41	0.003050		
S6-23°C	262.8	33.46	0.002348		
Average	266.9	33.98	0.002635	102.58	3.265
S1-500°C	229.0	29.16	0.00656	45.85	1.460
S2-500°C	217.2	27.65	0.00676	52.02	1.656
S3-500°C	189.8	24.17	0.007128	62.94	2.003
S4-500°C	172.1	21.91	0.005809		
S5-500°C	181.2	23.07	0.006235		
S6-500°C	200.1	25.48	0.00644		
Average	198.2	25.24	0.006489	53.60	1.706

P_C: maximum measured compression load, f_c': concrete cylinder compressive strength at 28 days, ε_c: strain at f_c', P_T: maximum measured tensile load, f_{sp}: splitting tensile strength.

Table A.6: GFRP pullout tests results

SP. #	Temp.	$F_{b,u}$	SAF	ε_R	UBS	SABS	RUBS/ UBS
	°C	kN	mm	mm	MPa	mm	
1		5.915	3.896	1.198	1.883	2.697	
2	23	6.156	3.742	1.247	1.960	2.495	
3		6.913	4.429	1.400	2.200	3.028	
Average		6.328	4.022	1.282	2.014	2.740	100%
1		4.750	3.005	1.011	1.512	1.994	
2	125	4.382	3.058	0.932	1.395	2.125	
3		4.647	3.050	0.989	1.479	2.061	
Average		4.593	3.038	0.977	1.462	2.060	72.6%
1		2.848	2.393	0.665	0.906	1.728	
2	250	3.141	2.612	0.733	1.000	1.879	
3		3.463	2.877	0.808	1.102	2.069	
Average		3.150	2.627	0.735	1.003	1.892	49.8%
1		1.337	1.281	0.341	0.426	0.939	
2	320	1.217	1.395	0.311	0.388	1.084	
3		1.393	1.476	0.356	0.443	1.121	
Average		1.316	1.384	0.336	0.419	1.048	20.8%
1		22.352	6.725	4.528	7.115	2.197	
2	23 +	21.150	7.135	4.284	6.732	2.850	
3	End cap	19.663	6.399	3.983	6.259	2.416	
Average		21.055	6.753	4.265	6.702	2.488	332%
1		17.104	6.962	4.367	5.444	2.595	
2	320 +	14.625	5.918	3.734	4.655	2.184	
3	End cap	15.234	6.433	3.890	4.849	2.543	
Average		15.654	6.438	3.997	4.983	2.441	247%

$F_{b,u}$: maximum measured force, SAF: stroke at maximum force, ε_R: bar elongation, UBS: bond strength, SABS: slip at maximum bond strength, RUBS: residual ultimate bond strength, EC: end cap

Table A.7: BFRP pullout tests results

SP. #	Temp.	$F_{b,u}$	SAF	ε_R	UBS	SABS	RUBS/ UBS
	°C	kN	mm	mm	MPa	mm	
1		7.619	3.700	1.105	2.425	2.595	
2	23	8.513	3.386	1.234	2.710	2.152	
3		8.635	3.820	1.252	2.749	2.568	
Average		8.256	3.635	1.197	2.628	2.438	100%
1		6.098	3.113	0.924	1.941	2.189	
2	125	6.225	3.210	0.943	1.981	2.267	
3		7.036	3.083	1.066	2.239	2.017	
Average		6.453	3.136	0.978	2.054	2.158	78.2%
1		2.885	2.241	0.477	0.918	1.764	
2	250	3.263	2.820	0.540	1.038	2.280	
3		3.535	2.426	0.585	1.125	1.842	
Average		3.227	2.496	0.534	1.027	1.962	39.1%
1		1.977	1.124	0.364	0.629	0.760	
2	320	1.532	1.382	0.282	0.488	1.100	
3		1.714	1.452	0.315	0.545	1.137	
Average		1.741	1.319	0.320	0.554	0.999	21.1%
1		27.212	6.256	3.946	8.662	2.311	
2	23 +	28.437	6.860	4.123	9.052	2.736	
3	End cap	25.538	5.878	3.703	8.129	2.175	
Average		27.062	6.332	3.924	8.614	2.407	328%
1		19.298	5.892	3.551	6.143	2.341	
2	320 +	23.125	7.566	4.256	7.361	3.310	
3	End cap	20.625	8.959	3.796	6.565	5.163	
Average		21.016	7.472	3.868	6.690	3.605	255%

$F_{b,u}$: maximum measured force, SAF: stroke at maximum force, ε_R: bar elongation, UBS: bond strength, SABS: slip at maximum bond strength, RUBS: residual ultimate bond strength, EC: end cap

Table A.8: CFRP pullout tests results

SP. #	Temp.	$F_{b,u}$	SAF	ε_R	UBS	SABS	RUBS /UBS
	°C	kN	mm	mm	MPa	mm	
1		25.925	5.622	2.079	8.252	3.543	
2	23	25.205	4.873	2.021	8.023	2.852	
3		27.463	5.645	2.202	8.742	3.443	
Average		26.198	5.380	2.101	8.339	3.279	100%
1		23.554	5.385	2.049	7.497	3.336	
2	125	20.109	4.827	1.750	6.401	3.078	
3		22.357	4.616	1.945	7.117	2.671	
Average		22.007	4.943	1.915	7.005	3.028	84.0%
1		14.520	3.847	1.379	4.622	2.468	
2	250	15.375	3.794	1.460	4.894	2.334	
3		14.401	3.237	1.368	4.584	1.869	
Average		14.765	3.626	1.402	4.700	2.224	56.4%
1		4.276	2.008	0.503	1.361	1.504	
2	320	4.677	2.134	0.551	1.489	1.583	
3		5.580	2.391	0.657	1.776	1.734	
Average		4.844	2.177	0.570	1.542	1.607	18.5%
1		30.625	6.252	2.456	9.748	3.796	
2	23 +	27.587	5.543	2.212	8.781	3.330	
3	End cap	26.024	6.375	2.087	8.284	4.288	107.2
Average		28.079	6.056	2.252	8.938	3.805	%
1		21.721	4.528	2.558	6.914	1.970	
2	320 +	20.673	4.281	2.434	6.580	1.847	
3	End cap	23.097	4.731	2.720	7.352	2.011	
Average		21.830	4.513	2.570	6.949	1.943	83.3%
1	375	2.719	2.729	0.462	0.865	2.267	10.4%

$F_{b,u}$: maximum measured force, SAF: stroke at maximum force, ε_R: bar elongation, UBS: bond strength, SABS: slip at maximum bond strength, RUBS: residual ultimate bond strength, EC: end cap

Table A.9: Steel bars pullout tests results

SP. #	Temp.	$F_{b,u}$	SAF	ε_R	UBS	SABS	RUBS/ UBS
	°C	kN	mm	mm	MPa	mm	
1		29.67	5.27	0.83	9.44	2.61	
2	23	38.84	4.36	1.08	12.36	3.27	
3		38.09	3.72	1.06	12.13	2.66	
Average		35.54	4.45	0.99	11.31	2.85	100%
1		33.36	3.68	1.04	10.62	2.64	
2	125	33.78	3.64	1.05	10.75	2.58	
3		33.63	4.06	1.05	10.71	3.01	
Average		33.59	3.79	1.05	10.69	2.74	94.5%
1		27.73	3.22	0.85	8.83	2.37	
2	250	29.52	3.12	0.90	9.40	2.21	
3		28.10	3.13	0.86	8.94	2.27	
Average		28.45	3.16	0.87	9.06	2.28	80.0%
1		25.93	2.68	0.79	8.26	1.89	
2	325	28.21	3.01	0.86	8.98	2.16	
3		23.48	2.45	0.71	7.47	1.74	
Average		25.87	2.71	0.79	8.24	1.93	72.8%
1		19.57	2.74	0.58	6.23	2.15	
2	375	25.67	3.23	0.77	8.17	2.46	
3		23.50	3.48	0.70	7.48	2.78	
Average		24.59	3.35	0.73	7.83	2.62	69.2%

$F_{b,u}$: maximum measured force, SAF: stroke at maximum force, ε_R: bar elongation, UBS:bond strength, SABS: slip at maximum bond strength, RUBS: residual ultimate bond strength, EC: end cap

Table A.10: Characteristics of load-deflection diagram for GFRP-RC beams with and without end cap before and after heating

Beam Type		Sample #	$P_{exp-ult}$	$\Delta_{exp-ult}$	P_{exp-cr}	Δ_{exp-cr}	Δ_{exp-s}	I.S	S.2nd	S.R
N.T.	Without End Cap	Sample1	30.035	13.746	9.756	0.835	7.713	11688	3856	67%
		Sample1	35.466	12.728	12.235	0.900	6.803	10560	4149	61%
		Sample1	32.414	13.365	10.296	0.679	5.147	15380	5106	67%
		Average	32.638	13.280	10.762	0.804	6.554	12543	4370	65%
	With End Cap	Sample1	60.556	19.121	13.297	0.498	4.463	26761	5801	78%
		Sample1	56.871	19.583	12.976	0.462	4.208	28074	4854	83%
		Sample1	57.886	16.029	13.617	0.462	4.042	29523	6147	79%
		Average	58.438	18.244	13.297	0.474	4.238	28119	5601	80%
H.T.	Without End Cap	Sample1	6.355	19.777	1.655	0.460	--	3599	692	81%
		Sample1	8.384	20.707	1.425	0.346	--	4121	768	81%
		Sample1	5.821	19.424	1.422	0.321	--	4492	1099	76%
		Average	6.853	19.969	1.501	0.376	--	4071	853	79%
	With End Cap	Sample1	26.648	19.103	3.898	0.468	6.274	8337	1952	77%
		Sample1	30.011	22.532	3.845	0.524	7.000	7348	1940	74%
		Sample1	26.700	17.770	3.044	0.497	5.314	6127	2275	63%
		Average	27.786	19.802	3.596	0.496	6.196	7270	2056	72%

$P_{exp-ult}$, experimental ultimate load, $\Delta_{exp-ult}$, measured mid-span deflection at ultimate load, P_{exp-cr}, experimental cracking load, Δ_{exp-cr}, measured mid-span deflection at cracking load, I.S., initial stiffness, S.2nd, stiffness after cracking, S.R., reduction in stiffness, Δ_{exp-s}, experimental mid-span deflection at theoretical service load

Table A.11: Characteristics of load-deflection diagram for BFRP-RC beams with and without end cap before and after heating

Beam Type		Sample #	$P_{exp-ult}$	$\Delta_{exp-ult}$	P_{exp-cr}	Δ_{exp-cr}	Δ_{exp-s}	I.S	S.2nd	S.R
N.T.	Without End Cap	Sample1	43.713	13.690	12.343	0.870	6.995	14194	4423	69%
		Sample1	35.736	11.674	11.589	0.962	7.373	12035	3458	71%
		Sample1	36.259	10.585	11.883	0.937	6.211	14088	3796	73%
		Average	38.569	11.983	11.938	0.923	6.860	13440	3892	71%
	With End Cap	Sample1	68.726	22.675	13.350	0.462	3.245	28926	7170	75%
		Sample1	87.202	24.238	13.290	0.444	3.225	29987	5660	81%
		Sample1	84.692	23.687	15.330	0.480	3.430	31998	5203	84%
		Average	80.207	23.533	13.990	0.462	3.300	30304	6011	80%
H.T.	Without End Cap	Sample1	7.262	17.143	1.185	0.396	--	2996	1341	55%
		Sample1	6.728	14.505	1.968	0.568	--	3467	1780	49%
		Sample1	7.796	15.931	1.706	0.506	--	3369	1163	65%
		Average	7.262	15.860	1.620	0.490	--	3277	1428	56%
	With End Cap	Sample1	47.579	23.048	2.189	0.426	4.322	5140	3506	32%
		Sample1	49.502	20.524	3.806	0.498	3.360	7647	4065	47%
		Sample1	44.963	17.717	2.131	0.248	4.379	8616	3267	62%
		Average	47.348	20.430	2.709	0.391	4.020	7134	3613	49%

$P_{exp-ult}$, experimental ultimate load, $\Delta_{exp-ult}$, measured mid-span deflection at ultimate load, P_{exp-cr}, experimental cracking load, Δ_{exp-cr}, measured mid-span deflection at cracking load, I.S., initial stiffness, S.2nd, stiffness after cracking, S.R., reduction in stiffness, Δ_{exp-s}, experimental mid-span deflection at theoretical service load

Table A.12: Characteristics of load-deflection diagram for CFRP-RC beams with and without end cap before and after heating

Beam Type		Sample #	$P_{exp-ult}$	$\Delta_{exp-ult}$	P_{exp-cr}	Δ_{exp-cr}	Δ_{exp-s}	I.S	S.2nd	S.R
N.T.	Without End Cap	Sample1	84.030	10.989	12.289	0.746	2.891	16492	8474	49%
		Sample1	98.152	12.229	15.254	1.018	2.741	16587	10144	39%
		Sample1	87.736	11.094	13.457	0.642	2.553	21363	9160	57%
		Average	89.973	11.437	13.667	0.802	2.728	18147	9260	48%
	With End Cap	Sample1	94.251	16.224	13.751	0.480	2.500	30465	7596	75%
		Sample1	85.280	13.222	14.471	0.490	2.733	36025	6940	80%
		Sample1	89.712	17.592	13.617	0.638	2.974	29986	7575	74%
		Average	89.748	15.679	13.946	0.536	2.736	32159	7370	76%
H.T.	Without End Cap	Sample1	29.423	16.466	1.121	0.261	10.957	4297	2448	43%
		Sample1	31.666	15.040	1.762	0.550	7.945	2889	1824	37%
		Sample1	34.817	17.749	1.869	0.428	9.636	4366	1988	54%
		Average	31.969	16.418	1.584	0.413	9.513	3851	2087	46%
	With End Cap	Sample1	61.837	23.012	2.136	0.409	6.942	5222	2801	46%
		Sample1	54.361	27.153	2.881	0.881	7.635	3271	2827	14%
		Sample1	66.216	23.776	3.097	0.853	7.936	5541	2367	57%
		Average	60.805	24.647	2.705	0.714	7.505	4678	2665	43%

$P_{exp-ult}$, experimental ultimate load, $\Delta_{exp-ult}$, measured mid-span deflection at ultimate load, P_{exp-cr}, experimental cracking load, Δ_{exp-cr}, measured mid-span deflection at cracking load, I.S., initial stiffness, S.2nd, stiffness after cracking, S.R. reduction in stiffness, Δ_{exp-s}, experimental mid-span deflection at theoretical service load

Table A.13: Characteristics of load-deflection diagram for Steel-RC beams before and after heating

		Sample #	$P_{exp-ult}$	$\Delta_{exp-ult}$	P_{exp-cr}	Δ_{exp-cr}	$P_{exp-yield}$	$\Delta_{exp-yield}$	Δ_{exp-s}	I.S	S.2nd	S.R
Steel	N.T.	Sample1	77.780	10.380	19.0	1.350	70.447	6.383	1.686	14285	11756	17.70%
		Sample1	78.420	10.120	22.0	1.540	70.717	6.105	1.72	14930	11610	22.24%
		Sample1	72.210	12.870	21.0	1.239	66.75	5.346	1.355	18450	11121	39.72%
		Average	76.137	11.123	20.667	1.376	69.305	5.945	1.587	15888	11496	26.55%
	H.T.	Sample1	70.595	12.403	3.471	0.428	64.561	8.482	2.82	8360	8000	4.31%
		Sample1	72.197	14.363	3.097	0.284	61.463	7.092	2.34	12850	9400	26.85%
		Sample1	65.468	14.292	2.19	0.250	60.449	8.661	3.03	8760	7340	16.21%
		Average	69.420	13.686	2.919	0.321	62.158	8.078	2.730	9.990	8.247	15.79%

$P_{exp-ult}$, experimental ultimate load, $\Delta_{exp-ult}$, measured mid-span deflection at ultimate load, P_{exp-cr}, experimental cracking load, Δ_{exp-cr}, measured mid-span deflection at cracking load, I.S., initial stiffness, S.2nd, stiffness after cracking, S.R., reduction in stiffness, Δ_{exp-s}, experimental mid-span deflection at theoretical service load

Table A.14: Strain measurements of concrete and different reinforcing bars at ultimate loads

Temp.			GFRP		BFRP		CFRP		Steel			
		Sample #	ε_c x 10^{-6}	ε_f x 10^{-6}	ε_c x 10^{-6}	ε_f x 10^{-6}	ε_c x 10^{-6}	ε_f x 10^{-6}	ε_c x 10^{-6} ult	ε_s x 10^{-6} ult	ε_c x 10^{-6} yield	ε_s x 10^{-6} yield
N.T.	Without End Cap	Sample1	1349	5370	1680	5897	2766	7067	5290	7760	2710	3750
		Sample1	1501	4993	1646	4711	2964	7766	5843	7320	3013	2973
		Sample1	1387	5893	1795	4617	2489	6600	5120	5650	2933	2265
		Average	1412	5419	1707	5075	2740	7144	5418	6910	2885	2996
	With End Cap	Sample1	2983	10562	2489	9087	2792	6473				
		Sample1	3463	10982	2746	10877	3045	7082				
		Sample1	3591	11189	2831	11122	2578	6552				
		Average	3346	10911	2689	10362	2805	6702				
H.T.	Without End Cap	Sample1	1066	1317	1308	1605	3060	2916	4858	N.A	2450	2720
		Sample1	1151	1911	1417	2068	2948	2709	6428	N.A	3038	1996
		Sample1	1008	1703	1604	1933	3758	2879	7318	N.A	4350	2364
		Average	1075	1644	1443	1869	3255	2835	6201	N.A	3279	2360
	With End Cap	Sample1	3432	6000	3750	7946	4531	6634				
		Sample1	4577	6387	4041	8035	4312	6621				
		Sample1	4270	5922	4199	6686	4835	7601				
		Average	4093	6103	3997	7556	4559	6952				

ε_f, FRP strain at ultimate load, ε_c, concrete strain at ultimate or yield load, ε_s =steel strain at yield or ultimate load

Table A.15: Ductility indices and overall ductility factors of GFRP-RC beams

Temp.	End Caps	Sample #	E_{el} kN.mm	E_{inel} kN.mm	E_{total} kN.mm	μ	P_{-m} kN	Δ_{-m} mm	$P_{exp\text{-}ult}$ kN	$\Delta_{exp\text{-}ult}$ mm	$P_{exp\text{-}ult}$ / P_m	$\Delta_{exp\text{-}ult}$ / Δ_m	ODF
Normal	Without End Cap	Sample1	71.5	192.7	264.1	2.348	18.67	6.00	30.04	13.75	1.61	2.29	3.68
		Sample1	86.7	200.4	287.1	2.156	24.26	7.38	35.47	12.73	1.46	1.72	2.52
		Sample1	66.8	238.9	305.7	2.787	23.70	5.25	32.41	13.37	1.37	2.55	3.48
		Average	75.0	210.6	285.6	2.430	22.21	6.21	32.64	13.28	1.47	2.14	3.14
	With End Cap	Sample1	148.0	616.0	764.0	3.081	27.26	5.33	60.56	19.12	2.22	3.59	7.97
		Sample1	138.6	618.5	757.1	3.231	21.79	3.89	56.87	19.58	2.61	5.03	13.14
		Sample1	138.5	475.5	614.0	2.717	27.46	4.86	57.89	16.03	2.11	3.30	6.95
		Average	141.7	570.0	711.7	3.010	25.50	4.69	58.44	18.24	2.29	3.89	8.91
High	Without End Cap	Sample1	10.0	67.2	77.2	4.368	--	--	6.36	19.78	--	--	--
		Sample1	22.6	88.0	110.6	2.950	--	--	8.38	20.71	--	--	--
		Sample1	6.7	77.8	84.5	6.806	--	--	5.82	19.42	--	--	--
		Average	13.1	77.7	90.8	4.708	--	--	6.85	19.97	--	--	--
	With End Cap	Sample1	180.9	129.9	310.8	1.359	14.33	7.62	26.65	19.10	1.86	2.51	4.66
		Sample1	163.0	245.8	408.8	1.754	13.29	7.37	30.01	22.53	2.26	3.06	6.91
		Sample1	133.2	149.2	282.4	1.560	11.70	5.00	26.70	17.77	2.28	3.55	8.11
		Average	159	175	334	1.558	13.10	6.66	27.79	19.80	2.12	2.97	6.30

E_{el}, elastic energy, E_{inel}, inelastic energy, E_{total}, total energy, μ, ductility index, P_m, force at 0.001 concrete strain (0.0021 in case of heated concrete), Δ_m, deflection corresponding to P_m, $P_{exp\text{-}ult}$, measure ultimate load capacity, $\Delta_{exp\text{-}ult}$, deflection at ultimate load capacity, ODF, overall ductility factor

Table A.16: Ductility indices and overall ductility factors of BFRP-RC beams

Temp.	End Caps	Sample #	E_{el} kN.mm	E_{inel} kN.mm	E_{total} kN.mm	μ	P_{-m} kN	Δ_{-m} mm	$P_{exp-ult}$ kN	$\Delta_{exp-ult}$ mm	$P_{exp-ult}$ / P_m	$\Delta_{exp-ult}$ / Δ_m	ODF
Normal	Without End Cap	Sample1	107.1	252.0	359.1	2.176	25.55	6.61	43.71	13.69	1.71	2.07	3.55
		Sample1	86.5	151.9	238.4	1.878	23.45	6.31	35.74	11.67	1.52	1.85	2.82
		Sample1	92.5	149.5	242.0	1.808	25.16	5.75	36.26	10.59	1.44	1.84	2.66
		Average	95.3	184.4	279.8	1.954	24.72	6.22	38.57	11.98	1.56	1.93	3.01
	With End Cap	Sample1	215.8	888.7	1104.5	3.059	34.97	5.64	68.73	22.68	1.97	4.02	7.90
		Sample1	344.6	1026.1	1370.7	2.489	38.42	6.25	87.20	24.24	2.27	3.88	8.81
		Sample1	288.6	1035.7	1324.3	2.794	40.90	6.39	84.69	23.69	2.07	3.71	7.68
		Average	283	983.5	1266.5	2.781	38.10	6.09	80.21	23.53	2.11	3.86	8.13
High	Without End Cap	Sample1	16.1	73.6	89.7	3.287	--	--	7.26	17.14	--	--	--
		Sample1	11.4	66.8	78.2	3.940	--	--	6.73	14.51	--	--	--
		Sample1	15.8	70.6	86.3	3.241	--	--	7.80	15.93	--	--	--
		Average	14.4	70.3	84.7	3.489	--	--	7.26	15.86	--	--	--
	With End Cap	Sample1	313.9	365.5	679.4	1.582	19.80	5.54	47.58	23.05	2.40	4.16	10.00
		Sample1	271.8	395.8	667.6	1.728	20.87	4.70	49.50	20.52	2.37	4.37	10.36
		Sample1	275.9	183.1	459.0	1.332	20.90	5.98	44.96	17.72	2.15	2.96	6.37
		Average	287.2	314.8	602	1.547	20.52	5.41	47.35	20.43	2.31	3.78	8.72

E_{el}, elastic energy, E_{inel}, inelastic energy, E_{total}, total energy, μ, ductility index, P_m, force at 0.001 concrete strain (0.0021 in case of heated concrete), Δ_m, deflection corresponding to P_m, $P_{exp-ult}$, measure ultimate load capacity, $\Delta_{exp-ult}$, deflection at ultimate load capacity, ODF, overall ductility factor

Table A-17: Ductility indices and overall ductility factors of CFRP-RC beams

Temp.	End Caps	Sample #	E_{el} kN.mm	E_{inel} kN.mm	E_{total} kN.mm	μ	P_{-m} kN	Δ_{-m} mm	$P_{exp-ult}$ kN	$\Delta_{exp-ult}$ mm	$P_{exp-ult}$ / P_m	$\Delta_{exp-ult}$ / Δ_m	ODF
Normal	Without End Cap	Sample1	353.6	177.7	531.3	1.251	34.22	3.44	84.03	10.99	2.46	3.19	7.84
		Sample1	463.7	244.9	708.6	1.264	34.26	3.16	98.15	12.23	2.86	3.87	11.09
		Sample1	343.5	245.6	589.1	1.358	36.73	3.19	87.74	11.09	2.39	3.47	8.30
		Average	386.9	222.7	609.7	1.291	35.07	3.27	89.97	11.44	2.57	3.50	8.99
	With End Cap	Sample1	386.0	647.0	1033.0	1.838	39.86	3.73	94.25	16.22	2.36	4.35	10.28
		Sample1	292.5	430.5	723.0	1.736	37.11	3.71	85.28	13.22	2.30	3.57	8.20
		Sample1	351.0	760.0	1111.0	2.083	39.38	4.29	89.71	17.59	2.28	4.10	9.34
		Average	343.2	612.5	955.7	1.886	38.78	3.91	89.75	15.68	2.31	4.01	9.28
High	Without End Cap	Sample1	192.7	88.9	281.6	1.231	20.11	9.26	29.42	16.47	1.46	1.78	2.60
		Sample1	186.5	111.6	298.1	1.299	22.38	7.71	31.67	15.04	1.42	1.95	2.76
		Sample1	233.8	123.5	357.3	1.264	18.28	7.58	34.82	17.75	1.91	2.34	4.46
		Average	204.3	108.0	312.3	1.265	20.25	8.18	31.97	16.42	1.58	2.01	3.17
	With End Cap	Sample1	543.8	272.3	816.1	1.250	25.36	7.67	61.84	23.01	2.44	3.00	7.32
		Sample1	495.0	428.8	923.8	1.433	23.73	7.91	54.36	27.15	2.29	3.43	7.86
		Sample1	632.0	206.0	838.0	1.163	23.06	7.92	66.22	23.78	2.87	3.00	8.62
		Average	556.9	302.3	859.3	1.282	24.05	7.83	60.81	24.65	2.53	3.15	7.96

E_{el}, elastic energy, E_{inel}, inelastic energy, E_{total}, total energy, μ, ductility index, P_m, force at 0.001 concrete strain (0.0021 in case of heated concrete), Δ_m, deflection corresponding to P_m , $P_{exp-ult}$, measure ultimate load capacity, $\Delta_{exp-ult}$, deflection at ultimate load capacity, ODF, overall ductility factor

Table A.18: Ductility of steel-RC beams

Beam Type	Sample #	E_{total} (kN.mm)	$\Delta_{exp-ult}$ mm	$\Delta_{exp-yield}$ mm	$Ductility = \dfrac{\Delta_{exp-ult}}{\Delta_{exp-yield}}$
STEEL-RC- Normal Temperature	S1	555.3	10.380	6.383	1.63
	S2	565.5	10.120	6.105	1.66
	S3	755.6	12.870	5.346	2.41
	Average	625.5	11.123	5.945	1.897
STEEL-RC- High Temperature	S1	543.6	12.403	8.482	1.46
	S2	727.0	14.363	7.092	2.03
	S3	627.0	14.292	8.661	1.65
	Average	632.5	13.686	8.078	1.713

E_{total}, total absorbed energy, $\Delta_{exp-ult}$, deflection at ultimate load capacity, $\Delta_{exp-yield}$, deflection at yield load
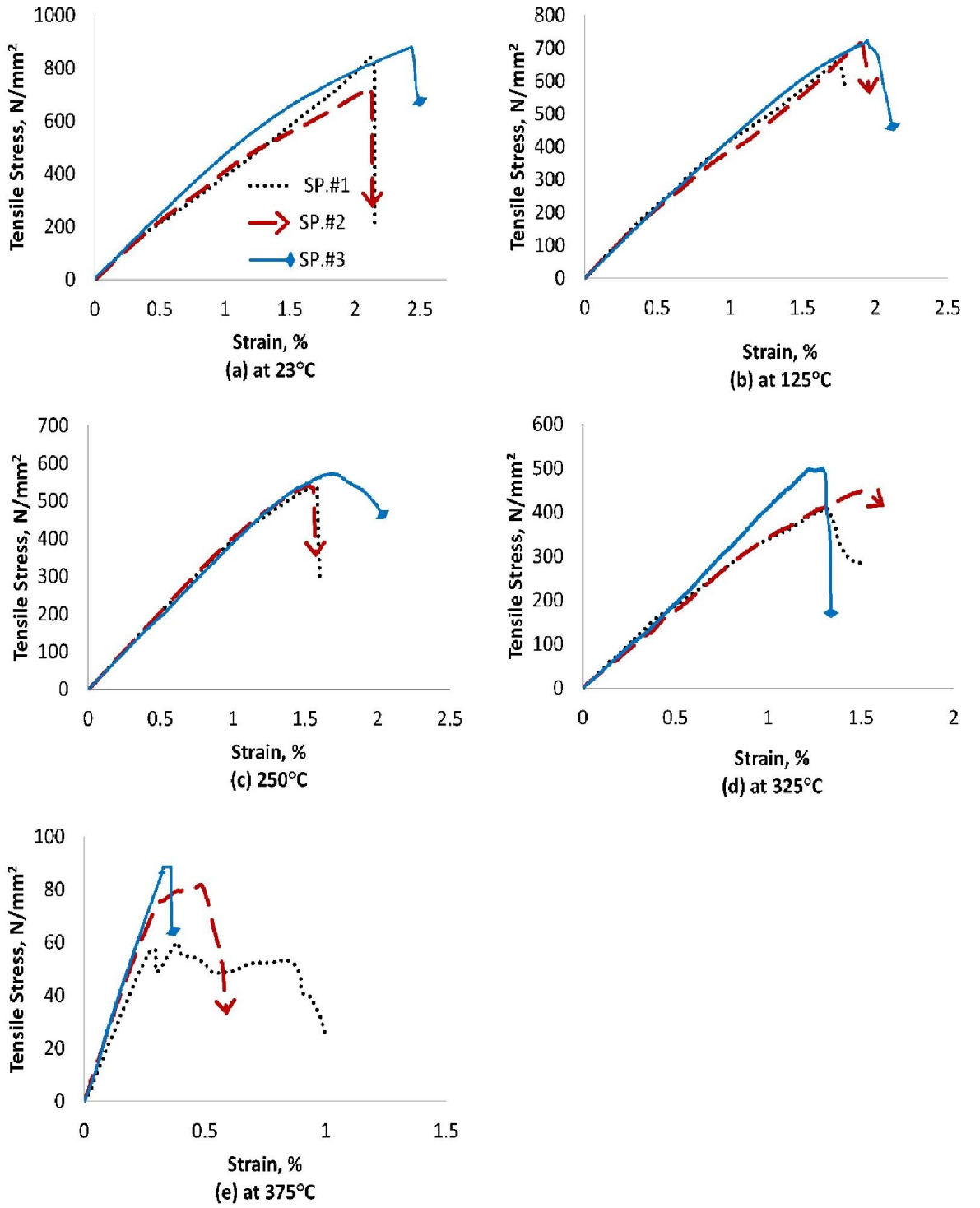
Fig A.1 Stress-strain diagram for triplicate GFRP bars under elevated temperatures
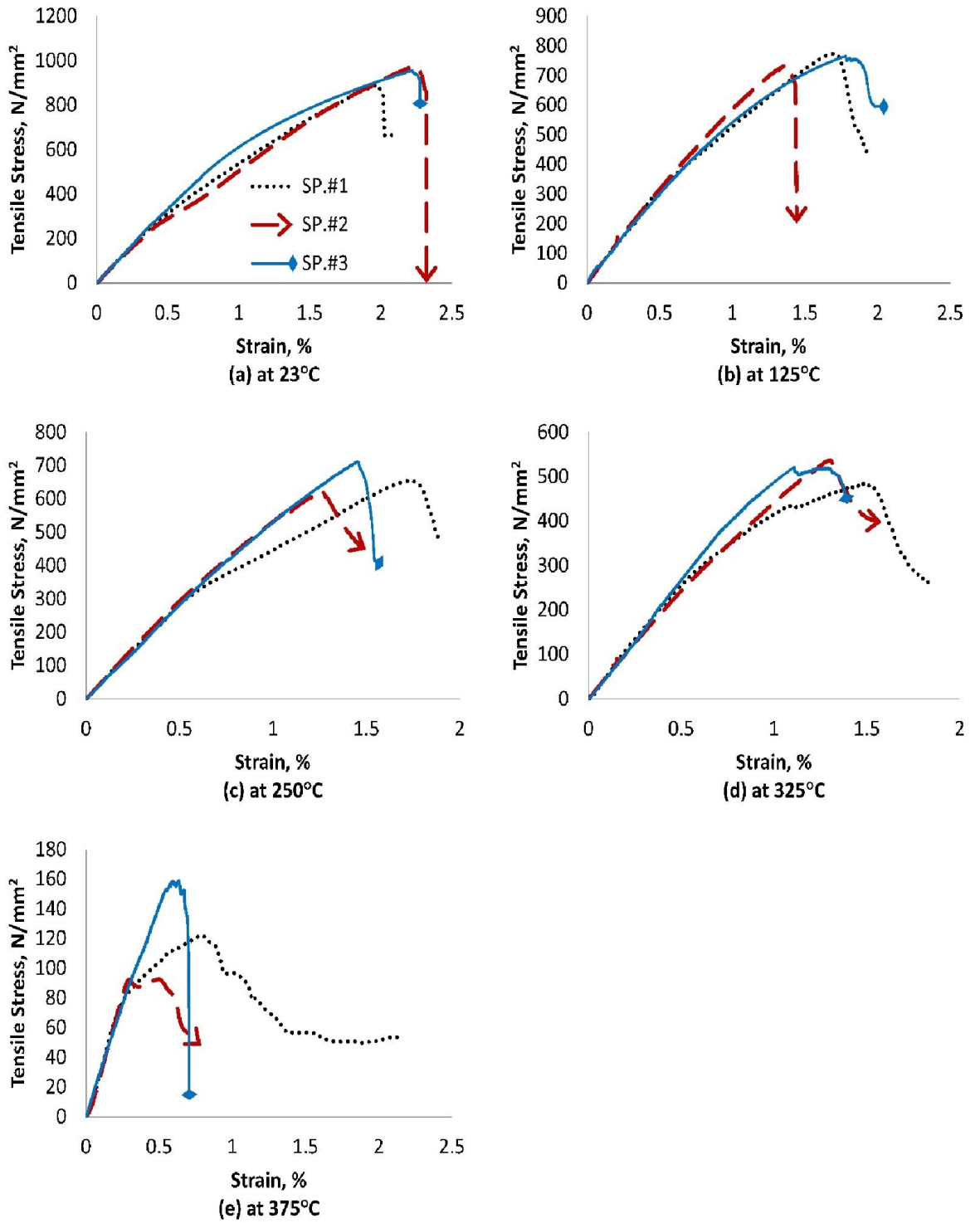
Fig A.2 Stress-strain diagram for triplicate BFRP bars under elevated
temperatures
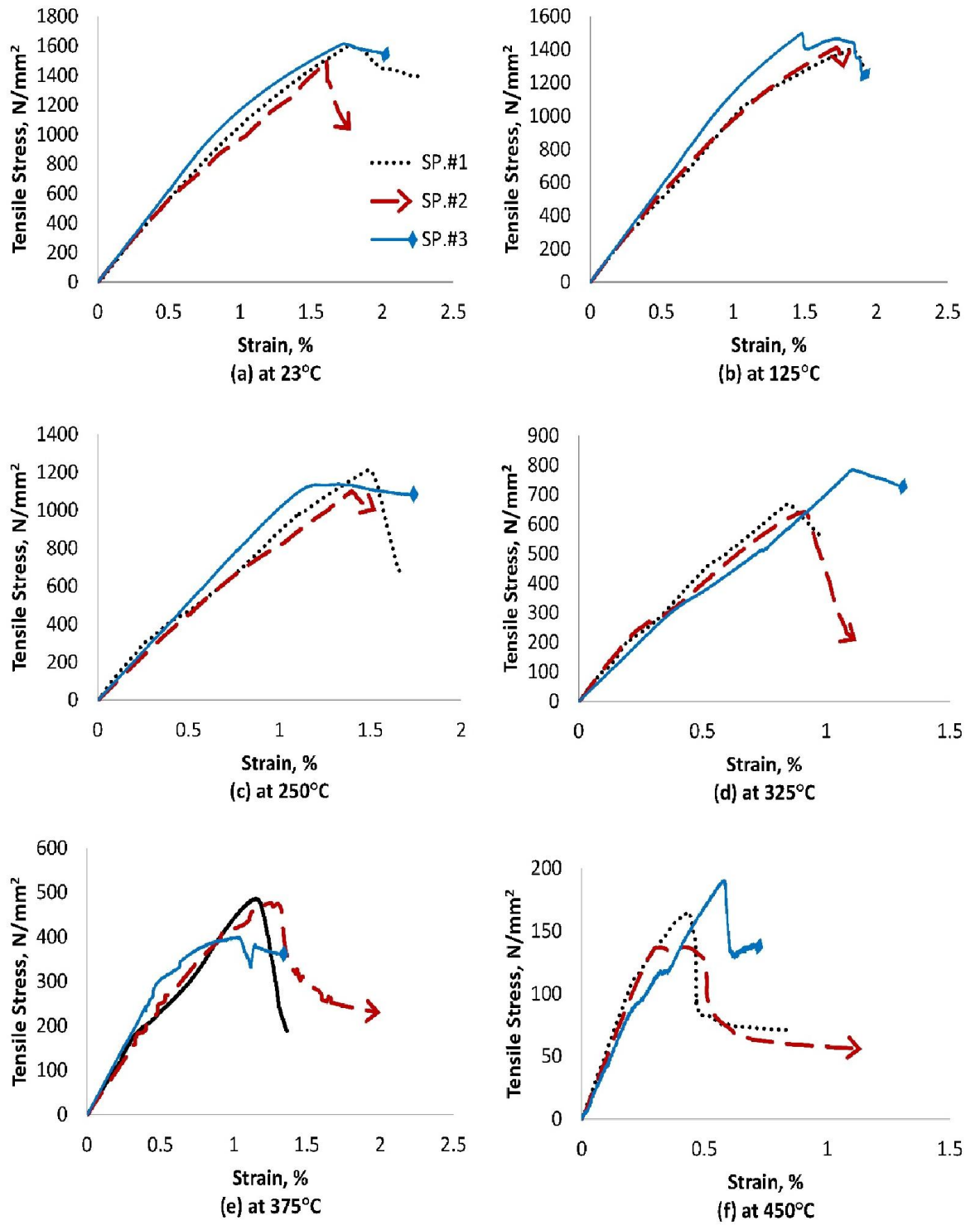
Fig A.3 Stress-strain diagram for triplicate CFRP bars under elevated
temperatures
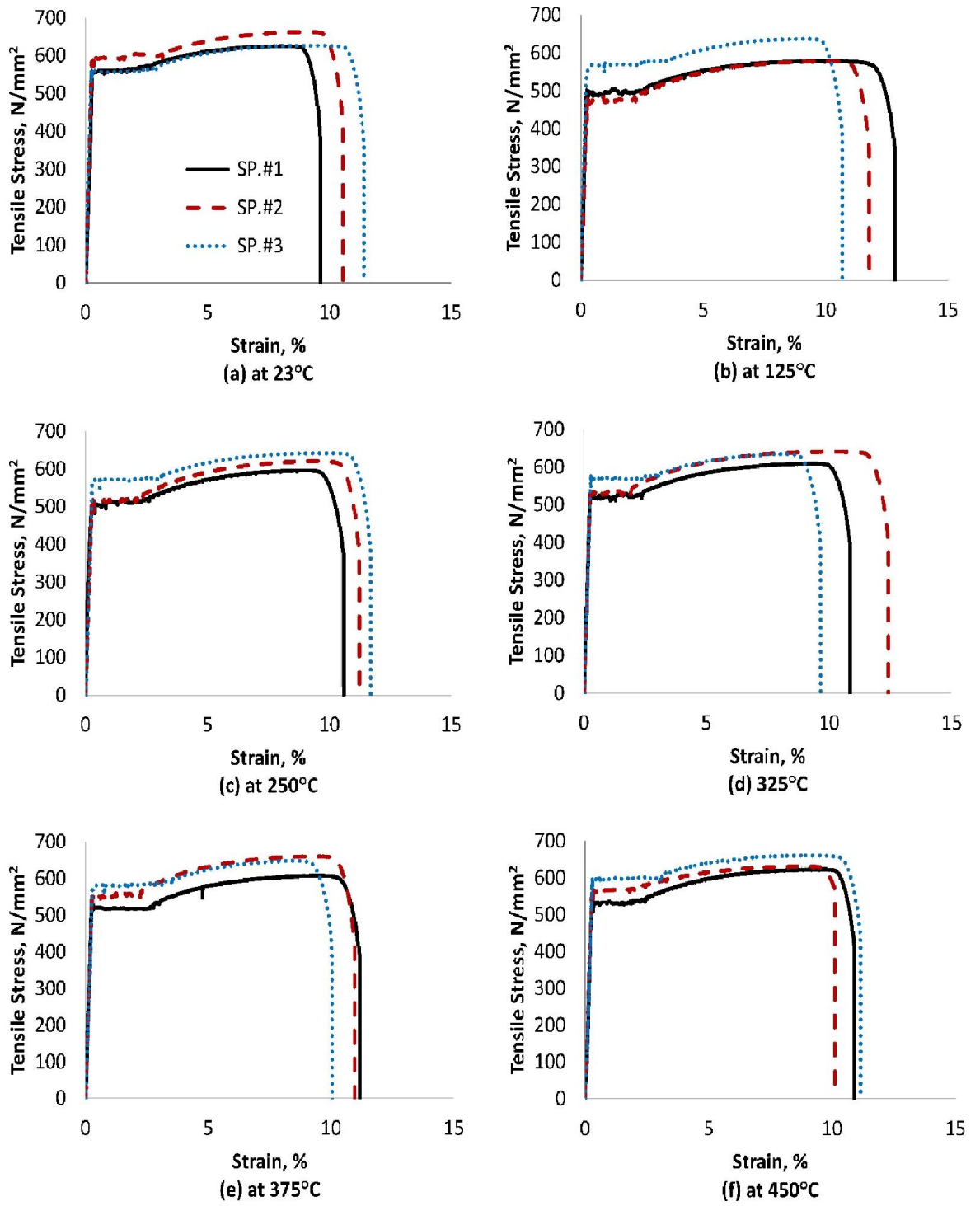
Fig A.4 Stress-strain diagram for triplicate steel bars under elevated temperatures
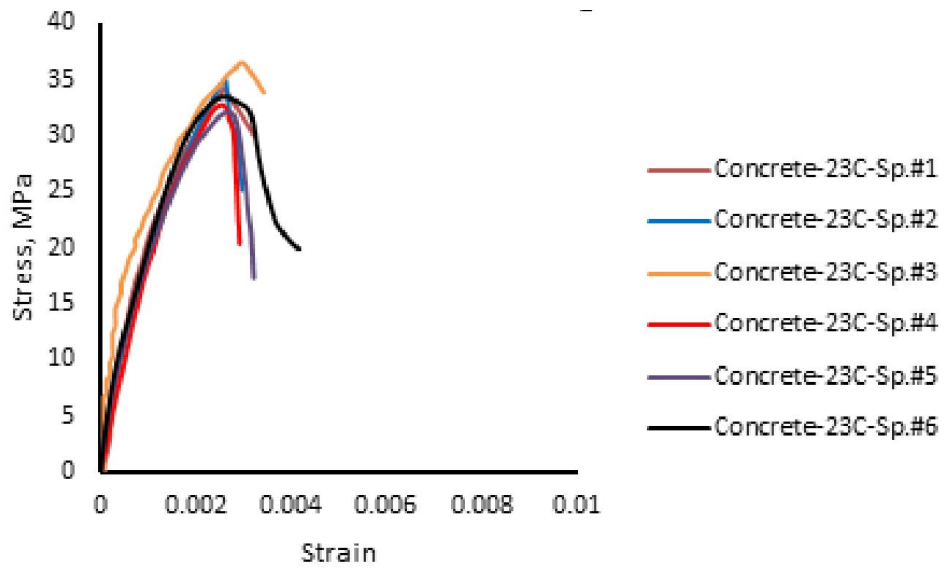
(a) at 23°C
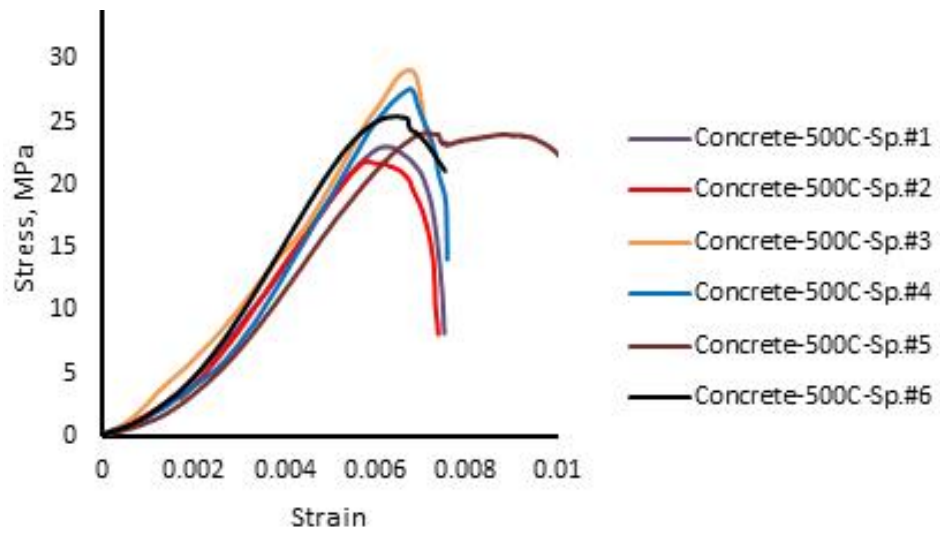
(b) at 500°C

Fig A.5: Compressive stress versus strain for concrete before and after exposure to 500°C
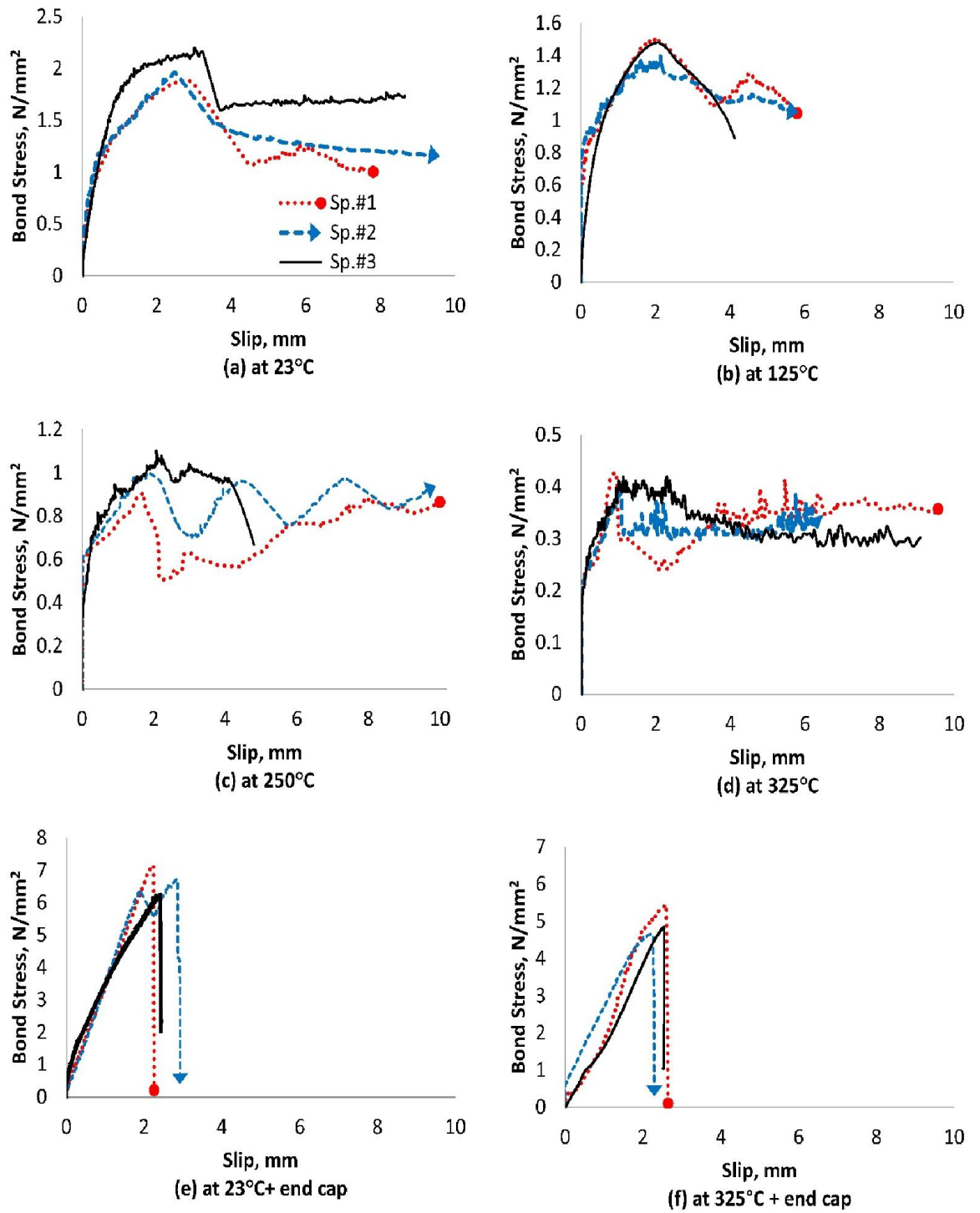
Fig A.6: Bond stress-strain curves for triplicate GFRP bars under elevated temperatures
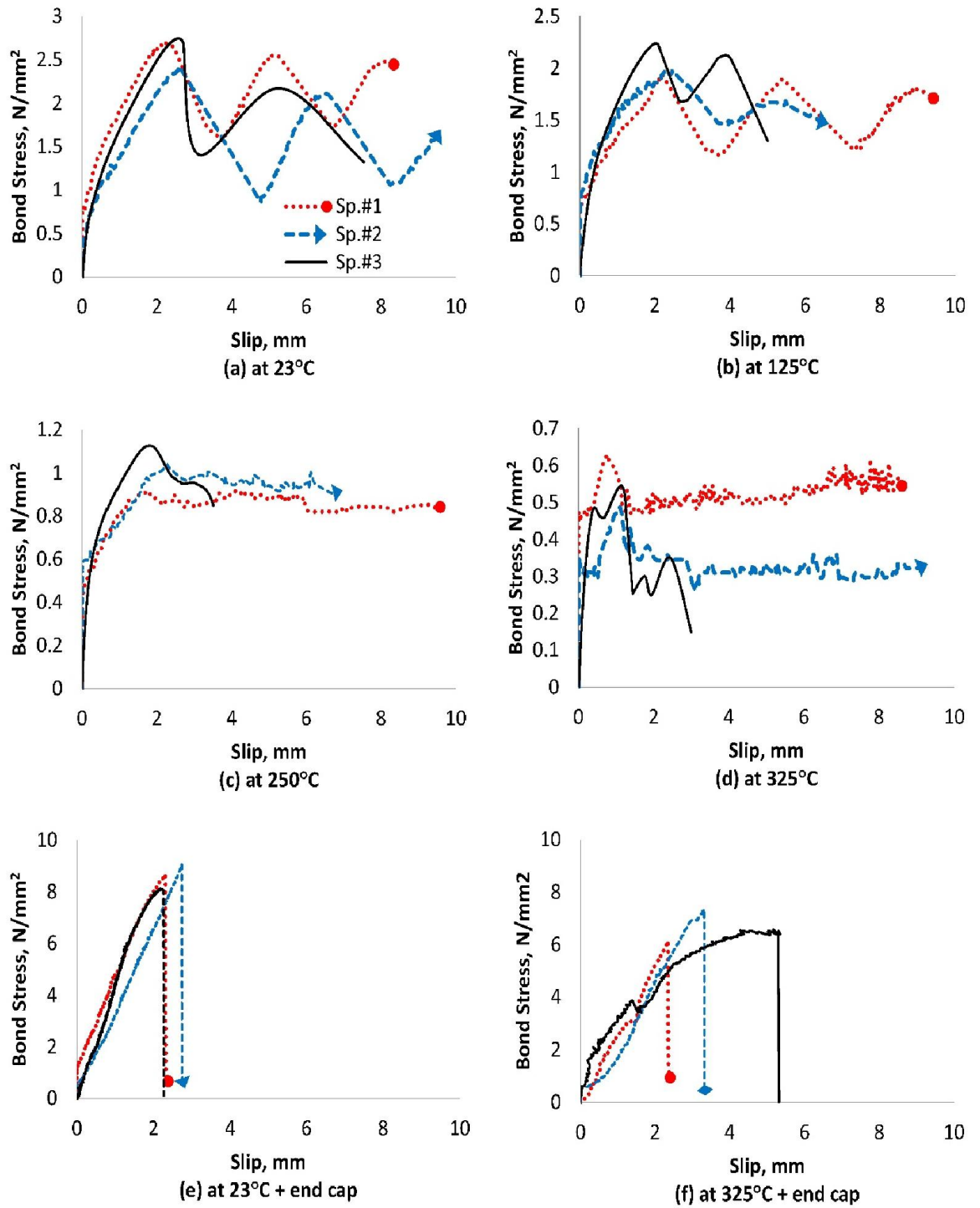
Fig A.7: Bond stress-strain curves for triplicate BFRP bars under elevated temperatures
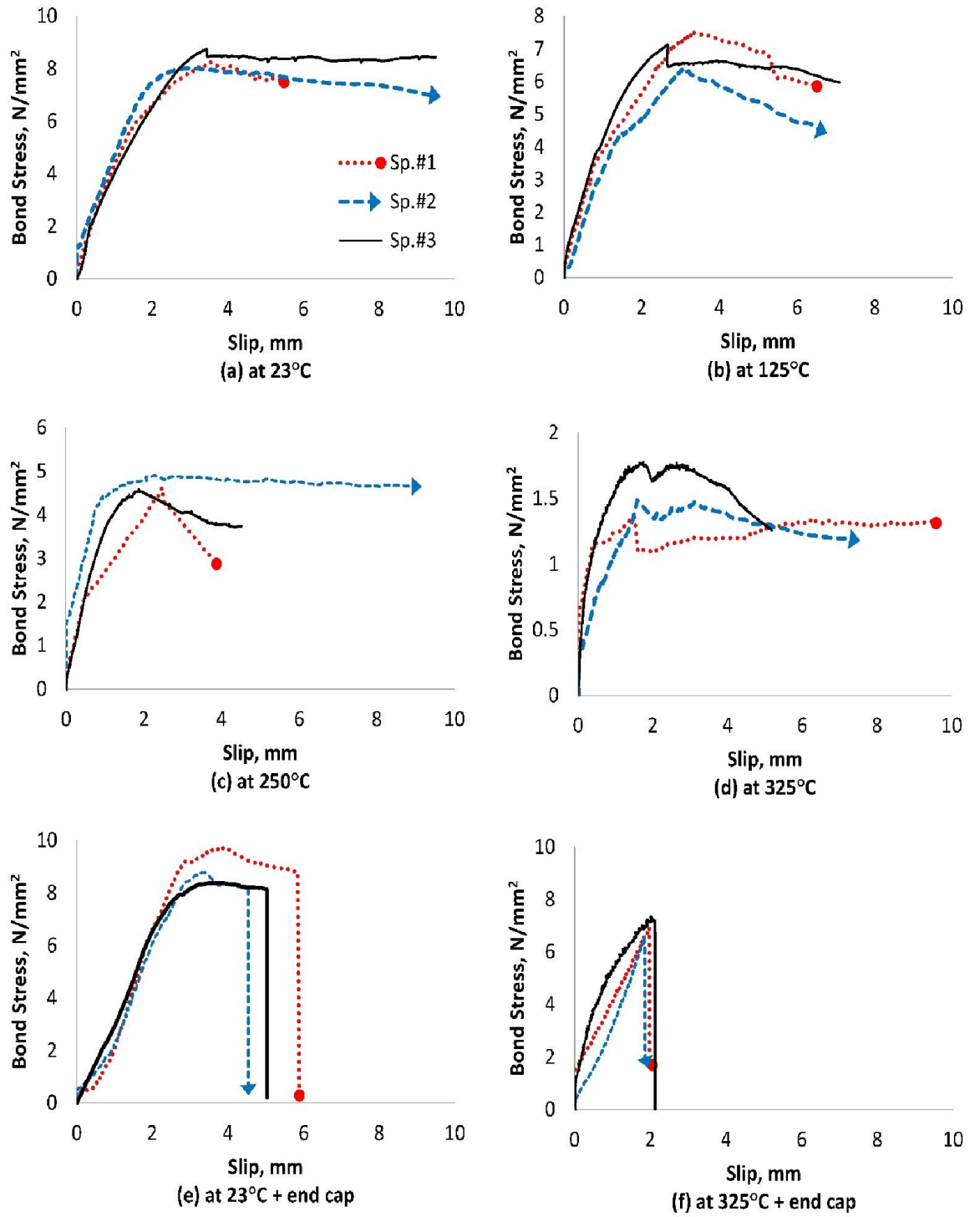
Fig A.8: Bond stress-strain curves for triplicate CFRP bars under elevated temperatures
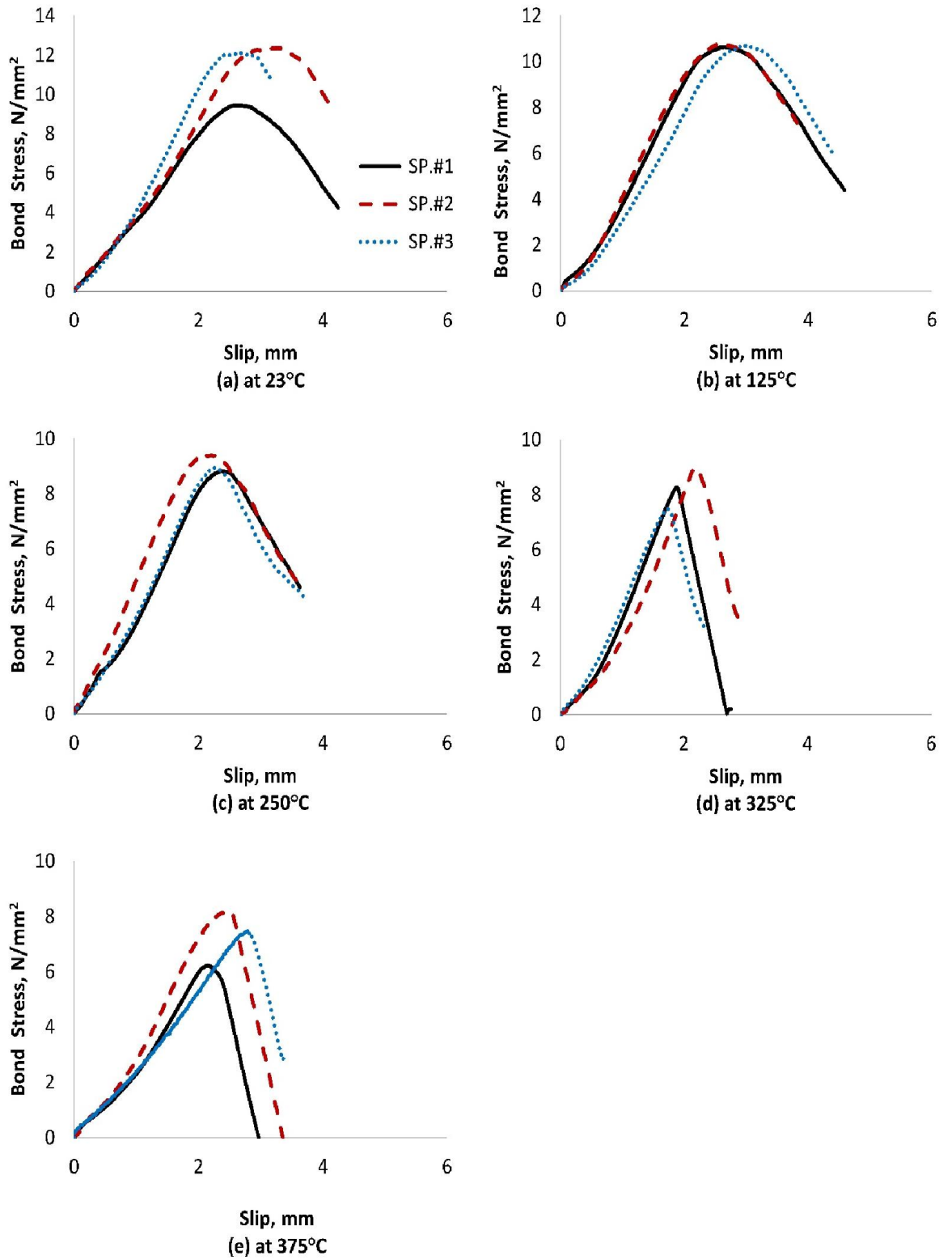
Fig A.9: Bond stress-strain curves for triplicate steel bars under elevated temperatures
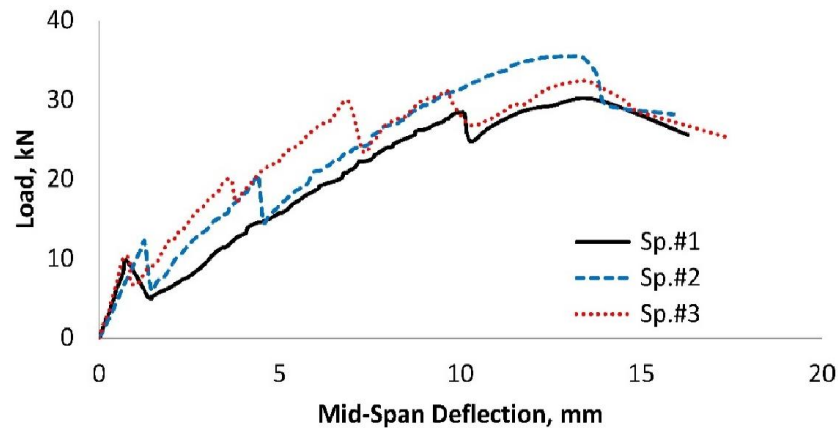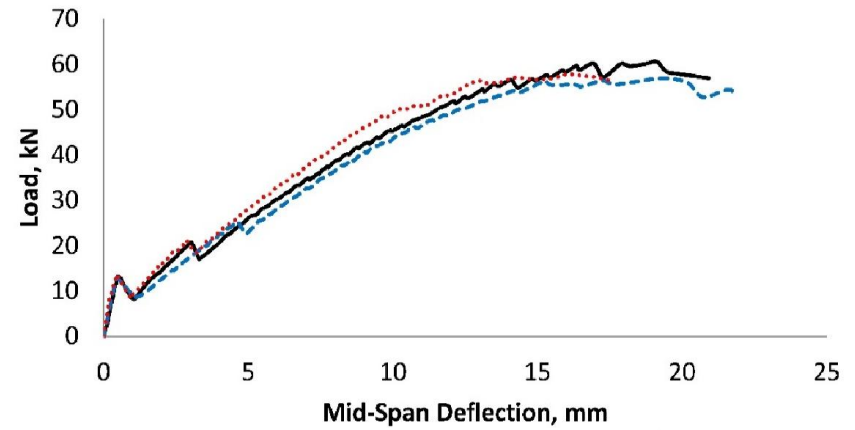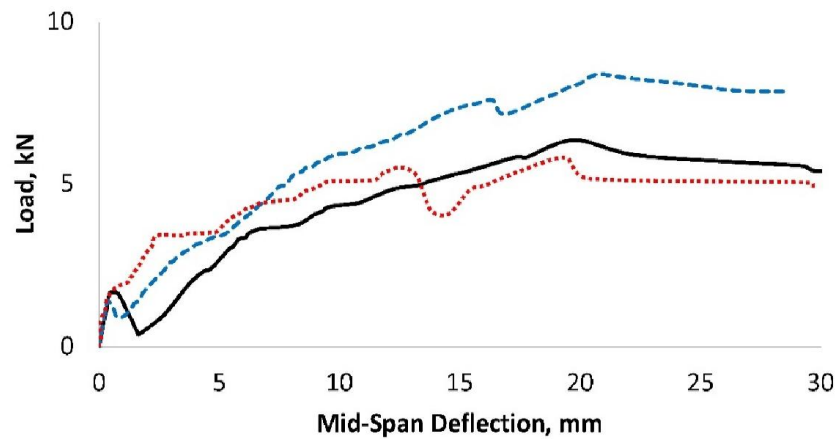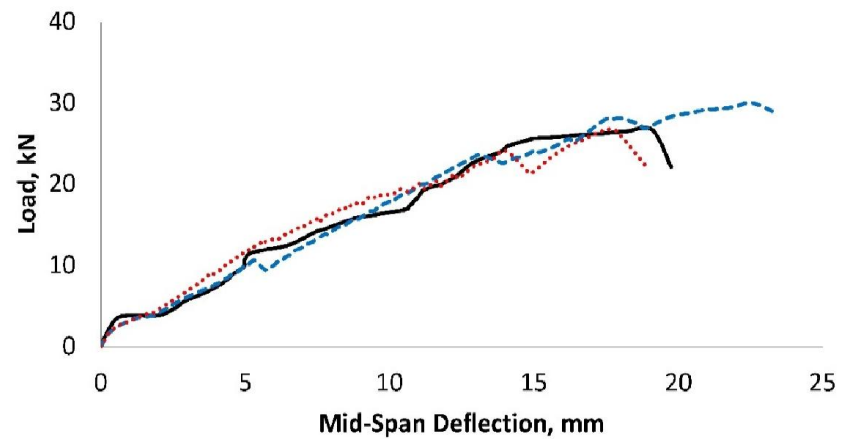
Fig. A.10 Load-deflection behavior of GFRP-RC beams with and without end cap anchorage at different exposure temperatures
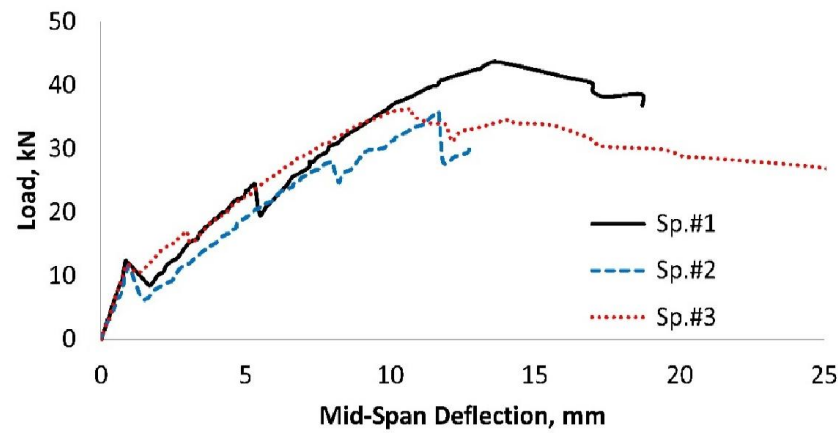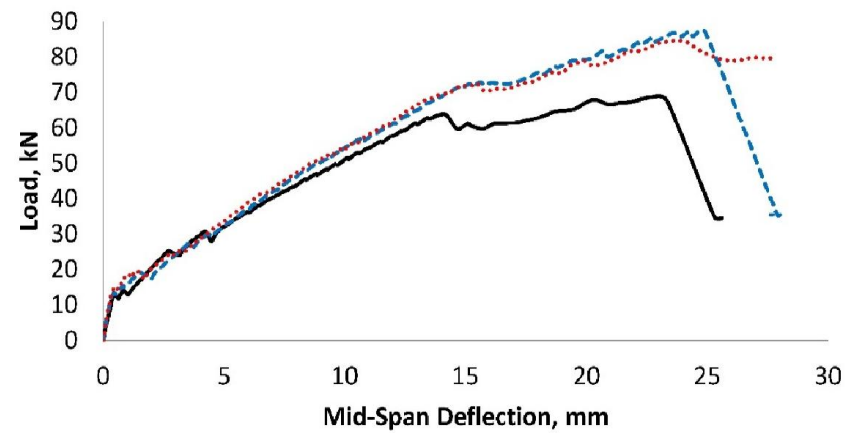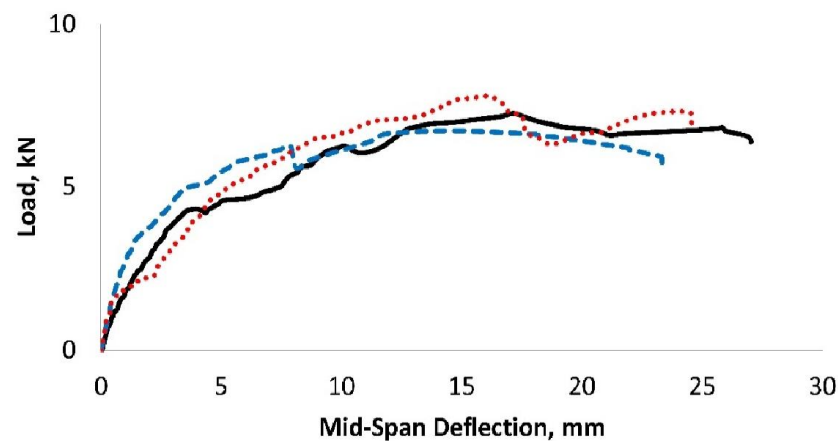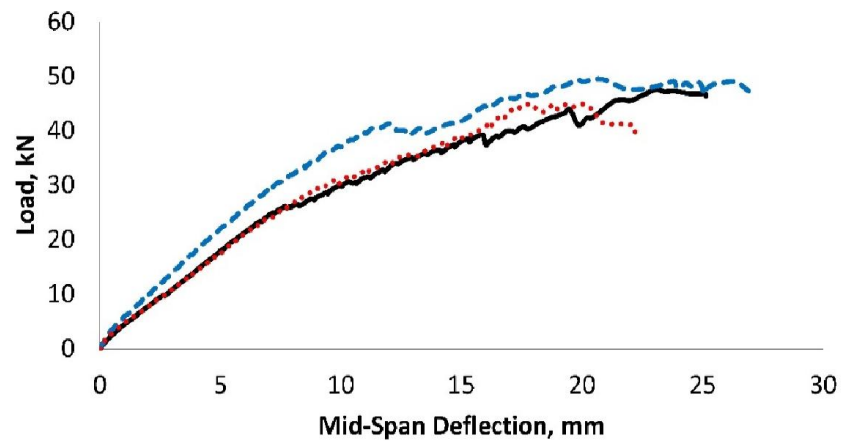
Fig. A.11 Load-deflection behavior of BFRP-RC beams with and without end cap anchorage at different exposure temperatures
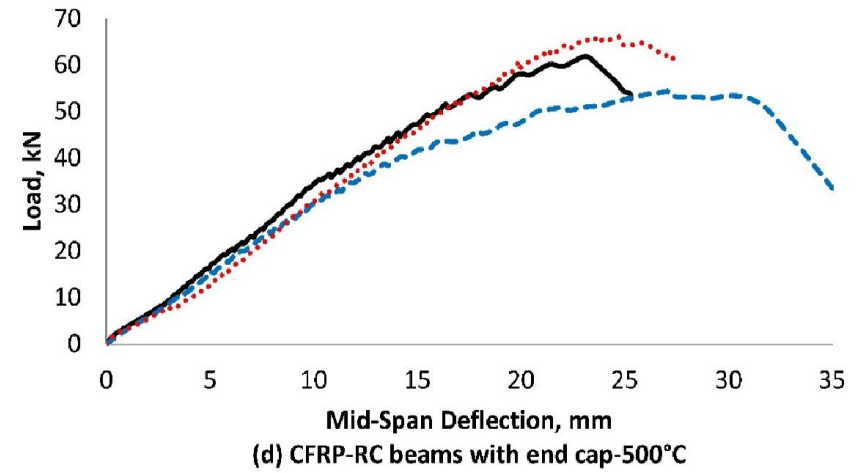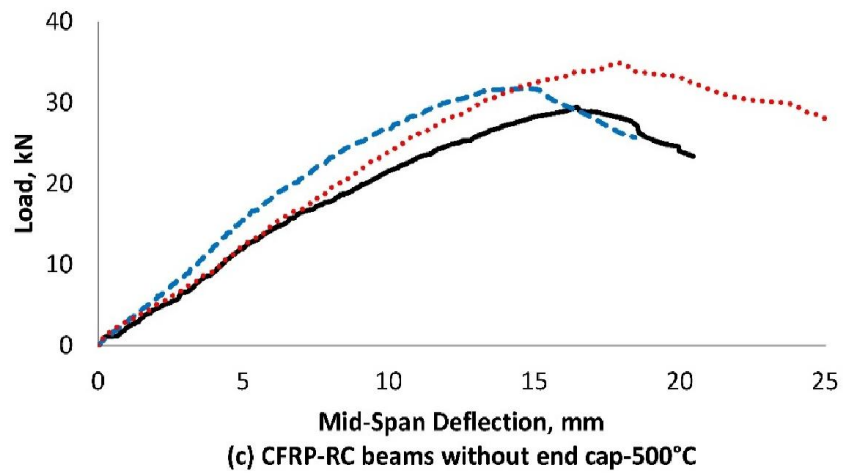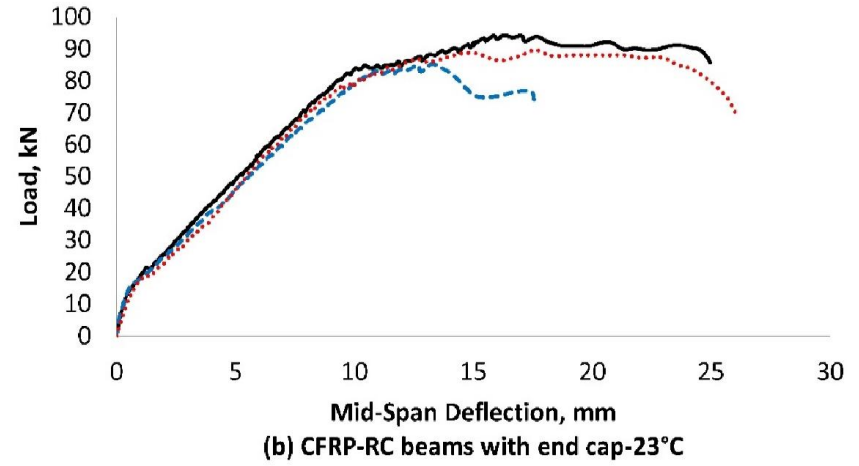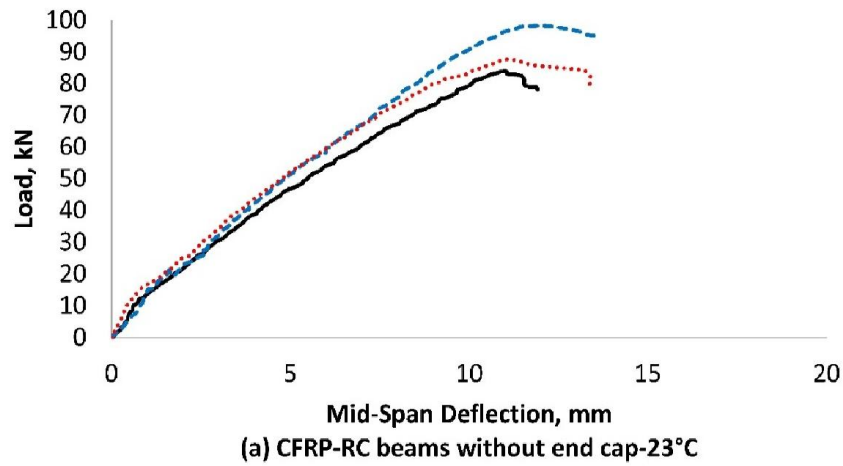
Fig. A.12 Load-deflection behavior of CFRP-RC beams with and without end cap anchorage at different exposure temperatures
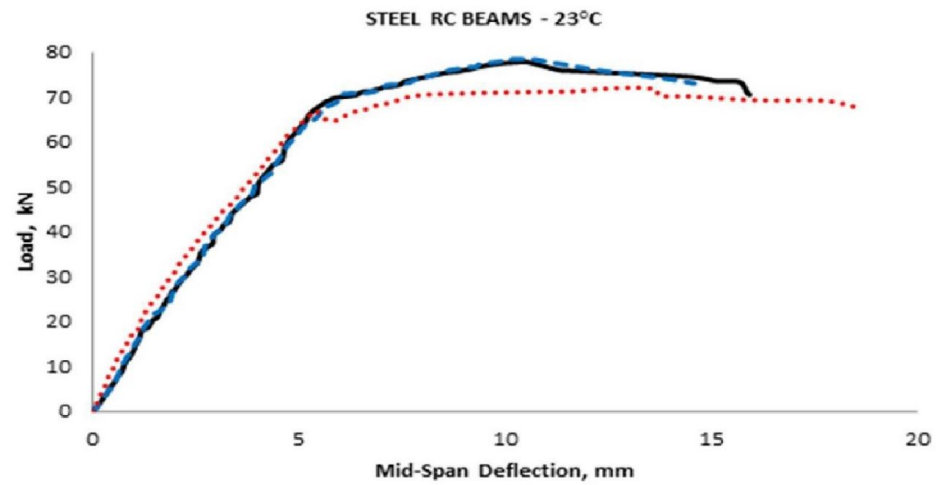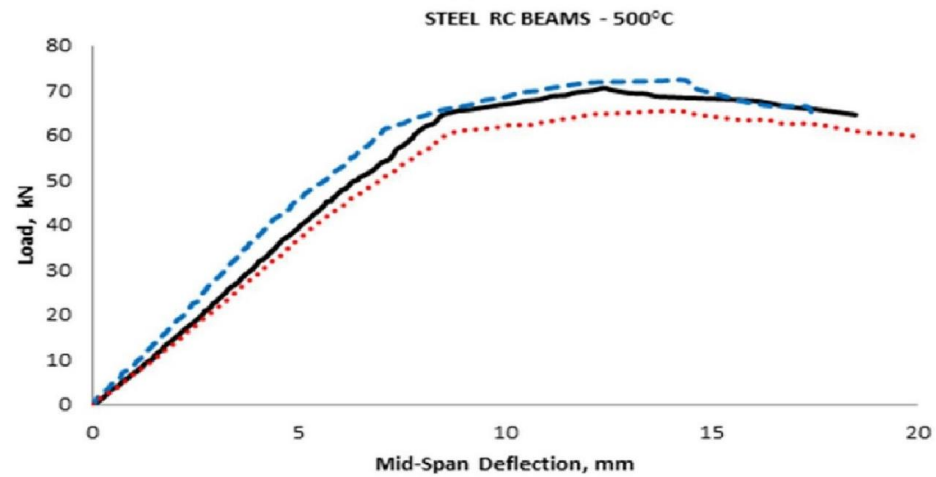
Fig. A.13 Load-deflection behavior of steel-RC beams at different exposure temperatures
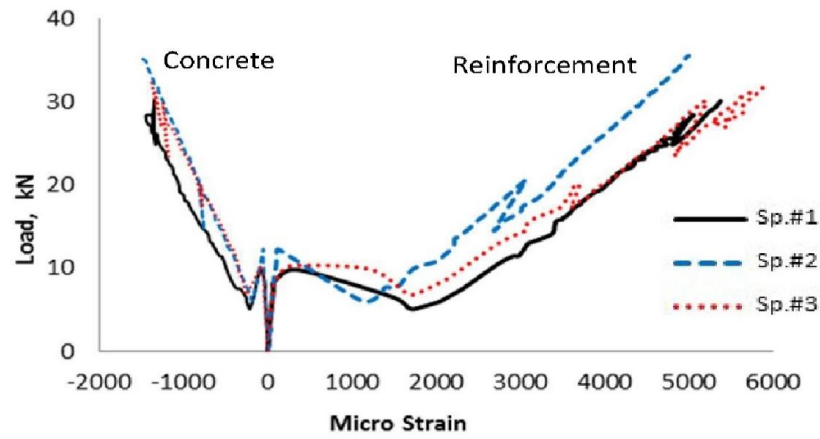
(a) N.T. without end caps
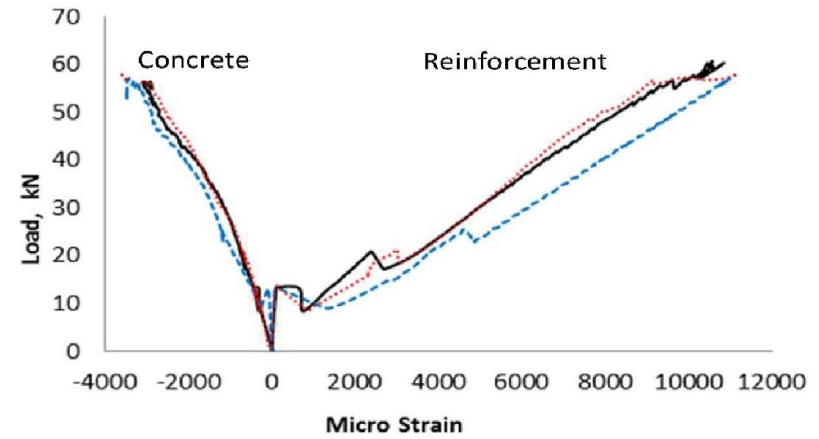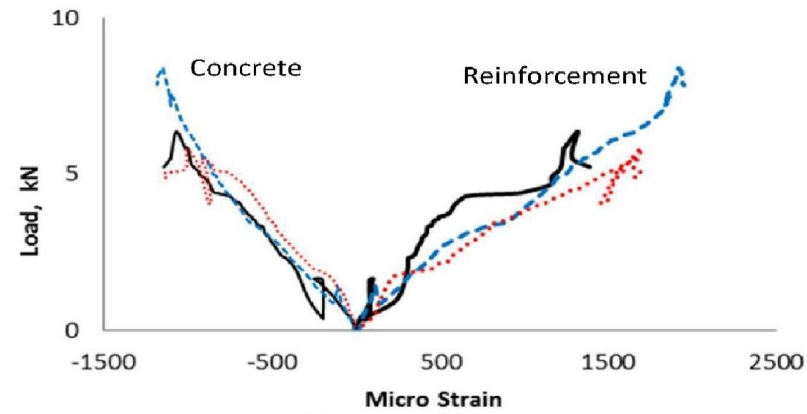
(b) N.T. with end caps

(c) H.T. without end caps
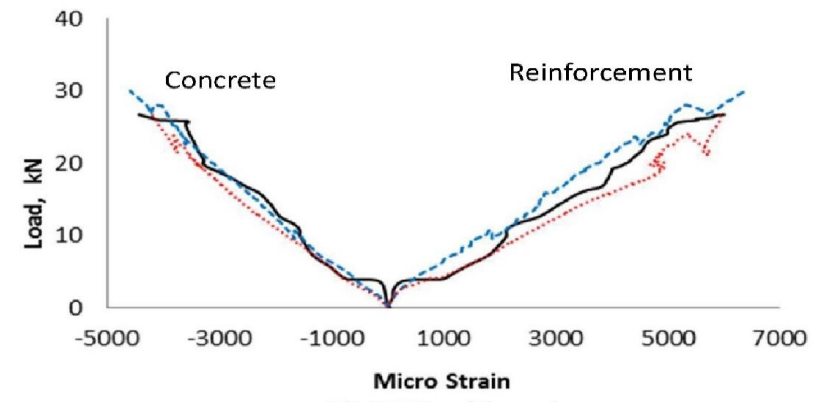
(d) H.T. with end caps

Fig. A.14: Strains in concrete and reinforcement bars in GFRP–RC beams, with and without end caps, tested under flexural before and after exposure to 500°C
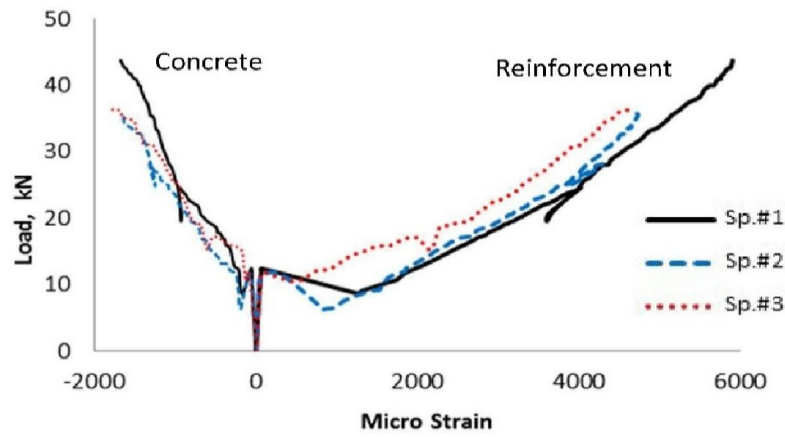
(a) N.T. without end caps
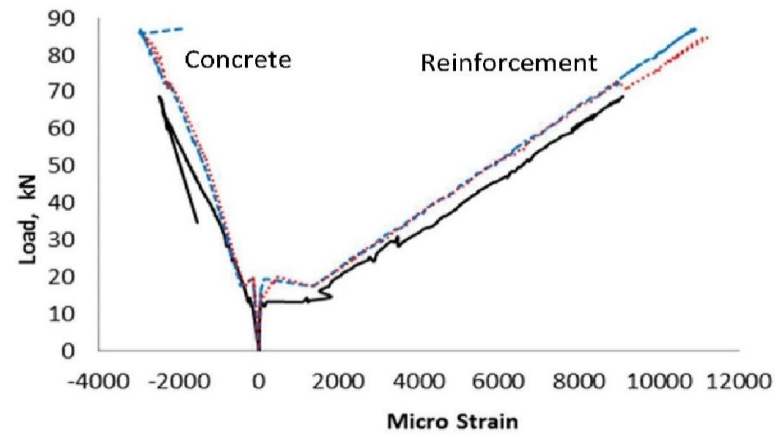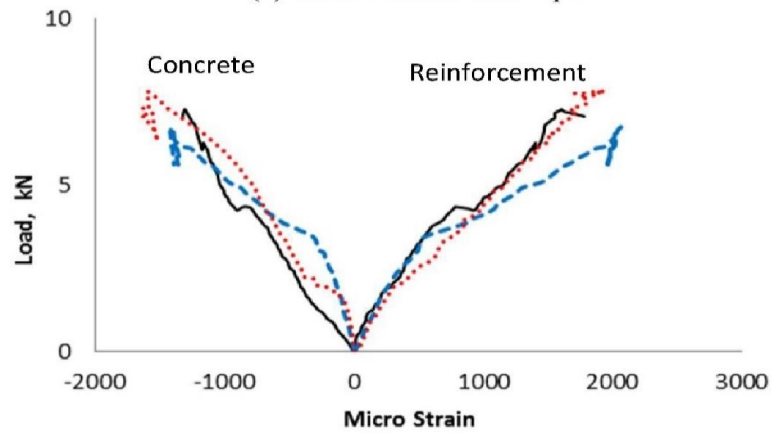
(b) N.T. with end caps

(c) H.T. without end caps
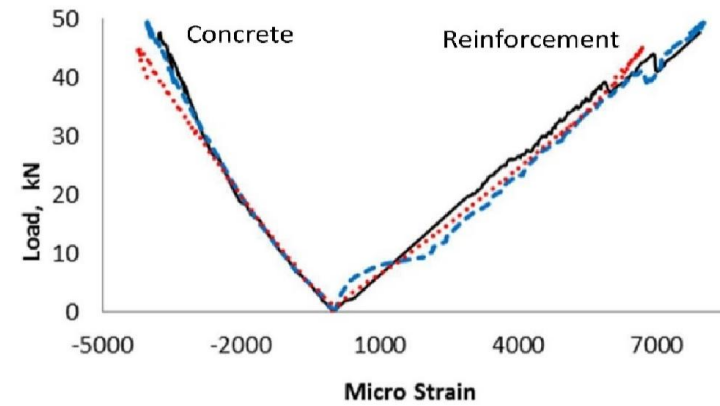
(d) H.T. with end caps

Fig. A.15: Strains in concrete and reinforcement bars in BFRP–RC beams, with and without end caps, tested under flexural before and after exposure to 500°C
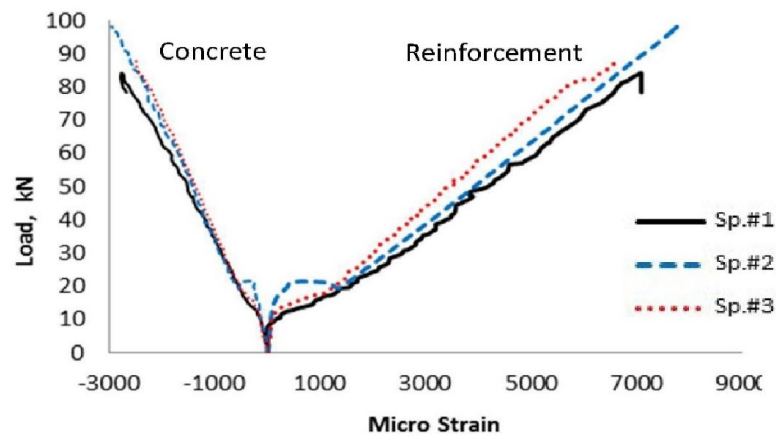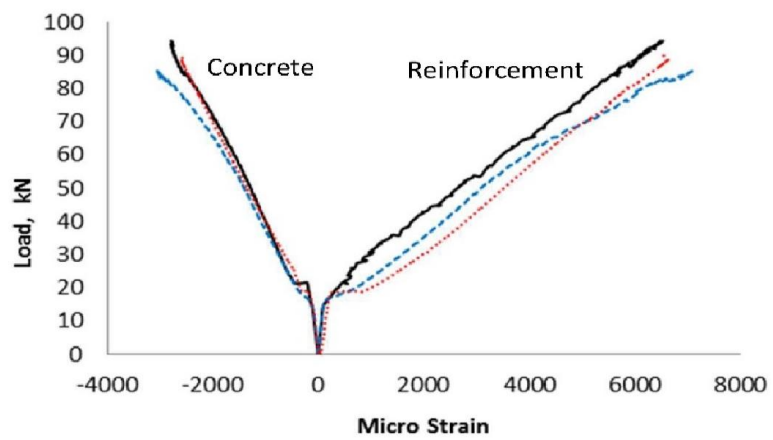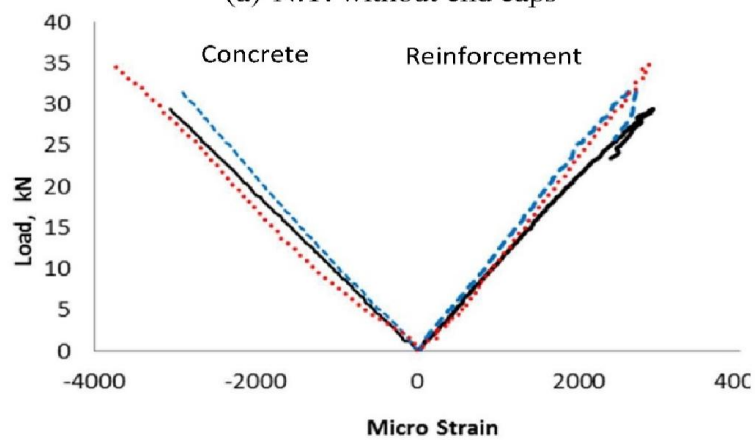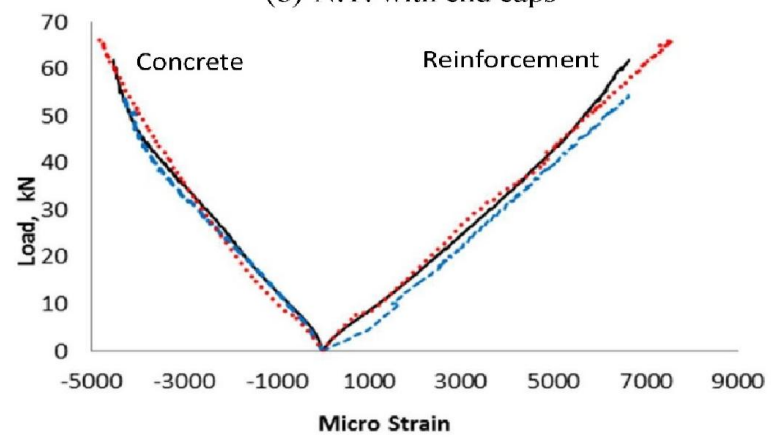
Fig. A.16: Strains in concrete and reinforcement bars in CFRP–RC beams, with and without end caps, tested under flexural before and after exposure to 500°C
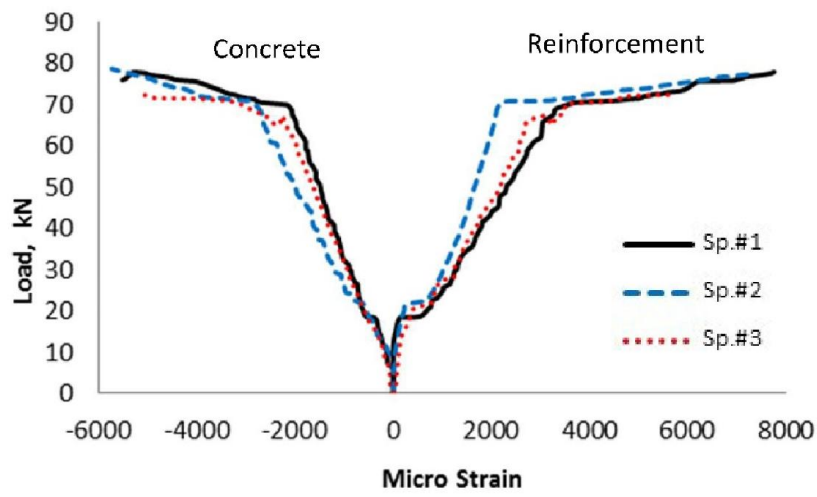
(a) N.T.
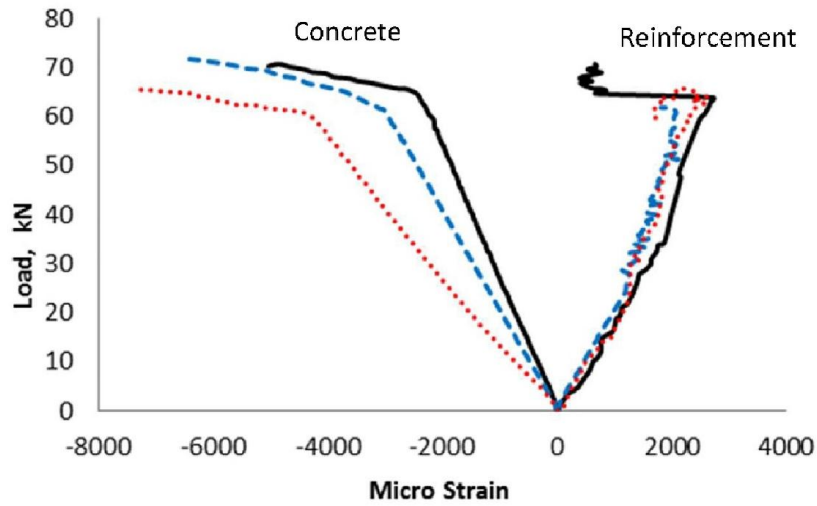
(b) H.T.

Fig. A.17: Strains in concrete and reinforcement bars in steel–RC beams, tested under flexural before and after exposure to 500°C

Appendix B: Theoretical Prediction of Flexural Capacity of FRP-RC beams

B1.   Theoretical prediction of flexural capacity of GFRP-RC beams at normal temperature

E_f =47,140 MPa

Reduced f_{ult-f} =571.2 MPa

ρ_f /ρ_b = 1.035 >1.0   ==> crushing concrete mode failure

Extreme fiber compressive strain = ultimate concrete strain ε_{cu} = 0.003
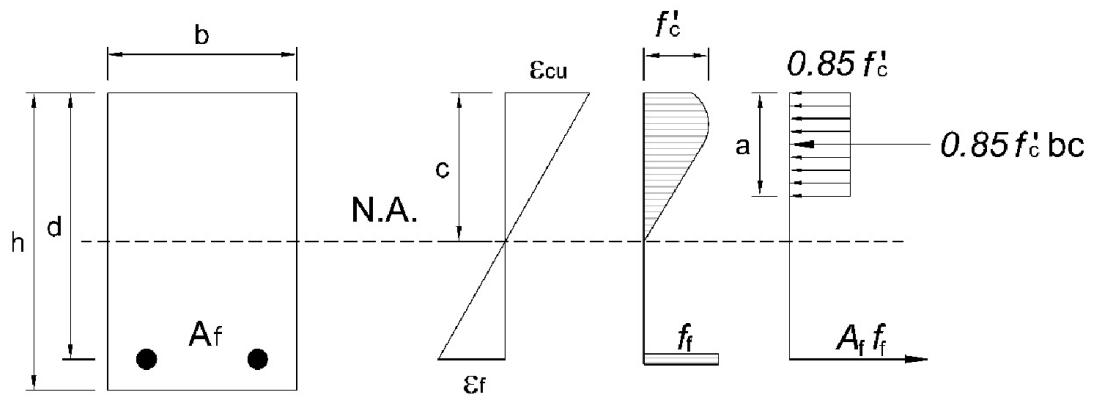
(Refer Fig. 5.10)

$FRP\ tensile\ stress\ at\ time\ of\ concrete\ crushing = f_f$

$$f_f = \sqrt{\left(\frac{E_f \varepsilon_{CU}}{2}\right)^2 + \left(\frac{0.85\beta_1 f_c' E_f \varepsilon_{CU}}{\rho_f}\right)} - \frac{E_f \varepsilon_{CU}}{2} \le f_{ult-f} = 571 \text{ MPa}$$

$$f_f = \sqrt{\left(\frac{47140 \times 0.003}{2}\right)^2 + \left(\frac{0.85 \times 0.80714 \times 34 \times 47140 \times 0.003}{0.008391}\right)} - \frac{47140 \times 0.003}{2}$$

$$= 560.2 MPa < f_{ult-} = 571.2 \text{ MPa}\quad \text{OK}$$

$$\varepsilon_f = \frac{f_f}{E_f} = \frac{560.2}{47140} = 0.011885$$

$Tensile\ force\ in\ reinforcemnet\ T_m = A_f f_f = 157.08 \times 560.2 = 88,007\ N$

$$= 88.0\ kN$$

$$a = \frac{A_f f_f}{0.85 f_c' b} = \frac{157.08 \times 560.2}{0.85 \times 34 \times 130} = 23.43 \ mm \rightarrow c = \frac{a}{\beta_1} = \frac{23.43}{0.80714} = 29.02 \ mm$$

$$M_n = T_m \left(d - \frac{a}{2} \right) = 88.0 \times \left(144 - \frac{23.43}{2} \right) \times 10^{-6} = 11.64 \ kN.m$$

Or M_n can be directly calculated from the below equation:

$$M_n = A_f f_f d \left(1 - \frac{0.59 \rho_f f_f}{f_c'} \right)$$

$$= 157.08 \times 560.2 \times 144 \times \left(1 - \frac{0.59 \times 0.008391 \times 560.2}{34} \right) \times 10^{-6} = 11.64 \ kN.m$$
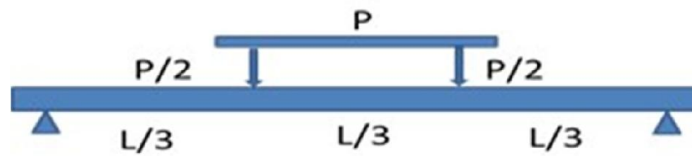
(Refer Fig. 5.7)

$$For \ four \ point \ loaded \ beam, P_n = \frac{6 M_n}{L} = \frac{6 \times 11.64}{1.05} = 66.52 \ kN$$

<u>Check of bond capacity of GFRP in the Concrete beam at normal temperature:</u>

The tensile force is transferred to the bars though bar-concrete bond. The bond stress distributions are not constant along the reinforcement bars so the average mean values of the bond will be used to indicate the bond strength between the bars and concrete. From previous presented pullout -test results, Average bond strength capacity between different FRP and concrete at normal and high temperature are summarized in the following table:

τ MPa	Carbon	Glass	BASALT	Steel
at 23°C	8.338	2.014	2.628	7.480
at 320°C	1.533	0.419	0.554	3.923
+end cap at 23°C	8.937	6.703	8.614	
+end cap at 320°C	6.948	4.983	6.690	

Ultimate bond capacity of GFRP with concrete $\tau_{max} = 2.014 \ MPa$

For FRP bar , ultimate nond force $= \pi\, \tau_{max} d_b\, S$
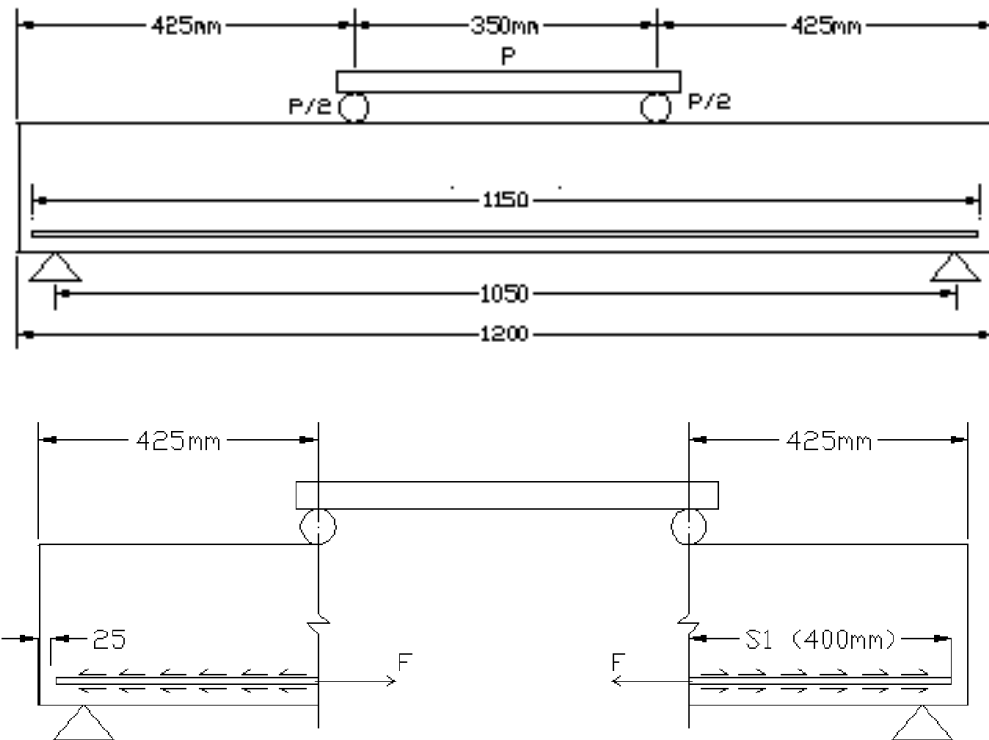
(Refer Fig. 5.12)

For two GFRP bars $F = 2\times\pi\, \tau_{max} d_b\, S = 2\times\pi\times2.014\times10\times400 = 50.617\ \text{kN}$

$$< T_m = 88.0\ kN$$

Maximum bond force capacity between GFRP and concrete is lower than the maximum tensile force capacity so bond failure between GFRP and concrete is expected before reaching to concrete crushing and flexural capacity of the beam should be recalculate as follows.

The ACI compression stress block is not applicable because the maximum concrete strain didn't reach its ultimate value of 0.003 therefore an approximate stress distribution in the concrete should be used according to the strain level reached using Hognestad Model.

1.   First step is to assume that the concrete stress is less than its peak & strain is less than ε_o. Parabolic distribution of concrete compressive stress of maximum value f_c is assumed   (note: parabolic area = 2/3 f_c c)
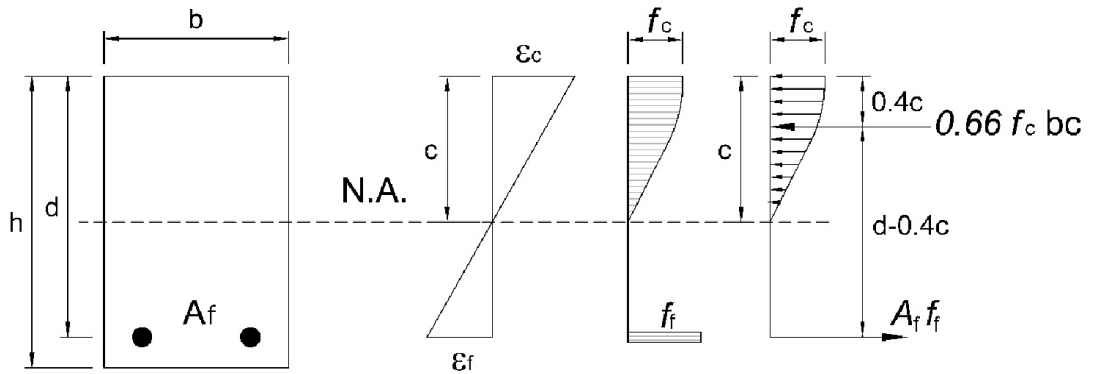
(Refer Fig. 5.11)

2.   Assume $f_c = f_c' = 34$ MPa

F (maximum Bond capacity Force) =50,617 N=50.617 kN (from previous page)

$$Maximum\ FRP\ strain\ \varepsilon_f = \frac{F}{A_f E_f} = \frac{50.617}{157.08 \times 47140} = 0.006835$$

$$Compression\ force\ C\ = \frac{2}{3} f_c cb = \frac{2}{3} \times 34 \times 130 \times c$$

Using internal forces equilibrium, C = F

$$\frac{2}{3} \times 34 \times 130 \times c = 50,617 \rightarrow c = 17.177\ mm$$

$$\varepsilon_c = \frac{c\ \varepsilon_f}{d-c} = \frac{17.177 \times 0.006835}{144 - 17.177} = 0.0009288$$

Using concrete stress $-$ strain curve proposed by Hognestad 1955,

concrete compressive stress f_c

$$= \begin{cases} f_c' \left(\frac{\varepsilon_c}{\varepsilon_o}\right)\left(2 - \frac{\varepsilon_c}{\varepsilon_o}\right) & if\ \varepsilon_c \leq \varepsilon_o \\ f_c' \left[1 - \left(0.15 \times \frac{\varepsilon_c - \varepsilon_o}{\varepsilon_{cu} - \varepsilon_o}\right)\right] & if\ \varepsilon_o < \varepsilon_c \leq \varepsilon_{cu} \end{cases}$$

where ε_o *strain at peak stress* $= \frac{1.8 f_c'}{E_c} = \frac{1.8 f_c'}{4700\sqrt{f_c'}} = \frac{1.8 \times 34}{4700\sqrt{34}} = 0.0022331$

$$f_c = f_c' \left(\frac{\varepsilon_c}{\varepsilon_o}\right)\left(2 - \frac{\varepsilon_c}{\varepsilon_o}\right) = 34 \times \left(\frac{0.0009288}{0.002233}\right)\left(2 - \frac{0.0009288}{0.002233}\right) = 22.35 \, MPa$$

3.   By trial and error, repeat the previous step using initially f_c = 22.35 MPa, until we find the correct stress value f_c.

It was found that fc = 26.906 MPa

c= 21.707 mm

ε_c = 0.001213

$$M_n = F(d - 0.4c) = 50.617 \times (144 - 0.4 \times 21.707) \times 10^{-6} = 6.85 \, kN.m$$

$$For \; four \; point \; loaded \; beam, P_n = \frac{6M_n}{L} = \frac{6 \times 6.85}{1.05} = 39.14 \, kN$$

<u>Check of bond capacity of GFRP bar with end cap in the concrete beam at normal temperature:</u>

$Ultimate \; bond \; capacity \; of \; GFRP \; with \; concrete \; \tau_1 = 2.014 \, MPa$

$Ultimate \; bond \; capacity \; between \; GFRP, epoxy \; and \; SS \; cap \; \tau_2 = 6.703 \, MPa$

$For \; one \; FRP \; bar \; with \; end \; cap, ultimate \; bond \; force \; = \pi \, d_b \, (S_1 \, \tau_1 + S_2 \, \tau_2)$
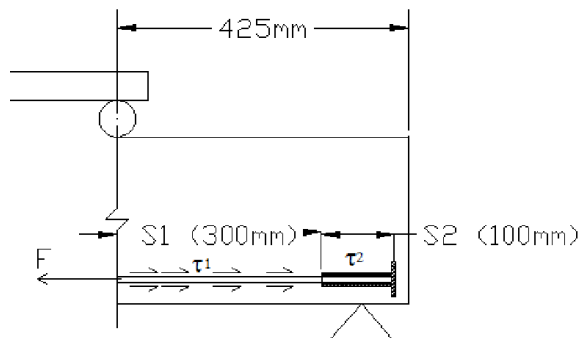
Fig. B.1

$For \; two \; GFRP \; bars \; F \; = \; 2 \times \pi \, d_b \, (S_1 \, \tau_1 + S_2 \, \tau_2)$

$= \; 2 \times \pi \times 10 \times (300 \times 2.014 + 100 \times 6.703) = 80.08 \; kN < \; T$

$= 88.0 \, kN$

Maximum bond force capacity between GFRP bars with end cap and concrete is lower than the maximum tensile force in the reinforcement of the beam at concrete crushing failure which means that bond between GFRP and concrete is expected to fail before reaching to concrete crushing and flexural capacity of the beam should be recalculate similar to previous steps:

1. Assume $f_c = f_c' = 34$ MPa

F (maximum Bond capacity Force) = 80,080 N = 80.08 kN (from previous page)

$$Maximum\ FRP\ strain\ \varepsilon_f = \frac{F}{A_f E_f} = \frac{80.08}{157.08 \times 47140} = 0.010815$$

$$Compression\ Force\ C = \frac{2}{3} f_c cb = \frac{2}{3} \times 34 \times 130 \times c$$

Using internal forces equilibrium, C = F

$$\frac{2}{3} \times 34 \times 130 \times c = 80,080 \rightarrow c = 27.176\ mm$$

$$\varepsilon_c = \frac{c\ \varepsilon_f}{d - c} = \frac{27.176 \times 0.010815}{144 - 27.176} = 0.002516 > \varepsilon_o$$

$$where\ \varepsilon_o\ strain\ at\ peak\ stress\ = \frac{1.8 f_c'}{E_c} = \frac{1.8 f_c'}{4700 \sqrt{f_c'}} = \frac{1.8 \times 34}{4700 \sqrt{34}} = 0.0022331$$

This means that the concrete compressive stress had exceeded its peak values and existed in the linear part of the curve between its peak stress (fc') and the crushing stress (0.85fc')

$$Using\ concrete\ stress - strain\ curve\ proposed\ by\ Hognestad, for\ \varepsilon_c > \varepsilon_o$$

$$f_c = f_c' \left[1 - \left(0.15 \times \frac{\varepsilon_c - \varepsilon_o}{\varepsilon_{cu} - \varepsilon_o} \right) \right]$$

$$= f_c' \left[1 - \left(0.15 \times \frac{0.002516 - 0.002233}{0.003 - 0.002233} \right) \right] = 0.94471 f_c' = 32.12\ MPa$$
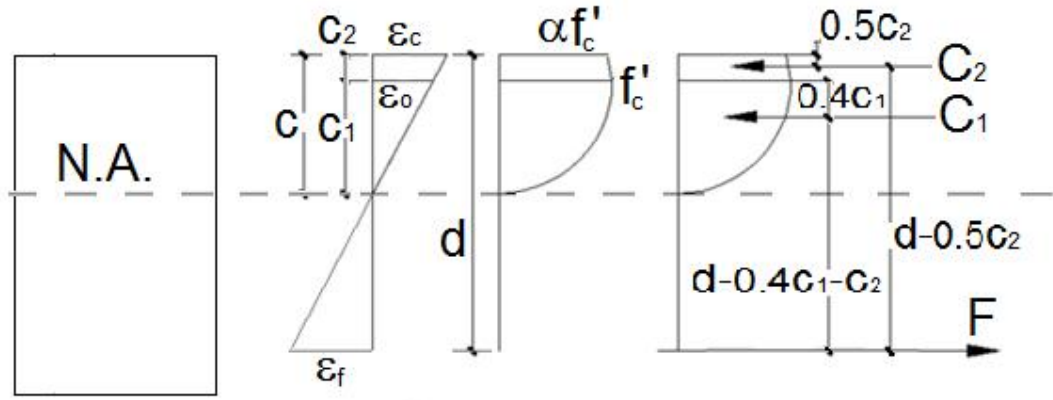
Fig. B-2

1. Assume $f_c = \alpha\, f_c' = 0.94471\, f_c' = 32.12$ MPa

Compression Force $C = \left[\dfrac{2}{3} f_c' c_1 b\right] + \left[\left(\dfrac{1+\alpha}{2}\right) f_c' c_2 b\right]$

$c_2 = \left(\dfrac{\varepsilon_c - \varepsilon_o}{\varepsilon_o}\right) c_1 \quad \& \quad c_1 = \left(\dfrac{\varepsilon_o}{\varepsilon_c}\right) c$

Compression Force $C = C_1 + C_2 = \left[\dfrac{2}{3} f_c' c_1 b\right] + \left[\left(\dfrac{1+\alpha}{2}\right)\left(\dfrac{\varepsilon_c - \varepsilon_o}{\varepsilon_o}\right) c_1 f_c' b\right]$

$\qquad = f_c' c\, b \left(\dfrac{\varepsilon_o}{\varepsilon_c}\right)\left[\left(\dfrac{2}{3}\right) + \left(\dfrac{1+\alpha}{2}\right)\left(\dfrac{\varepsilon_c - \varepsilon_o}{\varepsilon_o}\right)\right]$

Using internal forces equilibrium, $C = T_m$

$f_c' c\, b \left(\dfrac{\varepsilon_o}{\varepsilon_c}\right)\left[\left(\dfrac{2}{3}\right) + \left(\dfrac{1+\alpha}{2}\right)\left(\dfrac{\varepsilon_c - \varepsilon_o}{\varepsilon_o}\right)\right] = T_m$

$\qquad 34 \times 130 \times c \times \left(\dfrac{0.002233}{0.002516}\right)\left[\left(\dfrac{2}{3}\right) + \left(\dfrac{1+0.94471}{2}\right)\left(\dfrac{0.002516 - 0.002233}{0.002233}\right)\right]$

$\qquad\qquad = 80,080 \qquad\qquad \rightarrow c = 25.844\ mm$

$\varepsilon_c = \dfrac{c\,\varepsilon_f}{d-c} = \dfrac{25.844 \times 0.010815}{144 - 25.844} = 0.0023655 > \varepsilon_o$

Using concrete stress − strain curve proposed by Hognestad 1955, for $\varepsilon_c > \varepsilon_o$

$f_c = f_c' \left[1 - \left(0.15 \times \dfrac{\varepsilon_c - \varepsilon_o}{\varepsilon_{cu} - \varepsilon_o}\right)\right] = f_c' \left[1 - \left(0.15 \times \dfrac{0.0023655 - 0.002233}{0.003 - 0.002233}\right)\right]$

$\qquad\qquad = 0.974\, f_c'$

2. By trial and error, repeat the previous steps using initially $f_c = \alpha\, f_c' = 0.974\, f_c'$ MPa until we find the correct stress value f_c.

It was found that $f_c = 32.8$ MPa,

c= 26.263 mm, c1=24.3117 mm, c2= 1.9517 mm, and $\varepsilon c = 0.00241$.

$$Compression\ Force\ \ C_1 = \left[\frac{2}{3}f_c'c_1b\right] = \left[\frac{2}{3}\times34\times24.3117\times130\right]\times10^{-3}$$

$$= 71.638\ kN$$

$$Compression\ Force\ \ C_2 = \left(\frac{f_c + f_c'}{2}\right)c_2b = \left(\frac{32.8 + 34}{2}\right)\times1.9517\times130\times10^{-3}$$

$$= 8.474\ kN$$

$$M_n = [C_1(d - 0.4c_1 - c_2)] + [C_2(d - 0.5c_2)]$$

$$= [71.638\times(144 - \langle0.4\times24.3117\rangle - 1.9517)] + [8.474\times(144 - \langle0.5\times1.9517\rangle)]$$

$$= 10.69\ kN.m$$

$$For\ four\ point\ loaded\ beam, P_n = \frac{6M_n}{L} = \frac{6\times10.69}{1.05} = 61.0\ kN$$

B2. Theoretical prediction of flexural capacity of BFRP-RC beams at normal temperature :

E_f =65,850 MPa

Reduced f_{ult-f} =752 MPa

ρ_f /ρ_b = 1.3 >1.0   ==> crushing concrete mode failure

Extreme fiber compressive strain = ultimate concrete strain ε_{cu} = 0.003
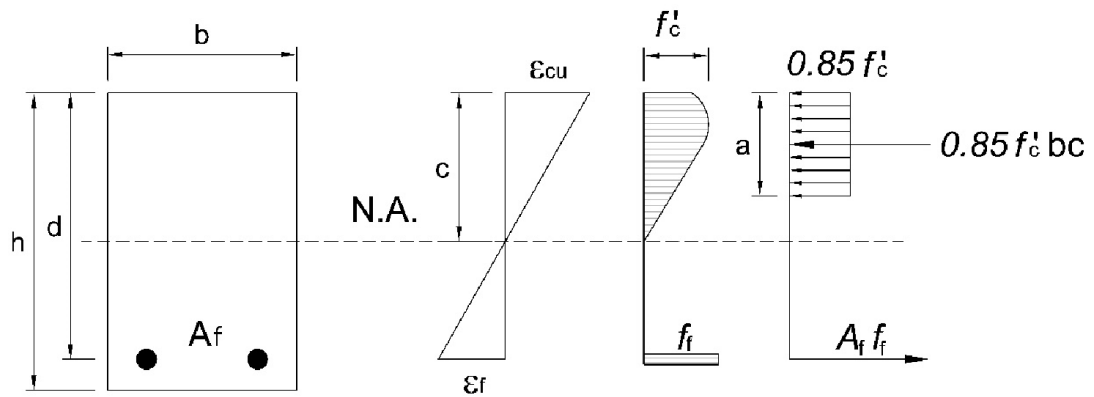
(Refer Fig. 5.10)

FRP tensile stress at time of concrete crushing = f_f

$$f_f = \sqrt{\left(\frac{E_f \varepsilon_{CU}}{2}\right)^2 + \left(\frac{0.85 \beta_1 f_c' E_f \varepsilon_{CU}}{\rho_f}\right)} - \frac{E_f \varepsilon_{CU}}{2} \le f_{ult-f} = 571 \text{ MPa}$$

$$f_f = \sqrt{\left(\frac{65850 \times 0.003}{2}\right)^2 + \left(\frac{0.85 \times 0.80714 \times 34 \times 65850 \times 0.003}{0.008391}\right)} - \frac{65850 \times 0.003}{2}$$

$$= 648.85 \text{ } MPa < f_{ult-f} = 752 \text{ MPa} \quad \text{OK}$$

$$\varepsilon_f = \frac{f_f}{E_f} = \frac{648.85}{65850} = 0.0098533$$

Tensile force in reinforcemnet $T_m = A_f f_f = 157.08 \times 648.85 = 101,921 \text{ } N$

$$= 101.92 \text{ } kN$$

$$a = \frac{A_f f_f}{0.85 f_c' b} = \frac{157.08 \times 648.84}{0.85 \times 34 \times 130} = 27.13 \text{ } mm \rightarrow c = \frac{a}{\beta_1} = \frac{34.86}{0.80714} = 33.61 \text{ } mm$$

$$M_n = T_m \left(d - \frac{a}{2}\right) = 101.92 \times \left(144 - \frac{27.13}{2}\right) \times 10^{-6} = 13.29 \, kN.m$$

$$For \; four \; point \; loaded \; beam, P_n = \frac{6M_n}{L} = \frac{6 \times 13.29}{1.05} = 75.94 \, kN$$

Check of bond capacity of BFRP in the Concrete beam at normal temperature:

$Ultimate \; Bond \; capacity \; of \; BFRP \; with \; concrete \; \tau_{max} = 2.628 \, MPa$

$For \; FRP \; Bar \, , Ultimate \; Bond \; Force \; = \pi \, \tau_{max} d_b \, S$

For two GFRP bars $F = 2 \times \pi \, \tau_{max} d_b \, S = 2 \times \pi \times 2.628 \times 10 \times 400 = 66.048$ kN

$$< \; T_m = 101.92 \, kN$$

Maximum bond force capacity between BFRP and concrete is lower than the maximum tensile force in the bars at concrete crushing failure stage so bond failure between BFRP and concrete is expected before reaching to concrete crushing and flexural capacity of the beam to be recalculate similar to previous GFRP beam design:

1. First step is to assume that the concrete stress is less than its peak & strain is less than ε_o . Parabolic distribution of concrete compressive stress of maximum value f_c is assumed (note: parabolic area = 2/3 f_c c)
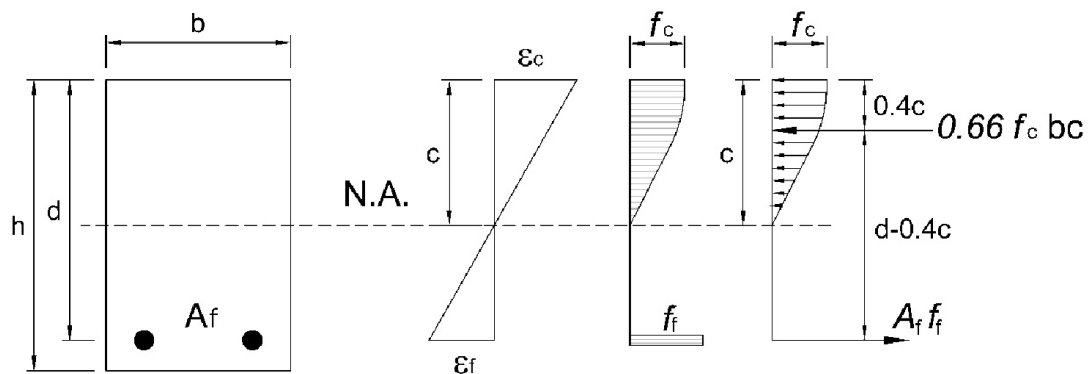
(Refer Fig. 5.11)

2. Assume $f_c = f_c' = 34$MPa

F (maximum Bond capacity Force) =66,048 N=66.048 kN

$$Maximum \; FRP \; strain \; \varepsilon_f = \frac{F}{A_f E_f} = \frac{66,048}{157.08 \times 65850} = 0.00639$$

Compression Force $C = \dfrac{2}{3}f_c cb = \dfrac{2}{3} \times 34 \times 130 \times c$

Using internal forces equilibrium, $C = F$

$\dfrac{2}{3} \times 34 \times 130 \times c = 66{,}048 \rightarrow c = 22.415 \; mm$

$\varepsilon_c = \dfrac{c\,\varepsilon_f}{d-c} = \dfrac{22.415 \times 0.00639}{144 - 22.415} = 0.001178 \; < \varepsilon_o$

$where \; \varepsilon_o \; strain \; at \; peak \; stress \; = \dfrac{1.8 f_c'}{E_c} = \dfrac{1.8 f_c'}{4700\sqrt{f_c'}} = \dfrac{1.8 \times 34}{4700\sqrt{34}} = 0.0022331$

$Using \; concrete \; stress - strain \; curve \; proposed \; by \; Hognestad \; 1955,$

$f_c = f_c' \left(\dfrac{\varepsilon_c}{\varepsilon_o}\right)\left(2 - \dfrac{\varepsilon_c}{\varepsilon_o}\right) = 34 \times \left(\dfrac{0.001178}{0.002233}\right)\left(2 - \dfrac{0.001178}{0.002233}\right) = 26.4 \; MPa$

3. By trial and error, repeat the previous steps using initially $f_c = 26.4$ MPa, until

   we find the correct stress value f_c.

It was found that $f_c = 29.34$ MPa

c= 25.975 mm and $\varepsilon_c = 0.001406$

$M_n = F(d - 0.4c) = 66{,}048 \times (144 - 0.4 \times 25.975) \times 10^{-6} = 8.825 \; kN.m$

$For \; four \; point \; loaded \; beam, P_n = \dfrac{6 M_n}{L} = \dfrac{6 \times 8.825}{1.05} = 50.42 \; kN$

Check of bond capacity of BFRP bar with end cap in the concrete beam at normal
temperature:
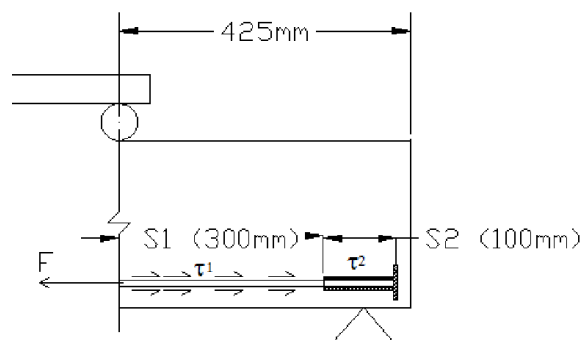
(Refer Fig. B.1)

Ultimate bond capacity of BFRP with concrete $\tau_1 = 2.628 \, MPa$

Ultimate bond capacity between BFRP, epoxy and S.S.cap $\tau_2 = 8.614 \, MPa$

For FRP Bar with end cap, ultimate bond force $= \pi \, d_b \, (S_1 \, \tau_1 + S_2 \, \tau_2)$

For two GFRP bars $F = 2 \times \pi \, d_b \, (S_1 \, \tau_1 + S_2 \, \tau_2)$

$$= 2 \times \pi \times 10 \times (300 \times 2.628 + 100 \times 8.614) = 103.66 \, \text{kN} > T_m$$

$$= 101.92 \, kN$$

Maximum bond force capacity between BFRP bars with end cap and concrete is higher than the maximum tensile force in the reinforcement of the beam at concrete crushing failure stage which means that concrete is expected to reach crushing strain before reaching the de-bonding stage and flexural capacity of the beam is the same previously calculated value of 13.29 kN.m.

B3. Theoretical prediction of flexural capacity of CFRP-RC beams at normal temperature

E_f =119,000 MPa

Reduced f_{ult-f} =1414 MPa

ρ_f / ρ_b = 2.524 >1.0   ==> crushing concrete mode failure

Extreme fiber compressive strain = ultimate concrete strain ε_{cu} = 0.003
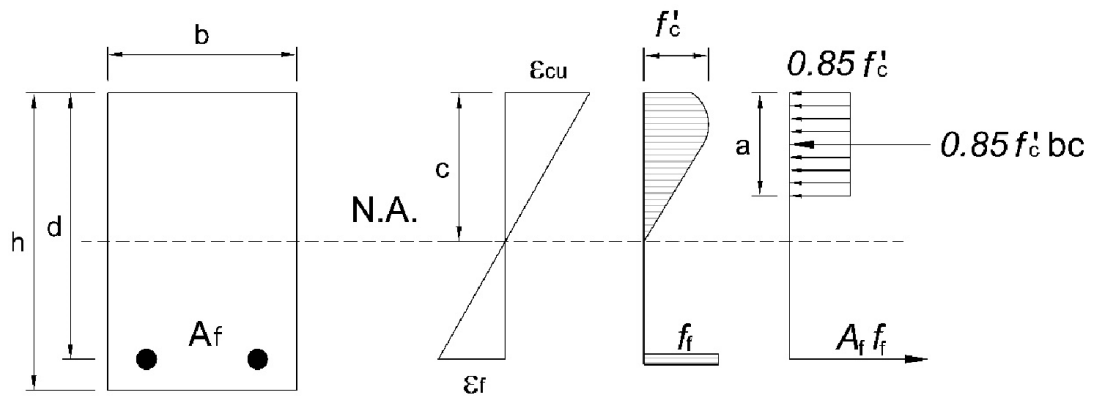
(Refer Fig. 5.10)

$FRP \; tensile \; stress \; at \; time \; of \; concrete \; crushing = f_f$

$$f_f = \sqrt{\left(\frac{E_f \varepsilon_{CU}}{2}\right)^2 + \left(\frac{0.85\beta_1 f_c' E_f \varepsilon_{CU}}{\rho_f}\right)} - \frac{E_f \varepsilon_{CU}}{2} \le f_{ult-f} = 1414 \text{ MPa}$$

$$f_f = \sqrt{\left(\frac{119,000 \times 0.003}{2}\right)^2 + \left(\frac{0.85 \times 0.80714 \times 34 \times 119,000 \times 0.003}{0.008391}\right)}$$

$$- \frac{119,000 \times 0.003}{2} = 833.78 MPa < f_{ult-f} = 1414 \text{ MPa} \quad OK$$

$$\varepsilon_f = \frac{f_f}{E_f} = \frac{833.78}{119,000} = 0.007007$$

$Tensile \; force \; in \; reinforcemnet \; T_m = A_f f_f = \; 157.08 \times 833.78 = 130,970 \; N$

$$= 130.97 \; kN$$

$$a = \frac{A_f f_f}{0.85 f_c' b} = \frac{157.08 \times 833.78}{0.85 \times 34 \times 130} = 34.86 \; mm \to c = \frac{a}{\beta_1} = \frac{34.86}{0.80714} = 43.19 mm$$

$$M_n = T_m \left(d - \frac{a}{2} \right) = 130,970 \times \left(144 - \frac{34.86}{2} \right) \times 10^{-6} = 16.57 \, kN.m$$

$$For \ four \ point \ loaded \ beam, P_n = \frac{6M_n}{L} = \frac{6 \times 16.57}{1.05} = 94.69 \, kN$$

Check of bond capacity of CFRP in the concrete beam at normal temperature:

$$Ultimate \ Bond \ capacity \ of \ CFRP \ with \ concrete \ \tau_{max} = 8.338 \, MPa$$
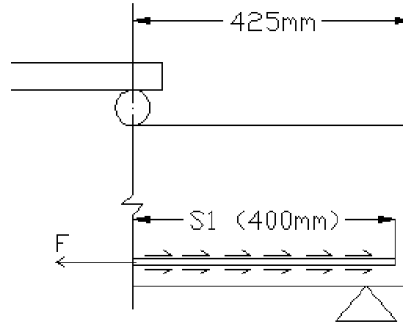
(Refer Fig. B-1)

$$For \ each \ FRP \ Bar \ , Ultimate \ Bond \ Force = \pi \ \tau_{max} d_b \ S$$

For two CFRP bars F $= 2 \times \pi \ \tau_{max} d_b \ S = 2 \times \pi \times 8.338 \times 10 \times 400 = $ 209.5 kN

$$> T_m = 130.97 \, kN$$

Maximum bond force capacity is higher than the maximum tensile force capacity so no bond failure between CFRP bars and concrete is expected at normal temperature.

Note:

The ultimate force capacity P_n calculated from the flexural capacity of this CFRP-RC is higher than its P_n calculated from the beam shear capacity, which means that shear failure is expected to occur before reaching the flexural failure due to concrete crushing.

Maximum Compressive stress/ strain and maximum tensile FRP stress/ strain can be calculated at time of shear failure as follows:

1. Assume that the concrete stress is less than its peak and strain is less than ε_o. Parabolic distribution of concrete compressive stress of maximum value f_c is assumed   (note: parabolic area = 2/3 f_c c)
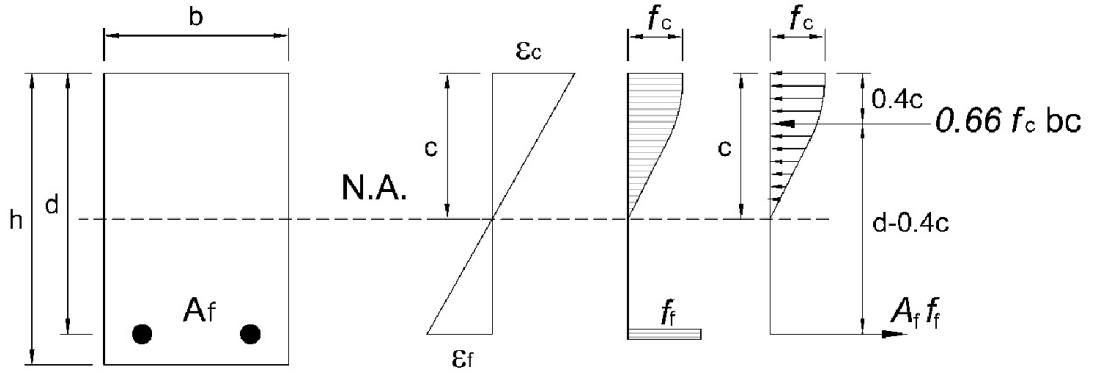
(Refer Fig. 5.11)

P_n from shear capacity calculation = 85.74

$$M = \frac{PL}{6} = \frac{85.74 \times 1.05}{6} = 15.0 \ kN.m$$

$$\varepsilon_o \ strain \ at \ peak \ stress \ \ = \frac{1.8f_c'}{E_c} = \frac{1.8f_c'}{4700\sqrt{f_c'}} = \frac{1.8 \times 34}{4700\sqrt{34}} = 0.0022331$$

Compression Force C $= \frac{2}{3}f_ccb = \frac{2}{3} \times f_c' \left(\frac{\varepsilon_c}{\varepsilon_o}\right)\left(2 - \frac{\varepsilon_c}{\varepsilon_o}\right) \times b \times c$

FRP Tensile Force $T_m = \varepsilon_f E_f A_f = \left(\frac{d-c}{c}\right)\varepsilon_c E_f A_f$

Using internal forces equilibrium, C = T_m

$$\frac{2}{3} \times f_c' \left(\frac{\varepsilon_c}{\varepsilon_o}\right)\left(2 - \frac{\varepsilon_c}{\varepsilon_o}\right) \times b \times c = \left(\frac{d-c}{c}\right)\varepsilon_c E_f A_f \qquad\qquad eq.\#1$$

$$M_n = T_m(d - 0.4c) = \left(\frac{d-c}{c}\right)\varepsilon_c E_f A_f(d - 0.4c) = 15.0 \ kN.m \qquad\qquad eq.\#2$$

Solving the above two equations with two unknowns (c and ε_c), we find that c = 40.06 mm and ε_c = 0.002415 > ε_o = 0.002233. This means that at this loading, the concrete compressive stress exceeded its peak value and existed in the linear part of the curve between its peak stress (f_c') and the crushing stress (0.85f_c')
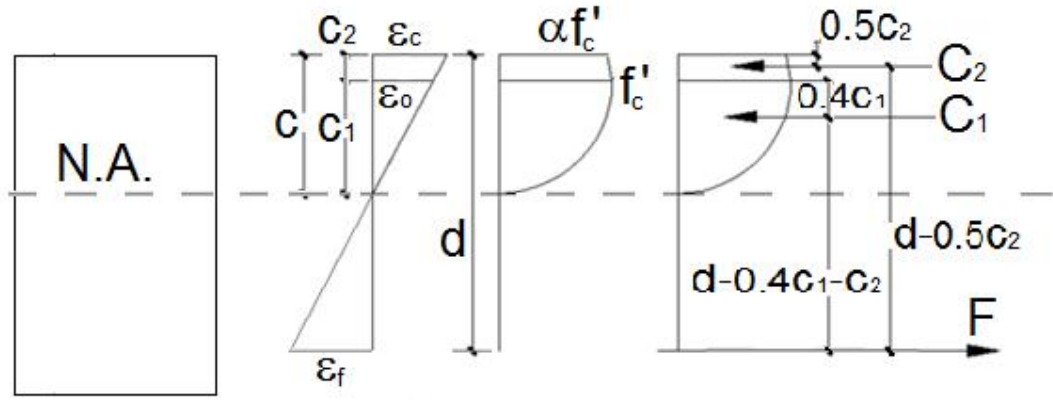
(Refer Fig. B.2)

$$c_2 = \left(\frac{\varepsilon_c - \varepsilon_o}{\varepsilon_c}\right)c$$

$$c_1 = \left(\frac{\varepsilon_o}{\varepsilon_c}\right)c$$

$$f_c = \alpha f_c' = f_c'\left[1 - \left(0.15\times\frac{\varepsilon_c - \varepsilon_o}{\varepsilon_{cu} - \varepsilon_o}\right)\right] =$$

Compression force $C = C_1 + C_2 = \left[\frac{2}{3}f_c'c_1 b\right] + \left[\left(\frac{1+\alpha}{2}\right)f_c'c_2 b\right]$

$$C = \left[\frac{2}{3}f_c'bc\left(\frac{\varepsilon_o}{\varepsilon_c}\right)\right] + \left[\left(\frac{1+\alpha}{2}\right)\left(\frac{\varepsilon_c - \varepsilon_o}{\varepsilon_c}\right)cf_c'b\right]$$

$$= f_c'c\,b\left[\left(\frac{2}{3}\right)\left(\frac{\varepsilon_o}{\varepsilon_c}\right) + \left(\frac{1+\alpha}{2}\right)\left(\frac{\varepsilon_c - \varepsilon_o}{\varepsilon_c}\right)\right]$$

FRP Tensile Force $T = \varepsilon_f E_f A_f = \left(\frac{d-c}{c}\right)\varepsilon_c E_f A_f$

Using internal forces equilibrium, C = F

$$f_c'c\,b\left[\left(\frac{2}{3}\right)\left(\frac{\varepsilon_o}{\varepsilon_c}\right) + \left(\frac{1+\alpha}{2}\right)\left(\frac{\varepsilon_c - \varepsilon_o}{\varepsilon_c}\right)\right] = \left(\frac{d-c}{c}\right)\varepsilon_c E_f A_f \quad eq.\#1$$

$$\alpha = \left[1 - \left(0.15\times\frac{\varepsilon_c - \varepsilon_o}{\varepsilon_{cu} - \varepsilon_o}\right)\right] \quad eq.\#2$$

$$M_n = [C_1(d - 0.4c_1 - c_2)] + [C_2(d - 0.5c_2)]$$

$$15 = \left[\frac{2}{3} f_c' bc \left(\frac{\varepsilon_o}{\varepsilon_c}\right) \left(d - 0.4c \left(\frac{\varepsilon_o}{\varepsilon_c}\right) - \left(\frac{\varepsilon_c - \varepsilon_o}{\varepsilon_c}\right) c\right)\right]$$

$$+ \left[\left(\frac{1+\alpha}{2}\right) \left(\frac{\varepsilon_c - \varepsilon_o}{\varepsilon_c}\right) c f_c' b \left(d - 0.5 \left(\frac{\varepsilon_c - \varepsilon_o}{\varepsilon_c}\right) c\right)\right] \qquad eq. \#3$$

Solving the above three equations with three unknowns (c, α and ε_c), we find that:

At expected shear failure mode,

c = 38.964 mm   ,

f_c = 0.98345 f_c' = 33.4374 MPa

ε_c = 0.002318 > ε_o = 0.002233

ε_f = 0.006248

f_f = 743 Mpa
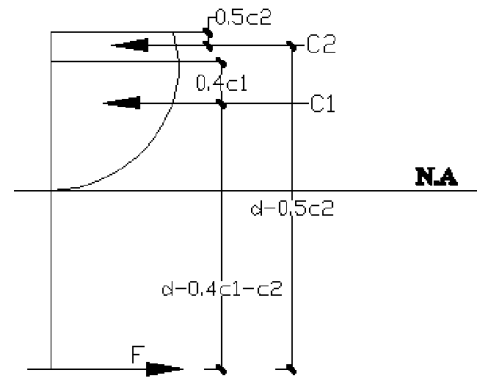
B4. Theoretical prediction of flexural capacity of GFRP-RC beams after exposure to high temperature

E_f =37,390 MPa, reduced f_{ult-f} =316.4 MPa

f_c'=25.2 MPa at T=500°C

β_1=0.85

ρ_f / ρ_b = 0.557131 <1.0 ==> FRP rupture failure mode before crushing concrete

FRP reached its maximum tensile strength while concrete still below its crushing strain stage.

Stress-strain relationship for concrete at High temperature

Concrete compressive stress f_c at any strain level can be evaluated using concrete stress-strain curve proposed by EuroCode EN1992-1-2:2004, which consists of two parts, parabolic shape curve up to peak stress (at strain ε_0) then descending linear branch up to ε_{cu}, as follows:

$$f_{c,T} = \left(\frac{3\varepsilon_{c,T} f_{c,T}'}{\varepsilon_{o,T}\left[2 + \left(\frac{\varepsilon_{c,T}}{\varepsilon_{o,T}}\right)^3\right]} \right)$$

$$\rightarrow f_{c,500} = \left(\frac{3\varepsilon_{c,T} f_{c,500}'}{0.015\left[2 + \left(\frac{\varepsilon_{c,T}}{0.015}\right)^3\right]} \right)$$
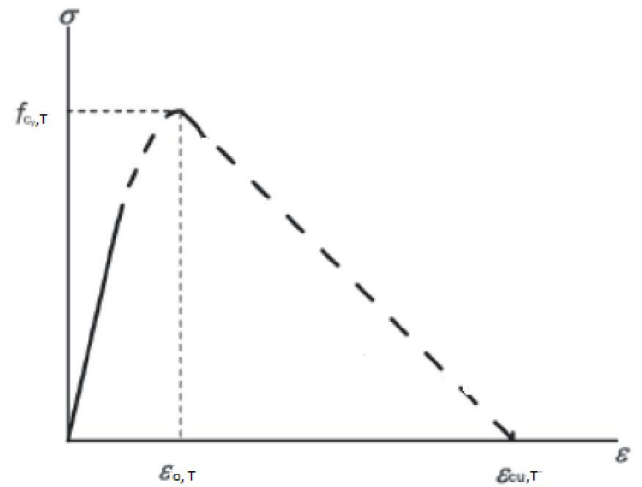
(Refer Fig. 5.9)

As per EN1992 code, for concrete exposed to 500°C, ε_0 = 0.015 and ε_{cu} = 0.025

Flexural capacity of the beam should be calculated as follows:

1. Assume that the concrete stress is less than its peak & strain is less than ε_0.

   Parabolic distribution of concrete compressive stress of maximum value f_c is assumed   (note: parabolic area = 2/3 f_c c)

$$\text{Maximum FRP strain } \varepsilon_{ult-f} = \frac{f_{ult-f}}{E_f} = \frac{316.4}{37,390} = 0.008462$$

$$\text{Tensile force in reinforcemnet } T_m = A_f f_{ult-f} = 157.08 \times 316.4$$

$$= 49,700N = 49.7 \, kN$$
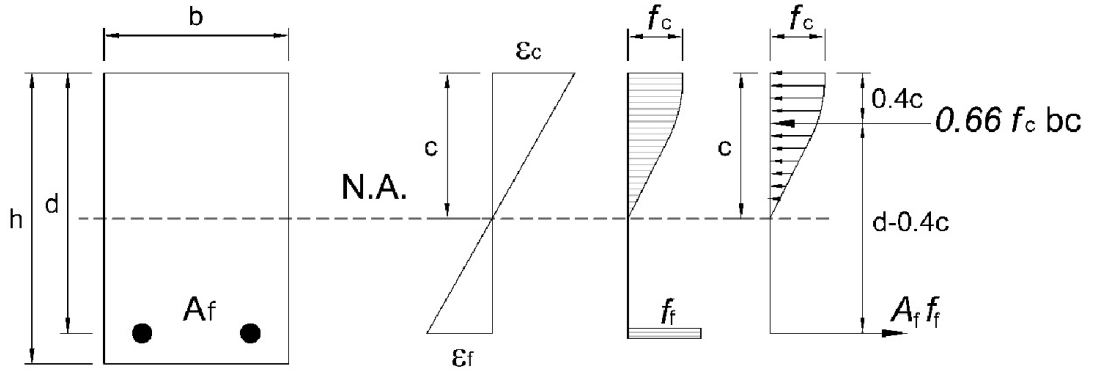
(Refer Fig. 5.11)

2. Assume $f_c = f_c' = 25.2$ MPa

Compression Force $C = \dfrac{2}{3} f_c cb = \dfrac{2}{3} \times 25.2 \times 130 \times c$

Using internal forces equilibrium, $C = T_m$

$$\frac{2}{3} \times 25.2 \times 130 \times c = 49,700 \rightarrow c = 22.7565 \, mm$$

$$\varepsilon_c = \frac{c \, \varepsilon_{ult-f}}{d - c} = \frac{22.7565 \times 0.008462}{144 - 22.7565} = 0.0015883 < \varepsilon_o$$

$Using \, EN1992 \, concrete \, stress - strain \, curve, \qquad at \, 500°C$

$$f_c = \left(\frac{3\varepsilon_{c,T} f_{c,500}'}{0.015 \left[2 + \left(\frac{\varepsilon_{c,T}}{0.015} \right)^3 \right]} \right) = \left(\frac{3\varepsilon_{c,T} \times 25.2}{0.015 \left[2 + \left(\frac{\varepsilon_{c,T}}{0.015} \right)^3 \right]} \right)$$

$$= \left(\frac{3 \times 0.0015883 \times 25.2}{0.015 \left[2 + \left(\frac{0.0015883}{0.015} \right)^3 \right]} \right) = 4.0 MPa$$

3. By trial and error, repeat the previous steps using initially $f_c = 4.0$ MPa, until

finding the correct stress value f_c.

It was found that f_c = 11.356 MPa, c= 50.497 mm and ε_c = 0.004570.

$$M_n = T(d - 0.4c) = 49.7 \times (144 - 0.4 \times 50.497) \times 10^{-6} = 6.153 \ kN.m$$

$$For \ four \ point \ loaded \ beam, P_n = \frac{6M_n}{L} = \frac{6 \times 6.153}{1.05} = 35.16 \ kN$$

Check of bond capacity of GFRP bars in the concrete beam after exposure to high temperature:

$Ultimate \ Bond \ capacity \ of \ GFRP \ with \ concrete \ after \ exposure \ to \ 320°C \ \tau_{max}$
$= 0.419 \ MPa$

$For \ FRP \ bar, ultimate \ bond \ force \ = \pi \ \tau_{max} d_b \ S$

For two GFRP bars $F \ = \ 2 \times \pi \ \tau_{max} d_b \ S \ = \ 2 \times \pi \times 0.419 \times 10 \times 400 = \ 10.530 \ kN$

$$< \ T_m = 49.7 \ kN$$

For GFRP-RC beams exposed to high temperature, maximum bond force capacity between GFRP bars and concrete is lower than the maximum tensile force capacity in the bars so bond failure between GFRP and concrete is expected before reaching to bar maximum tensile capacity and flexural capacity of the beam to be recalculate similar to previous cases.
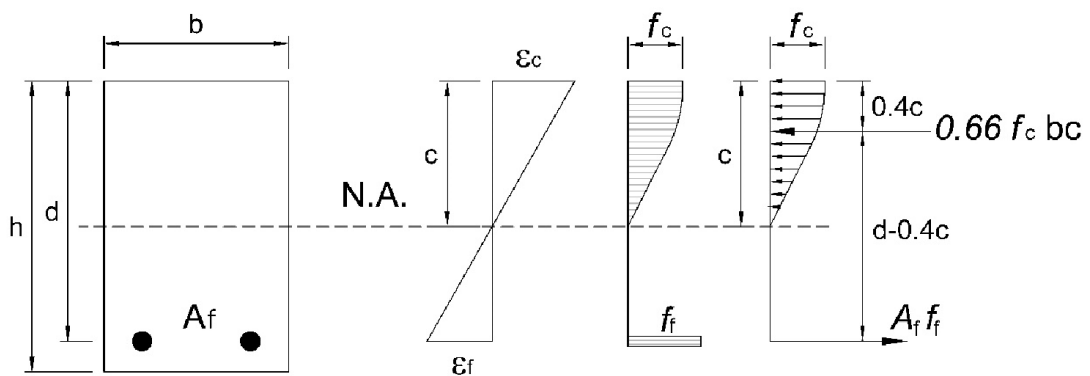
(Refer Fig. 5.11)

1. Assume f_c =11.356 MPa (from previous step)

F (maximum bond capacity force) =10,530 N=10.530 kN

$$\text{Maximum FRP strain } \varepsilon_f = \frac{F}{A_f E_f} = \frac{10,530}{157.08 \times 37,390} = 0.001793$$

$$\text{Compression Force C} = \frac{2}{3} f_c c b = \frac{2}{3} \times 11.356 \times 130 \times c$$

Using internal forces equilibrium, C = F

$$\frac{2}{3} \times 11.356 \times 130 \times c = 10,530 \rightarrow c = 10.699 \; mm$$

$$\varepsilon_c = \frac{c \, \varepsilon_f}{d - c} = \frac{10.699 \times 0.001793}{144 - 10.699} = 0.000144 < \varepsilon_o$$

$$Using \; EN1992 \; concrete \; stress - strain \; curve, \qquad at \; 500°C$$

$$f_c = \left(\frac{3\varepsilon_{c,T} f'_{c,500}}{0.015 \left[2 + \left(\frac{\varepsilon_{c,T}}{0.015} \right)^3 \right]} \right) = \left(\frac{3\varepsilon_{c,T} \times 25.2}{0.015 \left[2 + \left(\frac{\varepsilon_{c,T}}{0.015} \right)^3 \right]} \right)$$

$$= \left(\frac{3 \times 0.000144 \times 25.2}{0.015 \left[2 + \left(\frac{0.000144}{0.015} \right)^3 \right]} \right) = 0.363 \; MPa$$

2. By trial and error, repeat the previous steps using initially f_c = 0.363 MPa, until finding the correct stress value f_c.

It was found that f_c = 2.419 MPa, c= 50.22 mm and ε_c = 0.000960

$$M_n = F(d - 0.4c) = 10,530 \times (144 - 0.4 \times 50.22) \times 10^{-6} = 1.3048 \; kN.m$$

$$For \; four \; point \; loaded \; beam, P_n = \frac{6M_n}{L} = \frac{6 \times 1.3048}{1.05} = 7.46 \; kN$$

Check of bond capacity of GFRP bar with end cap in the concrete beam after exposure to high temperature:

$$Ultimate \; Bond \; capacity \; of \; GFRP \; with \; concrete \; after \; exposure \; to \; 320°C \quad \tau_1$$

$$= 0.419 \; MPa$$

$$Ult. \; bond \; capacity \; between \; GFRP, epoxy \; and \; steel \; cap \; after \; exposure \; to \; 320°C \; (\tau_2)$$

$$= 4.983 \; MPa$$

$$For \; FRP \; bar \; with \; end \; cap \, , ultimate \; bond \; force \; = \pi \, d_b \, (S_1 \, \tau_1 + S_2 \, \tau_2)$$

For two GFRP bars with steel end cap $F = 2 \times \pi \, d_b \, (S_1 \, \tau_1 + S_2 \, \tau_2)$

$$= 2 \times \pi \times 10 \times (300 \times 0.419 + 100 \times 4.983) = 39.2 \text{ kN} < T_m$$

$$= 49.7 kN$$
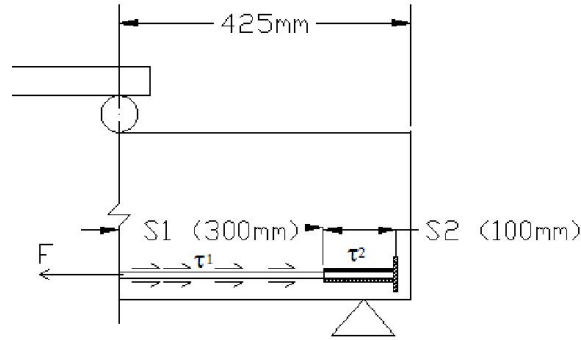
(Refer fig. B1)

Maximum bond force capacity between GFRP bars with end cap and concrete is lower than the maximum tensile force in the reinforcement of the beam at failure stage which means that de-bonding is expected before reaching the FRP rupture failure and flexural capacity of the beam should be calculated again similar to previous cases.

1. Assume that the concrete stress is less than its peak & strain is less than ε_o. Parabolic distribution of concrete compressive stress of maximum value f_c is assumed (note: parabolic area = 2/3 f_c c)

2. Assume $f_c = f_c' = 11.356$ MPa

F (maximum Bond capacity Force) =39,200 N=39.2 kN

$$Maximum \ FRP \ strain \ \varepsilon_f = \frac{F}{A_f E_f} = \frac{39{,}200}{157.08 \times 37{,}390} = 0.006674$$

$$Compression \ Force \ C = \frac{2}{3} f_c c b = \frac{2}{3} \times 11.356 \times 130 \times c$$

Using internal forces equilibrium, C = F

$$\frac{2}{3} \times 11.356 \times 130 \times c = 39{,}200 \rightarrow c = 39.829 \ mm$$

$$\varepsilon_c = \frac{c \, \varepsilon_f}{d - c} = \frac{39.829 \times 0.006676}{144 - 39.829} = 0.002552 < \varepsilon_o$$
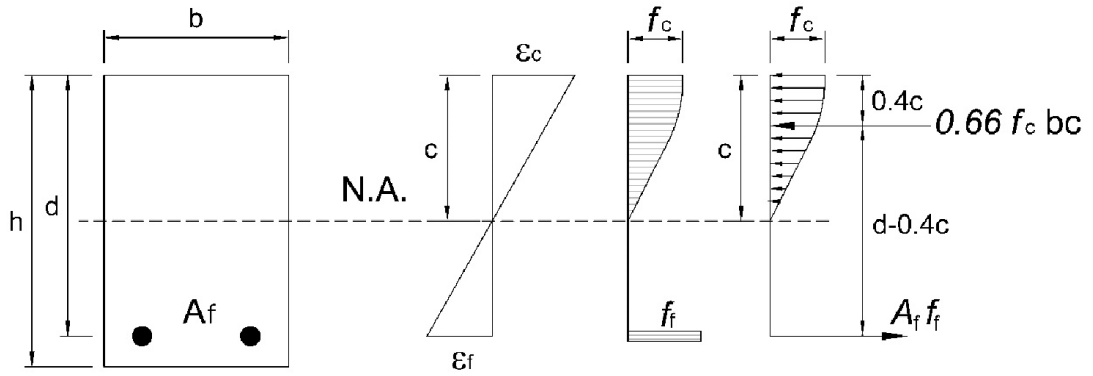
(Refer Fig. 5.11)

Using EN1992 concrete stress − strain curve ,   at 500°C

$$f_c = \left(\frac{3\varepsilon_{c,T} f'_{c,500}}{0.015 \left[2 + \left(\frac{\varepsilon_{c,T}}{0.015}\right)^3\right]} \right) = \left(\frac{3\varepsilon_{c,T} \times 25.2}{0.015 \left[2 + \left(\frac{\varepsilon_{c,T}}{0.015}\right)^3\right]} \right)$$

$$= \left(\frac{3 \times 0.002552 \times 25.2}{0.015 \left[2 + \left(\frac{0.002552}{0.015}\right)^3\right]} \right) = 6.415 \ MPa$$

3. By trial and error, repeat the previous steps using initially f_c = 6.415 MPa, until finding the correct stress value f_c.

It was found that fc = 8.983 MPa, c= 50.355 mm and ε_c = 0.003589

$$M_n = F(d - 0.4c) = 39.2 \times (144 - 0.4 \times 50.355) \times 10^{-6} = 4.855 \ kN.m$$

$$For \ four \ point \ loaded \ beam, P_n = \frac{6M_n}{L} = \frac{6 \times 4.855}{1.05} = 27.74 \ kN$$

B5. Theoretical prediction of flexural capacity of BFRP-RC beams after exposure to high temperature

E_f =51,890 MPa

Reduced f_{ult-f} =408 MPa

f_c'=25.2 MPa

β_1=0.85

$\rho_f /\rho_b = 0.681$ <1.0 ==> FRP rupture failure mode before crushing concrete

FRP reached its maximum tensile strength while concrete still below its crushing strain stage.

Flexural capacity of the beam should be calculated as follows:

- Assume that the concrete stress is less than its peak and strain is less than ε_o. Parabolic distribution of concrete compressive stress of maximum value f_c is assumed

   (Note: parabolic area = 2/3 f_c c)
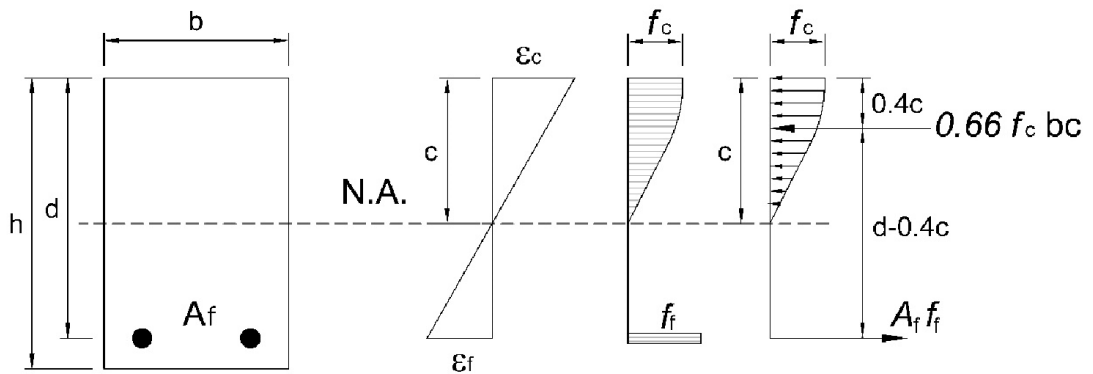
(Refer Fig. 5.11)

$$Maximum\ FRP\ strain\ \varepsilon_{ult-f} = \frac{f_{ult-f}}{E_f} = \frac{408}{51,890} = 0.007863$$

$$Tensile\ force\ in\ reinforcemnet\ \ T_m = A_f f_{ult-f} = 157.08×408 = 64,090\ N$$

$$= 64.09\ kN$$

- Assume $f_c = f_c'$ =25.2MPa

Compression Force $C = \frac{2}{3}f_c cb = \frac{2}{3} \times 25.2 \times 130 \times c$

Using internal forces equilibrium, $C = T_m$

$\frac{2}{3} \times 25.2 \times 130 \times c = 64{,}090 \rightarrow c = 29.345 \ mm$

$\varepsilon_c = \frac{c \ \varepsilon_{ult-f}}{d - c} = \frac{29.345 \times 0.007863}{144 - 29.345} = 0.002013 \ < \varepsilon_o$

Using EN1992 concrete stress − strain curve ,   at 500°C

$$f_c = \left(\frac{3\varepsilon_{c,T}f'_{c,500}}{0.015 \left[2 + \left(\frac{\varepsilon_{c,T}}{0.015} \right)^3 \right]} \right) = \left(\frac{3\varepsilon_{c,T} \times 25.2}{0.015 \left[2 + \left(\frac{\varepsilon_{c,T}}{0.015} \right)^3 \right]} \right)$$

$$= \left(\frac{3 \times 0.002013 \times 25.2}{0.015 \left[2 + \left(\frac{0.002013}{0.015} \right)^3 \right]} \right) = 5.065 \ MPa$$

3. By trial and error, repeat the previous steps using initially $f_c = 5.065$ MPa, until finding the correct stress value f_c.

   It was found that $f_c = 12.876$ MPa, c= 57.434 mm and $\varepsilon c = 0.005217$

$M_n = F(d - 0.4c) = 64.09 \times (144 - 0.4 \times 57.434) \times 10^{-6} = 7.756 \ kN.m$

For four point loaded beam, $P_n = \frac{6M_n}{L} = \frac{6 \times 7.756}{1.05} = 44.32 \ kN$

<u>Check of bond capacity of BFRP bars in the concrete beam after exposure to high temperature:</u>

Ultimate bond capacity of BFRP with concrete after exposure to 320°C (τ_{max}) = 0.555 MPa

For FRP bar, ultimate bond force $= \pi \ \tau_{max} d_b \ S$

For two GFRP bars $F = 2 \times \pi \ \tau_{max} d_b \ S = 2 \times \pi \times 0.555 \times 10 \times 400 = 13.95$ kN

$< \ T_m = 64.09 \ kN$

For BFRP-RC beams exposed to high temperature, maximum bond force capacity between BFRP bars and concrete is lower than the maximum tensile force capacity in the bars so bond failure between BFRP and concrete is expected before reaching to bar maximum tensile capacity and flexural capacity of the beam to be recalculate similar to previous cases.

(Refer Fig. 5.11)
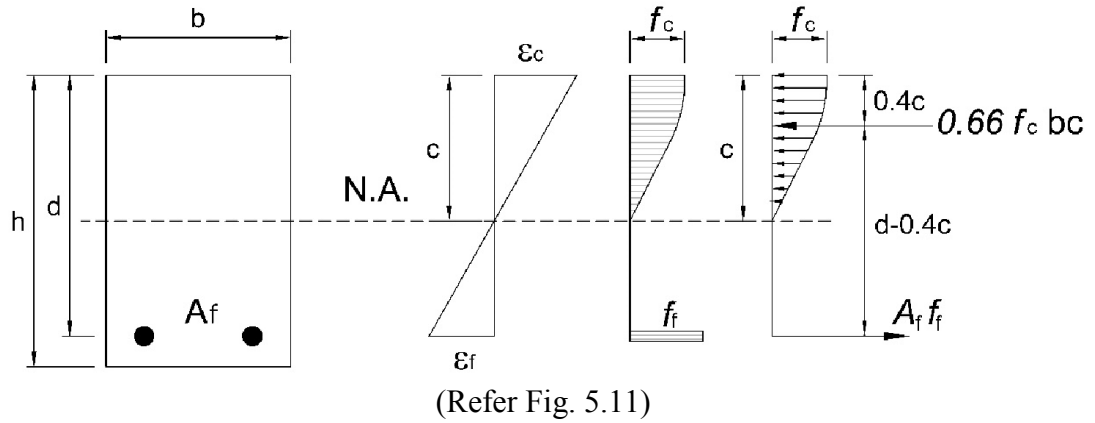
1. Assume f_c =12.876 MPa

F (maximum Bond capacity Force) =13,950 N=13.95 kN

$$Maximum\ FRP\ strain\ \varepsilon_f = \frac{F}{A_f E_f} = \frac{13,950}{157.08\times51,890} = 0.001711$$

$$Compression\ force\ C = \frac{2}{3}f_c cb = \frac{2}{3}\times12.876\times130\times c$$

Using internal forces equilibrium, C = F

$$\frac{2}{3}\times12.876\times130\times c = 13,950 \rightarrow c = 12.501\ mm$$

$$\varepsilon_c = \frac{c\ \varepsilon_f}{d - c} = \frac{12.501\times 0.001711}{144 - 12.501} = 0.000163 < \varepsilon_o$$

$Using\ EN1992\ concrete\ stress - strain\ curve,\qquad at\ 500°C$

$$f_c = \left(\frac{3\varepsilon_{c,T}f'_{c,500}}{0.015\left[2 + \left(\frac{\varepsilon_{c,T}}{0.015}\right)^3\right]}\right) = \left(\frac{3\varepsilon_{c,T}\times25.2}{0.015\left[2 + \left(\frac{\varepsilon_{c,T}}{0.015}\right)^3\right]}\right)$$

$$= \left(\frac{3 \times 0.000163 \times 25.2}{0.015 \left[2 + \left(\frac{0.000163}{0.015} \right)^3 \right]} \right) = 0.41 \ MPa$$

2. By trial and error, repeat the previous steps using initially f_c =0.41 MPa, until finding the correct stress value f_c.

I was found that fc = 2.8242 MPa, c= 56.99 mm and ε_c = 0.001121

$$M_n = F(d - 0.4c) = 13{,}950 \times (144 - 0.4 \times 56.99) \times 10^{-6} = 1.6908 \ kN.m$$

$$For \ four \ point \ loaded \ beam, P_n = \frac{6M_n}{L} = \frac{6 \times 1.6908}{1.05} = 9.66 \ kN$$

<u>Check of bond capacity of BFRP bar with end cap in the concrete beam after exposure to high temperature:</u>
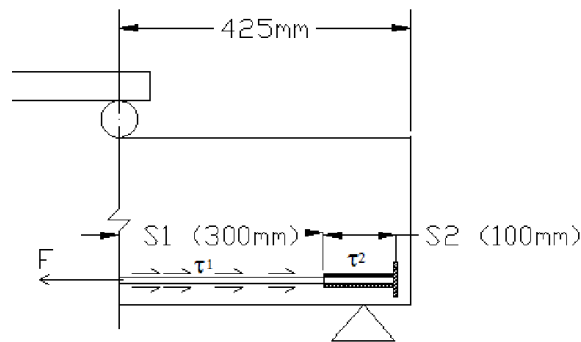
(Fig. B.1)

$Ultimate \ bond \ capacity \ of \ GFRP \ with \ concrete \ after \ exposure \ to \ 320°C \ (\tau_1)$

$$= 0.555 \ MPa$$

$Ult. \ bond \ capacity \ between \ GFRP, epoxy \ and \ steel \ cap \ after \ exposure \ to \ 320°C \ (\tau_2)$

$$= 6.69 \ MPa$$

$For \ FRP \ Bar \ with \ end \ cap , Ultimate \ Bond \ Force \ = \pi \ d_b \ (S_1 \ \tau_1 + S_2 \ \tau_2)$

For two GFRP bars with steel end cap F $= 2 \times \pi \ d_b \ (S_1 \ \tau_1 + S_2 \ \tau_2)$

$$= 2 \times \pi \times 10 \times (300 \times 0.555 + 100 \times 6.69) = 52.5 \ kN < T$$

$$= 64.09 \ kN$$

Maximum bond force capacity between BFRP bars with end cap and concrete is lower than the maximum tensile force in the reinforcement of the beam at FRP rupture failure

which means that de-bonding is expected before reaching the FRP rupture failure and flexural capacity of the beam should be calculated again similar to previous cases.

1. First step is to assume that the concrete stress is less than its peak and strain is less than ε_o. Parabolic distribution of concrete compressive stress of maximum value f_c is assumed   (note: parabolic area = 2/3 f_c c)
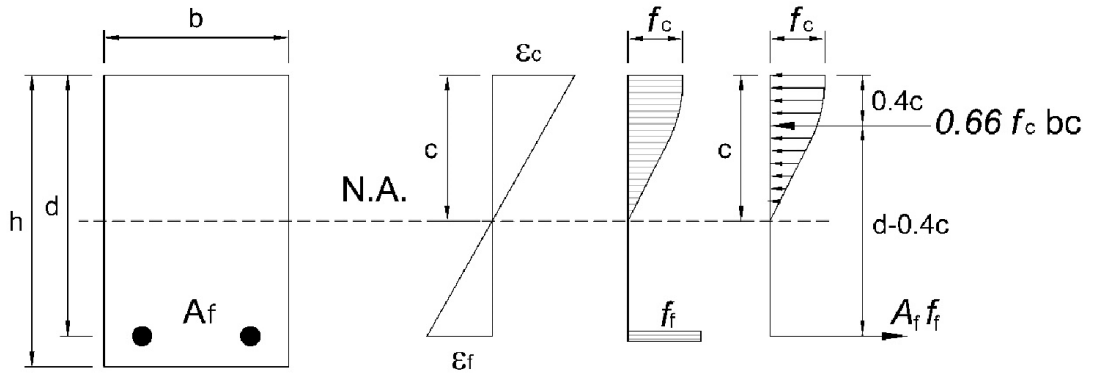
(Refer Fig. 5.11)

2. Assume $f_c = f_c' = 12.876$ MPa

F (maximum Bond capacity Force) =52,500 N=52.5 kN

$$Maximum\ FRP\ strain\ \varepsilon_f = \frac{F}{A_f E_f} = \frac{52,500}{157.08 \times 51,890} = 0.006441$$

$$Compression\ Force\ C = \frac{2}{3} f_c cb = \frac{2}{3} \times 12.876 \times 130 \times c$$

Using internal forces equilibrium, C = F

$$\frac{2}{3} \times 12.876 \times 130 \times c = 52,500 \rightarrow c = 47.048\ mm$$

$$\varepsilon_c = \frac{c\ \varepsilon_f}{d - c} = \frac{47.048 \times 0.006441}{144 - 47.048} = 0.003126 < \varepsilon_o$$

$Using\ EN1992\ concrete\ stress - strain\ curve,$ $at\ 500°C$

$$f_c = \left(\frac{3\varepsilon_{c,T} f_{c,500}'}{0.015 \left[2 + \left(\frac{\varepsilon_{c,T}}{0.015} \right)^3 \right]} \right) = \left(\frac{3\varepsilon_{c,T} \times 25.2}{0.015 \left[2 + \left(\frac{\varepsilon_{c,T}}{0.015} \right)^3 \right]} \right)$$

$$= \left(\frac{3 \times 0.003126 \times 25.2}{0.015 \left[2 + \left(\frac{0.003126}{0.015} \right)^3 \right]} \right) = 7.841 \; MPa$$

- By trial and error, repeat the previous steps using initially f_c = 7.841 MPa, until finding the correct stress value f_c.

I was found that f_c = 10.585 MPa, c= 57.228 mm, and ε_c = 0.004248

$$M_n = F(d - 0.4c) = 52{,}500 \times (144 - 0.4 \times 57.228) \times 10^{-6} = 6.358 \; kN.m$$

$$For \; four \; point \; loaded \; beam, P_n = \frac{6M_n}{L} = \frac{6 \times 6.358}{1.05} = 36.33 \; kN$$

B6. Theoretical prediction of flexural capacity of CFRP-RC beams after exposure to high temperature

E_f =80,410 MPa

Reduced f_{ult-f} =630 MPa

f_c'=25.2 MPa

β_1=0.85

ρ_f / ρ_b = 1.0487 >1.0   ==> crushing concrete mode failure

$$Maximum\ CFRP\ strain\ \varepsilon_{ult-f} = \frac{f_{ult-f}}{E_f} = \frac{630}{80,410} = 0.007835$$

Concrete Strain at peak stress ε_0 = 0.015 > 0.007835 ==> FRP rupture is expected before concrete crushing.

Flexural capacity of the beam should be calculated as follows:

1. Assume that the concrete stress is less than its peak and strain is less than ε_0.

   Parabolic distribution of concrete compressive stress of maximum value f_c is assumed   (note: parabolic area = 2/3 f_c c)
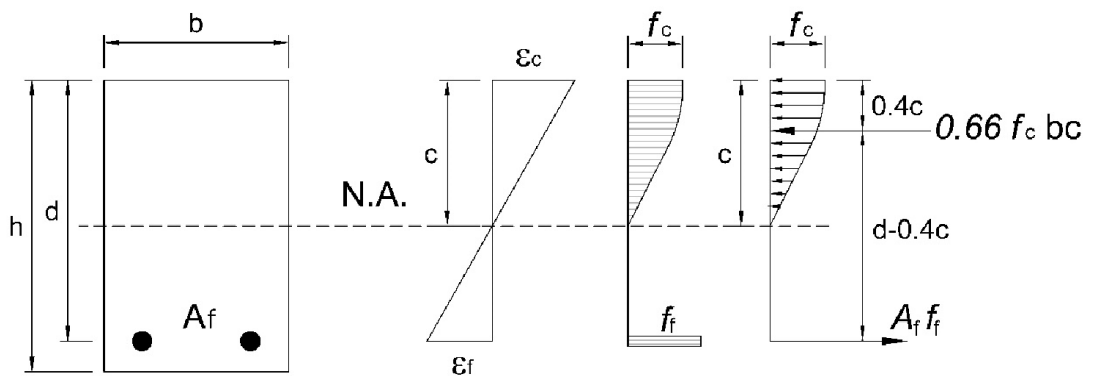
(Refer Fig. 5.11)

2. Assume $f_c = f_c'$ =25.2MPa

$$\varepsilon_{ult-f} = \frac{f_{ult-f}}{E_f} = \frac{630}{80,410} = 0.007835$$

$$Maximum\ Tensile\ force\ in\ reinforcemnet\ T = A_f f_{ult-f} = 157.08 \times 630$$

$$= 98{,}9607N = 98.96\ kN$$

$$\text{Compression Force C} = \frac{2}{3} f_c cb = \frac{2}{3} \times 25.2 \times 130 \times c$$

Using internal forces equilibrium, $C = T_m$

$$\frac{2}{3} \times 25.2 \times 130 \times c = 98{,}960 \rightarrow c = 45.3115\ mm$$

$$\varepsilon_c = \frac{c\ \varepsilon_{ult-f}}{d-c} = \frac{43.3115 \times 0.00783}{144 - 43.3115} = 0.003597\ < \varepsilon_o$$

$$Using\ EN1992\ concrete\ stress - strain\ curve, \qquad at\ 500°C$$

$$f_c = \left(\frac{3\varepsilon_{c,T} f'_{c,500}}{0.015 \left[2 + \left(\frac{\varepsilon_{c,T}}{0.015} \right)^3 \right]} \right) = \left(\frac{3\varepsilon_{c,T} \times 25.2}{0.015 \left[2 + \left(\frac{\varepsilon_{c,T}}{0.015} \right)^3 \right]} \right)$$

$$= \left(\frac{3 \times 0.003597 \times 25.2}{0.015 \left[2 + \left(\frac{0.003957}{0.015} \right)^3 \right]} \right) = 9.0\ MPa$$

3. By trial and error, repeat the previous steps using initially f_c = 9.0 MPa, until finding the correct stress value f_c.

It was found that f_c = 16.678 MPa, c= 67.976 mm and ε_c = 0.007005

$$M_n = F(d - 0.4c) = 98.96 \times (144 - 0.4 \times 67.976) \times 10^{-6} = 11.56\ kN.m$$

$$For\ four\ point\ loaded\ beam, P_n = \frac{6M_n}{L} = \frac{6 \times 11.56}{1.05} = 66.05\ kN$$

Check of bond capacity of CFRP bars in the concrete beam after exposure to high temperature:

$Ultimate\ bond\ capacity\ of\ CFRP\ with\ concrete\ after\ exposure\ to\ 320°C\ (\tau_{max})$
$= 1.533\ MPa$

$$For\ FRP\ bar, ultimate\ bond\ force\ = \pi\ \tau_{max} d_b\ S$$

For two CFRP bars $F = 2 \times \pi\, \tau_{max} d_b\, S = 2 \times \pi \times 1.533 \times 10 \times 400 = 38.53$ kN

$$< T_m = 98.96\ kN$$

For CFRP-RC beams exposed to high temperature, maximum bond force capacity between CFRP bars and concrete is lower than the maximum tensile force capacity in the bars at concrete crushing failure so bond failure between CFRP and concrete is expected before reaching to concrete crushing and flexural capacity of the beam to be recalculate similar to previous cases.

1. Assume that the concrete stress is less than its peak and strain is less than ε_o. Parabolic distribution of concrete compressive stress of maximum value f_c is assumed   (note: parabolic area = 2/3 f_c c)

2. Assume fc = fc' =16.79 MPa

F (maximum Bond capacity Force) =38,530 N=38.53 kN

$$Maximum\ FRP\ strain\ \varepsilon_f = \frac{F}{A_f E_f} = \frac{38,530}{157.08 \times 80,410} = 0.003051$$

$$Compression\ Force\ C = \frac{2}{3} f_c cb = \frac{2}{3} \times 16.79 \times 130 \times c$$
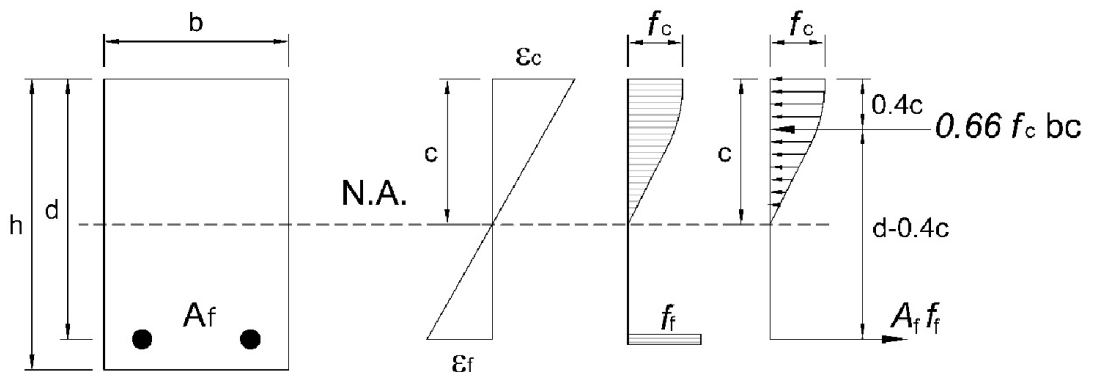
(Refer Fig. 5.11)

Using internal forces equilibrium, C = F

$$\frac{2}{3} \times 16.79 \times 130 \times c = 38,530 \rightarrow c = 26.47\ mm$$

$$\varepsilon_c = \frac{c\ \varepsilon_f}{d - c} = \frac{26.47 \times 0.003051}{144 - 26.47} = 0.000687 < \varepsilon_o$$

*Using EN*1992 *concrete stress* − *strain curve,*   *at* 500°*C*

$$f_c = \left(\frac{3\varepsilon_{c,T} f'_{c,500}}{0.015 \left[2 + \left(\frac{\varepsilon_{c,T}}{0.015}\right)^3\right]} \right) = \left(\frac{3\varepsilon_{c,T} \times 25.2}{0.015 \left[2 + \left(\frac{\varepsilon_{c,T}}{0.015}\right)^3\right]} \right)$$

$$= \left(\frac{3 \times 0.000687 \times 25.2}{0.015 \left[2 + \left(\frac{0.000687}{0.015}\right)^3\right]} \right) = 1.731 \; MPa$$

3. By trial and error, repeat the previous steps using initially f_c = 1.731 MPa, until we find the correct stress value f_c.

4. It was found that f_c = 6.647 MPa, c= 66.875 mm, ε_c = 0.002645

$$M_n = F(d - 0.4c) = 55.4 \times (144 - 0.4 \times 66.875) \times 10^{-6} = 4.517 \; kN.m$$

$$For \; four \; point \; loaded \; beam, P_n = \frac{6M_n}{L} = \frac{6 \times 4.517}{1.05} = 25.81 \; kN$$

Check of bond capacity of CFRP bar with end cap in the concrete beam after exposure to high temperature:
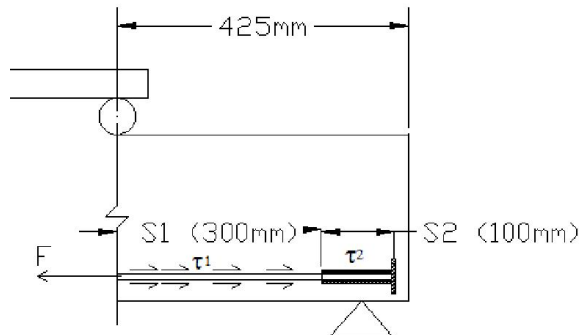
(Refer Fig. B.1)

Ultimate Bond capacity of CFRP with concrete after exposure to 320°*C*

$\tau_1 = 1.533 \; MPa$

Ult. Bond capacity between CFRP, epoxy and steel cap after exposure to 320°*C*

$\tau_2 = 6.948 \; MPa$

For FRP bar with end cap, ultimate bond force $= \pi \, d_b \, (S_1 \, \tau_1 + S_2 \, \tau_2)$

For two CFRP bars with steel end cap $F = 2 \times \pi \, d_b \, (S_1 \tau_1 + S_2 \tau_2)$

$$= 2 \times \pi \times 10 \times (300 \times 1.533 + 100 \times 6.948) = 72.55 \text{ kN} < T_m$$

$$= 96.267 \, kN$$

Maximum bond force capacity between CFRP bars with end cap and concrete is lower than the maximum tensile force in the reinforcement of the beam at concrete crushing failure which means that de-bonding is expected before reaching crushing strain of concrete and flexural capacity of the beam should be calculated again similar to previous cases.

1. Assume that the concrete stress is less than its peak & strain is less than ε_o. Parabolic distribution of concrete compressive stress of maximum value f_c is assumed

2. Assume $f_c = f_c' = 16.79$ MPa

F (maximum Bond capacity Force) =72,552 N=72.55 kN

$$Maximum \; FRP \; strain \; \varepsilon_f = \frac{F}{A_f E_f} = \frac{72,552}{157.08 \times 80,410} = 0.005744$$

$$Compression \; Force \; C = \frac{2}{3} f_c cb = \frac{2}{3} \times 16.79 \times 130 \times c$$
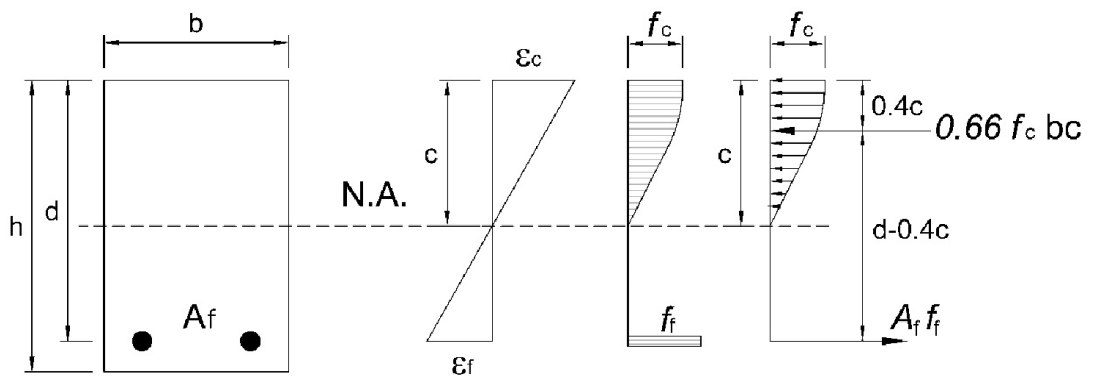
(Refer Fig. 5.11)

Using internal forces equilibrium, C = F

$$\frac{2}{3} \times 16.79 \times 130 \times c = 72,552 \rightarrow c = 49.836 mm$$

$$\varepsilon_c = \frac{c \, \varepsilon_f}{d - c} = \frac{49.836 \times 0.005744}{144 - 49.836} = 0.00304 < \varepsilon_o$$

Using EN1992 concrete stress − strain curve,   at 500°C

$$f_c = \left(\frac{3\varepsilon_{c,T} f'_{c,500}}{0.015 \left[2 + \left(\frac{\varepsilon_{c,T}}{0.015} \right)^3 \right]} \right) = \left(\frac{3\varepsilon_{c,T} \times 25.2}{0.015 \left[2 + \left(\frac{\varepsilon_{c,T}}{0.015} \right)^3 \right]} \right)$$

$$= \left(\frac{3 \times 0.00304 \times 25.2}{0.015 \left[2 + \left(\frac{0.00304}{0.015} \right)^3 \right]} \right) = 7.629 \, MPa$$

3. By trial and error, repeat the previous steps using initially f_c = 7.629 MPa, until

finding the correct stress value f_c.

4. It was found that f_c = 12.448 MPa, c= 67.25 mm and ε_c = 0.005033

$$M_n = F(d - 0.4c) = 72{,}552 \times (144 - 0.4 \times 67.25) \times 10^{-6} = 8.496 \, kN.m$$

For four point loaded beam, $P_n = \dfrac{6M_n}{L} = \dfrac{6 \times 8.496}{1.05} = 48.55 \, kN$

Appendix C: Theoretical Prediction of Flexural Capacity of Steel-RC beams

C1. Theoretical Prediction of Flexural Capacity of Steel -RC Beams at Normal Temperature

f_y =571 MPa and Es= 228 GPa

fc' =34 MPa

Extreme fiber compressive strain at failure = ultimate concrete strain ε_{cu} = 0.003

$Tensile\ force\ in\ reinforcemnet\ T_m = A_s f_y = 157{\times}571 = 89{,}647\ N$

$$= 89.65\ kN$$

$$a = \frac{T_m}{0.85 f_c' b} = \frac{89{,}647}{0.85{\times}34{\times}130} = 23.86\ mm \rightarrow c = \frac{a}{\beta_1} = \frac{23.86}{0.80714} = 29.56\ mm$$

$$M_n = T_m \left(d - \frac{a}{2}\right) = 89.65{\times}\left(144 - \frac{23.86}{2}\right){\times}10^{-6} = 11.84\ kN.m$$

$$For\ four\ point\ loaded\ beam, P_n = \frac{6M_n}{L} = \frac{6{\times}11.84}{1.05} = 67.66\ kN$$

From assumption that plain section before loading remain plain after loading, so strain in concrete and reinforcement is proportional to the distance from neutral axis:

$$\varepsilon_s = \frac{(d - c)\varepsilon_{cu}}{c} = \frac{(144 - 29.56){\times}\ 0.003}{29.56} = 0.0116 > \varepsilon_y = \frac{571}{228{,}000} = 0.0025$$

Which means that the steel bars yielded before reaching the concrete ultimate strain.

<u>Check of bond capacity of Steel in the Concrete beam at normal temperature:</u>

$Average\ bond\ capacity\ of\ steel\ bar\ with\ concrete\ (\tau_{max}) = 7.48\ MPa$

$For\ FRP\ bar, ultimate\ bond\ force\ = \pi\ \tau_{max} d_b\ S$

For two steel bars $F = 2{\times}\pi\ \tau_{max} d_b\ S = 2{\times}\pi{\times}7.48{\times}10{\times}400 = 187.9\ kN$

$$> T_m = 89.65\ kN$$

Which means that bond between steel bars and concrete are highly perfect up to failure.

C2. **Theoretical Prediction of Flexural Capacity of Steel -RC Beams at High Temperature**

f_y =547 MPa

E_s = 210 GPa

f_c' =25.2 MPa

Assume extreme fiber compressive strain = ultimate concrete strain ε_{cu} = 0.003

$Tensile\ force\ in\ reinforcemnet\ T_m = A_s f_y = 157 \times 547 = 85,880N$

$$= 85.88\ kN$$

$$a = \frac{T_m}{0.85 f_c' b} = \frac{85,880}{0.85 \times 25.2 \times 130} = 30.84\ mm \to c = \frac{a}{\beta_1} = \frac{30.84}{0.85} = 36.28\ mm$$

$$M_n = T_m \left(d - \frac{a}{2}\right) = 88.0 \times \left(144 - \frac{30.84}{2}\right) \times 10^{-6} = 11.042\ kN.m$$

$$For\ four\ point\ loaded\ beam, P_n = \frac{6M_n}{L} = \frac{6 \times 11.042}{1.05} = 63.1\ kN$$

$$\varepsilon_s = \frac{(d - c)\varepsilon_{cu}}{c} = \frac{(144 - 36.28) \times 0.003}{36.28} = 0.00891 > \varepsilon_y = \frac{547}{210,000} = 0.0026$$

Which means that the steel bars yielded before reaching the concrete ultimate strain.

<u>Check of bond capacity of Steel in the Concrete beam at high temperature:</u>

$Average\ bond\ capacity\ of\ steel\ bar\ with\ concrete\ \tau_{max} = 3.923\ MPa$

$For\ FRP\ bar, ultimate\ bond\ force\ = \pi\ \tau_{max} d_b\ S$

For two steel bars F $= 2 \times \pi\ \tau_{max} d_b\ S = 2 \times \pi \times 3.923 \times 10 \times 400 = 98.55$ kN

$$> T_m = 85.88\ kN$$

Which means that bond between steel bars and concrete are still perfect up to failure.